

STABLE ISOTOPES REVEAL A DISCONNECT BETWEEN BIOTIC AND ABIOTIC
HYDROLOGICAL PROCESSES IN A SEASONALLY-DRY, SEMI-ARID
WATERSHED

by

Ryan James McCutcheon

A thesis
submitted in partial fulfillment
of the requirements for the degree of
Master of Science in Hydrologic Sciences
Boise State University

August 2015

© 2015

Ryan James McCutcheon

ALL RIGHTS RESERVED

BOISE STATE UNIVERSITY GRADUATE COLLEGE

DEFENSE COMMITTEE AND FINAL READING APPROVALS

of the thesis submitted by

Ryan James McCutcheon

Thesis Title: Stable Isotopes Reveal a Disconnect Between Biotic and Abiotic Hydrological Processes in a Seasonally-Dry, Semi-Arid Watershed

Date of Final Oral Examination: 04 May 2015

The following individuals read and discussed the thesis submitted by student Ryan James McCutcheon, and they evaluated his presentation and response to questions during the final oral examination. They found that the student passed the final oral examination.

James McNamara, Ph.D.	Chair, Supervisory Committee
Shawn Benner, Ph.D.	Member, Supervisory Committee
Alejandro Flores, Ph.D.	Member, Supervisory Committee
Matthew Kohn, Ph.D.	Member, Supervisory Committee

The final reading approval of the thesis was granted by James McNamara, Ph.D., Chair of the Supervisory Committee. The thesis was approved for the Graduate College by John R. Pelton, Ph.D., Dean of the Graduate College.

ACKNOWLEDGEMENTS

First and foremost, I would like to thank my Supervisory Committee chair, Dr. James McNamara. Dr. McNamara helped me through some of the more trying times of my graduate career by showing interest in not only my research but also my career goals and general well-being. He never once voiced doubts about my research, even when I may have held reservations myself. Without his expertise, inspiration, and patience, this thesis would not have been possible. I would also like to thank my Supervisory Committee, Dr. Shawn Benner, Dr. Matthew Kohn, and Dr. Alejandro Flores for their expertise and support of my thesis work. Dr. Matthew Kohn granted me essential access to the Stable Isotope Laboratory and built the vacuum extraction line used to remove water from plants and soils, Dr. Flores provided crucial modeling advice, and Dr. Benner helped refine the scope of my research and focus on the most important topics. Lastly, I would like to express my gratitude for the help of Research Scientists Samantha Evans and Pam Aishlin. Samantha taught me how to use all of the equipment in the Stable Isotopes Laboratory and assisted in correcting the isotope values of water containing organic contaminants. She also offered an abundance of insightful research advice throughout the thesis process. Pam Aishlin was a vital contributor to my thesis work because she introduced me to Dry Creek Experimental Watershed, taught me how to collect and store water samples for isotopic analysis, and also install and collect data from weather stations, stream gauging stations, and soil moisture sensors.

ABSTRACT

Until recently, it had been thought that humid catchment woody plants transpired primarily mobile soil water that would otherwise flow to streams or recharge groundwater. However, several recent studies have suggested that trees in seasonally-dry humid catchments use primarily tightly-bound, immobile soil water that does not fully mix with new precipitation or participate in translatory flow. McDonnell (2014) called this existence of two, hydrologically-distinct, water pools “the two water worlds hypothesis.” This ecohydrological behavior has important implications for understanding a wide range of catchment processes, including the spatial and temporal variability of evapotranspiration and nutrient cycling, and our abilities to accurately model those processes. Yet, similar studies have not been conducted in drier environments. This study aims to improve our understanding of semi-arid woody plant root water sources. Isotopic analyses were conducted on the xylem water of nine common semi-arid woody plant species, in conjunction with bulk soil water, groundwater, and streamwater samples. The isotopic concentrations of plant xylem water and potential root water sources were plotted in dual-isotope space and qualitatively assessed. Additionally, the SISUS model was used to computationally characterize all feasible water source contributions to each plant individual. In total, 112 out of 121 plant samples had isotope values indicative of use of at least fractional immobile soil water use. These findings were consistent, regardless of plant species, geographic location, or time of sample collection. Nevertheless, some Yellow willow, Fire willow, Chokecherry, Rabbitbrush, Douglas-fir,

and Ponderosa pine individuals plotted between immobile and mobile water sources, and were modeled to use greater than 30% mobile water sources (groundwater and streamwater) in the late growing season. Additionally, median modeled use of mobile water sources increased for each field site between July and September, indicating that many plants may have actively rooted to groundwater as the soil column dried significantly below the permanent wilting point. Therefore, we accept the two water worlds hypothesis in terms of immobile soil water use, regardless of mobile soil water availability. However, we also acknowledge that many semi-arid woody plants also use mobile groundwater and streamwater sources.

TABLE OF CONTENTS

ACKNOWLEDGEMENTS	iv
ABSTRACT	v
LIST OF TABLES	x
LIST OF FIGURES	xv
LIST OF ABBREVIATIONS.....	xxiii
CHAPTER ONE: INTRODUCTION.....	1
CHAPTER TWO: SCIENTIFIC BACKGROUND	6
2.1 Soil Water Mobility, Field Capacity and Permanent Wilting Point	6
2.2 Water Isotopes in the Natural Environment.....	7
2.3 Meteoric Water Lines and Evaporation Water Lines	10
2.4 Isotopic Evidence for Two Water Worlds in Seasonally-Dry, Humid Catchments.....	12
2.5 Vegetation-Water Dynamics in Semi-Arid Watersheds	16
CHAPTER THREE: STUDY AREA – DRY CREEK EXPERIMENTAL WATERSHED .	18
3.1 Watershed Instrumentation	18
3.2 Topography and Drainage Patterns.....	19
3.3 Geology and Soil Characteristics.....	20
3.4 Climate and Soil Moisture	21
3.5 Woody Plant Life.....	22
CHAPTER FOUR: MATERIALS AND METHODS.....	24

4.1 Identifying Mobile and Immobile Water	24
4.2 Sampling and Storage	25
4.3 Sample Water Extraction	27
4.4 Stable Isotope Analysis.....	30
4.5 Los Gatos Research Liquid Water Isotope Analyzer.....	31
4.6 SISUS Modeling	32
CHAPTER FIVE: RESULTS	35
5.1 Spatiotemporal Variability of Catchment Water Inputs and Storage Reservoirs .	35
Inputs: Precipitation	35
Water Storage: Unsaturated Zone	37
Water Storage: Groundwater	42
Water Storage: Streamwater	44
5.2 Visual Assessment of Dual-Isotope Plots	46
Bulk Soil Water.....	46
Groundwater and Streamwater	46
Woody Plant Xylem Water	47
5.3 SISUS Modeled Feasible Water Source Contributions to Plant Xylem Water	51
CHAPTER SIX: DISCUSSION	53
6.1 The Two Water Worlds Hypothesis	53
6.2 Spatiotemporal Variability of Woody Plant Root Water Sources	55
6.3 Inter-Species Variability of Woody Plant Root Water Sources.....	57
Hillslope Shrubs.....	57
Deciduous Hillslope Trees	59

Coniferous Hillslope Trees	61
Riparian Zone Trees.....	62
CHAPTER SEVEN: CONCLUSIONS	65
REFERENCES	66
APPENDIX A.....	71
Tables.....	71
APPENDIX B.....	113
Figures.....	113
APPENDIX C.....	154
Los Gatos Liquid Water Isotope Analyzer – Correcting for Spectral Interference Caused by Organic Contaminants.....	154

LIST OF TABLES

Table 1	Dry Creek Experimental Watershed soil properties and characteristics (USDA NRCS Web Soil Survey 01-09-12). LG = Lower Gauge, TL = Treeline, BG = Bogus South. Locations are depicted in Figure 4. 72
Table 2	Dry Creek Experimental Watershed soil texture and moisture properties (adapted from Smith, 2010). θ = Volumetric Moisture Content. HN and HS are used as proxies for Bogus South. MHN and MHS are used as proxies for Treeline. LN and LS are used as proxies for Lower Gauge. Locations are depicted in Figure 4. 73
Table 3	Woody plant stem water removal efficiency. Stem samples were collected from the base of tree branches or cored from the trunk at breast height (Ponderosa pine and Douglas-fir), sliced into roughly 2 cm segments and stored in pyrex test tubes capped with parafilm. Water was removed via cryogenic vacuum distillation (West, 2006). Remaining water was calculated by re-weighing the sample after placing the evacuated sample in an oven at 110°C for 24 hours. μ = gravimetric moisture content. LG = Lower Gauge, TL = Treeline, BG = Bogus South. Locations are depicted in Figure 4. 74
Table 4	Bulk soil water cryogenic vacuum extraction efficiency. Samples were stored in test tubes and capped with parafilm. Silica wool was placed above the soil during extraction to ensure that soil was not lost to the vacuum. Remaining water was calculated by re-weighing the sample after placing the evacuated sample in an oven at 110°C for 24 hours. μ = gravimetric moisture content. LG = Lower Gauge, TL = Treeline, BG = Bogus South. Locations are depicted in Figure 4. 75
Table 5	Dry Creek Experimental Watershed precipitation $\delta^2\text{H}$ and $\delta^{18}\text{O}$ values (‰) (adapted from Tappa, 2013). BR = Bogus Ridge. LDP = Lower Deer Point, TL = Treeline, LW = Lower Weather. BG precipitation isotope values are likely between LDP and BR values (based off of the precipitation isotopic concentration relation to elevation; Tappa, 2013). LW data is used as a proxy for Lower Gauge precipitation. Locations are depicted in Figure 4. 77

Table 6	Dry Creek Experimental Watershed seasonally-weighted mean precipitation isotope values. LG = Lower Gauge, TL = Treeline, BG = Bogus South. Locations are depicted in Figure 4.	84
Table 7	Dry Creek Experimental Watershed plant and soil sample locations. NAD 83 Datum. Soils associated with a plant were sampled from within 5m of the plant trunk. LG = Lower Gauge, TL = Treeline, BG = Bogus South. Distance to Stream = the distance to Dry Creek or Treeline Stream. Distance to Tributary = the distance to the nearest tributary of Dry Creek or Treeline Stream. Locations are depicted in Figure 4.....	85
Table 8	Dry Creek Experimental Watershed bulk soil water $\delta^2\text{H}$ values (‰). Columns are organized by depth of bulk soil sample. Bulk soil water samples were taken from within 5 m of the plant individual listed in the first column. LG = Lower Gauge, TL = Treeline, BG = Bogus South. Locations are depicted in Figure 4. Soil sample coordinates are listed in Table 7.....	87
Table 9	Dry Creek Experimental Watershed soil $\delta^{18}\text{O}$ values (‰). Columns are organized by depth of bulk soil sample. Bulk soil water samples were taken from within 5 m of the plant individual listed in the first column. LG = Lower Gauge, TL = Treeline, BG = Bogus South. Locations are depicted in Figure 4. Soil sample coordinates are listed in Table 7.	90
Table 10	Spatiotemporal analysis of soil water $\delta^{18}\text{O}$ variance in Dry Creek Experimental Watershed. Field sites included Lower Gauge, Treeline and Bogus South (Figure 4). Lower gauge aspects are N-facing and S-facing, Treeline aspects are NE-facing and SW-facing and Bogus South aspects are E-facing and SW-facing. Depths of soil analyzed included 10 cm, 25 cm, 45 cm, 70 cm and 100 cm depths. Sampling dates were grouped into nearest spatial neighbor groups for each field site (e.g., BG on 07-08-2012, TL on 07-09-2012 and LG on 07-10-2012).....	93
Table 11	Dry Creek Experimental Watershed groundwater $\delta^2\text{H}$ and $\delta^{18}\text{O}$ isotope values (‰). BGS is a freshwater spring located between Bogus South and Lower Deer Point. LGW is a residential well located near Lower Gauge. BBW is a well at Bogus Basin Ski Resort. Locations are depicted in Figure 4.	94
Table 12	Dry Creek Experimental Watershed streamwater $\delta^2\text{H}$ and $\delta^{18}\text{O}$ Values. BG is located near the Dry Creek headwaters, while LG is the catchment outlet on Dry Creek. TL stream and TLTRIB are two ephemeral streams in the TL subcatchment. LGTRIB and TLTRIB are the tributaries entering Dry Creek and the Treeline stream near the respective gauging	

	stations. Samples collected prior to 2011 were handled by Pam Aishlin. Locations are depicted in Figure 4.	95
Table 13	Dry Creek Experimental Watershed woody plant xylem water $\delta^2\text{H}$ and $\delta^{18}\text{O}$ values (‰). LG = Lower Gauge, TL = Treeline, BG = Bogus South. Plant individuals ending in a letter represent multiple samples from the same branch. A = base of branch, while letters following A in the alphabet were collected from closer to the leaf surface. σ = standard deviation. Standard deviations were included because spectral interference corrections (refer to Appendix C), which create larger uncertainties in isotope values, were often needed for plant xylem water samples. Locations are depicted in Figure 4. Plant sample coordinates are listed in Table 7.	100
Table 14a	Stable Isotope Sourcing Using Sampling (SISUS) modeled median proportional source contributions to woody plant xylem water. Results represent the mean modeled proportional source contributions (% usage) of each potential water source. Bulk soil water isotope values were averaged at each sampled depth, at each field site, on each sampling date (e.g., 10 cm). The proportional source contributions are unbiased, and are derived from the differences between xylem water isotope values and source isotope values in dual-isotope ($\delta^2\text{H}$ and $\delta^{18}\text{O}$) plot space. For example, source water isotope values ($\delta^2\text{H}$ and $\delta^{18}\text{O}$) that plot near xylem water isotope values in dual-isotope space are likely to have a higher percent proportional contribution to the xylem water mixture. LG = Lower Gauge, TL = Treeline, BG = Bogus South. Locations are depicted in Figure 4. Plant sample coordinates are listed in Table 7.	104
Table 14b	Stable Isotope Sourcing Using Sampling (SISUS) modeled minimum proportional source contributions to woody plant xylem water. Results represent the mean minimum proportional source contributions (% usage) of each potential water source. Bulk soil water isotope values were averaged at each sampled depth, at each field site, on each sampling date (e.g., 10 cm). The proportional source contributions are unbiased, and are derived from the differences between xylem water isotope values and source isotope values in dual-isotope ($\delta^2\text{H}$ and $\delta^{18}\text{O}$) plot space. For example, source water isotope values ($\delta^2\text{H}$ and $\delta^{18}\text{O}$) that plot near xylem water isotope values in dual-isotope space are likely to have a higher percent proportional contribution to the xylem water mixture. LG = Lower Gauge, TL = Treeline, BG = Bogus South. Locations are depicted in Figure 4. Plant sample coordinates are listed in Table 7.	107
Table 14c	Stable Isotope Sourcing Using Sampling (SISUS) modeled maximum proportional source contributions to woody plant xylem water. Results represent the mean maximum proportional source contributions (%	

usage) of each potential water source. Bulk soil water isotope values were averaged at each sampled depth, at each field site, on each sampling date (e.g., 10 cm). The proportional source contributions are unbiased, and are derived from the differences between xylem water isotope values and source isotope values in dual-isotope ($\delta^2\text{H}$ and $\delta^{18}\text{O}$) plot space. For example, source water isotope values ($\delta^2\text{H}$ and $\delta^{18}\text{O}$) that plot near xylem water isotope values in dual-isotope space are likely to have a higher percent proportional contribution to the xylem water mixture. LG = Lower Gauge, TL = Treeline, BG = Bogus South. Locations are depicted in Figure 4. Plant sample coordinates are listed in Table 7..... 110

Table 15	LWIA Inter-run temporal variability of $m\text{BB}_{\text{standard}}$ and $m\text{NB}_{\text{standard}}$ output from the Los Gatos Research Liquid Water Isotope Analyzer, Spectral Contaminant Identifier Software. $m\text{BB}$ = broadband metric. $m\text{NB}$ = narrowband metric. n = number of samples in analysis..... 168
Table 16	One-tailed Wilcoxon rank sum test for LWIA measured $\delta^2\text{H}$ and $\delta^{18}\text{O}$ values. Measured isotope values were compared between standards where $m\text{NB} < 1$ and $m\text{NB} \geq 1$. The null hypothesis stated that these populations have the same isotope values ($h=0$). The alternate hypothesis stated that standards where $m\text{NB} > 1$ are more enriched than standards where $m\text{NB} < 1$ ($h=1$). n = number of samples in analysis. 168
Table 17	Plant xylem water and bulk soil water sample LWIA narrowband interference. n = number of samples analyzed. In total, 73.3 % of xylem water samples and 10.5% were found to contain narrowband absorber concentrations sufficient to significantly alter raw isotope value output. 169
Table 18	Intra-run LWIA $\delta^2\text{H}$ value sensitivity to narrowband absorbers. All trendlines are of the form $fx = -\ln(xa + 1)/b$ 169
Table 19	Intra-run LWIA $\delta^{18}\text{O}$ value sensitivity to narrowband absorbers. All trendlines are of the form $fx = -\ln(xa + 1)/b$ 170
Table 20	Inter-run LWIA $\delta^2\text{H}$ value sensitivity to narrowband absorbers. All trendlines are of the form $fx = -\ln(xa + 1)/b$ 170
Table 21	Intra-run LWIA $\delta^{18}\text{O}$ value sensitivity to narrowband absorbers. All trendlines are of the form $fx = -\ln(xa + 1)/b$. n = number of samples analyzed. 171
Table 22	LWIA isotope data piecewise narrowband spectral interference correction equations. All trendlines are of the form $fx = -\ln(xa + 1)/b$. $m\text{NB}$ = narrowband metric. n = number of samples analyzed. 171

Table 23	Clean water LWIA (IRIS) vs. Finnigan High Temperature Conversion Elemental Analyzer (IRMS) performance.	171
Table 24	LWIA (IRIS) vs. Finnigan High Temperature Conversion Elemental Analyzer (IRMS) plant xylem water $\delta^2\text{H}$ values (11-29-2012).....	172
Table 25	LWIA (IRIS) vs. Finnigan High Temperature Conversion Elemental Analyzer (IRMS) plant xylem water $\delta^{18}\text{O}$ values (11-29-2012).....	173

LIST OF FIGURES

Figure 1.	Dry Creek Hydrograph (Lower Gauge, 2012). Lower Gauge monitors discharge of Dry Creek at the outlet of Dry Creek Experimental Watershed. The gauge location is depicted in Figure 4.	114
Figure 2.	Treeline Stream Hydrograph (2012). Discharge only plots until late June because Treeline stream ceased to flow at this time. The gauge location is depicted in Figure 4.	115
Figure 3.	Dry Creek Hydrograph (Bogus South, 2012). Bogus South monitors discharge near the headwaters of Dry Creek. The gauge location is depicted in Figure 4.	116
Figure 4.	Dry Creek Experimental Watershed Topographic Map, including sampling sites, elevation, weather stations, stream gauges, and soil moisture monitoring stations. Refer to CHAPTER THREE: STUDY AREA or http://earth.boisestate.edu/drycreek/ for site descriptions.	117
Figure 5.	Dry Creek Experimental Watershed Slope Distribution, including sampling sites, elevation, weather stations, stream gauges, and soil moisture monitoring stations. Refer to CHAPTER THREE: STUDY AREA or http://earth.boisestate.edu/drycreek/ for site descriptions.	118
Figure 6.	Dry Creek Experimental Watershed Aspect Distribution, including sampling sites, elevation, weather stations, stream gauges, and soil moisture monitoring stations. Refer to CHAPTER THREE: STUDY AREA or http://earth.boisestate.edu/drycreek/ for site descriptions.	119
Figure 7.	Dry Creek Experimental Watershed flow accumulation, including sampling sites, elevation, weather stations, stream gauges, and soil moisture monitoring stations. Refer to CHAPTER THREE: STUDY AREA or http://earth.boisestate.edu/drycreek/ for site descriptions.	120
Figure 8.	Dry Creek Experimental Watershed spatiotemporal variation of precipitation and snow depth (2012). BR = Bogus Ridge, LDP = Lower Deer Point, TL = Treeline, LW = Lower Weather. Elevations: BR = 2114 m, LDP = 1850 m, TL = 1610 m, LW = 1151 m. Locations are depicted in Figure 4.	121

Figure 9.	Dry Creek Experimental Watershed spatiotemporal variation of temperature (2012). BR = Bogus Ridge, LDP = Lower Deer Point, TL = Treeline, LW = Lower Weather. Elevations: BR = 2114 m, LDP = 1850 m, TL = 1610 m, LW = 1151 m. Locations are depicted in Figure 4.	122
Figure 10.	Dry Creek Experimental Watershed spatiotemporal variation of solar radiation (2012). BR = Bogus Ridge, LDP = Lower Deer Point, TL = Treeline, LW = Lower Weather. Elevations: BR = 2114 m, LDP = 1850 m, TL = 1610 m, LW = 1151 m. Locations are depicted in Figure 4.	123
Figure 11.	Dry Creek Experimental Watershed spatiotemporal variation of relative humidity (2012). BR = Bogus Ridge, LDP = Lower Deer Point, TL = Treeline, LW = Lower Weather. Elevations: BR = 2114 m, LDP = 1850 m, TL = 1610 m, LW = 1151 m.....	124
Figure 12.	Dry Creek Experimental Watershed spatiotemporal variation in volumetric soil moisture content (2012). Field capacity and wilting point estimates from Smith (2010). HN is used as a proxy for BG soil moisture, field capacity and wilting point. MHN is used as a proxy for TL field capacity and wilting point. (a) LN, (b) Treeline, (c) HN. LN is used as a proxy for Lower Gauge soils and HN is used as a proxy for Bogus Gauge soils, though it is expected that BG soils generally contain more moisture than HN soils. Locations are depicted in Figure 4.....	125
Figure 13.	Total soil extracted water (grams) is plotted against vacuum evacuated soil water (%). Total extracted water is the sum of vacuum evacuated water and oven extracted water. Water was vacuum extracted from soils using cryogenic vacuum distillation (West et al., 2006 method) for 40 minutes. Remaining water was extracted via evaporation by placing samples in an oven at 100 °C for 24 hours. The percent vacuum evacuated water is calculated by vacuum evacuated water (g) / vacuum evacuated water (g) + 24 hour oven evaporated water (g).....	126
Figure 14.	Example water sample spectral absorption behavior (LGR LWIA run, 02-26-2012). The Los Gatos Research Liquid Water Isotope Analyzer uses the spectral absorbance features of water isotopologues as a proxy to calculate the concentrations of hydrogen and oxygen isotopes in each water sample.	127
Figure 15.	Example water sample spectral transmission behavior (LGR-LWIA run, 02-26-2012). The Los Gatos Research Liquid Water Isotope Analyzer uses the spectral absorbance features of water isotopologues as a proxy to calculate the concentrations of hydrogen and oxygen isotopes in each water sample. The Los Gatos Research Liquid Water Isotope Analyzer	

	uses the spectral absorbance features of water isotopologues as a proxy to calculate the concentrations of hydrogen and oxygen isotopes in each water sample.	127
Figure 16.	SISUS Modeling Output Example: Feasible water source contributions to the plant xylem water mixture. This model uses the Markov Chain Monte Carlo method to calculate unbiased proportional contribution estimates of each source (e.g., groundwater) to the mixture (woody plant xylem water). The x-axis labels percentage usage of each potential water source, while the y-axis labels the water source.	128
Figure 17.	Dry Creek Experimental Watershed Seasonally-Weighted LMWL. Precipitation data collected at Lower Weather, Treeline and Lower Deer Point field sites from 2009 to 2012. Refer to Tappa (2013) for data collection and weighting-method information. Locations are depicted in Figure 4.	129
Figure 18.	Lower Gauge Field Site Seasonally-Weighted LMWL. Precipitation data collected at Lower Weather from 2009 to 2012. Refer to Tappa (2013) for data collection and weighting-method information. This location is depicted in Figure 4.	130
Figure 19.	Treeline Field Site Seasonally-Weighted LMWL. Precipitation data collected at Treeline from 2009 to 2012. Refer to Tappa (2013) for data collection and weighting-method information. This location is depicted in Figure 4.	131
Figure 20.	Lower Deer Point Field Site Seasonally-Weighted LMWL. Precipitation data collected at Lower Deer Point 2009 to 2012. Refer to Tappa (2013) for data collection and weighting-method information. This LMWL was used as a proxy for a LMWL at Bogus South. This location is depicted in Figure 4.	132
Figure 21.	Dry Creek Experimental Watershed $\delta^2\text{H}$ and $\delta^{18}\text{O}$ isotope values (2012). Plotted values include water removed from trees, shrubs, streams, groundwater, and bulk soil water collected from 10 cm and 70 cm depths. Plant and soil samples collected from 03/27/2012 to 09/13/2012 are shown, while steamwater and groundwater samples were collected from 11/27/2011 to 10/9/2012. The Global Meteoric Water Line (Equation 4) and Dry Creek Experimental Watershed Seasonally-Weighted Local Meteoric Water Line (Equation 6) provide reference points for evaporative isotopic fractionation. The LMWL was derived from precipitation collected at Lower Gauge, Treeline and Lower Deer Point from 2009 to 2012 (see Tappa, 2013 for data and LMWL weighting method). Locations are depicted in Figure 4.	133

- Figure 22. Lower Gauge (location depicted in Figure 4) $\delta^2\text{H}$ and $\delta^{18}\text{O}$ isotope values (2012). Samples shown include trees, shrubs, streams, groundwater, and soil water at 10 cm, 25 cm, 45 cm and 70 cm depths. Woody plants sampled from the Lower Gauge field site include Chokecherry, Hackberry, Rabbitbrush, Sagebrush, Water birch and Yellow willow. Groundwater was sampled on 03-23-2012 from a residential well near Lower Gauge (Table 8). Streamwater was sampled during each field site visit. The Global Meteoric Water Line (Equation 4) and Seasonally-Weighted Local Meteoric Water Line (Equation 7) from precipitation collected at Lower Gauge from 2009 to 2012 provide reference points for evaporative isotopic fractionation (see Tappa, 2013 for data and LMWL weighting method). (a) 04-08-2012, (b) 06-04-2012, (c) 07-10-2012, (d) 09-13-2012..... 134
- Figure 23. Treeline (location depicted in Figure 4) $\delta^2\text{H}$ and $\delta^{18}\text{O}$ isotope values (2012). Samples shown include trees, shrubs, streams, groundwater, and soil water at 10 cm, 25 cm, 45 cm, 70 cm and 100 cm depths. Woody plants sampled from Treeline field site include Chokecherry, Sagebrush, Yellow willow, Fire willow and Ponderosa pine. Groundwater was sampled during each field site visit from a freshwater spring between Lower Deer Point and Bogus Gauge (Table 8). The Global Meteoric Water Line (Equation 4) and Seasonally-Weighted Local Meteoric Water Line (Equation 8) from precipitation collected at Treeline from 2009 to 2012 provide reference points for evaporative isotopic fractionation. (a) 03-27-2012, (b) 05-17-2012, (c) 07-09-2012, (d) 09-07-2012. 135
- Figure 24. Bogus South (location depicted in Figure 4) $\delta^2\text{H}$ and $\delta^{18}\text{O}$ isotope values (2012). Samples shown include trees, shrubs, streams, groundwater, and soil water at 10 cm, 25 cm, 45 cm, 70 cm and 100 cm depths. Woody plants sampled from Treeline field site include Chokecherry, Sagebrush, Yellow willow, Fire willow and Ponderosa pine. Groundwater was sampled during each field site visit from a freshwater spring between Lower Deer Point and Bogus Gauge (Table 8). The Global Meteoric Water Line (Equation 4) and Seasonally-Weighted Local Meteoric Water Line (Equation 7) from precipitation collected at Bogus South from 2009 to 2012 provide reference points for evaporative isotopic fractionation. Note that the axes were shrunk and some evaporatively-enriched soil water isotope values plotted outside of the axis limits. This was done in an effort to zoom in on the plants because Bogus South plants and bulk soil water lie closer to streamwater and groundwater values than other field sites. (a) 06-06-2012, (b) 07-08-2012, (c) 09-04-2012. 136
- Figure 25. Lower Gauge soil pit $\delta^{18}\text{O}$ values. Each line represents a linear interpolation between $\delta^{18}\text{O}$ value data points from bulk soil water

	collected at 10 cm, 25 cm, 45 cm and 70 cm depths. Note that the legend denotes soil pits dug on each sampling date, within 5 meters of a specific plant individual (Table 7). This location is depicted in Figure 4. (a) 04-08-2012, (b) 06-04-2012, (c) 07-10-2012, (d) 09-13-2012	137
Figure 26.	Treeline soil pit $\delta^{18}\text{O}$ values. Each line represents a linear interpolation between $\delta^{18}\text{O}$ value data points from bulk soil water collected at 10 cm, 25 cm, 45 cm and 70 cm depths. Note that the legend denotes soil pits dug on each sampling date, within 5 meters of a specific plant individual (Table 7). This location is depicted in Figure 4. (a) 10-14-2011, (b) 03-27-2012, (c) 05-17-2012, (d) 07-09-2012, (e) 09-07-2012.....	138
Figure 27.	HN (a field site proxy for Bogus South) soil pit $\delta^{18}\text{O}$ values. Each line represents a linear interpolation between $\delta^{18}\text{O}$ value data points from bulk soil water collected at 10 cm, 25 cm, 45 cm and 70 cm depths. Note that the legend denotes soil pits dug on each sampling date, within 5 meters of a specific plant individual (Table 7). This location is depicted in Figure 4. (a) 06-06-2012, (b) 07-08-2012, (c) 09-04-2012	139
Figure 28.	Temporal variability of Dry Creek Experimental Watershed groundwater and stream water $\delta^{18}\text{O}$ values (2012). High elevation groundwater was acquired from a freshwater spring between Lower Deer Point and Bogus South (BGS) and a well near Bogus Basin (BBW), while low elevation groundwater (LGW) was acquired from a residential well near Lower Gauge. Note that groundwater from LGW was only collected once. LG = Lower Gauge. TL = Treeline. BG = Bogus South. Locations are depicted in Figure 4.	140
Figure 29.	Temporal variability of Dry Creek Experimental Watershed streamwater and groundwater (outliers removed) along the LMWL (2012). Groundwater (BGS/BBW) was acquired from a freshwater spring between BG and a well near Bogus Basin, while Groundwater (LGW) was acquired from a residential well near LG. Locations are depicted in Figure 4.	141
Figure 30.	SISUS modeled Isotopic Mixing Convex Hull output for Treeline samples collected on 03-27-2012. This location is depicted in Figure 4.	142
Figure 31.	SISUS modeled Isotopic Mixing Convex Hull output for Treeline samples collected on 05-17-2012. This location is depicted in Figure 4.	143

Figure 32.	SISUS modeled Isotopic Mixing Convex Hull output for Treeline samples collected on 09-07-2012. This location is depicted in Figure 4.	144
Figure 33.	Lower Gauge (07-10-2012) SISUS modeled woody plant individual mean feasible contributions (y-axis) of water sources (x-axis) for each successfully modeled woody plant (Table 14). The bar represents the median, while the errorbars represent the minimum and maximum modeled source contributions to the plant individual. This location is depicted in Figure 4.	145
Figure 34.	Lower Gauge (09-13-2012) SISUS modeled woody plant individual mean feasible contributions (y-axis) of water sources (x-axis) for each successfully modeled woody plant (Table 14). The bar represents the median, while the errorbars represent the minimum and maximum modeled source contributions to the plant individual. This location is depicted in Figure 4.	146
Figure 35.	Treeline (07-09-2012) SISUS modeled woody plant individual mean feasible contributions (y-axis) of water sources (x-axis) for each successfully modeled woody plant (Table 14). The bar represents the median, while the errorbars represent the minimum and maximum modeled source contributions to the plant individual. This location is depicted in Figure 4.	147
Figure 36.	Treeline (09-07-2012) SISUS modeled woody plant individual mean feasible contributions (y-axis) of water sources (x-axis) for each successfully modeled woody plant (Table 14). The bar represents the median, while the errorbars represent the minimum and maximum modeled source contributions to the plant individual. This location is depicted in Figure 4.	148
Figure 37.	Bogus South (06-06-2012) SISUS modeled woody plant individual mean feasible contributions (y-axis) of water sources (x-axis) for each successfully modeled woody plant (Table 14). The bar represents the median, while the errorbars represent the minimum and maximum modeled source contributions to the plant individual. This location is depicted in Figure 4.	149
Figure 38.	Bogus South (07-08-2012) SISUS modeled woody plant individual mean feasible contributions (y-axis) of water sources (x-axis) for each successfully modeled woody plant (Table 14). The bar represents the median, while the errorbars represent the minimum and maximum modeled source contributions to the plant individual. This location is depicted in Figure 4.	150

Figure 39.	Bogus South (09-04-2012) SISUS modeled woody plant individual mean feasible contributions (y-axis) of water sources (x-axis) for each successfully modeled woody plant (Table 14). The bar represents the median, while the errorbars represent the minimum and maximum modeled source contributions to the plant individual. This location is depicted in Figure 4.	151
Figure 40.	SISUS modeled mean field site scale proportional contributions of source water to woody plant xylem water. The bars of the graph represent the average of the median feasible source contributions for each plant individual modeled at each field site, collected on each sampling date. Locations are depicted in Figure 4.	152
Figure 41.	SISUS modeled mean field site scale proportional contributions of source water to woody plant xylem water. The bars of the graph represent the average of the median feasible source contributions for each plant individual modeled at each field site, collected on each sampling date. Locations are depicted in Figure 4.	153
Figure 42.	LWIA measured standards values vs. actual known isotope values (09-25-2012)	174
Figure 43.	LWIA Isotopic Analysis Standard Group Example (08-02-2012)	175
Figure 44.	LWIA intra-run $mNB_{standard}$ temporal variability (run on 09-25-2012) ..	176
Figure 45.	LWIA inter-run δ^2H sensitivity to narrowband absorbers. All trendlines are of the form $fx = -\ln(xa + 1)/b$. Note that 95% represents confidence bounds on the All data fit.	177
Figure 46.	LWIA $\delta^{18}O$ sensitivity to narrowband absorbers. All trendlines are of the form $fx = -\ln(xa + 1)/b$. Note that 95% represents confidence bounds on the All data fit.	178
Figure 47.	LWIA δ^2H residuals plots for the all data function (top) and the function generated using on $mNB < 10$ (bottom).	179
Figure 48.	LWIA $\delta^{18}O$ residuals plots for the all data function (top) and the function generated using only $mNB < 10$ data (bottom).	180
Figure 49.	LWIA fitted δ^2H isotope value correction functions. All trendlines are of the form $fx = -\ln(xa + 1)/b$	181
Figure 50.	Fitted $\delta^{18}O$ isotope value correction function. All trendlines are of the form $fx = -\ln(xa + 1)/b$	182

Figure 51.	LWIA vs. FINNIGAN TC/EA IRMS $\delta^2\text{H}$ values.....	183
Figure 52.	LGR LWIA vs. FINNIGAN TC/EA IRMS $\delta^{18}\text{O}$ values	184

LIST OF ABBREVIATIONS

DCEW	Dry Creek Experimental Watershed
GMWL	Global Meteoric Water Line
LMWL	Local Meteoric Water Line
IRMS	Isotope Ratio Mass Spectrometer (or Spectrometry)
IRIS	Isotope Ratio Infrared Spectrometer (or Spectrometry)
LGR	Los Gatos Research
LWIA	Liquid Water Isotope Analyzer
LWIA-PAS	Liquid Water Isotope Analyzer Post Analysis Software
LWIA-SCI	Liquid Water Isotope Analyzer Spectral Contaminant Identifier
LG	Lower Gauge Field Site
TL	Treeline Field Site
BG	Bogus South Field Site
LDP	Lower Deer Point Field Site
HN	High North-Facing Field Site
LGW	Lower Gauge Well
BGS	Bogus Gauge Spring
BBW	Bogus Basin Well
mNB	Narrowband metric
mBB	Broadband metric

CHAPTER ONE: INTRODUCTION

The capacity of hillslope soils to store and transmit water determines, in part, how precipitation is partitioned into streamflow, groundwater recharge, and evapotranspiration in upland catchments. Vegetation strongly influences hydrologic partitioning by accessing and transpiring stored soil water. Until recently, it had been thought that trees transpired primarily mobile soil water that would otherwise flow to streams or recharge groundwater (Renée Brooks, Barnard, Coulombe, & McDonnell, 2010). Recent work, however, suggests that trees tend to use water that is tightly-bound to soil particles, called immobile water, while streams and groundwater receive water flowing under the influence of gravity, called mobile water (Cody Hale, 2011; Goldsmith et al., 2012; Renée Brooks et al., 2010). McDonnell (2014) posed the “two water worlds hypothesis” to place this phenomenon in a testable framework. The two water worlds hypothesis simply states that vegetation and streams return different pools of water to the hydrosphere. This behavior has important implications for understanding a wide range of catchment hydrological processes, and our abilities to accurately model those processes, including the spatial and temporal variability of evapotranspiration and nutrient cycling. Yet, the two water world hypothesis has only been evaluated in a few studies, most of which were conducted in forested catchments in humid, energy-limited environments (e.g., Cody Hale, 2011; Goldsmith et al., 2012; Renée Brooks et al., 2010; Penna et al., 2013).

Catchments in the seasonally-dry, semi-arid climate of the intermountain western U.S. process water inputs differently than their seasonally-dry humid climate counterparts. The seasonally-dry nature of these two climates is consistent, as wet winters produce high water inputs without the demands of evapotranspiration, and dry summers extract water from soil via evapotranspiration. However, in more humid catchments, soil moisture usually remains above the permanent wilting point (Renée Brooks et al., 2010) and plant growth is generally energy limited. In contrast, extensive evapotranspiration in semi-arid climate catchments often reduces soil moisture to levels significantly below the permanent wilting point. As a result, plant growth is generally water limited. Additionally, mountainous terrains with steep elevation gradients and aspect variability impose systematic variability on air temperature, precipitation magnitude and phase, vegetation, and soils. This variability is greater in semi-arid catchments than humid catchments due to increased aridity. The purpose of this study is to investigate the presence or absence of two water worlds within the high spatial and temporal variability of environmental conditions characteristic of semi-arid mountain catchments.

Mobile and immobile water are end-members in a continuum of the potential for soil water to flow by gravity and pressure, as opposed to cling to soils via tension. Mobile soil water generally exhibits a pressure head greater than -0.05 m and can be extracted using suction lysimeters (Torres, Dietrich, Montgomery, Anderson, & Loague, 1998). Immobile water is soil water that is held at tension greater than gravitational forces, thus remaining relatively stagnant in the soil. Some mixing of these two water pools does occur at the pore scale (Torres et al., 1998), however, their residence times generally differ enough that their waters acquire unique chemical and isotopic compositions (Renée

Brooks et al., 2010). Recently, researchers have learned to use the stable isotopes of water to differentiate these water pools.

The natural abundances of stable isotopes of water have emerged as valuable tools for tracing plant root water sources over the past several decades (Clark and Fritz, 1997). Water molecules contain stable isotopes of hydrogen (^1H , ^2H) and oxygen (^{16}O , ^{17}O , ^{18}O) and natural isotopic fractionation processes cause the concentrations of these isotopes to vary within the environment. However, once water migrates beneath approximately 10 cm depth in the soil column, hydrogen and oxygen isotopes do not fractionate unless exposed to geothermal systems (Barnes & Allison, 1988; Wythers, Lauenroth, & Paruelo, 1999). Additionally, plant roots generally do not fractionate isotopic concentrations (White, Cook, Lawrence, Broecker, 1985). The conservative nature and natural spatiotemporal variability of the stable isotopes of water thus makes them ideal tracers of plant root water uptake processes.

Since the discovery that plant roots do not fractionate isotopic concentrations, many have used stable isotopes of water as tracers to characterize plant water sources (Brunel, Walker, Dighton, & Monteny, 1997; Flanagan, Ehleringer, & Marshall, 1992; Flanagan & Ehleringer, 1991). However, until recently most of these studies used a single-isotope approach where only $^2\text{H}/^1\text{H}$ or $^{18}\text{O}/^{16}\text{O}$ isotope ratios were analyzed (McDonnell, 2014). This approach has often been used to identify the depth of root water uptake. However, recent findings that plants may be selectively transpiring tightly-bound immobile water causes us to question the validity of findings gleaned from the single-isotope approach. Additionally, it is difficult to use this approach to differentiate mobile and immobile water pools. In contrast, use of both hydrogen and oxygen isotope

concentrations allows for comparison of samples to the meteoric water line, a crucial reference point for evaporative isotopic enrichment and water pool differentiation (McDonnell, 2014).

The dual-isotope approach has increased in popularity since its potential to characterize hydrological pools has been realized. Since then, three dual-isotope approach studies have been conducted in humid, Mediterranean climate catchments. Renée Brooks et al. (2010) studied *Pseudotsuga menziesii* in H.J. Andrews Experimental Watershed (Oregon Cascade Range), Cody Hale (2011) studied *Pseudotsuga menziesii* and *Alnus rubra* in the Alsea River Watershed (Central Oregon Coastal Range), and Goldsmith et al. (2012) studied *Q. lanceifolia*, *Q. ocoteifolia*, *A. latifolia*, *Clethra mexicana*, *A. jorullensis*, *A. latifolia*, *C. mexicana*, and *M. glaberrima* in two tropical montane cloud forest watersheds near Veracruz, Mexico. Isotopic analyses at each field site suggested that trees transpire water from a tightly-bound, immobile water pool (Cody Hale, 2011; Goldsmith et al., 2012; Renée Brooks et al., 2010). These findings were consistent in all 3 of these studies, regardless of tree species, season, or soil moisture availability.

The suggestion that humid catchments exhibit two, hydrologically-distinct water worlds has important implications for understanding a wide range of catchment hydrological processes. It is therefore crucial that this hypothesis is investigated in other ecohydrological settings. This study examines the two water worlds hypothesis in a seasonally-dry, semi-arid watershed. Our hypothesis is that semi-arid ecosystem woody plants use immobile soil water that is hydrologically disconnected from streams and groundwater. We used Dry Creek Experimental Watershed (DCEW) as a field laboratory to test this hypothesis and explore the following research questions in a seasonally-dry,

semi-arid catchment: Do two water worlds exist across a semi-arid climatic gradient throughout the growing season? How extensive is woody plant water source spatiotemporal variability? How does water use behavior vary between plant species and populations?

To address these questions, we periodically sampled woody plant stems, soil water, groundwater and streamwater at several locations in DCEW during the 2012 growing season (and preliminary samples from the 2011 growing season). Following sample collection, cryogenic vacuum distillation was employed to extract water from plant stems and soil samples. Next we used an Isotope Ratio Infrared Spectrometer, the Los Gatos Liquid Water Isotope Analyzer, to conduct isotopic analyses on our water samples. Additional post-processing was needed to correct isotope values for spectral interference caused by organic contaminants in plant xylem water and soil water samples. We used the corrected stable isotope values to apply the dual-isotope approach, and compare sample isotopic concentrations to local meteoric water lines, in an effort to differentiate hydrological pools and characterize the most prevalent woody plant water sources. Lastly, we used the SISUS mixing model (Erhardt, Wolf, Ben-David, & Bedrick, 2014) to quantitatively evaluate our dual-isotope visual analyses and identify feasible water source contributions to plant xylem water.

CHAPTER TWO: SCIENTIFIC BACKGROUND

2.1 Soil Water Mobility, Field Capacity, and Permanent Wilting Point

Material properties largely govern the ability of soil to retain water against the forces of gravity and plant root water uptake (e.g., transpiration). Most hydrological research describes these material properties as thresholds at which gravity drainage and plant root water uptake cease to occur. These thresholds are commonly defined as specific moisture contents. The moisture content at which gravity drainage ceases has been termed “field capacity” (Veihmeyer and Hendrickson, 1949), and the moisture content at which transpiration ceases has been termed “permanent wilting point” (Briggs and Shantz, 1912). However, the pervasive use of specific moisture content constants to define these thresholds has been widely criticized. Field capacity has been scrutinized because the end point for gravity drainage is largely ambiguous, due to dependence upon boundary conditions and scale (Twarakavi, Sakai, & Šimůnek, 2009). Wilting point has been criticized because the actual wilting point is dependent upon the plant individual, and varies largely between plant species. Additionally, perennial plants adapted to arid environments can sometimes virtually cease transpiring with no evidence of wilting.

Nevertheless, field capacity and permanent wilting point have seen continued use in hydrological and biological literature because they are generally consistent with observed soil water dynamics and plant behavior. For example, there tends to be a moisture content at which the forces of soil water tension exceed the forces of gravity, and gravity drainage is greatly reduced. This moisture content tends to align with the

highest tension water that suction lysimeters can extract from the soil, where water pressure head is less than -0.05 m. Additionally, there is a lesser soil moisture content, below which, most plants can no longer extract water.

In this study, we use the terms field capacity and permanent wilting point to distinguish the two water worlds and discuss ecohydrological processes. For example, we assume that changes in soil moisture storage after soils have drained to field capacity are caused by evapotranspiration alone. Additionally, we assume that woody plants transpiring water from soil when the moisture content is below the permanent wilting point must possess unique adaptations to extract water from exceedingly dry soils.

2.2 Water Isotopes in the Natural Environment

The isotopic composition ($^2\text{H}/^1\text{H}$ and $^{18}\text{O}/^{16}\text{O}$ ratios) of water varies naturally by equilibrium and kinetic fractionation processes, governed by mass differences and caused by changes in phase. Equilibrium fractionation occurs at chemical equilibrium (relative humidity $\approx 100\%$), whereas kinetic fractionation occurs out of chemical equilibrium (relative humidity $< 100\%$). The isotopic composition of precipitation is primarily governed by kinetic fractionation factors during initial evaporation, the meteoric history of the precipitating air mass and equilibrium fractionation factors during condensation (Kendall and McDonnell, 1998). Following condensation, water is again exposed to evaporative kinetic fractionation factors.

Water vapor condensation generally occurs at or near chemical equilibrium and is therefore described as an equilibrium fractionation process. The isotopic composition of precipitation is largely governed by the rainout process where heavier water isotopes (e.g., ^{18}O and ^2H) become enriched in the liquid and solid phases, while lighter water

isotopes (e.g., ^{16}O and ^1H) become enriched in the gas phase. In an ideal, isolated parcel of air, equilibrium fractionation (and the rainout process) can be described as a Rayleigh process such that:

EQUATION 1

$$R_v = R_0 f^{(\alpha-1)}$$

where R_v is the isotopic ratio ($^{18}\text{O}/^{16}\text{O}$ or $^2\text{H}/^1\text{H}$) of residual atmospheric vapor at a point in time, R_0 is the initial isotope ratio of the vapor, f is the fraction of vapor remaining, and α is the fractionation factor between condensation and vapor (Bowen, 2010).

The magnitude of α is controlled by the temperature of the precipitating air mass and phase of the condensate (Bowen, 2010). Lower temperatures and larger phase transitions (e.g., gas to solid) promote larger differences between the zero point energies of vapor and condensate, and therefore greater isotopic fractionation factors for both hydrogen and oxygen (Kendall and McDonnell, 1998). The magnitude of f is governed by the saturation vapor pressure, which is driven by temperature and pressure (Bowen, 2010). Variable α and f values lead to increased heavy isotope depletion with increasing latitude, altitude, distance inland, and precipitation amount (Dansgaard, 1964).

Differences between hydrogen and oxygen isotope equilibrium fractionation factors cause hydrogen isotopes to fractionate more readily than oxygen isotopes during condensation. In fact, the $^2\text{H}/^1\text{H}$ equilibrium fractionation factor is 8 times greater than that of $^{18}\text{O}/^{16}\text{O}$ due to the relative atomic mass differences of these isotopes. For instance, ^2H is 100% heavier than that of ^1H , while the ^{18}O is 12.5% heavier than ^{16}O , making the relative mass difference 8 times larger for $^2\text{H}/^1\text{H}$ than $^{18}\text{O}/^{16}\text{O}$. This causes the slope of the meteoric water line ($\delta^{18}\text{O}$ vs. $\delta^2\text{H}$) to be 8.

Unfortunately, predicting real world precipitation isotopic concentrations is more complex than the Rayleigh equation for three reasons. First, the isolated parcel of air assumption of the Rayleigh equation is violated in the real world due to atmospheric mixing (Cappa, Hendricks, DePaolo, & Cohen, 2003). Second, R_0 does not truly exist because there is a continuous replenishment of water vapor to the atmosphere via evapotranspiration (Ingraham & Taylor, 1991). Third, real world precipitation interacts with atmospheric vapor and experiences partial evaporation after initial condensation (Lee, Fung, Depaolo, & Henning, 2007). Despite these shortcomings, the Rayleigh equation describes the basic processes governing isotopic fractionation during water condensation.

Evaporation is thus commonly described as a kinetic fractionation process. During evaporation, the heavier water isotopes (e.g., ^{18}O and ^2H) become enriched in the liquid phase, while the lighter water isotopes (e.g., ^{16}O and ^1H) are more likely to remain in the vapor phase (Kendall & McDonnell, 1998). Kinetic fractionation factors of hydrogen and oxygen are dependent upon humidity, salinity and temperature (Clark and Fritz, 1997). Humidity has the greatest effect because more arid conditions cause an air parcel to be farther out of equilibrium, causing a greater kinetic fractionation factor (Clark and Fritz, 1997). The effect of humidity on evaporative kinetic fractionation of hydrogen and oxygen isotopes is defined as the following (Clark and Fritz, 1997):

EQUATION 2

$$10^3 \ln \alpha^{18}\text{O}_{l-v} = 14.2(1 - h)\text{‰} \quad (\text{a})$$

$$10^3 \ln \alpha^{2}\text{H}_{l-v} = 12.5(1 - h)\text{‰} \quad (\text{b})$$

where l is liquid, v is vapor, h is relative humidity and α is the equilibrium fractionation factor between condensation and vapor.

Given that the relative humidity in Dry Creek Experimental Watershed usually ranges between 20% and 50% during the growing season, the slope of the evaporation line is usually between 4 and 5. This causes water pools experiencing evaporation to exhibit isotope signals that fall to the right of the meteoric water line (slope of 8). The dual-isotope approach, with the context of meteoric water lines and evaporation water lines provides useful tools for identifying varying degrees of equilibrium and kinetic isotopic fractionation within a catchment, thereby differentiating water pools that have undergone unique fractionation processes.

2.3 Meteoric Water Lines and Evaporation Water Lines

The meteoric water line is a linear trendline that describes the relationship between $^{18}\text{O}/^{16}\text{O}$ and $^2\text{H}/^1\text{H}$ isotope ratios in precipitation. The isotopic ratios of hydrogen and oxygen are reported in delta (δ) notation which is an expression of a per mille deviation from Vienna Standard Mean Ocean Water (VSMOW) and defined as:

EQUATION 3

$$\delta \text{‰} = (R_{\text{sample}}/R_{\text{VSMOW}} - 1) * 1000$$

where $R = ^{18}\text{O}/^{16}\text{O}$ or $^2\text{H}/^1\text{H}$ isotope ratio. Note that the $\delta^2\text{H}$ and $\delta^{18}\text{O}$ values of VSMOW are equal to zero.

The global meteoric water line (GMWL) describes the global relationship between precipitation $\delta^{18}\text{O}$ and $\delta^2\text{H}$ values (Craig, 1961) and is expressed as:

EQUATION 4

$$\delta^2\text{H} \text{‰} = 8 * \delta^{18}\text{O} + 10 \text{‰}$$

The slope of 8 is the result of the hydrogen equilibrium fractionation factor being 8 times greater than that of oxygen. The y-intercept of 10 ‰ is caused by the average kinetic evaporative fractionation associated with evaporation from the ocean surface (Dansgaard, 1964). Precipitation isotope values plot at various locations along the GMWL due to the varying equilibrium fractionation factors present during condensation (Tappa, 2013). When precipitation plots above or below the GMWL it indicates that kinetic fractionation caused by evaporation was greater than or less than the global mean evaporative kinetic fractionation, respectively. This can be caused by unusually arid or humid conditions during initial evaporation or significant contributions of secondary evaporation to the precipitating air parcel. In locations where local meteoric conditions differ significantly from the global average, the creation of a local meteoric water line (LMWL) can be a useful exercise. LMWL may have slightly different slopes and y-intercepts than the GMWL and knowledge of this may improve isotopic analyses.

As soon as water vapor condenses into a liquid or solid, it is again subject to kinetic evaporative enrichment. Kinetic fractionation factors have a proportionately larger effect on oxygen isotope ratios than hydrogen isotope ratios (Equations 2a and 2b). This causes evaporatively-enriched soil water to plot below the local meteoric water line. As a result, the evaporation water line plots at slopes less than the meteoric water line, commonly between 4 and 7 (Kendall & McDonnell, 1998). The slope of the line decreases with increased aridity. Characterizing the local evaporation water line can help us to correlate kinetically-fractionated isotopic concentrations with initial precipitation isotopic concentrations and improve our understanding of vadose zone water flow mechanisms.

2.4 Isotopic Evidence for Two Water Worlds in Seasonally-Dry, Humid Catchments

The relationships between oxygen and hydrogen isotopes in water described in Section 2.3 have been used to investigate the two water worlds hypothesis (Cody Hale, 2011; Goldsmith et al., 2012; McDonnell, 2014; Renée Brooks et al., 2010). In each of the seasonally-dry humid catchment studies, groundwater, streamwater and mobile soil water (extracted via suction lysimeter) plotted on or near the local meteoric water line, while bulk soil water and tree xylem water (extracted via cryogenic vacuum distillation) plotted below the LMWL. Bulk soil water contains both mobile (when available) and immobile soil water. Consequently, it is assumed that the immobile soil water fraction of bulk soil water is the portion with isotope values that plot significantly beneath the LMWL. Given that plant root water uptake does not fractionate hydrogen or oxygen isotopes, these studies assume that the tree xylem water isotopic signal is the integrated isotopic concentration of root water sources. Therefore, they suggest that these trees must be using immobile soil water rather than mobile soil water, groundwater or streamwater as their primary water sources (Cody Hale, 2011; Goldsmith et al., 2012; Renée Brooks et al., 2010).

The primary reason bulk soil water containing a significant proportion of immobile soil water plots below the meteoric water line is kinetic evaporative fractionation or mixing with evaporatively-enriched water. The slope of the meteoric water line is 8, while the slope of the evaporation line is commonly between 4 and 7, depending upon atmospheric conditions. In contrast, mobile soil water, groundwater and streamwater plot on or near the LWML, similar to precipitation. This isotopic signal persists through all forms of mobile water for three reasons. First, the more mobile the

water, the shorter its residence time on the soil surface and within the shallow soil column where it is exposed to evaporative forcings. Second, there is a progressive dampening of the kinetic evaporative enrichment signal with increased soil depth, regardless of water content, because the proportion of the infiltration pathway that occurs within the evaporatively-enriched shallow soil column decreases with depth. Third, mixing of mobile and immobile water in the soil column may be limited by the abundance of macropore flow, as up to 80% of the water that reaches the stream or groundwater reservoir flows through macropores (Beven & Germann, 1982). Macropore flow, or preferential flow, decreases the length of the flowpath of infiltrating water and increases the rate of flow, making it less likely that an infiltrating water particle would mix with immobile soil water.

Our understanding of soil physical properties and the isotopic concentrations of soil water in these preliminary studies elucidate potential causes for areas of widely varying hydraulic conductivity in the vadose zone. Nevertheless, the use of immobile water by trees in humid catchments is counter-intuitive for a number of reasons. First, many previously assumed that translatory flow occurred during the rainy season in humid climates (Hewlett & Hibbert, 1967; Horton & Hawkins, 1965; Renée Brooks et al., 2010). However, isotope analyses at H.J. Andrews Experimental Watershed suggested that some tightly-bound water persisted in small pores through the rainy season and was removed only by evapotranspiration (Renée Brooks et al., 2010; Hale 2011). Second, tree roots are expected to take up water from the water source that requires the least amount of energy to obtain (McDonnell, 2014). Third, transpiration from trees is often described as the primary source of the diel signal (Figure 1; Figure 2; Figure 3) in streamflow

(Graham, Barnard, Kavanagh, & McNamara, 2012). If none of the trees are transpiring water from mobile water sources, then what is the source of the diel signal?

The concept of translatory flow is that precipitation infiltrates the soil column and displaces antecedent soil moisture, pushing it deeper into the soil and ultimately into the stream or groundwater reservoir (Hewlett & Hibbert, 1967; Horton & Hawkins, 1965). This type of subsurface flow is generally expected to occur in humid catchments because the rate of rainfall often exceeds the rate of infiltration, suggesting that the shallow soil column should become saturated, and cause a soil moisture pulse to migrate through the soil column. Hypothetically, if translatory flow occurred throughout the vadose zone of a watershed, all plants would extract mobile, stream-bound or groundwater recharge bound soil water, effectively intercepting water from streams by transpiring it back into the atmosphere. This ideal setting is a one water world scenario. However, despite the expectation of translatory flow during the rainy season in humid catchments, Renée Brooks et al. (2010) found evidence to the contrary in H.J. Andrews Experimental Watershed. Renée Brooks et al. (2010) suggested that early rainy season precipitation events filled small soil pores, where that water remained, until removed by evapotranspiration in the dry season. Empirical evidence for this stems from the depleted isotope ratios found at depth in the soil column in H.J. Andrews Experimental Watershed (Renée Brooks et al., 2010). During each sampling campaign, deep bulk soil water isotope ratios plotted lower along the local meteoric water line than streamwater or the annual average precipitation isotope ratio (Renée Brooks et al., 2010). The proposed mechanism for this soil column isotope signal is the rainout effect, governed by Rayleigh distillation of heavy isotopes (Equation 1) (Clark and Fritz, 1997; Dansgaard, 1964;

Renée Brooks et al., 2010). As precipitation events progress, the isotope ratio of precipitation becomes more isotopically depleted. In H.J. Andrews Experimental Watershed, the isotopically-depleted late event precipitation appears to have filled deeper and deeper soil pores as the storm progressed, with deep bulk soil water isotopic concentrations nearly matching late precipitation event isotopic concentrations (Renée Brooks et al., 2010). These bulk soil isotopic concentrations persisted in the soil column through the rainy season, suggesting that shallow soil water (with a more enriched isotopic signal) did not fully mix with later storm event precipitation. This is indicative of preferential flow rather than translatory flow.

McDonnell (2014) also suggests that it's counter-intuitive for trees to use water that is energetically more difficult to obtain. Plants transport water from roots to leaves via sap flow through xylem tissue, where xylem sap flow is primarily governed by the water potential gradient. Water potential is defined as the potential energy of water. For example, water at high pressure has greater potential energy than water at low pressure. During transpiration, plants create a low water potential environment at the leaf surface via evaporation from stomata, which pulls water resources with higher water potential from the soil towards the leaves. Given the tendency for natural systems to flow from areas of the highest energy to lowest energy, many would expect the root water source with the highest water potential to be extracted from the soil first. Instead, these studies suggest that trees are largely using immobile soil water held at pressures between -0.05 mPa and -15 mPa (between the extraction limit of suction lysimeters and cryogenic vacuum distillation), regardless of mobile water availability.

Lastly, if trees and streams are hydrologically disconnected during the growing season, then what is the hydrological process causing a diel signal in small to medium catchment hydrographs worldwide (e.g., Figure 1; Figure 2; Figure 3)? Many small to medium catchment streams have been shown to exhibit discharge signals that peak at night and trough during the day. The cause of these fluctuations in streamflow has largely been assumed to be plants taking up stream-bound soil water or groundwater from the subsurface and transpiring it into the atmosphere (Graham et al., 2012). We can rule out evaporation as those sole cause of diel fluctuations in streamflow because evaporation only affects the top 10 cm of the soil column, and diel signals persist in streams occupying dry ecosystems where shallow soils become hydrologically disconnected from the stream. Therefore, if plants are not transpiring stream-bound, mobile water, we are left without a mechanism to describe the diel discharge fluctuations present in streams.

2.5 Vegetation-Water Dynamics in Semi-Arid Watersheds

The two water worlds findings in humid catchments has been interesting and largely unexpected. However, it is important to recognize the differences between humid and semi-arid ecohydrologic settings so that we do not falsely interpret differences between data sets. For example, hydrological circumstances conducive to translatory flow are rarer in semi-arid climates, as antecedent soil moisture storage is likely to be lesser, and storms are less often of a duration and intensity capable of saturating the soil column. Nevertheless, snowmelt events and large rain storms in semi-arid catchments should be equally capable of generating translatory flow. Additionally, we know that semi-arid ecosystem woody plants interact differently with hydrological pools than humid ecosystem species. For example, hillslope plants in semi-arid ecosystems are often more

starved for water resources, as the soil water reservoir is drier during the growing season. As a result, many of these plants have adapted to extract water from soil when the water content is below the permanent wilting point, or root to groundwater, in an effort to extend their growing season and access water resources through unusually dry summers. Despite these differences, characterizing semi-arid ecosystem woody plant root water sources will further our understanding of hydrological processes in this environment and help direct future vegetation water use research. Inter-comparison of dual-isotope analyses may reveal ecohydrologic similarities and differences between biota and subsurface flow in these environments.

CHAPTER THREE: STUDY AREA – DRY CREEK EXPERIMENTAL WATERSHED

Dry Creek Experimental Watershed (DCEW) is an approximately 27 km² Northeasterly trending semi-arid basin, ranging from 1033 to 2136 m elevation. It is located approximately 16 km northeast of Boise, Idaho in the Boise Front mountain foothills (McNamara, Chandler, Seyfried, & Achet, 2005). The catchment is maintained by Boise State University, and is used as a watershed sciences laboratory (<http://earth.boisestate.edu/drycreek>). It is instrumented with five weather stations, seven stream gauges, and eleven soil monitoring stations (Figure 4).

3.1 Watershed Instrumentation

The meteorological stations record precipitation, snow depth, air temperature, shortwave radiation, volumetric soil moisture, and soil temperature. Five meteorological stations (Lower Weather, Treeline Weather, Lower Deer Point, Lower Deer Point Ridge, and Bogus Ridge) are located at elevations of 1151, 1610, and 1720, 1850, and 2114 m respectively. These weather stations are used to monitor and describe the high spatiotemporal variability of meteorological variables in the catchment. A high topographic gradient of approximately 200 m/km and aspect-governed solar radiation promote extensive heterogeneity in weather patterns.

The stream gauges are located at integral locations along Dry Creek Experimental Watershed's drainage system. Bogus South is located at 1680 m elevation, near the headwaters of the primary stream draining the catchment (Dry Creek). Con1West and Con1East are situated at 1347 m elevation, at the first major tributary intersection with

Dry Creek. Con1East monitors the flow of Dry Creek, while Con1West monitors the flow of an unnamed southeasterly flowing tributary. Con2East (1158 m) and Con2Main (1143 m) and are located near the second major confluence along Dry Creek. Con2East monitors the flow from a major tributary named Shingle Creek, while Con2Main monitors flow in Dry Creek a few meters downstream of the Dry Creek-Shingle Creek intersection. Lower Gauge (1036 m) is located at the catchment outlet along Dry Creek.

Soil monitoring stations are located on north and south facing aspects at several points along the topographic gradient in DCEW. All soil monitoring stations (with the exception of the Treeline location) consist of four quadrilateral soil pits, spaced 2 to 6 meters apart, dug from surface to bedrock. These soil monitoring stations were placed at locations meant to represent the characteristic soil properties of their immediate area (Smith, 2010). Each soil monitoring pit contains ECH₂O EC-TM sensors at multiple depths between the surface and soil-bedrock interface. These sensors are hard wired to data loggers that record volumetric soil moisture and soil temperature at each respective depth at ten minute intervals (Smith, 2010).

3.2 Topography and Drainage Patterns

DCEW is comprised of an approximately 1100 meter elevation gradient. The landscape is comprised of steep slopes and is highly dissected by streams (Williams, 2005). Slope gradients average about 29% on north-facing slopes, and about 21% on south-facing slopes (Figure 5; Figure 6) (Smith, 2010). Dry Creek Experimental Watershed is drained by a dendritic drainage system (Figure 7). The primary catchment outlet is Dry Creek, a perennial stream with headwaters originating near Bogus Ridge, at an elevation of 2100 m, and terminating at its confluence with the Boise River at about

800 m of elevation (Williams, 2005). Dry Creek and its principal tributary Shingle Creek are the only perennial streams in DCEW. Shingle Creek and Dry Creek are primarily groundwater fed, as is evidenced by their perennial nature, despite very little summer rainfall. However, despite the groundwater fed nature of these streams, they exhibit a large diel signal during the spring and summer, suggesting that transpiration has a significant impact on streamflow (Figure 1; Figure 2; Figure 3) (Graham, Barnard, Kavanagh, & McNamara, 2013). The persistence of gaining and losing stream reaches along Dry Creek has also been well documented (personal communication with Alex Frye, 2013). Frye found spatiotemporal variability in the gaining and losing natures of 200 m stream reaches, suggesting heterogeneity in groundwater flow, streambed hydraulic conductivity, or transpiration in areas hydrologically connected to streamflow. Many unnamed ephemeral streams feed Shingle Creek and Dry Creek following snowmelt. Smaller ephemeral streams commonly dry up between May and August and remain dry until a large snowmelt event takes place (Figure 8; Figure 2). The Bogus South, Treeline Stream and Lower Gauge hydrographs all show the characteristic springtime increases in discharge that occur in conjunction with snowmelt and the rainy season (Figure 1; Figure 2; Figure 3).

3.3 Geology and Soil Characteristics

DCEW is underlain by the Atlanta Lobe, Cretaceous-aged Idaho Batholith. The bedrock consists of highly-erodible medium-grained and coarse-grained biotite granodiorite. Soils are gravelly loams to gravelly sands (commonly ≤ 1 m deep) created by erosion of the granodiorite bedrock and deposition of wind-blown loess (Gribb, Forkutsa, Hansen, Chandler, & McNamara, 2009). Soils are generally deeper and have a

finer texture on north-facing slopes than south-facing slopes (personal observation). Bogus South Gauge consists of the Eagleson-Kosh Complex, while Treeline consists of the Roney-Kisky-Olation Complex, and Lower Gauge features the Shimo-Kisky Complex (Table 1). Soils on opposing aspects differ significantly (Table 1); however these differences were less significant as elevation increased. Wilting point (-3 mPa) soil volumetric moisture content ranges from 0.06 to 0.10 and field capacity (-0.03 mPa) ranges from 0.18 to 0.25 (Smith, 2010).

3.4 Climate and Soil Moisture

DCEW's topographic gradient is accompanied by a significant climatic gradient of increasing precipitation and decreasing temperature with elevation (Figure 8; Figure 9). Precipitation, temperature and the growing season are out of phase, with most precipitation falling during winter months as snow in the higher elevations, and as rain and snow in the lower elevations (Figure 8; Figure 9). Solar radiation increases and relative humidity decreases during the summer, while correlations with elevation are less evident (Figure 10; Figure 11).

The growing season, assumed to be when average daily temperatures exceed 5°C, generally occurs from April to November (Smith, 2010). This estimate generally aligned with the 2012 season (Figure 9), although the only part of DCEW averaging above 5°C into November is the LW area. In contrast, the majority of annual precipitation occurs from November through April (Smith, 2010), where average annual precipitation ranges from 400 mm at lower elevations to 900 mm at upper elevations near Dry Creek headwaters. Precipitation during the 2012 season was near these averages (Figure 8), although approximately 100 mm of precipitation fell before November. Due to the fact

that precipitation and the growing season are out of phase with one another, warm temperatures are not always accompanied by abundant soil moisture supply for plants. This issue is exacerbated by shallow soils containing limited pore space for soil moisture storage in much of DCEW (Table 1; Table 2; Figure 12). July through September have warm temperatures, abundant solar radiation and low relative humidity that would allow for high plant productivity given adequate water supply (Figure 9; Figure 10; Figure 11). As a result, late rainy season precipitation affects have a great effect on woody plant health and productivity in this area (personal observation).

3.5 Woody Plant Life

A Sagebrush-steppe ecosystem dominates hillslopes at lower elevations (e.g., near Lower Gauge). All aspects are covered with grasses, Sagebrush, Rabbitbrush, and Bitterbrush. Wetter soils on north-facing aspects also promote the growth of deciduous trees including Chokecherry, Red elderberry and Red osier dogwood, while south-facing aspects generally only support Nettleleaf Hackberry trees within or adjacent to ephemeral stream channels. The riparian zone is dominated by Water birch and Yellow willow. Biomass per unit area is much greater in the riparian zone of Dry Creek than on adjacent hillslopes.

Mid-elevations of the watershed (e.g., near Treeline) comprise a transition zone between the Sagebrush-steppe ecosystem at low elevations and an Evergreen ecosystem at high elevations. Vegetation on north-facing aspects transitions to an Evergreen ecosystem at lower elevations than south-facing aspects. However, the Treeline location captures this transition zone on both NE and SW facing aspects. Grasses, Sagebrush,

Ceanothus, Ponderosa pine, Bitter cherry and Chokecherry cover the hillslopes, while thin riparian zones are filled with Yellow willow and Fire willow.

Higher elevations (e.g., near Bogus South) support an Evergreen dominated ecosystem, with plant species including Douglas-fir, Ponderosa pine, Bitter cherry, Chokecherry and Maple. Overall, biomass per unit area is greater here than at lower elevations. Hillslope and riparian vegetation is similar in both biomass density and species distribution, though the riparian zone supports more Maple and Bitter cherry trees. Tall Ponderosa pine and Douglas-fir shade the hillslope understory during much of the day, creating relatively similar soil moisture characteristics within north-facing and south-facing hillslopes. Greater soil moisture uniformity is likely the cause of greater plant cover uniformity between north-facing and south-facing aspects.

CHAPTER FOUR: MATERIALS AND METHODS

We evaluate the two water world hypothesis (see Introduction) in two ways. First, we conduct a visual assessment of dual-isotope plots. Second the SISUS mixing model was used to statistically test our visual evaluations of dual-isotope plots by modeling feasible contributions of potential water sources to each plant individual. Inputs to our dual-isotope plots included oxygen and deuterium isotopic concentrations of precipitation (in the form of seasonally-weighted local meteoric water lines), groundwater, streamwater and bulk soil water sampled at 10 cm, 25 cm, 45 cm, 70 cm and 100 cm depths (when available). SISUS modeling inputs all of the above, with the exception of precipitation isotope values.

4.1 Identifying Mobile and Immobile Water

When visually assessing dual-isotope plots, source waters are determined to be mobile or immobile by their proximity to the seasonally-weighted local meteoric water line (LMWL). Mobile water sources are assumed to be isotopically similar to precipitation and therefore plot on or near the LMWL (see Scientific Background). Immobile water sources are assumed to plot significantly below the LMWL (see Scientific Background). Plant roots generally do not fractionate water isotopes upon water uptake. Consequently, we can assume that plant xylem water isotopic concentrations are the integral of the isotopic concentrations of the water sources taken up by the roots. Using this knowledge, lines were constructed and used as thresholds to characterize water pools and woody plant water use.

Seasonally-weighted local meteoric water lines (precipitation isotope data and weighting factor established by Tappa, 2013) including 95% confidence intervals were created for the Lower Gauge, Treeline, and Lower Deer Point locations (Lower Deer Point was used as a proxy for Bogus South). The LMWL and lower boundary of the 95% confidence interval were the thresholds used to differentiate between water pools. Under the assumption that mobile water isotope values mimic those of precipitation, data points that plot on or above the LMWL are suggested to contain primarily mobile water. Items that plot between the LMWL and lower boundary of the 95% confidence interval are likely to contain at least a fractional proportion of immobile water. Finally, items that plot below the lower boundary of the 95% confidence interval are said to contain primarily immobile water. In the remainder of this section, we describe the methods used to collect and process plant stem, soil, and water samples, laboratory methods used to conduct isotopic analyses, and use of the SISUS model to determine feasible plant water sources.

4.2 Sampling and Storage

Three field sampling sites known as Lower Gauge, Treeline, and Bogus South were selected from within Dry Creek Experimental Watershed (Figure 4). Criteria for site selection included the presence of vegetative cover representative of the area, adjacency to a stream, dedicated stream gaging instrumentation and nearby weather and precipitation collection stations. Field sites were also selected to vary significantly in elevation, as significant climatic and vegetative gradients accompany the elevation gradient in DCEW. Lower Gauge is located at 1036 m on north-facing and south-facing aspects, Treeline at 1610 m on northeast-facing and southeast-facing aspects, and Bogus

South at 1680 m (although the adjacent hillslopes rise to much higher elevations) on east-facing and southwest-facing aspects.

Plant stems, streamwater, precipitation, and soil samples (at 10cm, 25cm, 45cm, 70cm, and 100cm where available) were collected from all three sampling sites multiple times throughout the 2011 and 2012 growing seasons (note that most of the 2011 sample year had to be discarded due to cryogenic vacuum extraction error and is thus not included in the results). Multiple soil samples from each depth were collected from each hillslope. Streamwater was collected from Dry Creek, Treeline Stream, and ephemeral streams near Lower Gauge and the semi-catchment outlet of Treeline Stream. Precipitation (when available) was collected from precipitation collection buckets within the Lower Gauge and Treeline sites, and at Lower Deer Point. Our plant sampling campaign was designed to sample the most dominant trees and shrubs at each field site. The most commonly sampled plants included *Pinus ponderosa* (Ponderosa pine), *Pseudotsuga menziesii* (Douglas fir), *Prunus virginiana* (Chokecherry), *Artemesia tridentate* (Sagebrush), *Ericameria nosiosa* (Rabbitbrush), *Salix lucida* (Yellow willow), and *Betula occidentalis* (Water birch). Less commonly sampled plants include *Celtis reticulata* (Netleaf hackberry) and *Salix scouleriana* (Fire willow).

Precipitation and stream water samples were collected in 20ml vials. Plant stem and soil samples were placed into Kimble Chase 19x150mm test tubes sealed with parafilm. Hardwood plant stem samples were collected by clipping unsuberized branch segments near the base of the branch. Multiple branches were collected from trees with thin branches (≤ 8 mm). Each branch was quickly cut into roughly 2 cm segments with the bark left on. Softwood tree stems (Douglas fir or Ponderosa pine) were collected using

the same methods as hardwood samples when the tree diameter was less than 30 cm. Softwood trees with a diameter greater than 30 cm were cored using an increment borer.

Following placement into a storage container, all samples were immediately placed into a cooler loaded with LIFOAM Freez Paks to maintain a refrigerated temperature until they arrived to the Boise State University. Plant stem samples were stored in a Biocold Environmental Inc freezer room at -20°C . Precipitation and stream water samples were stored in a Biocold Environmental Inc stability refrigerator room at 3°C . Following plant and soil water extraction, water samples were transferred into 1 dram Kimble Chase glass vials with inverted caps and transported to a refrigerator at 3°C in the Boise State University Stable Isotopes Laboratory. Precautions were taken to minimize post-extraction evaporative enrichment by limiting exposure to the open atmosphere, turbulence during transport, and headspace in each vial.

4.3 Sample Water Extraction

Water was extracted from plant stem and soil samples using cryogenic vacuum distillation. The vacuum apparatus was constructed by Matt Kohn at Boise State University. It consists of two individual stainless-steel units attached to a 1-inch glass manifold. A Welch 1400 DuoSeal Vacuum Pump designed by Thomas Industries Inc. was used to lower pressure within the independent units. Pressure was monitored with a Welch Vacuum Gauge Tube Model 1516A that connected the manifold and a Welch Pressure Gauge. This unit commonly reported vacuum pressures of 10 to 15 millitorr. Two Kimble Chase 19x150mm test tubes (one containing a plant or soil sample and the other empty) were attached to the stainless-steel units using Ultratorr vacuum fittings or Swagelok pipe connectors lined with appropriately sized Swagelok ferrules.

To extract water from plant and soil samples, test tubes containing the samples were dipped into liquid nitrogen, evacuated down to ≤ 30 millitorr and then sealed off from the vacuum manifold. After sealing off the unit, the test tube containing the sample was placed into an oven at 100 °C, while the empty test tube was dipped in liquid nitrogen, catalyzing diffusion of water from the sample test tube to the empty test tube. For soil samples, glass wool was packed into the sample test tube above the soil to prevent soil particles from being vacuumed. Care was taken to ensure that glass wool did not compromise the air-tight seal between the sample test tube and the unit.

Plant samples were evacuated for 120 minutes and soil samples for 40 minutes. Although accurate stable isotope values of water samples can be attained without extracting 100% of the water (Araguás-Araguás, Rozanski, Gonfiantini, & Louvat, 1995), variance in the morphology of the material in question may be responsible for variance in the required water extraction time (West, 2006); therefore caution must be used when selecting a length of time for water extraction from a given material. West (2006) used a similar vacuum setup, and suggested that plant samples need to be vacuumed for 60 to 75 minutes, while sandy soils require 30 minutes. However, plant species analyzed in this study differ from those vacuumed by West (2006), and slight vacuum setup differences are inevitable, so we increased water extraction times to 2 hours for plant stems and 40 minutes for bulk soil as a precautionary measure.

Some of the plant and soil samples were weighed by a Mettler Toledo PB3002-S scale after vacuum water extraction, baked in an oven at 100 °C for 24 hours, and then re-weighed to test for complete extraction of water, as incomplete extraction could result in isotopically enriched water samples. The empirical standard deviation of measured

weight using this scale was approximately 0.05g. The average stem water removed was 100.49% mass, with a standard deviation of 1.31% (Table 3). We also tested 38 soil samples, where the average amount of soil water removed was 95.43% mass, with a standard deviation of 6.91% (Table 4).

Results for plants were encouraging, considering that the standard deviation of weight output for this machine is 0.05g and the largest amount of water evaporated by the oven was 0.03g. At first glance, the results for the soil samples are disconcerting, as the percent water evacuated by the vacuum extraction line ranges from 74.88% to 100%. There were 8 instances where the remnant soil moisture was greater than 0.10 g. These instances indicate that the vacuum extraction line did not evacuate all water from the soil sample. However, further investigation reveals that the percent of soil water evacuated is related to volumetric moisture content (Figure 13).

When volumetric soil moisture (θ) dips below 0.08, which is below the permanent wilting point at each field site (Table 2), less than 100% of the water is extracted by the vacuum extraction line (Figure 13). This is likely due to strongly bound water that is not released below 110 °C, known as heat-labile water (Ingraham & Shadel, 1992). The lower the soil water content, the larger the fraction of heat-labile water to total soil water. In Dry Creek Experimental Watershed, soils dry throughout the summer, as was the case in 2012 when the soil samples in Table 4 and Figure 13 were collected. This table shows that soil samples where less than 90% of water was evacuated were only found at the LG site, and only in June or later in the growing season. This is as expected, because lower elevation sites in DCEW (e.g., Lower Gauge) receive very little precipitation and climatic conditions are conducive to evapotranspiration that dries the soil (Figure 8; Figure 9;

Figure 10; Figure 11). It is also important to note that the standard deviation for the Mettler Toledo scale was 0.05g and therefore a large proportion of the supposedly unevacuated water could be due to machine error.

4.4 Stable Isotope Analysis

A 4th generation Los Gatos Research (LGR) Liquid Water Isotope Analyzer (LWIA) housed in the Boise State University Stable Isotopes Laboratory was used to measure $^2\text{H}/^1\text{H}$ and $^{18}\text{O}/^{16}\text{O}$ ratios for all water samples. Stable isotope values were reported in delta notation, in units of per mil (‰). Vienna Standard Mean Ocean Water (VSMOW) was the standard to which all stable isotope ratios were compared, where VSMOW isotope ratios are $^2\text{H}/^1\text{H} = 155.76$ ppm and $^{18}\text{O}/^{16}\text{O} = 2005.20$ ppm. The LWIA is an Isotope Ratio Infrared Spectrometer (IRIS), a viable new alternative to Isotope Ratio Mass Spectrometry (IRMS) for liquid water stable isotope analysis. Boise State University Stable Isotopes lab also houses a Finnigan High Temperature Conversion Elemental Analyzer (IRMS). The LWIA was chosen over the more traditional IRMS machine because it requires less money and skill to run, has a higher overall throughput, and allows users to bypass the chemical conversion steps necessary when using IRMS (Schultz, Griffis, Lee, Baker., 2011; West & Goldsmith, 2010). There are several methods of preparing liquid water for an IRMS machine, but each is time consuming and often compromises accuracy (Kerstel & Meijer, 2005).

Despite the advantages of the IRIS method for liquid water stable isotope analysis, IRMS is more commonly used for plant and soil water. IRIS machines were found to be susceptible to spectral interference caused by contaminants commonly co-distilled with plant and soil water, and therefore less reliable than IRMS for this

application (Brand, 2010; West & Goldsmith, 2010; West, 2006). However, recent contaminant detection software releases have made IRIS systems manufactured by Los Gatos Research and Picarro viable alternatives to IRMS for plant and soil water isotopic analyses (Brian Leen, Berman, Liebson, & Gupta, 2012; Schultz et al., 2011). When this project was proposed, we believed that the advantages of using the LGR LWIA for our liquid water samples warranted the post-processing procedures required to correct stable isotope values for spectral interference caused by these contaminants.

4.5 Los Gatos Research Liquid Water Isotope Analyzer

The LWIA requires ½ ml liquid water samples. By default, the machine collects six samples (injections) of liquid water from each vial (LWIA Post Analysis Software User's Guide Version 2.1). Once the needle is injected into a sample vial, a small portion of the sample water is evaporated to the gas phase and transported to the absorption cavity, where a laser emits an infrared light signal. Transmission (and absorption) of the infrared signal is continuously recorded, and a fitting routine (Equation 5) is applied to the recorded transmission data.

EQUATION 5

$$I(v) = \frac{b_0 + b_1v + b_2v^2 + \dots}{1 + G(V_1 + V_2 + V_3 + \dots)}$$

where v is the relative laser frequency, $I(v)$ is the measured laser transmission, b_n are the baseline coefficients, G is the cavity gain factor, and V_n are Voigt functions (Brian Leen et al., 2012).

Spectral transmission and absorption (Volts) vs. Frequency (GHz) fits can be viewed during or after a LWIA run (Figure 14; Figure 15). Note that the highly characteristic rotational and vibrational stretching and bending motions of water

isotopologues gives each isotopologue a unique spectral absorbance signature (Kerstel & Meijer, 2005). The machine uses these unique spectral absorbance signatures to indirectly measure isotope ratios of $^{18}\text{O}/^{16}\text{O}$ and $^2\text{H}/^1\text{H}$ for each injection. All data recorded by the LWIA can be loaded into the LWIA Post Analysis Software package (LWIA-PAS), which eliminates errant injections via a flagging process and produces sample average isotope values and standard deviations (Kerstel & Meijer, 2005). Ultimately, we had to employ additional post-processing techniques to correct raw LGR LWIA isotope values for spectral interference caused by organic contaminants commonly found in plant and soil water (Appendix C). With additional processing, plant water $\delta^2\text{H}$ and $\delta^{18}\text{O}$ values agreed to within 2.64 ‰ and 0.48 ‰ of a Finnigan High Temperature Conversion Elemental Analyzer IRMS.

4.6 SISUS Modeling

SISUS is a mass balance mixing model that can be applied to a number of applications to evaluate feasible proportional contributions of sources to a mixture (Erhardt et al., 2014). This model was chosen over pure Bayesian mixing models because it can cope with multiple sources (number of sources is greater than the number of isotopes + 1). Using a large number of potential water sources is important for this study because soil water isotope values are the result of hydrological processes, and vary over a continuum rather than existing as discrete sources with associated isotope values (e.g., the isotope value of a food item in one's diet). SISUS is similar to IsoSource (Phillips & Gregg, 2003), however modeled feasible source contributions are more exact due to the use of an approximate Bayesian large sampling procedure as opposed to the deterministic

approach used by IsoSource, which requires a relatively arbitrary user-specified tolerance input to the model (Erhardt et al., 2014).

In this study, SISUS model inputs included $\delta^2\text{H}$ and $\delta^{18}\text{O}$ values of water pools (potential sources) and plant xylem water (the mixture). The solution space was constructed by mapping the 2-dimensional isotope ratio data space ($\delta^2\text{H}$ and $\delta^{18}\text{O}$) to the x-dimensional proportion solution space (x = the number of potential water source inputs to the model). The solution space axes represent potential water contributions of each source (between 0 and 1). SISUS uses the double description method to define the vertices and boundaries of the solution polytope (Fukuda & Prodon, 1996). The solution polytope is the intersection of the two isotope ratio ($\delta^2\text{H}$ and $\delta^{18}\text{O}$) planes with the x-dimensional proportion solution space. Note that if the number of sources exceeds the number of isotopes + 1, then the solution polytope represents an infinite amount of possible solutions. SISUS randomly samples 10,000 exact solutions (feasible water source contributions to the plant xylem water mixture) from the solution convex polytope using the random directions symmetric mixing algorithm (Smith, 1980). To do this, the model chooses a starting point inside the solution space and sets a counter to keep track of the number of samples taken from the solution space. Next it generates a random direction inside the solution polytope and draws a line segment through the current sampling point, along the chosen direction, to two edges of the polytope. The next sampling point is chosen randomly from that line segment. After sampling in this manner 10,000 times from the polytope, the model has collected a representative sample, converging to a uniform distribution over the solution polytope (Erhardt et al., 2014). Standard Markov chain Monte Carlo diagnostics are used to monitor convergence of the

algorithm. After a model run is completed, SISUS produces statistics summarizing the feasible water source contributions to the plant xylem water mixture, which can be viewed in tables and figures (e.g., Figure 16).

It is important to note that the SISUS model assumes that isotope values are exact, and does not account for uncertainty (e.g., $\delta^{18}\text{O}$ uncertainty $\approx 0.48\%$ and $\delta^2\text{H}$ uncertainty $\approx 2.64\%$; see Appendix C). As a result, modeled feasible water source contributions to plant xylem water are likely to contain a more finite range of possible solutions for each source than would be the case had we included uncertainty in our analyses. Additionally, we are more than 5 times more confident in our $\delta^{18}\text{O}$ values than our $\delta^2\text{H}$ values. However, $\delta^2\text{H}$ source water values commonly varied more than 5 times that of $\delta^{18}\text{O}$ source water values, counteracting the effects of this uncertainty imbalance in our analyses. We also wanted to run both isotopes simultaneously in the SISUS model to persist with the dual-isotope approach used in our visual assessments of scatter plots. Lastly, we wanted to avoid the water pool differentiation shortcomings of the single-isotope modeling approach (see Introduction).

CHAPTER FIVE: RESULTS

Following a description of the spatiotemporal variability of hydrogen and oxygen isotopic concentrations in hydrological pools and woody plant xylem water, we evaluate woody plant water sourcing by visually assessing the proximity of plant water isotopic values to water sources in dual-isotope space. However, plants may use water from multiple sources simultaneously, and there are infinite possible water sourcing solutions when the number of potential sources is greater than the number of isotopes plus one. These factors can make visual assessment alone deceiving. To improve our isotopic analyses, we use the SISUS mixing model to compute feasible source contributions to the xylem water of each plant individual (see Materials and Methods). SISUS results are used in conjunction with dual-isotope plot assessments to evaluate the two water worlds hypothesis in the discussion section.

5.1 Spatiotemporal Variability of Catchment Water Inputs and Storage Reservoirs

Inputs: Precipitation

The Dry Creek Experimental Watershed precipitation isotopic signal (Table 5) is described by the seasonally-weighted local meteoric water line (Equation 6; Figure 17), derived from precipitation collected at three sites (Lower Gauge, Treeline and Lower Deer Point) spanning the watershed's elevation gradient.

EQUATION 6

$$\delta^2H = 7.483(\delta^{18}O) + 0.688$$

Smaller spatial scale seasonally-weighted local meteoric water lines were also constructed for Lower Gauge (Equation 7; Figure 18), Treeline (Equation 8; Figure 19) and Lower Deer Point, which was used as a proxy for the Bogus South location (Equation 9; Figure 20).

EQUATION 7

$$\delta^2H = 7.414(\delta^{18}O) - 2.125$$

EQUATION 8

$$\delta^2H = 7.698(\delta^{18}O) + 4.953$$

EQUATION 9

$$\delta^2H = 7.614(\delta^{18}O) + 3.850$$

All local meteoric water lines were weighted using the methods outlined for the Treasure Valley by Tappa (2013). Tappa (2013) states that the dry season (June 1st to September 31st) precipitation water line exhibits a shallower slope and decreased y-intercept relative to the rainy season. The differences between rainy season and dry season LMWL equations are likely caused by decreased relative humidity causing increased secondary evaporation after precipitation exits clouds during dry season precipitation events (Peng, Mayer, Harris, & Krouse, 2007; Tappa, 2013). Tappa (2013) also discovered a positive correlation ($r = 0.63$) between amount-weighted average precipitation $\delta^{18}O$ values and average surface temperature during individual precipitation events. This trend translates to a very strong negative correlation ($r = -0.98$) between weighted precipitation $\delta^{18}O$ values and elevation, where $\delta^{18}O$ values decrease by 2.3 ‰ per km elevation gain (Tappa, 2013). This trend was evident when comparing the seasonally-weighted mean precipitation isotope values for Lower Gauge and Treeline locations (Table 6); however,

interestingly, Lower Deer Point had a LMWL indicative of slightly more secondary evaporation than Treeline, despite being located at a higher elevation (1610 m and 1720 m, respectively). Nevertheless, precipitation isotopic compositions were significantly different at each field site, and field site scale LMWL were used to improve dual-isotope analyses.

Precipitation falling at higher elevations is generally more likely to plot above the Dry Creek Experimental Watershed LMWL, while precipitation at lower elevations is more likely to plot below the catchment LMWL. This is exemplified by the varying slopes and intercepts of the smaller spatial scale local meteoric water lines (Equation 7; Equation 8; Equation 9). This trend is largely caused by lower elevation sites having lower average relative humidity, which increases the frequency that secondary evaporation occurs. Given the lesser slope of the Lower Gauge LMWL, we can assume that the inclusion of low elevation sites in the DCEW LMWL linear regression analysis is largely responsible for the slope of the catchment LMWL being significantly lower than the GMWL. Dry season precipitation at all elevations is also a factor, due to lower relative humidity and increased secondary evaporation.

Water Storage: Unsaturated Zone

In dual-isotope space, isotope values of bulk soil water (geographic location of samples in Table 7; isotope values in Table 8 and Table 9) generally plotted below the LMWL, with shallower soil samples plotting the farthest below the line (Figure 21). This trend is indicative of kinetic evaporative enrichment (refer to Scientific Background). Bulk soil water values also generally plotted farther below the LMWL as the growing season progressed, increasing the isotopic spatial variability within the soil column

(Figure 22; Figure 23; Figure 24). There are likely two reasons why this trend occurred. First, the shallow soil experiences greater evaporative enrichment in the summer (see Scientific Background), as relative humidity is lower and temperature is higher, causing greater evaporative forcings. Second, the fraction of immobile soil water contained in bulk soil water samples increases over the course of the growing season. Draining of mobile water to groundwater or streamflow leaves only the more isotopically-enriched immobile soil water fraction behind. Immobile soil water generally plots farther below the LMWL and also lower along the LMWL than mobile soil water (Renée Brooks et al., 2010).

The mechanisms by which the differences in soil moisture residence time lead to unique isotopic concentrations in mobile and immobile soil water are complex; however, the natures of precipitation isotopic concentrations, evapotranspiration and unsaturated flow are likely to all contribute to this phenomenon. Evaporation and transpiration remove water from the soil over the course of the growing season (spring and summer) until soil water tension is too great for roots to extract water. Little summer precipitation occurs to refill soil pores (although summer precipitation more often has an evaporatively-enriched isotopic signal). Due to lack of summer precipitation, antecedent soil moisture is held at higher and higher tensions over the course of the growing season as water is continuously removed via evapotranspiration. Finally, during the fall rainy season, precipitation typically infiltrates downward through the soil column, refilling soil pores that have been largely depleted by evapotranspiration. During these refill infiltration events, pores with the smallest neck and body diameters are the first to fill and last to drain (Selker et al., 1999). As a result, the smallest pores, which are likely to

contain relatively immobile water, fill with water that has mixed with shallow antecedent soil moisture that has been exposed to isotopic evaporative enrichment all summer long. This shallow antecedent soil moisture is extremely enriched by this time (e.g., Figure 22d; Figure 23d). As a result, small soil pores are most likely to contain immobile soil water, and that immobile water is likely to contain a large proportion of water that has been evaporatively enriched.

In DCEW, bulk soil water stable isotope values plotted lower along the LMWL with increased soil depth, exhibiting a more depleted isotopic signal than shallow bulk soil water throughout the growing season (Figure 22; Figure 23; Figure 24). Some have suggested that this is indicative of the rainout effect causing the more isotopically-depleted late event precipitation to fill deeper and deeper soil pores as storms progress (Renée Brooks et al., 2010). However due to the seasonality of precipitation (Figure 8) and subsequent infiltration (Figure 12) in DCEW, we suggest that this phenomenon may be the result of varying infiltration depths associated with variably sized, isotopically-unique precipitation events. Summer precipitation plots significantly higher along local meteoric water lines in this area (Tappa, 2013). Soil moisture data demonstrates that very little water infiltrated below 15 cm depth from May to mid-September at Lower Gauge or Treeline, or from June to mid-September at HN (a soil moisture site used as a proxy for Bogus South) (Figure 12). This means that the enriched isotopic signal of summer precipitation is typically only mixing with shallow soil moisture. In contrast, the more isotopically-depleted winter and spring precipitation is largely responsible for filling deeper soil pores with water. Furthermore, it is doubtful that the trend of isotopic-depletion with soil depth was governed by differential mixing of evaporatively-enriched

soil water alone, because deep soil water isotope values consistently plotted lower along the LMWL as the growing season progressed. This trend occurred in the absence of precipitation or increased soil moisture. As a result, we suggest that spatiotemporal variation of bulk soil water isotope values was governed primarily by evaporative enrichment of shallow soil water, subsequent infiltration and partial mixing with shallow soil water, and also the fact that bulk soil water samples contained increasingly large immobile water fractions as the growing season progressed. The rainout effect described in Brooks et al. (2010) may have also contributed to these isotopic trends. Depth differences (soil pit scale variability) correlated best with bulk soil water isotopic concentrations during the latter two sampling campaigns (07-08-2012 to 09-13-2012) (Table 10). However, latitude differences (catchment scale variability) correlated best during the first two sampling campaigns (03-27-2012 to 06-06-2012). This transition from catchment-scale isotopic controls to soil pit scale controls occurred as the frequency of precipitation events and relative humidity at each field site plummeted.

On the hillslope scale, heterogeneous soil texture, variable bedrock depth, and vegetative cover influence soil water flow and evaporative processes, contributing to the extensive isotopic variability seen at each sampling site (Figure 22; Figure 23; Figure 24). Variable proportions of mobile and immobile water (which contain unique isotopic signatures) in bulk soil water also contributed to this variability. Individual soil pit $\delta^{18}\text{O}$ values are plotted against soil depth at Lower Gauge, Treeline and Bogus South (Figure 25; Figure 26; Figure 27). Plotting isotopic concentrations at each depth, in individual soil pits helps us to better understand the hillslope-scale isotopic variability. These figures show that the trends of increased isotopic depletion with depth, and greater

evidence of evaporative enrichment in shallow soils are consistent in the majority of soil pits at each field site. The evaporative enrichment signal is particularly discernible in the shallow soil column in July and September (e.g., Figure 25c; Figure 25d; Figure 26d; Figure 26e; Figure 27c).

On a catchment scale in a mountainous watershed, spatial variability of the isotopic signal is largely governed by a variable precipitation input signal (Tappa, 2013) and climatic differences between field sites (Figure 9; Figure 10; Figure 11) causing greater variations in kinetic evaporative enrichment than is likely present on the hillslope scale. On average, all depths of soil water were more isotopically depleted and closer to the GMWL at Bogus South than at lower elevation sites (Figure 22; Figure 23; Figure 24). This is largely caused by the negative linear relationship between elevation and precipitation isotopic concentration (Tappa, 2013). In addition, relative humidity is generally higher and temperatures lower, at higher elevations. Since relative humidity and temperature are drivers of evaporation, there is less evaporative isotopic enrichment at higher elevations (Figure 11; Figure 9).

In summary, bulk soil water isotopic concentrations have the highest spatial and temporal variability of all potential plant root water sources in DCEW. On a soil pit scale, shallow soil water (10 cm - 25 cm) tended to be more isotopically enriched than deep soil water (45 cm – 100 cm). Shallow soil water also typically became more isotopically enriched as the growing season progressed. Deep soil water tended to plot farther below the LMWL, but also lower along the LMWL as the growing season progressed. Extensive lateral spatial variability of isotopic concentrations existed at the hillslope scale; nevertheless, depth of bulk soil sample correlated significantly with isotopic

concentrations in the later growing season. On the DCEW catchment scale, soil water generally became more isotopically depleted (plotted lower along the LMWL) with increased latitude, as a result of more isotopically-depleted and overall larger precipitation events (Tappa, 2013). Caution must be exercised when using bulk soil water for plant water source analyses, as isotopic concentrations exhibited extensive spatiotemporal variability, as well as variable and sometimes ambiguous mechanisms causing such variability.

Water Storage: Groundwater

Groundwater was sampled six times from a spring near Bogus South (BGS), once from a well near lower gauge (LGW) on 3/4/2012 and once from a well at Bogus Basin Ski Resort on 3/4/2012 (Table 11). Four of the BGS groundwater samples and the Bogus Basin Ski Resort sample all plotted on or near the GMWL, with average isotope values of $\delta^2\text{H} = -120.48$ and $\delta^{18}\text{O} = -16.43$, and standard deviations of $\sigma = 1.34$ and $\sigma = 0.13$, respectively. The BGS groundwater samples plot closer to the GMWL than the Lower Deer Point seasonally-weighted LMWL. This discrepancy was likely caused by increased secondary evaporation of precipitation in the dry season (Tappa, 2013). This dry season precipitation is less likely to mix with groundwater because soils are drier, and therefore less hydrologically connected to groundwater during the dry season (Figure 12).

In contrast, groundwater from LGW plots below both the GMWL and Lower Gauge LMWL. These differences were likely caused for several reasons. First, groundwater at this location may be primarily derived from relatively local water sources. Second, kinetic evaporative enrichment of the soil column at the LG location is much more pervasive than at higher elevations. Therefore, even though mixing between

immobile soil water and mobile soil water may be limited, the extremely enriched isotopic signal present in the shallow soil column in late summer may be enough to enrich the local groundwater isotopic signal. Third, streamwater at the LG location is a losing reach of Dry Creek during the late summer and fall before the rainy season begins, meaning that streamwater is being lost to bedrock, and infiltrating downward to the water table and mixing with local groundwater (personal communication with Alex Frye, 2013). Upon evaluation of Figure 22d, we can see that the isotopic signals of late summer streamwater and groundwater near Lower Gauge are very similar, suggesting that streamwater may be contributing to the groundwater pool at this location.

Although groundwater isotopic concentrations are often assumed to approximate average precipitation values, BGS groundwater lies significantly lower along the GMWL than average seasonally-weighted precipitation from Lower Deer Point (used as a proxy for BG precipitation) (Figure 24). This likely occurs because more isotopically-depleted winter precipitation and snowmelt is more likely to infiltrate to the groundwater reservoir than the more isotopically-enriched summer precipitation, as a result of increased soil saturation in the colder months (Figure 12). LGW groundwater also plotted lower along the LMWL than average seasonally-weighted precipitation.

In summary, groundwater isotopic values at BGS and BBW remain relatively constant and plot near the GMWL and lower along the line than average precipitation throughout the 2012 growing season. This lack of isotopic concentration temporal variability was expected, as groundwater is the largest water storage reservoir in DCEW and also generally has the longest residence time. As a result, local groundwater isotopic values are less likely to be influenced by small-scale temporal variability in the

precipitation isotopic signal than smaller storage reservoirs such as the unsaturated zone or streams. LGW groundwater plots slightly below the LMWL, but above the Lower Gauge LMWL lower 95% confidence interval. Due to the consistency of the groundwater isotopic signal at BGS and BBW during the growing season, we suspect that the groundwater signal also remains relatively stable at the Lower Gauge location. This consistency allows for telling isotopic analyses with regards to plant use of groundwater.

Water Storage: Streamwater

Similar to groundwater, streamwater samples from Dry Creek (Lower Gauge and Bogus South) usually plotted near the GMWL (Table 12; Figure 28; Figure 29). This similarity may be the result of the stream being largely groundwater fed (personal communication with Alex Frye, 2013). Water from Dry Creek tended to have a more enriched isotopic signal as the growing season progressed. Lower elevation stream sampling sites typically had more enriched isotopic signals than high elevation sites. Three small ephemeral streams (two at Treeline and one at Lower Gauge) showed faster isotopic enrichment trends than Dry Creek. These differences may have been the result of the ephemeral streams being recharged by primarily new water, as opposed to Dry Creek which is primarily old water (groundwater) fed. New water in the form of runoff, unsaturated flow, or bedrock interface flow is more likely to be significantly influenced by short-term variability in the precipitation signal variability.

During the 2012 sampling campaign, the most depleted isotope values seen at Lower Gauge were sampled on 3/23/12, while the most enriched isotope values were seen on 9/13/12. Over this time, $\Delta\delta^2\text{H} = 8.59\text{‰}$ and $\Delta\delta^{18}\text{O} = 1.65\text{‰}$ (Table 9), which indicates an isotopic enrichment rate of 1.48 ‰ per month and 0.29 ‰ per month,

respectively. This change is expressed as a slope of 5.2 in dual-isotope space, which is similar to the slope of an evaporative kinetic fractionation line. This enrichment trend may have been caused by hyporheic exchange with increasingly isotopically-enriched soil water while the gaining (groundwater fed) reach of Dry Creek decreased in length as the growing season progressed (personal communication with Alex Frye, 2013).

Additionally, as the discharge of Dry Creek slowed rapidly throughout the growing season (Figure 1), the transit time of Dry Creek water from Bogus South to Lower Gauge would have greatly increased due to increased streambed friction and less direct water flow paths within the stream channel. This increased transit time would have catalyzed increased hyporheic exchange per unit water volume, along with increased exposure to the atmosphere which may have resulted in evaporative enrichment of the streamwater. Unfortunately, Dry Creek water was only collected at the Bogus South site from 5/19/12 to 9/4/12; however, over this short time period $\delta^2\text{H}$ and $\delta^{18}\text{O}$ values were enriched by 1.36 ‰ and 0.39 ‰, respectively. Although these small isotopic changes don't invoke confidence given the potential error associated with each measurement (Table 11), they do suggest that an isotopic enrichment trend may be occurring in the Dry Creek headwaters.

In summary, streamwater isotopic values are relatively stable, but unlike groundwater, streamwater becomes noticeably more isotopically enriched as the growing season progresses. Dry Creek water became slightly more enriched throughout the growing season at both the headwaters and the catchment outlet. Most of the enrichment is shown as streamwater isotope values plotting farther to the northeast along the GMWL. However, late summer Dry Creek samples from Lower Gauge suggest kinetic

evaporative enrichment or mixing with evaporatively-enriched soil water, as the isotope values plot significantly below the LMWL. Smaller ephemeral streams have less stable isotopic signals and show faster evaporative enrichment trends. Overall, DCEW stream isotopic signals are less stable than groundwater but more stable than bulk soil water. The relatively steady streamwater isotopic signals and predictable isotopic enrichment trends in DCEW streams suggest that we can be reasonably confident in our use of streamwater in plant water source analyses.

5.2 Visual Assessment of Dual-Isotope Plots

Bulk Soil Water

Bulk soil water samples extracted via cryogenic vacuum distillation plot below the LMWL the vast majority of the time (Figure 21). Bulk soil water contains both mobile (when available) and immobile soil water. In bulk soil samples containing an isotopically-relevant fraction of immobile water, the enriched isotopic signal of the immobile water causes the overall isotopic signal to plot below the LMWL. In total, 297 bulk soil samples from the 2012 growing season were analyzed, and only 29 plotted on or above the Dry Creek Experimental Watershed LMWL, 18 of which were collected during one sampling campaign on 03-27-2012 that followed a large rain on snow melting event at Treeline (Figure 8). This indicates that the vast majority of bulk soil samples collected from Dry Creek Experimental Watershed during the 2012 growing season contain an isotopically-recognizable fraction of immobile water.

Groundwater and Streamwater

The isotopic signals of groundwater (Table 8) and streamwater (Table 9) generally plot near the meteoric water lines, indicating that they are mixtures of primarily

mobile soil water inputs. Four of six groundwater samples plotted above the GMWL and Dry Creek Experimental Watershed LMWL (Figure 21). The two samples that plotted below the DCEW LMWL were an anomaly collected on 03/23/2012 from Bogus Gauge Spring and a groundwater sample taken from a well near Lower Gauge on 03/04/2012. Even with these early season anomalies, each groundwater sample plotted above the lower 95% confidence interval for the catchment LMWL. Streamwater isotope values from a given sampling site often exhibit notable isotopic enrichment as the growing season progresses. However, 14 of 21 stream samples plotted above the catchment LMWL, the rest of which were primarily samples from ephemeral streams. Similar to groundwater, each streamwater isotope value plotted above the lower 95% confidence interval for the catchment LMWL.

Woody Plant Xylem Water

The vast majority of woody plant xylem water isotope values (Table 13) plot below the meteoric water lines (Figure 21). In total, 121 plant xylem water samples were analyzed, and only 9 plotted on or above the Dry Creek Experimental Watershed LMWL. Xylem water isotope values were nearly as variable as bulk soil water isotope values in DCEW. However, given that bulk soil water samples containing recognizable fractions of immobile water were the only sampled water sources to plot significantly below the LMWL, 112 out of 121 plants are likely transpiring water that contains at least a significant fraction of immobile soil water. Out of those 112 plants, 88 plotted below the lower 95% confidence interval for the LMWL, indicating that it is likely that they are likely transpiring primarily, if not exclusively, immobile soil water.

In late March through early June, only one tree at Treeline and two trees at Bogus South plotted above the local meteoric water lines (Figure 22a; Figure 23a; Figure 23b; Figure 24a). In total, only 3 of the 60 sampled plants plotted above the LMWL. Additionally, only four trees at LG, seven at TL and six at BG plotted above the lower 95% LMWL confidence intervals. Altogether, only 17 of 60 samples showed evidence of potential proportional use of mobile water sources. Our confidence in this assessment is bolstered by the fact that the vast majority of plants plotted below bulk soil water isotope values at a time when bulk soils contained significant fractions of mobile water (Figure 12). The larger fraction of trees plotting nearer to the LMWL at Bogus South may be an artifact of using a LMWL derived from precipitation data from Lower Deer Point. For example, Bogus Ridge snowmelt had a much different average isotopic signal than LDP precipitation, and the geographic location of Bogus South field site is roughly half way between Lower Deer Point and Bogus Ridge (Figure 4).

In March and April, some of the disparity between mobile water and woody plant isotopic signals was likely caused by plants that were not yet actively transpiring plotting far to the northeast of bulk soil water isotope values, along an evaporative enrichment line. However, Ponderosa pines transpire year-round, and three out of four Ponderosa pines sampled on March 27th at Treeline plot significantly below the range of bulk soil water isotope values (Figure 23a). On April 8th at Lower Gauge (Figure 22a), one active Sagebrush and one Rabbitbrush show a similar trend. These Ponderosa pines, Sagebrush and Rabbitbrush are clearly transpiring because they did not plot along the evaporative enrichment line like the inactive plants. Nevertheless, they plot significantly below the range of bulk soil water isotope values, suggesting selective immobile soil water use,

even though they are rooted into soil that should contain abundant mobile water (Figure 12).

By mid-May, all but one sampled woody plant appear to be actively transpiring, as xylem water isotope values plot significantly to the southwest of their March plotting locations, indicating that these plants have taken up new water. On 05-17-2012 at Treeline, three out of the five Ponderosa pines, one of three Chokecherries, one of three Yellow willow, and all four Sagebrush plot significantly below the range of bulk soil water isotope values, below the lower 95% confidence interval for the LMWL (Figure 23b). We attribute these differences to the same cause as the March and April plant samples, where these plants are using immobile soil water held at higher tension than the average bulk soil water, which contains a unique, enriched isotopic signal. However, at this point in the growing season the xylem water of most plants plots more closely to the isotopic signals of bulk soil water. Six trees plot within or near the range of bulk soil water, while only one Chokecherry and one Ponderosa pine plot above the LMWL, and to the southwest of groundwater and streamwater isotope values, indicating that they may be transpiring mobile soil water.

Finally, during the June, July, and September sampling campaigns, plants typically plot within or very near the range of bulk soil water isotope values. The soil column had dried to below the permanent wilting point at each field site before the July sampling campaign (with the exception of the 15 cm sensor at LN) (Figure 12). With soils dried to this extent, one would expect that plants with root access to mobile water would actively take up water from that source, given that it should be energetically easiest to obtain. In fact, closer assessment of these plots reveals that some plants

sampled in July, and more frequently in September, plot on the upper threshold of the range of bulk soil water isotope values, in the general proximity of the groundwater and streamwater isotope values (Figure 22d; Figure 23d; Figure 24d). It is therefore possible that these plants are transpiring fractional contributions of mobile water sources in conjunction with immobile soil water. Nevertheless, 47 woody plants were sampled in July and September, and only one tree at TL and one tree at BG plotted on or above their respective local meteoric water lines. Zero trees or shrubs at Lower Gauge plotted above the lower 95% confidence interval for the LMWL. At Treeline, five trees plotted above this line in July, while three plotted above the line in September. At Bogus South, five trees plotted above the line in July, while seven plotted above the line in September. Again, Bogus South trees are the anomaly of the three field sites, as there is less certainty that they are using primarily immobile soil water sources.

If early season inactive woody plant samples are excluded from the analysis, dual-isotope plots show that 86 out of 92 plants plot below the local meteoric water lines. Out of 60 plants sampled in March through May, only 3 plotted above the LMWL, and out of 47 sampled in July through September, only 3 plotted above the LMWL. If we exclude both inactive plants and trees from Bogus South (where most trees plotted between the LMWL and lower 95% confidence interval for the LMWL), 70 of 89 trees and shrubs sampled plotted below the lower 95% confidence interval for the LMWL. This level of consistency suggests that the xylem water of the vast majority of plants contains a large fraction of immobile soil water throughout the growing season. However, it is important to note that plants may use more than one water source simultaneously. It is therefore possible that some of the presented plant isotope values represent mixtures of both

immobile and mobile water sources. To investigate this possibility, and ensure that our visual analyses are unbiased, we ran the SISUS mixing model to calculate feasible water source contributions to the xylem water of each individual plant sample.

5.3 SISUS Modeled Feasible Water Source Contributions to Plant Xylem Water

SISUS model inputs included $\delta^2\text{H}$ and $\delta^{18}\text{O}$ values of potential water sources and plant xylem water. Bulk soil water inputs were averaged at each depth for each field site. Field site depth average values were used for soil water model inputs because soil pit depth was highly variable (high boulder concentration) and isotope values at each depth exhibited high hillslope-scale variability. Given these inputs, the SISUS model provided solutions for 42 out of the 107 xylem water samples analyzed. Feasible source contributions to plant xylem water were calculated for each plant individual and each potential root water source. Minimum, median and maximum modeled plant water usage of each potential water source was highly variable (Table 14).

The vast majority of failed modeling attempts were the result of early growing season data sets. March and April sampling campaigns often yielded plant xylem water isotope values that plotted to the northeast, or below modeling solution space (e.g., Figure 30). May and June sampling campaigns also generally yielded plant xylem water isotope values that plotted below the solution space (e.g., Figure 31). In contrast, plant xylem water collected in July and September, when the vast majority of soil water was generally immobile, frequently plotted within the solution space (e.g., Figure 32). Consequently, SISUS yielded a number of modeled solutions at each field site.

Late growing season SISUS modeling revealed plant individuals using a wide variety of water sources at Lower Gauge (Figure 33; Figure 34), Treeline (Figure 35;

Figure 36) and Bogus South (Figure 37; Figure 38; Figure 39) field sites. These results illustrate several overarching trends. First of all, little is certain when the number of sources is greater than the number of isotope tracers plus one, as there are an infinite number of solutions to these xylem water mixtures. Plants with xylem water isotope values that plotted near the center of the solution isotope space generally had a wide range of feasible source contributions. Nevertheless, investigating the median modeled source contributions shows us that deep bulk soil water is the most common water source in July and September at each field site (Figure 40). However, many plants also appear to have contained larger fractions of groundwater and streamwater as the 2012 growing season progressed. Field site averaged mobile water source contributions (average of all modeled plant median source contributions on a given sampling date) to plant xylem water ranged from 13% (n=4) at Lower Gauge on 07-08-2012 to 44% (n=4) at Bogus South on 09-04-2012 (Figure 41). Note that Treeline 05-17-12 and Bogus South 06-06-12 sampling campaigns were excluded from this analysis due to few successfully modeled plant individuals. Some Yellow willow, Fire willow, Chokecherry, Rabbitbrush, Douglas-fir, and Ponderosa pine individuals were modeled to use greater than 30% mobile groundwater and streamwater.

CHAPTER SIX: DISCUSSION

6.1 The Two Water Worlds Hypothesis

Visual assessments of dual-isotope plots illustrate that woody plant xylem water plots below the LMWL the vast majority of the time, indicating that plants are transpiring at least a fractional contribution of immobile soil water (Figure 21). SISUS results validate this assumption, as xylem water sampled from trees and shrubs at each field site was generally modeled to contain larger proportions of immobile bulk soil water than mobile water sources. This extensive use of immobile water suggests that the two water worlds hypothesis may be applicable to semi-arid ecosystems. However, extensive spatiotemporal variability of water source isotope values exists in DCEW. Additionally, we sampled nine woody plant species that may interact with water resources in unique ways. Thus, a more detailed isotopic analysis is required to better evaluate the two water worlds hypothesis.

In the early growing season, when mobile soil water is generally available (Figure 12), actively-transpiring woody plants appear to use a water source that contains a unique isotopic signal that is not well represented by bulk soil water, streamwater or groundwater (Figure 22a; Figure 23a; Figure 23b). The immobile soil water collected in the late growing season (after soils dry to near or below wilting point) was the only sampled water source with an isotopic signal that plotted far enough below the local meteoric water line to potentially be the primary plant water source. Given that soil moisture generally decreased to below field capacity by mid-May to June (Figure 12),

indicating that soil water had become immobile, we can assume that limited mixing took place between mobile and immobile soil water pools during this time. Thus, we can infer that early season immobile soil water isotope values (e.g., 05-17-2012) are likely similar to late season Treeline immobile soil water isotope values (e.g., 09-07-2012).

Consequently, it is likely that the majority of plants were transpiring the unsampled immobile fraction of bulk soil water in the early growing season. This was unclear from visual inspection of the dual-isotope plots alone, because the isotopic signal of the larger fraction of mobile water overshadowed the isotopic signal of the small fraction of immobile water in bulk soil samples. As a result, the exact isotope values of early season immobile soil water are unknown.

In the late growing season (July and September), after the vast majority of soil dried to significantly below field capacity, woody plants at each field site appear to transpire water from immobile water pools. Water contained in bulk soil samples is generally more immobile when soil is this dry, and, not surprisingly, the isotope values of woody plant xylem water more closely match the isotope values of bulk soil water. This, in turn, yielded more telling visual assessments of dual-isotope plots and SISUS plant water sourcing results. SISUS results suggest that immobile water was the primary water source at each field site in the July and September sampling campaigns. However, the xylem water of some plants appears to contain greater than 30% water source contributions of groundwater and streamwater. Modeled contributions of mobile water to plant xylem water mixtures also increases as the growing season progresses. This shift from immobile soil water use to mobile groundwater and streamwater use is likely the

result of plants adapting to utilize alternative water sources as soil moisture content falls below permanent wilting point.

Isotopic tracer studies have suggested that some plants in relatively arid ecosystems actively root to mobile water (e.g., groundwater) to avoid wilting as a result of dry soils (Walter, 1971; Dawson & Ehleringer, 1991; Mensforth, Thorburn, Tyerman & Walker, 1994). In contrast, more humid catchments often present a nutrient-limited environment to plants, where soils remain above the permanent wilting point year-round. Although the vast majority of plants in DCEW appear to have adapted to transpire at least fractional contributions of immobile soil water, even when soil moisture content was below permanent wilting point, SISUS modeling suggests that increased use of groundwater or streamwater may also be a common adaptation to dry conditions.

6.2 Spatiotemporal Variability of Woody Plant Root Water Sources

The first collection of plant water samples at Treeline and Lower Gauge (03-27-2012 and 04-08-2012) shows that the majority of trees and shrubs exhibit isotopic signals unlike any of the potential root water sources (Figure 22a; Figure 23a; Figure 24a). These isotopic signals suggest that tree and shrub stem water has been subjected to a large amount of kinetic evaporative enrichment. This phenomenon may be the result of one of two scenarios. One possible scenario is that these plants are not yet actively transpiring this early in the year. If this were the case, water may have remained relatively stagnant within the stems of these plants for months. We typically assume that the stems of woody plants act as impermeable barriers to evaporation. However, bark is a porous material, and it may be possible that it breathes enough for xylem water to be subjected to evaporation, and therefore, isotopic evaporative enrichment, over the fall and winter

seasons. A second possible scenario is that these plants were taking up extremely evaporatively-enriched bulk soil water before entering senescence. If these plants had not begun actively transpiring in the new growing season and their bark acted as a perfect shield from evaporation, their stem water would reflect the isotopic signature of the last water taken up by the roots. We find the second possibility to be less likely due to the isotopically-depleted late growing season xylem water samples collected at Treeline in 2011 (see 10-14-11 and 11-29-11 sampling dates in Table 13). It is more likely that evaporative enrichment occurs through the bark when xylem water is relatively stagnant in the fall and winter seasons. The rate of such evaporation and its effect on plant water sourcing analyses is largely unknown and requires further investigation. At the very least, this early growing season data set exemplifies the need for accurate growing season definition when analyzing plant root water source under the assumption that the xylem water represents the isotopic signal of recently acquired water.

The SISUS modeling results were sparse in the early growing season. However, this is actually informative. We know that sampled plants were transpiring during the May and June sampling campaigns because the isotope values of their xylem water changed significantly from March and April values. Nevertheless, only three plant water source results were produced for the 37 plant samples collected during the May and June sampling campaigns. This is likely because we did not provide the correct water source inputs (immobile soil water isotope values) to the SISUS model, causing sourcing analyses to fail. Without the inclusion of immobile soil water isotope values in SISUS modeling solution space, sampled water sources could not account for the isotope values observed in the xylem water of woody plants in the early growing season. For example, it

was common for plants to plot significantly below the SISUS modeling solution space (e.g., Figure 31). Further research is needed to discern from what range of soil water tensions plant roots of different species are taking up water, and how such water might be extracted from the soil and analyzed isotopically (McDonnell, 2014).

Results from sampling campaigns during the active growing season showed a different trend, as trees and shrubs generally plotted both below the LMWL and within or near the range of sampled bulk soil water isotope values. However, it was not until the July and September sampling campaigns that plants more commonly plotted within the range of bulk soil water isotope values. SISUS results reflected this phenomenon, as the model produced water sourcing results for the majority of trees sampled in July and September, but failed for earlier sampling campaigns. Woody plant xylem water plotted within or below the range bulk soil water isotope values consistently over the course of the active growing season, increasing our confidence that woody plant use of immobile soil water is a full growing season phenomenon, rather than a seasonal trend. The few tree xylem water outliers that plotted above the LMWL during the active growing season typically plotted closest to deep bulk soil water isotope values, which occasionally plotted on or near the LMWL.

6.3 Inter-Species Variability of Woody Plant Root Water Sources

Hillslope Shrubs

Rabbitbrush (3 sampled at LG) and Sagebrush (3 sampled at LG and 4 at TL) generally had isotopic signals that were unique compared to co-occurring hillslope trees (Figure 22; Figure 23). This suggests that these shrubs may be competing for an entirely different water pool than the three other hillslope tree species and three riparian tree

species sampled at Lower Gauge and Treeline. Differences between tree and shrub water uptake behavior has been seen in a semi-arid environment before, where single-isotope analyses suggested that Rabbitbrush used groundwater, while Juniper and Pinyon used primarily summer precipitation, and Sagebrush used a combination of groundwater and summer precipitation (Flanagan et al., 1992). In the early growing season (03-27-2012 to 04-08-2012), Rabbitbrush and Sagebrush generally had isotopic signals closer to bulk soil water than deciduous trees (Figure 22a; Figure 23a). This may be caused by shrubs beginning to transpire earlier in the growing season than trees. In May and June, when all woody plants appear to be actively transpiring, Rabbitbrush and Sagebrush both tended to plot farther to the northeast than any of the hillslope or riparian trees, possibly indicating greater proportional use of immobile, shallow soil water. Finally, in the late growing season, July to September, both shrub species plot farther below the LMWL, but directly beneath tree isotope values. This may be indicative of use of soil water that is more immobile than the bulk soil water that we sampled. Given that exceedingly immobile soil water tends to plot farther below the LMWL, and shrubs in DCEW tend to plot farther below the LMWL than trees, it is possible that Sagebrush and Rabbitbrush have adapted to use water held at higher tension than trees in this area. Overall, Sagebrush and Rabbitbrush seem to be resourceful in their water acquisition behavior, by using immobile soil water long after its water content has fallen below the permanent wilting point. SISUS modeled feasible source contribution results also suggest that Rabbitbrush and Sagebrush may use significant fractional contributions of groundwater in the late growing season.

Deciduous Hillslope Trees

Sampled hillslope deciduous trees included Netleaf hackberry and Chokecherry. Netleaf hackberry xylem water (1 at LG) plotted within the range of bulk soil water isotope values from June to September. The Netleaf hackberry plotted farther below the LMWL as the growing season progressed, possibly illustrating use of increasingly immobile water. The trunk of this tree was approximately 1m away from an ephemeral stream that drained into Dry Creek near Lower Gauge. Note that areas of topographic convergence such as this were the only areas where Netleaf hackberry survived at this field site. This ephemeral stream had dried up at the surface before our June sampling campaign. However, the stream lied at a topographic convergence, so it is likely that shallow soil was saturated in June, but continued to dry as the summer progressed. SISUS model results suggested that this Hackberry was transpiring water with an isotopic signal similar to bulk soil water at 45 cm to 70 cm depth in July and September.

Chokecherry xylem water was sampled at all 3 field sites. Isotope values of Chokecherries at Lower Gauge plotted in the range of bulk soil water from 25 cm to 70 cm depth in June and July, while SISUS modeled use of primarily bulk soil water from 70 cm depth (Figure 22). On 09-13-2012, both Chokecherries plotted to the northeast of most bulk soil water samples, in the range of 10 cm to 25 cm bulk soil water isotope values. Given that no other plants plotted near this range, that shallow soil water was significantly below the permanent wilting point in mid-September, and the knowledge that woody plant xylem water may exhibit post-senescence evaporative fractionation, we suggest that these isotope values are indicative of Chokecherries entering senescence before other trees and shrubs. Chokecherries were only able to survive on north-facing

aspects at this location, indicating that this species is likely very water limited in this location.

Chokecherries at Treeline generally had isotopic signals that plotted within the range of bulk soil water from 45 cm to 100 cm depth (Figure 23). One exception, sampled in September, plotted on the LMWL, higher to the northeast towards groundwater than any bulk soil water isotope values. SISUS model results suggest that this Chokecherry may have used primarily groundwater at this time. This Chokecherry, TL-t11 lied high up the hillslope, roughly 37 m from Treeline Stream (Table 7). Therefore it is unlikely that its roots can reach groundwater (Schenk and Jackson, 2002), and this sample is considered an anomaly.

Chokecherries at Bogus South generally plotted within the range of bulk soil water from 45 cm to 100 cm depth. However, two of three Chokecherries plotted above the GMWL on 06-06-2012 along with some of the bulk soil water sampled at this time. It is therefore possible that these trees contain significant proportions of mobile soil water, as soils at HN were near field capacity in early June (Figure 12). Additionally, the snowpack on the hillslope to the north had only dissipated a month before this sampling campaign (Figure 8). In July and September, Chokecherries at BG generally plotted below the LMWL, within the range of bulk soil water from 45 cm to 100 cm depth. SISUS modeled source contributions confirm this assessment (Table 14). There is one outlier that plotted near the LMWL, near Dry Creek streamwater and local groundwater. SISUS results for this outlier suggest that the tree may have been using primarily groundwater and streamwater. This particular Chokecherry, BG-t5, lies just 5 m south of

the stream, so the possibility that it may have used groundwater or streamwater in response to drying soils should not be discounted.

Coniferous Hillslope Trees

Ponderosa pines were sampled from TL and BG field sites, while Douglas-fir were sampled at BG (Figure 23; Figure 24). Overall, Ponderosa pines and Douglas-firs had the most consistent isotopic signals of all sampled plant species. This may be largely the result of year-round photosynthesis. Ponderosa pines at TL (n=5) generally plotted farther below the GMWL than sampled bulk soil water sources on 03-27-2012 and 05-17-2012, with the exception of one Ponderosa pine, TL-t10, that plotted near deep bulk soil water on both dates (Figure 23). These results suggest use of immobile soil water. In July and early September, TL Ponderosa pines generally plotted within the 45 cm to 100 cm bulk soil isotope value range. However, on both sampling dates, two of the five sampled Ponderosa pines plotted nearer to the groundwater isotope value than most bulk soil water isotope values, indicating a possible proportional contribution of groundwater.

Unlike Treeline, Ponderosa pines at Bogus South plot within the bulk soil water isotope value range on every sampling date (Figure 24). SISUS model results suggest that these Ponderosa pines were using immobile soil water from 45 cm to 70 cm depth. Two Douglas-firs were sampled at BG, adjacent to Ponderosa pines. In June and July, the Douglas-firs plotted within the range of bulk soil water isotope values, usually closest to deep soil water. In contrast, in September, the two Douglas-firs plotted very near the Lower Deer Point LMWL, near the groundwater and streamwater isotope values. SISUS modeled results for two Douglas-fir indicate that they may have been using greater than 70% mobile water in July and September. These Douglas-firs lie 7 m and 14 m away

from Dry Creek (Table 7); therefore, these trees may have transitioned from bulk soil water use to groundwater use in the late growing season. They may be using groundwater and streamwater as a means of avoiding competition with the adjacent Ponderosa pines.

Riparian Zone Trees

Sampled riparian zone trees include Water birch (LG), Yellow willow (LG and TL) and Fire willow (TL) (Figure 22; Figure 23). Water birch generally plotted within the range of 25 cm to 70 cm bulk soil water isotope values, although generally nearer to groundwater isotope values than hillslope trees, possibly indicating a small proportional contribution of groundwater. SISUS results confirm that Water birch may have used roughly 20% to 30% groundwater and streamwater in September. Water birches generally plotted farther SSE of the LMWL as the growing season progressed (06-04-2012 to 09-13-2012). This trend is similar to the trend in the Netleaf hackberry xylem water isotopic signal, and may be indicative of the use of immobile soil water held at higher tension as the growing season progressed.

Yellow willow was sampled at Lower Gauge (n=1) and Treeline (n=3). None of the early season (03-27-2012 to 04-08-2012) xylem water samples plotted within the range of potential water sources. However, the Yellow willow sampled at Lower Gauge plotted along what looks like a kinetic evaporative enrichment line from 06-06-2012 to 09-13-2012. The 07-10-2012 and 09-13-2012 samples both plotted within the 25 cm to 70 cm bulk soil water range. SISUS results suggest that this Yellow willow was using primarily deep bulk soil water, but roughly 30% groundwater and streamwater in July and September.

The Yellow willows at Treeline showed a different, but equally interesting trend, and plotted within the range of bulk soil water on each sampling date from May to September. One Yellow willow plotted above the LMWL in May, but most plot closely to the isotopic signal of deep bulk soil water. The willows then plotted farther below the LMWL from 05-17-2012 to 07-09-2012, along what also looks like a kinetic evaporative enrichment line. The water source is difficult to discern on 05-17-2012, however, SISUS models it to be primarily shallow bulk soil water from 10 cm to 45 cm depth. On 07-09-2012, two Yellow willows were modeled to use large fractions of shallow soil water (Figure 35). However on 09-07-2012, these willows were modeled to use deep bulk soil water and groundwater (Figure 36). Note that Treeline stream flowed until the end of June (Figure 2). The stream may have kept adjacent soils wetter than the surrounding hillslopes, and these two willows were both located just 3 m from the edge of the stream (Table 7). It is likely that the shallow soil that these trees were accessing dried up and they had to actively root into deeper bulk soil water or a combination of groundwater and deep bulk soil water. The Fire willow plotted outside of the range of potential water sources on 03-27-2012 and 05-17-2012, and appeared to be in senescence during these early sampling campaigns. However, it plotted within the range of bulk soil water on 07-09-2012 and 09-07-2012, and its isotopic signal suggests that it may have transpired deeper bulk soil water, or a combination of groundwater and deeper soil water later in the growing season as Treeline stream dried up. SISUS results agree, suggesting that xylem water was composed of over 60% bulk soil water from roughly 100 cm depth.

Overall, the isotope values of Water birch, Yellow willow, and Fire willow indicate primarily immobile soil water use from May through early September. However,

many of the riparian trees plot closer to the LMWL (as well as groundwater and streamwater isotope values) than hillslope trees and shrubs. SISUS results suggest that these trees all use large proportional contributions of deep immobile soil water or groundwater in September. Groundwater use was overall more prevalent than streamwater use (Figure 40). However, streamwater was not available to Treeline site riparian trees in the late summer.

The isotopic signals of the nine woody plant species sampled from Dry Creek Experimental Watershed suggest species-unique adaptations to semi-arid environment conditions. Sagebrush and Rabbitbrush have unique isotopic signals, generally plotting below trees in dual-isotope space. Riparian trees and hillslope vegetation within rooting distance (25 m or less) of streams were more likely to contain significant contributions of mobile water than hillslope trees far away from streams. This finding validates our thought that these trees are generally not using mobile soil water, as plants far away from streams generally do not have root access to groundwater or streamwater, and isotopic evidence of mobile water use for these plants was limited. Further research is needed to constrain the range of tensions at which the roots of each of these tree and shrub species is capable of extracting water from the soil, and how to extract water held at this range of tensions for isotopic analysis. Until then, it will remain difficult to confidently define the depth of plant root water uptake because varying proportions of mobile and immobile water influence the bulk soil water isotopic signature, and we cannot be assured that these plants aren't discriminating against more mobile portions of bulk soil water.

CHAPTER SEVEN: CONCLUSIONS

Visual assessment of dual-isotope plots and SISUS modeled feasible water source contributions to plant xylem water agree that the most prevalent water source of trees and shrubs in Dry Creek Experimental Watershed is immobile soil water. These findings applied to woody plants at field sites ranging from 1036 m to 1680 m elevation, from a sage-steppe ecosystem to a Ponderosa pine ecosystem, and throughout the growing season. Woody plant species that used significant proportional contributions of immobile water included Chokecherry, Nettleleaf hackberry, Ponderosa pine, Douglas-fir, Yellow willow, Fire willow, Water birch, Sagebrush and Rabbitbrush. These results agree with previous results in seasonally-dry humid catchments (Renée Brooks et al., 2010; Hale, 2011; Goldsmith et al., 2012), which identified immobile soil water as the primary tree water source. While mobile soil water was not widely used, SISUS results indicate that riparian zone trees and hillslope trees and shrubs within rooting distance of streams often contained greater than 30% groundwater and streamwater in July and September. Therefore, we partially accept the two water worlds hypothesis in a semi-arid catchment, as it appears that immobile soil water is the primary woody plant water source in Dry Creek Experimental Watershed, regardless of mobile soil water availability, sampling site or species. However, we also suggest that many plants use significant proportional contributions of mobile groundwater or streamwater sources after the soil column dries below permanent wilting point.

REFERENCES

- Araguás-Araguás, L., Rozanski, K., Gonfiantini, R., & Louvat, D. (1995). Isotope effects accompanying vacuum extraction of soil water for stable isotope analyses. *Journal of Hydrology*. doi:10.1016/0022-1694(94)02636-P
- Barnes, C. J., & Allison, G. B. (1988). Tracing of water movement in the unsaturated zone using stable isotopes of hydrogen and oxygen. *Journal of Hydrology*. doi:10.1016/0022-1694(88)90184-9
- Beven, K., & Germann, P. F. (1982). Macropores and water flows in soils. *Wat. Resour. Res.*, 18(5), 1311–1325.
- Brand, W. A. (2010). RCM Letter to the Editor. *Rapid Communications in Mass Spectrometry*, 2687–2688. doi:10.1002/rcm
- Brian Leen, J., Berman, E. S. F., Liebson, L., & Gupta, M. (2012). Spectral contaminant identifier for off-axis integrated cavity output spectroscopy measurements of liquid water isotopes. *The Review of Scientific Instruments*, 83(4), 044305. doi:10.1063/1.4704843
- Brunel, J. P., Walker, G. R., Dighton, J. C., & Monteny, B. (1997). Use of stable isotopes of water to determine the origin of water used by the vegetation and to partition evapotranspiration. A case study from HAPEX-Sahel. *Journal of Hydrology*, 188-189, 466–481. doi:10.1016/S0022-1694(96)03188-5
- Cappa, C. D., Hendricks, M. B., DePaolo, D. J., & Cohen, R. C. (2003). Isotopic fractionation of water during evaporation. *Journal of Geophysical Research*, 108(D16). doi:10.1029/2003JD003597
- Cody Hale. (2011). Beyond the Paired-Catchment Approach: Isotope Tracing to Illuminate Stocks, Flows, Transit Time, and Scaling, 1–189. Retrieved from papers2://publication/uuid/3009CECC-7EE8-4B65-AC2F-F54B7FB75956
- Craig, H. (1961). Isotopic Variations in Meteoric Waters. *Science (New York, N.Y.)*, 133(3465), 1702–1703. doi:10.1126/science.133.3465.1702
- Dansgaard, W. (1964). Stable isotopes in precipitation. *Tellus A*. doi:10.3402/tellusa.v16i4.8993

- Dawson, T. E., & Ehleringer, J. R. (1991). Streamside trees that do not use stream water. *Nature*, 350(6316), 335–337. doi:10.1038/350335a0
- Dawson, T. E., & Pate, J. S. (1996). Seasonal water uptake and movement in root systems of Australian phraeatophytic plants of dimorphic root morphology: a stable isotope investigation. *Oecologia*. doi:10.1007/BF00582230
- Erhardt, E. B., Wolf, B. O., Ben-David, M., & Bedrick, E. J. (2014). Stable Isotope Sourcing Using Sampling. *Open Journal of Ecology*, 4(May), 289–298. doi:10.4236/oje.2014.46027
- Flanagan, Ehleringer, & Marshall. (1992). Differential uptake of summer precipitation among co-occurring trees and shrubs in a pinyon-juniper woodland. *Plant, Cell & ...*, 831–836. Retrieved from <http://onlinelibrary.wiley.com/doi/10.1111/j.1365-3040.1992.tb02150.x/abstract>
- Flanagan, L., & Ehleringer, J. (1991). Stable isotope composition of stem and leaf water: applications to the study of plant water use. *Functional Ecology*, 5(2). Retrieved from <http://www.jstor.org/stable/10.2307/2389264>
- Fukuda, K., & Prodon, A. (1996). Double Description Method Revisited. *Lecture Notes in Computer Science*, (1120), 91–111.
- Goldsmith, G. R., Muñoz-Villers, L. E., Holwerda, F., McDonnell, J. J., Asbjornsen, H., & Dawson, T. E. (2012). Stable isotopes reveal linkages among ecohydrological processes in a seasonally dry tropical montane cloud forest. *Ecohydrology*, 5(6), 779–790. doi:10.1002/eco.268
- Graham, C. B., Barnard, H. R., Kavanagh, K. L., & Mcnamara, J. P. (2012). Catchment scale controls the temporal connection of transpiration and diel fluctuations in stream flow. doi:10.1002/hyp
- Graham, C. B., Barnard, H. R., Kavanagh, K. L., & McNamara, J. P. (2013). Catchment scale controls the temporal connection of transpiration and diel fluctuations in streamflow. *Hydrological Processes*, 27(18), 2541–2556. doi:10.1002/hyp.9334
- Gribb, M. M., Forkutsa, I., Hansen, A., Chandler, D. G., & McNamara, J. P. (2009). The Effect of Various Soil Hydraulic Property Estimates on Soil Moisture Simulations. *Vadose Zone Journal*, 8(2), 321. doi:10.2136/vzj2008.0088
- Hewlett, J. D., & Hibbert, A. R. (1967). Factors affecting the response of small watersheds to precipitation in humid areas. In *Forest hydrology* (pp. 275–290).
- Horton, J. H., & Hawkins, R. H. (1965). Flow path of rain from soil surface to water table. *Soil Science*, 100(6), 377–383.

- Ingraham, N. L., & Shadel, C. (1992). A comparison of the toluene distillation and vacuum/heat methods for extracting soil water for stable isotopic analysis. *Journal of Hydrology*.
- Ingraham, N. L., & Taylor, B. E. (1991). Light stable isotope systematics of large-scale hydrologic regimes in California and Nevada. *Water Resources Research*.
- Kerstel, E. R. T., & Meijer, H. A. J. (2005). Optical isotope ratio measurements in hydrology. In *Isotopes in the Water Cycle: Past, Present and Future of a Developing Science* (pp. 109–123). Springer Netherlands.
- Lee, J., Fung, I., Depaolo, D. J., & Henning, C. C. (2007). Analysis of the global distribution of water isotopes using the NCAR atmospheric general circulation model. *Circulation*, *112*, 1–14. doi:10.1029/2006JD007657
- McDonnell, J. J. (2014). The two water worlds hypothesis: ecohydrological separation of water between streams and trees? *Wiley Interdisciplinary Reviews: Water*, *1*(August), n/a–n/a. doi:10.1002/wat2.1027
- McNamara, J. P., Chandler, D., Seyfried, M., & Achet, S. (2005). Soil moisture states, lateral flow, and streamflow generation in a semi-arid, snowmelt-driven catchment. *Hydrological Processes*, *19*(20), 4023–4038. doi:10.1002/hyp.5869
- Peng, H., Mayer, B., Harris, S., & Krouse, H. R. (2007). The influence of below-cloud secondary effects on the stable isotope composition of hydrogen and oxygen in precipitation at Calgary, Alberta, Canada. *Tellus, Series B: Chemical and Physical Meteorology*, *59*(4), 698–704. doi:10.1111/j.1600-0889.2007.00291.x
- Penna, D., Oliviero, O., Assendelft, R., Zuecco, G., Meerveld, I. (H. J. . Van, Anfodillo, T., ... Fontana, G. D. (2013). Tracing the Water Sources of Trees and Streams: Isotopic Analysis in a Small Pre-Alpine Catchment. *Procedia Environmental Sciences*, *19*, 106–112. doi:10.1016/j.proenv.2013.06.012
- Phillips, D. L., & Gregg, J. W. (2003). Source partitioning using stable isotopes: coping with too many sources. *Oecologia*, *136*(2), 261–9. doi:10.1007/s00442-003-1218-3
- Poulos, M. J., Pierce, J. L., Flores, A. N., & Benner, S. G. (2012). Hillslope asymmetry maps reveal widespread, multi-scale organization. *Geophysical Research Letters*, *39*(6), n/a–n/a. doi:10.1029/2012GL051283
- Renée Brooks, J., Barnard, H. R., Coulombe, R., & McDonnell, J. J. (2009). Ecohydrologic separation of water between trees and streams in a Mediterranean climate. *Nature Geoscience*, *3*(2), 100–104. doi:10.1038/ngeo722

- Renée Brooks, J., Barnard, H. R., Coulombe, R., & McDonnell, J. J. (2010). Ecohydrologic separation of water between trees and streams in a Mediterranean climate. *Nature Geoscience*, 3(2), 100–104. doi:10.1038/ngeo722
- Schultz, N. M., Griffis, T. J., Lee, X., & Baker, J. M. (2011). Identification and correction of spectral contamination in 2H/1H and 18O/16O measured in leaf, stem, and soil water. *Rapid Communications in Mass Spectrometry : RCM*, 25(21), 3360–8. doi:10.1002/rcm.5236
- Sessions, A. L. (2006). Seasonal changes in D/H fractionation accompanying lipid biosynthesis in *Spartina alterniflora*. *Geochimica et Cosmochimica Acta*, 70(9), 2153–2162. doi:10.1016/j.gca.2006.02.003
- Smith, T. J. (2010). USING SOIL MOISTURE TRENDS ACROSS TOPOGRAPHIC GRADIENTS TO EXAMINE CONTROLS ON SEMI-ARID ECOSYSTEM DYNAMICS By BOISE STATE UNIVERSITY GRADUATE COLLEGE, (May).
- Torres, R., Dietrich, W. E., Montgomery, D. R., Anderson, S. P., & Loague, K. (1998). Unsaturated zone processes and the hydrologic response of a steep, unchanneled catchment. *Water Resources Research*, 34(8), 1865. doi:10.1029/98WR01140
- Twarakavi, N. K. C., Sakai, M., & Šimůnek, J. (2009). An objective analysis of the dynamic nature of field capacity. *Water Resources Research*, 45(10), 1–9. doi:10.1029/2009WR007944
- West, a G., Goldsmith, G. R., Matimati, I., & Dawson, T. E. (2011). Spectral analysis software improves confidence in plant and soil water stable isotope analyses performed by isotope ratio infrared spectroscopy (IRIS). *Rapid Communications in Mass Spectrometry : RCM*, 25(16), 2268–74. doi:10.1002/rcm.5126
- West, A. (2006). Water extraction times for plant and soil materials used in stable isotope analysis. ... *Communications in Mass ...*, 1317–1321. doi:10.1002/rcm
- West, A., & Goldsmith, G. (2010). Discrepancies between isotope ratio infrared spectroscopy and isotope ratio mass spectrometry for the stable isotope analysis of plant and soil waters. ... *in Mass Spectrometry*, 1948–1954. doi:10.1002/rcm
- Williams, D. G. (2005). Ecohydrology of Water-Controlled Ecosystems: Soil Moisture and Plant Dynamics. *Eos, Transactions American Geophysical Union*, 86(38), 344. doi:10.1029/2005EO380008
- Wythers, K. R., Lauenroth, W. K., & Paruelo, J. M. (1999). Bare-Soil Evaporation Under Semiarid Field Conditions. *Soil Science Society of America Journal*, 63(5), 1341–1349.

Zhao, L., Xiao, H., Zhou, J., Wang, L., Cheng, G., Zhou, M., ... McCabe, M. F. (2011). Detailed assessment of isotope ratio infrared spectroscopy and isotope ratio mass spectrometry for the stable isotope analysis of plant and soil waters. *Rapid Communications in Mass Spectrometry : RCM*, 25(20), 3071–82.
doi:10.1002/rcm.5204

APPENDIX A

Tables

Table 1 Dry Creek Experimental Watershed soil properties and characteristics (USDA NRCS Web Soil Survey 01-09-12). LG = Lower Gauge, TL = Treeline, BG = Bogus South. Locations are depicted in Figure 4.

Location	Depth to Bedrock (cm)	Drainage Class	Depth to Water Table (cm)	Ksat of the Most Limiting Layer (cm/hr)	Water Capacity (cm)
BG (E and SW facing aspects)	25 - 100	Somewhat excessively drained to excessively drained	> 200	5 - 50	2.8 – 5.0
TL (N-facing aspect)	50 - 100	Somewhat excessively drained	> 200	5 - 15	7.0
Treeline (S-facing aspect)	25 - 50	Excessively drained	> 200	15 - 50	2.0
LG (N-facing aspect)	25 - 100	Excessively drained	> 200	15-50	1.8-3.0
LG (S-facing aspect)	25 - 50	Excessively drained	> 200	5-15	3.3

Table 2 Dry Creek Experimental Watershed soil texture and moisture properties (adapted from Smith, 2010). θ = Volumetric Moisture Content. HN and HS are used as proxies for Bogus South. MHN and MHS are used as proxies for Treeline. LN and LS are used as proxies for Lower Gauge. Locations are depicted in Figure 4.

Location	USDA Soil Texture Classification	Wilting Point (θ at -3 mPa)	Field Capacity (θ at -0.03 mPa)	Field Capacity (Empirically Estimated)
HN	Sandy loam	0.10	0.25	0.19
HS	Sandy loam	0.10	0.25	0.17
MHN	Sandy loam	0.10	0.25	0.19
MHS	Loamy sand	0.06	0.18	0.16
LN	Sandy loam	0.10	0.25	0.18
LS	Loamy sand (80%), Sandy loam (20%)	0.08	0.22	0.17

Table 3 **Woody plant stem water removal efficiency. Stem samples were collected from the base of tree branches or cored from the trunk at breast height (Ponderosa pine and Douglas-fir), sliced into roughly 2 cm segments and stored in pyrex test tubes capped with parafilm. Water was removed via cryogenic vacuum distillation (West, 2006). Remaining water was calculated by re-weighing the sample after placing the evacuated sample in an oven at 110°C for 24 hours. μ = gravimetric moisture content. LG = Lower Gauge, TL = Treeline, BG = Bogus South. Locations are depicted in Figure 4.**

Species	Location	Date Sampled	μ (g/g)	Evacuated Water (g)	Remaining Water (g)	Grams Evacuated Water (%)
Bitter cherry	TL	05/07/12	0.12	3.56	0.03	99.16
Water birch	LG	06/04/12	0.14	4.50	0.01	99.78
Sagebrush	LG	06/04/12	0.11	3.21	-0.03	100.94
Sagebrush	LG	06/04/12	0.10	2.72	-0.03	101.12
Pacific willow	LG	06/04/12	0.14	4.40	-0.07	101.62
Rabbitbrush	LG	06/04/12	0.08	2.05	-0.04	101.99
Bitter cherry	BG	07/08/12	0.13	3.90	0.05	98.73
Bitter cherry	BG	07/08/12	0.13	4.10	-0.01	100.24
Ponderosa pine	BG	07/08/12	0.08	2.04	-0.01	100.49
Ponderosa pine	BG	09/04/12	0.06	1.49	-0.03	102.05
Sagebrush	TL	09/07/12	0.03	0.97	0.03	97.00
Pacific willow	TL	09/07/12	0.11	3.16	0.03	99.06
Sagebrush	TL	09/07/12	0.06	1.75	0.00	100.00
Sagebrush	TL	09/07/12	0.08	2.13	0.00	100.00
Sagebrush	TL	09/07/12	0.12	3.70	0.00	100.00
Fire willow	TL	09/07/12	0.11	3.24	-0.01	100.31
Bitter cherry	TL	09/07/12	0.12	3.81	-0.03	100.79
Bitter cherry	TL	09/07/12	0.11	3.41	-0.04	101.19
Ponderosa pine	TL	09/07/12	0.09	2.30	-0.04	101.77
Sagebrush	TL	09/07/12	0.05	1.48	-0.03	102.07
Ponderosa pine	TL	09/07/12	0.06	1.48	-0.03	102.07

Table 4 Bulk soil water cryogenic vacuum extraction efficiency. Samples were stored in test tubes and capped with parafilm. Silica wool was placed above the soil during extraction to ensure that soil was not lost to the vacuum. Remaining water was calculated by re-weighing the sample after placing the evacuated sample in an oven at 110°C for 24 hours. μ = gravimetric moisture content. LG = Lower Gauge, TL = Treeline, BG = Bogus South. Locations are depicted in Figure 4.

Location	Aspect	Date Sampled	μ (g/g)	Evacuated Water (g)	Remaining Water (g)	Grams Evacuated Water (%)
LG	N	09/13/12	0.015	0.44	0.07	85.64
LG	N	09/13/12	0.018	0.47	0.13	77.85
LG	N	07/10/12	0.033	0.86	0.18	82.40
LG	N	09/13/12	0.033	0.94	0.08	91.82
LG	N	09/13/12	0.036	0.99	0.11	89.69
LG	N	09/13/12	0.065	1.57	0.07	95.51
LG	N	06/04/12	0.078	2.00	-0.02	101.01
LG	N	06/04/12	0.130	2.39	-0.01	100.42
LG	S	09/13/12	0.006	0.19	0.06	74.88
LG	S	07/10/12	0.013	0.41	0.03	92.39
LG	N	06/04/12	0.033	0.84	0.02	97.25
LG	N	07/10/12	0.043	1.27	0.09	93.13
LG	N	07/10/12	0.046	1.39	0.04	96.95
LG	N	07/10/12	0.047	1.25	0.03	97.37
LG	N	06/04/12	0.049	1.22	0.08	93.58
LG	N	06/04/12	0.053	1.45	0.00	100.00
LG	N	09/13/12	0.060	1.55	0.09	94.30
LG	N	06/04/12	0.060	1.63	0.12	92.94
LG	N	09/13/12	0.024	0.72	0.12	85.33
LG	N	09/13/12	0.025	0.73	0.16	81.68
LG	N	09/13/12	0.028	0.98	0.06	93.89
LG	N	07/10/12	0.032	0.99	0.14	87.32
LG	N	09/13/12	0.035	0.90	0.09	90.57
LG	N	07/10/12	0.040	1.26	0.06	95.18
LG	N	09/13/12	0.064	1.65	0.09	94.62
LG	N	07/10/12	0.025	0.79	0.12	86.46
LG	N	06/04/12	0.043	1.27	0.05	95.94
LG	N	06/04/12	0.044	1.27	0.04	96.67
TL	NE	05/17/12	0.082	1.70	0.01	99.42
TL	NE	05/17/12	0.102	2.28	-0.02	100.88
TL	SW	05/17/12	0.054	1.54	-0.05	103.36
TL	SW	05/17/12	0.090	1.93	-0.02	101.05
TL	SW	05/17/12	0.103	2.32	-0.08	103.57
TL	SW	05/17/12	0.125	2.58	-0.01	100.39
TL	NE	05/17/12	0.089	2.25	-0.02	100.90
TL	NE	05/17/12	0.121	2.75	0.00	100.00

TL	SW	05/17/12	0.083	1.93	-0.05	102.66
TL	SW	05/17/12	0.105	2.53	-0.01	100.40
TL	SW	05/17/12	0.108	2.54	-0.02	100.79
TL	SW	05/17/12	0.117	2.78	0.01	99.64
TL	NE	05/17/12	0.129	3.10	-0.05	101.64
TL	SW	05/17/12	0.111	2.71	-0.03	101.12
TL	NE	05/17/12	0.115	2.88	-0.03	101.05
TL	SW	05/17/12	0.113	2.87	-0.02	100.70
TL	SW	05/17/12	0.118	3.00	-0.03	101.01
TL	SW	05/17/12	0.104	2.86	-0.02	100.70
TL	SW	05/17/12	0.119	3.57	-0.03	100.85

Table 5 Dry Creek Experimental Watershed precipitation $\delta^2\text{H}$ and $\delta^{18}\text{O}$ values (‰) (adapted from Tappa, 2013). BR = Bogus Ridge. LDP = Lower Deer Point, TL = Treeline, LW = Lower Weather. BG precipitation isotope values are likely between LDP and BR values (based off of the precipitation isotopic concentration relation to elevation; Tappa, 2013). LW data is used as a proxy for Lower Gauge precipitation. Locations are depicted in Figure 4.

Location	Date	$\delta^2\text{H}$ (‰)	$\delta^{18}\text{O}$ (‰)
BR (snowmelt)	1/20/2012	-161.99	-22.17
BR (snowmelt)	1/24/2012	-104.47	-14.14
BR (snowmelt)	1/27/2012	-127.29	-16.61
BR (snowmelt)	2/2/2012	-146.64	-20.54
BR (snowmelt)	2/15/2012	-144.53	-19.95
BR (snowmelt)	2/15/2012	-114.1	-15.77
BR (snowmelt)	3/16/2012	-124.86	-16.42
BR (snowmelt)	3/17/2012	-116.57	-14.57
BR (snowmelt)	3/19/2012	-129.14	-16.94
BR (snowmelt)	3/21/2012	-135.86	-17.46
LDP	10/14/2009	-131.86	-15.51
LDP	10/14/2009	-169.81	-22.2
LDP	10/15/2009	-79.78	-9.97
LDP	10/15/2009	-63.46	-9.41
LDP	10/15/2009	-54.69	-7.64
LDP	10/19/2009	-88.57	-12.64
LDP	10/24/2009	-110.78	-15.09
LDP	10/30/2009	-88.63	-12.83
LDP	11/7/2009	-71.76	-10.56
LDP	11/13/2009	-150.39	-19.06
LDP	1/13/2010	-84.22	-11.37
LDP	1/20/2010	-131.73	-15.63
LDP	1/20/2010	-136.24	-17.27
LDP	3/29/2010	-118.34	-15.84
LDP	4/2/2010	-108.7	-14.57
LDP	4/15/2010	-125.44	-16.64
LDP	4/20/2010	-114.25	-15.17
LDP	4/21/2010	-110.42	-15.23
LDP	4/24/2010	-99.68	-12.43
LDP	5/7/2010	-101.36	-13.34
LDP	5/12/2010	-106.79	-14.07
LDP	5/19/2010	-103.61	-14.79
LDP	5/25/2010	-104.54	-14.23
LDP	5/28/2010	-100.8	-14.14
LDP	6/5/2010	-113.98	-15.2

LDP	6/7/2010	-110.87	-14.41
LDP	6/11/2010	-61.63	-8.36
LDP	6/21/2010	-71.25	-9.8
LDP	10/25/2010	-134.04	-18.47
LDP	10/27/2010	-79.52	-12.34
LDP	11/1/2010	-94.02	-13.84
LDP	11/8/2010	-126.88	-18.55
LDP	11/11/2010	-104.91	-15.2
LDP	11/15/2010	-98.53	-13.64
LDP	12/7/2010	-130.12	-16.84
LDP	1/17/2011	-148.73	-19.91
LDP	5/7/2011	-130.28	-17.78
LDP	5/16/2011	-129.08	-17.58
LDP	5/19/2011	-112.96	-15.15
LDP	5/26/2011	-83.75	-12.47
LDP	5/27/2011	-115.98	-16.06
LDP	6/7/2011	-100.52	-13.74
LDP	6/9/2011	-103.45	-14.71
LDP	6/29/2011	-84	-9.91
LDP	6/30/2011	-99.43	-12.31
LDP	9/11/2011	-70.64	-10.18
LDP	9/15/2011	-39.23	-3.19
LDP	9/16/2011	-52.59	-7.71
LDP	10/5/2011	-93.89	-13.54
LDP	10/7/2011	-167.9	-22.76
LDP	10/17/2011	-119.8	-16.48
LDP	11/5/2011	-112.21	-16.53
LDP	11/13/2011	-85.62	-13.04
LDP	11/22/2011	-167.41	-23.48
LDP	12/27/2011	-101.51	-13.63
LDP	12/31/2011	-100.36	-13.87
LDP	1/20/2012	-157.65	-21.76
LDP	1/22/2012	-100.55	-14.33
LDP	1/24/2012	-158.73	-21.37
LDP	1/27/2012	-104.95	-12.95
LDP	2/3/2012	-135.99	-18.44
LDP	2/15/2012	-133.19	-18.27
LDP	3/18/2012	-130.16	-17.56
LDP	3/19/2012	-124.73	-16.08
LDP	3/21/2012	-122.04	-15.74
LDP	3/27/2012	-96.29	-13.33
LDP	3/28/2012	-113.09	-15.05
LDP	4/19/2012	-105.75	-14.54

LDP	4/26/2012	-121.82	-16.58
LDP	4/27/2012	-110.39	-12.88
LDP	5/1/2012	-75.86	-11.09
LDP	5/5/2012	-92.18	-13.09
LDP	5/23/2012	-66.86	-9.86
LW	10/6/2009	-137.96	-19.2
LW	10/19/2009	-71.19	-9.59
LW	10/19/2009	-70.8	-9.69
LW	10/24/2009	-83.97	-10.63
LW	10/24/2009	-85.12	-10.81
LW	10/30/2009	-93.39	-12.69
LW	11/7/2009	-53.15	-7.15
LW	11/13/2009	-140.93	-18.66
LW	11/13/2009	-140.82	-18.65
LW	1/7/2010	-112.83	-15.65
LW	1/25/2010	-140.9	-17.87
LW	1/27/2010	-133.85	-18.1
LW	2/1/2010	-179.15	-23.77
LW	2/10/2010	-127.65	-15.35
LW	2/17/2010	-75.34	-9.42
LW	2/24/2010	-164.83	-20.85
LW	2/28/2010	-110.39	-12.95
LW	3/5/2010	-100.24	-12.65
LW	3/9/2010	-96.81	-12.79
LW	3/15/2010	-118.51	-14.75
LW	3/26/2010	-84.71	-11.51
LW	4/2/2010	-80.13	-9.93
LW	4/3/2010	-125.32	-15.95
LW	4/13/2010	-98.57	-12.35
LW	4/21/2010	-75.81	-10.54
LW	4/30/2010	-114.87	-14.96
LW	5/7/2010	-80.88	-10.71
LW	5/12/2010	-102.44	-13.79
LW	5/19/2010	-72.61	-10.22
LW	5/24/2010	-117.97	-16.04
LW	5/30/2010	-91.87	-12.27
LW	6/1/2010	-70.63	-6.94
LW	6/5/2010	-100.12	-12.39
LW	6/11/2010	-43.32	-4.75
LW	6/21/2010	-49.32	-5.72
LW	10/25/2010	-127.3	-16.33
LW	10/27/2010	-72.94	-11.43
LW	11/1/2010	-74.22	-10.22

LW	11/8/2010	-109.63	-15.45
LW	11/15/2010	-83.27	-11.35
LW	12/7/2010	-144.44	-19.59
LW	12/7/2010	-144.93	-19.8
LW	12/13/2010	-70.6	-10.24
LW	12/15/2010	-129.92	-17.2
LW	12/27/2010	-133.9	-17.96
LW	12/29/2010	-177.12	-23.35
LW	1/17/2011	-123.45	-16.19
LW	1/25/2011	-91.66	-12.8
LW	3/8/2011	-149.49	-19.3
LW	3/11/2011	-105.21	-13.89
LW	3/14/2011	-87.44	-10.61
LW	3/17/2011	-111.05	-14.41
LW	3/22/2011	-134.18	-18.17
LW	3/25/2011	-120.8	-16.53
LW	3/31/2011	-130.9	-17.19
LW	4/2/2011	-92.92	-12.85
LW	4/5/2011	-72.83	-9.86
LW	4/17/2011	-139.78	-18.84
LW	4/22/2011	-105	-13.25
LW	4/26/2011	-98	-13.25
LW	4/30/2011	-95.71	-12.79
LW	5/7/2011	-102.03	-12.75
LW	5/8/2011	-129.92	-17.19
LW	5/16/2011	-124.06	-16.73
LW	5/19/2011	-94.55	-12.79
LW	5/27/2011	-94.26	-12.72
LW	6/2/2011	-121.64	-16.51
LW	6/7/2011	-80.33	-11.14
LW	6/9/2011	-86.11	-12.09
LW	6/29/2011	-72.75	-7.23
LW	6/30/2011	-80.71	-7.52
LW	9/16/2011	-39.06	-5.04
LW	10/5/2011	-82.01	-11.21
LW	10/7/2011	-152.86	-20.46
LW	10/11/2011	-142.84	-18.32
LW	10/17/2011	-110.68	-14.79
LW	11/5/2011	-109.63	-15.77
LW	11/22/2011	-126.83	-17.34
LW	12/29/2011	-107.1	-13.51
LW	12/31/2011	-84.29	-11.25
LW	1/20/2012	-148.88	-20.26

LW	1/24/2012	-127.75	-16.59
LW	1/27/2012	-98.91	-12.08
LW	2/2/2012	-147.88	-20.16
LW	2/15/2012	-103.93	-13.98
LW	2/27/2012	-93.24	-11.83
LW	3/16/2012	-112.53	-14.88
LW	3/18/2012	-119.65	-15.35
LW	3/19/2012	-125.82	-16.58
LW	3/21/2012	-118.51	-15
LW	3/26/2012	-84.2	-12.35
LW	3/28/2012	-113.94	-15.27
LW	4/19/2012	-83.53	-10.24
LW	4/26/2012	-117.88	-15.34
LW	4/27/2012	-116.91	-15.37
LW	5/1/2012	-62.7	-7.5
LW	5/5/2012	-93.44	-12.75
LW	5/23/2012	-60.59	-7.86
TL	10/6/2009	-153.53	-21.27
TL	10/14/2009	-144.21	-18.35
TL	10/15/2009	-58.8	-8.64
TL	10/19/2009	-84.25	-12.38
TL	10/24/2009	-105.49	-14.32
TL	10/30/2009	-90.29	-12.75
TL	11/7/2009	-66.66	-10.15
TL	11/13/2009	-149.07	-19.81
TL	1/20/2010	-128.18	-16.56
TL	1/25/2010	-150.96	-19.74
TL	1/27/2010	-151.14	-19.94
TL	1/30/2010	-149.72	-19.49
TL	2/10/2010	-147.14	-19.07
TL	2/17/2010	-135.56	-17.26
TL	3/5/2010	-140.51	-18.14
TL	3/9/2010	-134.86	-17.56
TL	3/12/2010	-121.95	-15.72
TL	3/26/2010	-63.32	-7.82
TL	3/29/2010	-102.06	-13.27
TL	4/2/2010	-75.07	-10.13
TL	4/7/2010	-100.01	-12.89
TL	4/13/2010	-107.13	-13.81
TL	4/14/2010	-109.23	-14.24
TL	4/21/2010	-91.98	-12.59
TL	4/24/2010	-84.54	-11.06
TL	4/24/2010	-84.05	-11.09

TL	4/30/2010	-107.65	-13.85
TL	5/7/2010	-110.79	-15.48
TL	5/12/2010	-109.57	-15.5
TL	5/19/2010	-96.41	-13.25
TL	5/24/2010	-104.49	-14.64
TL	5/28/2010	-96.57	-13.4
TL	5/30/2010	-106	-14.45
TL	6/1/2010	-84.04	-10.5
TL	6/7/2010	-108.24	-13.69
TL	6/11/2010	-50.36	-6.43
TL	6/21/2010	-68.52	-9.61
TL	10/25/2010	-130.23	-17.48
TL	10/27/2010	-71.62	-11.79
TL	11/1/2010	-86.33	-12.58
TL	11/8/2010	-123.23	-17.59
TL	11/11/2010	-95.71	-13.97
TL	11/15/2010	-95.66	-13.1
TL	12/7/2010	-139.72	-19.34
TL	12/9/2010	-123.57	-16.85
TL	12/9/2010	-147.1	-20.6
TL	12/13/2010	-85.83	-12.44
TL	12/13/2010	-126.81	-17.85
TL	12/15/2010	-139.07	-19.26
TL	12/15/2010	-140.31	-19.15
TL	12/16/2010	-133.99	-18.13
TL	12/27/2010	-148.37	-19.72
TL	1/17/2011	-131.84	-17.99
TL	1/17/2011	-150.31	-20.2
TL	1/20/2011	-108.85	-15.01
TL	1/20/2011	-142.84	-19.07
TL	1/28/2011	-106.81	-14.82
TL	1/28/2011	-117.58	-14.66
TL	3/3/2011	-120.03	-15.63
TL	3/8/2011	-118.47	-15.81
TL	3/11/2011	-115.21	-15.1
TL	3/14/2011	-96.02	-13.04
TL	3/14/2011	-113.29	-15.09
TL	3/18/2011	-118.22	-16.03
TL	3/18/2011	-103.48	-14.28
TL	3/22/2011	-127.94	-17.13
TL	3/22/2011	-129.47	-17.22
TL	3/25/2011	-110.44	-15.64
TL	3/31/2011	-138.09	-18.18

TL	4/5/2011	-87.93	-12.73
TL	4/17/2011	-153.13	-21.14
TL	4/22/2011	-121.42	-15.77
TL	4/23/2011	-123.92	-16.63
TL	4/27/2011	-97.69	-13.78
TL	4/30/2011	-110.82	-14.82
TL	5/7/2011	-115.87	-15.16
TL	5/8/2011	-145.33	-19.78
TL	5/16/2011	-130.25	-17.52
TL	5/19/2011	-102.32	-13.66
TL	5/26/2011	-103.36	-14.79
TL	5/27/2011	-106.05	-14.69
TL	6/7/2011	-97.07	-13.46
TL	6/9/2011	-101.57	-14.57
TL	6/29/2011	-70.04	-7.41
TL	6/30/2011	-98.41	-11.59
TL	9/11/2011	-49.55	-6.37
TL	9/16/2011	-50.01	-7.07
TL	10/5/2011	-90.35	-12.5
TL	10/7/2011	-168.45	-22.6
TL	10/11/2011	-148.06	-19.6
TL	10/17/2011	-118.7	-16.34
TL	11/5/2011	-119.8	-15.98
TL	11/13/2011	-90.84	-13.99
TL	11/22/2011	-154.88	-21.78
TL	12/29/2011	-117.55	-15.73
TL	1/20/2012	-166.6	-22.57
TL	1/24/2012	-112.34	-15.87
TL	1/27/2012	-114.21	-14.99
TL	2/15/2012	-129.26	-17.7
TL	2/27/2012	-92.72	-12.69
TL	3/16/2012	-113.38	-15.55
TL	3/18/2012	-123.6	-16.27
TL	3/19/2012	-128.51	-16.1
TL	3/21/2012	-127.57	-16.82
TL	3/21/2012	-125.86	-16.42
TL	3/27/2012	-89.13	-12.89
TL	3/27/2012	-93.26	-13.27
TL	3/28/2012	-121.26	-15.89
TL	4/19/2012	-99.01	-13.6
TL	4/26/2012	-141.65	-19.15
TL	4/27/2012	-121.38	-16.53
TL	5/1/2012	-75.04	-10.38

TL	5/5/2012	-91.21	-12.56
TL	5/23/2012	-68.35	-9.78

Table 6 Dry Creek Experimental Watershed seasonally-weighted mean precipitation isotope values. LG = Lower Gauge, TL = Treeline, BG = Bogus South. Locations are depicted in Figure 4.

Location	$\delta^2\text{H}$	σ	$\delta^{18}\text{O}$	σ
DCEW	-110.12	27.54	-14.79	3.71
LG	-106.33	28.78	-14.00	4.14
TL	-112.72	26.21	-15.24	3.45
LDP	-109.63	27.57	-14.87	3.65

Table 7 Dry Creek Experimental Watershed plant and soil sample locations. NAD 83 Datum. Soils associated with a plant were sampled from within 5m of the plant trunk. LG = Lower Gauge, TL = Treeline, BG = Bogus South. Distance to Stream = the distance to Dry Creek or Treeline Stream. Distance to Tributary = the distance to the nearest tributary of Dry Creek or Treeline Stream. Locations are depicted in Figure 4.

Common Name	Plant	Aspect	Latitude	Longitude	Distance to Stream (m)	Distance to Tributary (m)
Chokecherry	BG-t5	E	43.742103	-116.099789	5	NaN
Chokecherry	BG-t6	SW	43.742128	-116.099425	6	NaN
Chokecherry	BG-t7	SW	43.741886	-116.099336	21	NaN
Douglas-fir	BG-t2	E	43.74142564	-116.0994307	7	NaN
Douglas-fir	BG-t4	E	43.74143813	-116.099612	14	NaN
Ponderosa pine	BG-t1	E	43.74142564	-116.0994307	6	NaN
Ponderosa pine	BG-t3	E	43.74143813	-116.099612	13	NaN
Ponderosa pine	BG-t8	SW	43.741833	116.099561	23	NaN
Chokecherry	LG-n-t2	N	43.68812009	-116.1783809	15	NaN
Chokecherry	LG-n-t4	N	43.68786243	-116.1783903	41	NaN
Netleaf hackberry	LG-s-t6	S	43.68845025	-116.1783581	25	1
Rabbitbrush	LG-n-s2	N	43.68815957	-116.1784719	12	NaN
Rabbitbrush	LG-n-s3	N	43.68790886	-116.1782153	33	NaN
Rabbitbrush	LG-s-s5	S	43.68893808	-116.178689	69	NaN
Sagebrush	LG-n-s1	N	43.68821195	-116.178339	14	NaN
Sagebrush	LG-n-s5	N	43.68765045	-116.1782956	63	NaN
Sagebrush	LG-s-s1	S	43.68844329	-116.178352	19	7
Sagebrush	LG-s-s2	S	43.68844329	-116.178352	25	1
Water birch	LG-n-t1	N	43.68826166	-116.1783232	1	NaN
Water birch	LG-s-t1	S	43.68828219	-116.1784062	1	4
Water birch	LG-s-t10	S	43.68834724	-116.1789129	4	NaN
Water birch	LG-s-t3	S	43.68836082	-116.178643	6	NaN
Yellow willow	LG-s-t2	S	43.6884355	-116.1786365	1	NaN
Chokecherry	TL-t11	SW	43.72983514	-116.1393271	37	NaN
Chokecherry	TL-t5	SW	43.73049648	-116.139181	26	10
Chokecherry	TL-t7	SW	43.73038692	-116.1394114	7	NaN
Ponderosa pine	TL-t1	NE	43.73002566	-116.1391113	7	NaN

Ponderosa pine	TL-t10	SW	43.72982961	-116.139343	38	NaN
Ponderosa pine	TL-t6	SW	43.73050578	-116.1392054	26	13
Ponderosa pine	TL-t8	NE	43.73051341	-116.1399757	3	NaN
Ponderosa pine	TL-t9	NE	43.73055322	-116.1399651	4	NaN
Sagebrush	TL-s1	S	43.73014217	-116.1389019	15	NaN
Sagebrush	TL-s2	S	43.73073134	-116.1396845	29	NaN
Sagebrush	TL-s3	NE	43.73012767	-116.1399178	43	NaN
Sagebrush	TL-s4	NE	43.72981972	-116.1393533	38	NaN
Fire willow	TL-t4	SW	43.73027788	-116.1391005	12	3
Yellow willow	TL-t12	SW	43.73045323	-116.139701	3	NaN
Yellow willow	TL-t2	SW	43.73019054	-116.1390822	3	NaN
Yellow willow	TL-t3	SW	43.73039505	-116.1394285	3	NaN

Table 8 Dry Creek Experimental Watershed bulk soil water $\delta^2\text{H}$ values (‰). Columns are organized by depth of bulk soil sample. Bulk soil water samples were taken from within 5 m of the plant individual listed in the first column. LG = Lower Gauge, TL = Treeline, BG = Bogus South. Locations are depicted in Figure 4. Soil sample coordinates are listed in Table 7.

Plant	Date Sampled	$\delta^2\text{H}$ 10 cm	$\delta^2\text{H}$ 25 cm	$\delta^2\text{H}$ 45 cm	$\delta^2\text{H}$ 70 cm	$\delta^2\text{H}$ 100 cm
BG-t1	11/29/11	-104.82	-126.67			
BG-t1	06/06/12	-103.41	-108.02			
BG-t1	07/08/12	-100.89				
BG-t1	09/04/12	-104.90	-119.45		-127.84	
BG-t2	11/29/11					
BG-t2	06/06/12		-120.49			
BG-t2	07/08/12			-109.54		
BG-t2	09/04/12		-126.00	-121.29		
BG-t3	11/29/11			-135.98	-127.13	
BG-t3	06/06/12	-120.73		-131.36	-121.73	-117.92
BG-t3	07/08/12			-117.47	-127.84	-129.67
BG-t3	09/04/12	-81.10		-137.71		
BG-t5	06/06/12	-127.61	-126.53			
BG-t5	07/08/12	-122.55				
BG-t5	09/04/12	-109.46	-126.43			
BG-t6	06/06/12	-117.11		-118.27	-144.73	
BG-t6	07/08/12	-123.39		-138.09	-131.25	
BG-t6	09/04/12	-128.80	-147.44	-128.61		
BG-t7	06/06/12	-118.52	-122.18	-124.02	-123.64	-124.82
BG-t7	07/08/12	-121.10			-125.91	
BG-t7	09/04/12	-128.83	-105.89	-120.96	-125.39	
LG-n-s1	08/15/11	-98.27		-120.71		
LG-n-s1	11/27/11	-126.40	-118.01	-123.09	-118.08	-133.17
LG-n-s1	04/08/12	-107.85	-106.72	-115.90	-119.71	
LG-n-s1	06/04/12	-111.95	-109.74	-106.27		
LG-n-s1	07/10/12	-103.05	-104.29	-117.07	-124.57	
LG-n-s1	09/13/12		-102.65	-127.15	-129.45	
LG-n-s2	04/08/12	-103.58	-114.83	-112.10		
LG-n-s2	06/04/12			-109.66		
LG-n-s2	09/13/12	-110.23	-145.32	-142.40		
LG-n-s2	07/10/12	-108.25	-115.29	-125.30	-147.79	
LG-n-s3	06/29/11	-127.73	-121.01			
LG-n-s3	04/08/12	-102.85	-113.99	-120.48		
LG-n-s3	06/04/12	-98.91	-106.18	-133.97		
LG-n-s3	07/10/12	-116.66	-122.63	-130.41	-128.19	

LG-n-s3	09/13/12	-132.90		-151.05		
LG-n-s5	08/15/11			-135.72		
LG-n-s5	04/08/12	-138.27	-118.23	-124.25	-136.08	
LG-n-s5	06/04/12	-118.08	-133.81	-127.23	-127.82	
LG-n-s5	07/10/12	-113.53	-144.92	-140.36	-139.30	
LG-n-s5	09/13/12	-114.34	-130.37	-138.56		
LG-n-t1	08/02/11		-125.05	-128.46		
LG-n-t1	08/15/11		-118.53			
LG-n-t1	04/08/12	-112.31				
LG-n-t1	06/04/12	-102.77			-111.91	
LG-n-t1	07/10/12	-97.42	-115.50	-115.73	-134.14	
LG-n-t1	09/13/12	-100.44	-123.66			
LG-n-t2	07/15/11	-118.84				
LG-n-t2	08/15/11	-125.78				
LG-n-t2	04/08/12	-114.17	-105.72	-117.65		
LG-n-t2	06/04/12		-108.57	-124.55		
LG-n-t2	09/13/12	-105.83	-117.71			
LG-n-t3	06/29/11	-112.26	-122.95			
LG-n-t3	08/15/11	-105.74				
LG-n-t4	06/29/11	-123.97	-105.13		-137.28	
LG-n-t4	04/08/12	-105.26	-111.94	-120.09		
LG-n-t4	06/04/12	-126.97	-132.98	-131.20		
LG-n-t4	07/10/12	-110.63	-127.49	-114.58		
LG-n-t4	09/13/12	-117.07	-121.35	-139.69		
LG-n-t7	08/02/11	-130.49				
LG-s-s2	07/19/11	-108.13				
LG-s-s2	11/27/11	-102.09		-133.16		
LG-s-s2	06/04/12	-118.98	-122.43			
LG-s-s2	07/10/12	-108.61	-128.47	-131.79		
LG-s-s2	09/13/12	-107.04	-114.23			
LG-s-s5	07/19/11			-120.63		
LG-s-s5	11/27/11					
LG-s-s5	04/08/12	-111.82				
LG-s-s5	06/04/12	-94.38	-106.89			
LG-s-s5	07/10/12	-123.80				
LG-s-s5	09/13/12	-127.02	-103.15			
LG-s-t1	04/08/12	-133.81				
LG-s-t1	06/04/12	-118.23	-121.68	-104.26		
LG-s-t1	09/13/12	-98.82		-132.84	-133.90	
LG-s-t2	07/10/12	-113.65	-112.05			
LG-s-t10	06/04/12	-111.98	-102.87	-106.42		
TL-s1	03/27/12	-104.39	-123.50	-126.27	-124.61	
TL-s1	05/17/12	-112.49	-108.99	-116.16	-121.68	-125.63

TL-s1	09/07/12			-130.18	-145.77	
TL-s2	03/27/12	-127.62		-128.89		
TL-s2	05/17/12	-117.27	-117.74	-120.25		
TL-s2	07/09/12	-96.39				
TL-s2	09/07/12	-95.74		-137.93		
TL-s3	03/27/12	-111.01	-123.81	-130.98	-139.49	
TL-s3	05/17/12	-117.75	-109.84	-129.96	-133.57	
TL-s3	07/09/12	-112.16		-149.38	-143.15	
TL-s3	09/07/12	-130.73		-124.00	-134.16	-139.93
TL-t1	03/27/12	-129.69	-124.46	-126.28	-124.12	
TL-t1	05/17/12	-116.82		-126.19		-126.95
TL-t1	07/09/12	-101.39		-133.36	-138.91	
TL-t1	09/07/12			-147.45	-140.10	-139.47
TL-t10	10/14/11	-133.44	-123.76	-135.26	-140.82	
TL-t10	03/27/12	-117.78	-121.78	-126.04		
TL-t10	07/09/12	-118.24			-135.32	-139.88
TL-t10	09/07/12			-136.31	-149.91	-161.36
TL-t11	05/17/12		-109.75			
TL-t13	08/11/11	-125.73	-123.94	-126.09		
TL-t13	10/14/11		-120.63			
TL-t2	08/11/11					
TL-t2	10/14/11	-142.44	-131.19	-135.67	-138.17	
TL-t2	07/09/12	-116.71		-123.90	-129.22	-128.03
TL-t2	09/07/12	-124.92				
TL-t3	05/17/12	-116.35	-123.94			
TL-t3	09/07/12	-127.85	-130.22			
TL-t4	10/14/11	-135.94				
TL-t4	05/17/12	-121.03	-120.43			
TL-t4	07/09/12	-93.83	-115.14			
TL-t4	09/07/12	-99.58	-108.90			
TL-t5	08/11/11	-125.08			-131.79	
TL-t5	10/14/11		-134.69	-136.75	-136.92	
TL-t5	03/27/12	-103.02		-120.67		
TL-t5	05/17/12	-128.60	-112.25	-117.44	-122.29	-131.55
TL-t5	07/09/12	-63.97		-128.13	-123.09	-137.55
TL-t5	09/07/12	-98.23			-103.44	
TL-t7	05/17/12	-120.77	-115.72	-120.23	-122.99	-123.57
TL-t8	10/14/11	-143.34				
TL-t8	03/27/12		-121.23			
TL-t8	05/17/12	-126.76	-113.81			
TL-t8	07/09/12		-132.16			
TL-t8	09/07/12	-99.18	-104.61			
TL-t9	10/14/11	-110.19	-110.35	-126.72		

Table 9 Dry Creek Experimental Watershed soil $\delta^{18}\text{O}$ values (%). Columns are organized by depth of bulk soil sample. Bulk soil water samples were taken from within 5 m of the plant individual listed in the first column. LG = Lower Gauge, TL = Treeline, BG = Bogus South. Locations are depicted in Figure 4. Soil sample coordinates are listed in Table 7.

Plant Individual	Date Sampled	$\delta^{18}\text{O}$ 10 cm	$\delta^{18}\text{O}$ 25 cm	$\delta^{18}\text{O}$ 45 cm	$\delta^{18}\text{O}$ 70 cm	$\delta^{18}\text{O}$ 100 cm
BG-t1	11/29/11	-13.22	-16.18			
BG-t1	06/06/12	-15.20	-15.30			
BG-t1	07/08/12	-11.91				
BG-t1	09/04/12	-8.73	-9.84		-17.01	
BG-t2	11/29/11					
BG-t2	06/06/12		-15.72			
BG-t2	07/08/12			-13.39		
BG-t2	09/04/12		-16.18	-14.75		
BG-t3	11/29/11			-16.25	-16.10	
BG-t3	06/06/12	-15.57		-15.90	-15.08	-16.35
BG-t3	07/08/12			-12.69	-14.85	-16.97
BG-t3	09/04/12	-5.37		-16.55		
BG-t5	06/06/12	-16.32	-17.56			
BG-t5	07/08/12	-12.47				
BG-t5	09/04/12	-10.49	-13.69			
BG-t6	06/06/12	-15.23		-16.47	-19.51	
BG-t6	07/08/12	-14.44		-18.40	-17.69	
BG-t6	09/04/12	-15.73	-17.39	-16.48		
BG-t7	06/06/12	-13.78	-14.98	-15.47	-15.42	-15.52
BG-t7	07/08/12	-15.37			-15.16	
BG-t7	09/04/12	-13.95	-8.69	-16.16	-15.88	
LG-n-s1	08/15/11	-10.75		-14.12		
LG-n-s1	11/27/11	-16.01	-13.16	-13.73	-13.51	-16.55
LG-n-s1	04/08/12	-13.79	-13.54	-14.60	-15.18	
LG-n-s1	06/04/12	-14.43	-14.46	-12.28		
LG-n-s1	07/10/12	-5.56	-8.20	-11.44	-14.47	
LG-n-s1	09/13/12		-6.34	-14.42	-15.93	
LG-n-s2	04/08/12	-12.06	-14.84	-14.39		
LG-n-s2	06/04/12			-13.07		
LG-n-s2	09/13/12	-8.63	-15.43	-16.26		
LG-n-s2	07/10/12	-8.13	-11.22	-11.90	-18.33	
LG-n-s3	06/29/11	-14.53	-14.08			
LG-n-s3	04/08/12	-12.88	-14.19	-13.66		
LG-n-s3	06/04/12	-8.89	-11.05	-17.01		
LG-n-s3	07/10/12	-10.64	-15.34	-15.34	-15.40	

LG-n-s3	09/13/12	-14.74		-17.01		
LG-n-s5	08/15/11			-16.88		
LG-n-s5	04/08/12	-17.41	-13.64	-15.77	-17.15	
LG-n-s5	06/04/12	-13.67	-15.73	-15.36	-15.91	
LG-n-s5	07/10/12	-10.25	-18.26	-18.23	-17.13	
LG-n-s5	09/13/12	-8.84	-11.64	-17.13		
LG-n-t1	08/02/11		-13.54	-15.10		
LG-n-t1	08/15/11		-11.94			
LG-n-t1	04/08/12	-14.42				
LG-n-t1	06/04/12	-11.39			-12.58	
LG-n-t1	07/10/12	-8.01	-12.74	-14.43	-14.52	
LG-n-t1	09/13/12	-6.44	-13.75			
LG-n-t2	07/15/11	-12.14				
LG-n-t2	08/15/11	-12.10				
LG-n-t2	04/08/12	-12.65	-12.57	-16.40		
LG-n-t2	06/04/12		-11.49	-15.18		
LG-n-t2	09/13/12	-4.73	-11.07			
LG-n-t3	06/29/11	-11.91	-15.09			
LG-n-t3	08/15/11	-11.44				
LG-n-t4	06/29/11	-15.19	-9.02		-16.78	
LG-n-t4	04/08/12	-11.80	-14.02	-15.16		
LG-n-t4	06/04/12	-14.68	-15.41	-16.14		
LG-n-t4	07/10/12	-9.61	-15.73	-12.25		
LG-n-t4	09/13/12	-9.55	-13.12	-16.55		
LG-n-t7	08/02/11	-16.26				
LG-s-s2	07/19/11	-10.05				
LG-s-s2	11/27/11	-14.27		-16.39		
LG-s-s2	06/04/12	-14.81	-15.46			
LG-s-s2	07/10/12	-5.47	-15.11	-16.02		
LG-s-s2	09/13/12	-4.05	-9.07			
LG-s-s5	07/19/11			-13.68		
LG-s-s5	11/27/11					
LG-s-s5	04/08/12	-13.72				
LG-s-s5	06/04/12	-8.55	-11.84			
LG-s-s5	07/10/12	-14.87				
LG-s-s5	09/13/12	-16.48	-1.41			
LG-s-t1	04/08/12	-17.03				
LG-s-t1	06/04/12	-15.28	-15.77	-10.08		
LG-s-t1	09/13/12	-3.61		-14.71	-15.98	
LG-s-t2	07/10/12	-11.82	-12.56			
LG-s-t10	06/04/12	-13.50	-13.04	-13.45		
TL-s1	03/27/12	-14.93	-16.85	-17.59	-17.68	
TL-s1	05/17/12	-14.17	-13.74	-14.90	-15.77	-16.31

TL-s1	09/07/12			-12.66	-18.82	
TL-s2	03/27/12	-17.87		-17.85		
TL-s2	05/17/12	-15.01	-15.71	-15.80		
TL-s2	07/09/12	-8.14				
TL-s2	09/07/12	-1.24		-16.57		
TL-s3	03/27/12	-14.63	-17.84	-17.98	-19.75	
TL-s3	05/17/12	-14.76	-14.39	-17.14	-17.60	
TL-s3	07/09/12	-8.87		-19.01	-18.28	
TL-s3	09/07/12	-16.06		-15.37	-17.39	-17.80
TL-t1	03/27/12	-18.15	-17.15	-17.72	-17.12	
TL-t1	05/17/12	-14.35		-16.35		-17.07
TL-t1	07/09/12	-9.45		-17.40	-17.51	
TL-t1	09/07/12			-17.97	-16.80	-17.62
TL-t10	10/14/11	-16.23	-14.69	-16.96	-17.81	
TL-t10	03/27/12	-16.53	-17.03	-17.35		
TL-t10	07/09/12	-12.97			-17.36	-17.86
TL-t10	09/07/12			-18.14	-19.24	-20.79
TL-t11	05/17/12		-13.89			
TL-t13	08/11/11	-15.95	-15.56	-16.24		
TL-t13	10/14/11		-13.53			
TL-t2	08/11/11					
TL-t2	10/14/11	-18.47	-16.05	-16.82	-17.89	
TL-t2	07/09/12	-14.37		-15.26	-17.60	-18.24
TL-t2	09/07/12	-12.18				
TL-t3	05/17/12	-14.72	-16.13			
TL-t3	09/07/12	-10.01	-13.17			
TL-t4	10/14/11	-18.43				
TL-t4	05/17/12	-15.85	-15.80			
TL-t4	07/09/12	-5.39	-11.98			
TL-t4	09/07/12	-1.55	-7.93			
TL-t5	08/11/11	-14.06			-15.10	
TL-t5	10/14/11		-16.55	-15.96	-16.70	
TL-t5	03/27/12	-13.95		-14.96		
TL-t5	05/17/12	-16.11	-14.03	-14.48	-15.33	-16.69
TL-t5	07/09/12	-2.49		-15.45	-13.98	-17.53
TL-t5	09/07/12	-2.50			-5.80	
TL-t7	05/17/12	-15.20	-14.69	-15.43	-16.37	-16.27
TL-t8	10/14/11	-17.21				
TL-t8	03/27/12		-16.65			
TL-t8	05/17/12	-14.77	-14.40			
TL-t8	07/09/12		-16.04			
TL-t8	09/07/12	-6.03	-7.35			
TL-t9	10/14/11	-11.29	-13.06	-16.50		

Table 10 Spatiotemporal analysis of soil water $\delta^{18}\text{O}$ variance in Dry Creek Experimental Watershed. Field sites included Lower Gauge, Treeline and Bogus South (Figure 4). Lower gauge aspects are N-facing and S-facing, Treeline aspects are NE-facing and SW-facing and Bogus South aspects are E-facing and SW-facing. Depths of soil analyzed included 10 cm, 25 cm, 45 cm, 70 cm and 100 cm depths. Sampling dates were grouped into nearest spatial neighbor groups for each field site (e.g., BG on 07-08-2012, TL on 07-09-2012 and LG on 07-10-2012).

Date Range	Source	Sum Sq.	d.f.	Mean Sq.	F	p-value
All	Site	135.05	2	67.527	7.53	0.0006
	Aspect	10.73	1	10.731	1.2	0.2749
	Depth	729.79	4	182.448	20.34	0
	Error	2591.9	289	8.969		
	Total	3569.18	296			
03-27 to 04-28	Site	44.801	1	44.8011	22.95	0
	Aspect	0.005	1	0.005	0	0.9601
	Depth	18.959	3	6.3196	3.24	0.033
	Error	72.238	37	1.9524		
	Total	163.862	42			
05-17 to 06-06	Site	58.421	2	29.2107	12.06	0
	Aspect	2.495	1	2.4945	1.03	0.3137
	Depth	21.259	4	5.3146	2.19	0.0786
	Error	167.086	69	2.4215		
	Total	262.396	76			
07-08 to 07-10	Site	17.564	2	8.782	1.13	0.3309
	Aspect	2.522	1	2.522	0.32	0.5715
	Depth	436.934	4	109.234	14.05	0
	Error	412.186	53	7.777		
	Total	887.026	60			
09-04 to 09-13	Site	45.2	2	22.6	1.52	0.2286
	Aspect	14.22	1	14.218	0.95	0.3331
	Depth	740.03	4	185.008	12.4	0
	Error	835.23	56	14.915		
	Total	1658.26	63			

Table 11 Dry Creek Experimental Watershed groundwater $\delta^2\text{H}$ and $\delta^{18}\text{O}$ isotope values (‰). BGS is a freshwater spring located between Bogus South and Lower Deer Point. LGW is a residential well located near Lower Gauge. BBW is a well at Bogus Basin Ski Resort. Locations are depicted in Figure 4.

Location	Date Sampled	$\delta^2\text{H}$	$\delta^{18}\text{O}$
BBW	03/04/12	-120.25	-16.54
BGS	08/04/11	-123.09	-16.37
BGS	11/27/11	-121.62	-17.90
BGS	03/23/12	-128.98	-16.54
BGS	07/08/12	-120.66	-16.52
BGS	09/05/12	-121.52	-16.43
BGS	10/09/12	-121.46	-16.51
LGW	03/04/12	-116.03	-14.64

Table 12 Dry Creek Experimental Watershed streamwater $\delta^2\text{H}$ and $\delta^{18}\text{O}$ Values. BG is located near the Dry Creek headwaters, while LG is the catchment outlet on Dry Creek. TL stream and TLTRIB are two ephemeral streams in the TL subcatchment. LGTRIB and TLTRIB are the tributaries entering Dry Creek and the Treeline stream near the respective gauging stations. Samples collected prior to 2011 were handled by Pam Aishlin. Locations are depicted in Figure 4.

Stream Location	Date Sampled	$\delta^2\text{H}$	$\delta^{18}\text{O}$
BG	9/29/09	-117.98	-16.24
BG	2/12/10	-120.09	-16.14
BG	4/16/10	-121.17	-16.29
BG	5/8/10	-115.43	-15.93
BG	6/5/10	-117.91	-15.64
BG	6/11/10	-118.10	-15.52
BG	6/15/10	-119.32	-15.42
BG	9/15/10	-119.50	-16.32
BG	1/7/11	-122.58	-16.59
BG	3/14/11	-81.30	-8.91
BG	4/23/11	-122.76	-16.96
BG	5/19/11	-122.46	-16.73
BG	8/4/11	-121.42	-16.21
BG	8/8/11	-121.72	-16.41
BG	11/27/11	-120.31	-17.72
BG	6/6/12	-121.03	-16.49
BG	7/8/12	-120.66	-16.52
BG	9/4/12	-121.10	-16.34
LG	9/29/08	-115.47	-15.09
LG	10/6/09	-119.41	-15.88
LG	10/14/09	-112.33	-12.90
LG	10/15/09	-114.82	-15.36
LG	10/19/09	-114.59	-15.32
LG	10/24/09	-116.32	-15.45
LG	10/28/09	-117.02	-15.49
LG	10/30/09	-116.57	-15.58
LG	11/7/09	-116.47	-15.38
LG	11/13/09	-118.03	-15.68
LG	11/18/09	-117.67	-15.67
LG	12/26/09	-119.80	-15.92
LG	1/7/10	-118.71	-15.96
LG	1/11/10	-118.98	-15.96
LG	1/20/10	-117.71	-15.59
LG	1/25/10	-118.09	-15.55

LG	1/27/10	-109.58	-12.69
LG	2/1/10	-119.34	-15.82
LG	2/10/10	-118.28	-15.69
LG	2/17/10	-116.88	-15.31
LG	2/22/10	-117.70	-15.25
LG	3/5/10	-121.00	-15.77
LG	3/5/10	-120.27	-15.66
LG	3/20/10	-120.00	-15.67
LG	3/26/10	-118.63	-15.98
LG	3/30/10	-115.75	-15.35
LG	4/2/10	-117.77	-15.56
LG	4/13/10	-117.73	-15.25
LG	4/16/10	-119.00	-15.69
LG	4/18/10	-119.11	-16.02
LG	4/21/10	-115.84	-15.90
LG	4/21/10	-118.12	-15.79
LG	4/30/10	-114.97	-15.69
LG	5/7/10	-113.15	-15.55
LG	5/19/10	-114.29	-15.83
LG	5/24/10	-117.23	-15.47
LG	6/5/10	-116.52	-15.45
LG	6/11/10	-116.94	-15.46
LG	6/14/10	-116.59	-15.11
LG	6/17/10	-115.61	-14.76
LG	6/21/10	-115.45	-15.10
LG	7/13/10	-116.81	-15.04
LG	7/16/10	-117.48	-15.07
LG	8/3/10	-116.14	-14.93
LG	8/12/10	-115.00	-15.16
LG	8/23/10	-117.18	-15.31
LG	9/2/10	-117.14	-15.49
LG	9/9/10	-117.04	-15.57
LG	9/9/10	-115.83	-15.39
LG	10/15/10	-115.43	-15.56
LG	10/27/10	-116.40	-15.95
LG	11/1/10	-114.78	-16.07
LG	11/8/10	-118.33	-16.93
LG	11/11/10	-117.47	-15.89
LG	11/15/10	-117.13	-15.64
LG	12/3/10	-119.82	-16.07
LG	12/9/10	-119.95	-16.36
LG	12/16/10	-120.50	-16.16
LG	12/27/10	-119.75	-15.58

LG	1/18/11	-124.76	-16.47
LG	1/31/11	-122.46	-16.53
LG	3/3/11	-119.83	-15.72
LG	3/14/11	-120.43	-15.58
LG	3/25/11	-122.07	-16.47
LG	4/4/11	-123.34	-16.79
LG	4/23/11	-122.35	-16.64
LG	4/27/11	-121.48	-16.50
LG	5/8/11	-122.35	-16.68
LG	5/10/11	-122.02	-16.47
LG	6/28/11	-120.48	-16.06
LG	7/4/11	-120.72	-15.90
LG	7/9/11	-120.17	-15.83
LG	7/10/11	-120.10	-16.11
LG	8/1/11	-120.32	-16.11
LG	8/2/11	-119.99	-16.05
LG	8/15/11	-119.60	-15.35
LG	8/16/11	-119.13	-15.85
LG	8/17/11	-118.31	-15.80
LG	9/9/11	-118.49	-15.82
LG	9/20/11	-117.74	-15.84
LG	9/27/11	-117.67	-16.12
LG	10/11/11	-122.82	-16.46
LG	10/14/11	-120.11	-16.19
LG	11/27/11	-118.54	-17.17
LG	1/22/12	-127.63	-17.20
LG	3/4/12	-122.59	-16.62
LG	3/23/12	-123.72	-16.78
LG	3/25/12	-123.76	-16.56
LG	4/8/12	-122.10	-16.36
LG	6/4/12	-118.70	-16.04
LG	7/10/12	-118.84	-16.13
LG	9/13/12	-115.13	-15.13
LG	10/9/12	-115.73	-15.63
LGTRIB	3/25/12	-125.36	-16.47
LGTRIB	4/8/12	-126.97	-15.83
TL	1/13/10	-122.83	-16.07
TL	1/20/10	-121.36	-15.80
TL	1/25/10	-120.56	-15.86
TL	1/27/10	-120.28	-15.73
TL	2/1/10	-120.20	-15.79
TL	2/10/10	-121.64	-15.70
TL	2/12/10	-121.16	-15.80

TL	2/17/10	-122.35	-15.85
TL	2/24/10	-123.03	-16.11
TL	2/26/10	-123.94	-16.11
TL	3/5/10	-128.11	-16.54
TL	3/7/10	-127.17	-16.36
TL	3/9/10	-125.12	-16.27
TL	3/12/10	-123.73	-15.87
TL	3/15/10	-126.12	-16.21
TL	3/20/10	-121.05	-15.73
TL	3/26/10	-117.68	-15.56
TL	3/29/10	-116.97	-15.26
TL	4/2/10	-117.71	-15.43
TL	4/3/10	-118.91	-15.46
TL	4/7/10	-119.69	-15.53
TL	4/13/10	-119.49	-15.38
TL	4/14/10	-119.22	-15.42
TL	4/15/10	-120.06	-15.50
TL	4/21/10	-115.39	-15.35
TL	4/22/10	-114.21	-15.32
TL	4/24/10	-114.42	-15.18
TL	4/30/10	-114.42	-15.28
TL	5/2/10	-114.30	-15.21
TL	5/12/10	-113.08	-15.02
TL	5/19/10	-112.64	-14.99
TL	5/24/10	-115.86	-15.66
TL	5/28/10	-113.67	-15.10
TL	6/1/10	-113.78	-15.02
TL	6/7/10	-106.84	-12.25
TL	6/11/10	-114.27	-14.84
TL	6/21/10	-112.55	-14.40
TL	12/9/10	-128.28	-17.35
TL	12/17/10	-125.08	-16.75
TL	12/27/10	-125.80	-16.76
TL	1/17/11	-139.14	-18.67
TL	1/20/11	-132.15	-17.71
TL	1/28/11	-131.73	-17.30
TL	2/4/11	-129.20	-16.75
TL	2/18/11	-119.77	-13.73
TL	3/3/11	-127.59	-16.76
TL	3/8/11	-130.21	-17.04
TL	3/11/11	-130.86	-17.27
TL	3/14/11	-128.47	-16.72
TL	3/17/11	-128.11	-16.76

TL	3/18/11	-128.47	-17.24
TL	3/22/11	-127.12	-17.17
TL	3/25/11	-126.34	-16.99
TL	3/31/11	-126.80	-17.27
TL	4/1/11	-125.57	-16.89
TL	4/15/11	-123.87	-16.93
TL	4/16/11	-124.25	-16.74
TL	4/22/11	-124.46	-16.77
TL	5/8/11	-122.30	-16.38
TL	5/16/11	-121.69	-16.33
TL	5/19/11	-122.47	-16.31
TL	6/3/11	-118.79	-15.98
TL	6/21/11	-118.06	-16.03
TL	3/4/12	-128.84	-17.09
TL	3/23/12	-126.12	-16.55
TL	5/17/12	-120.74	-16.05
TLTRIB	3/4/12	-126.60	-16.89
TLTRIB	3/23/12	-124.87	-16.87
TLTRIB	5/17/12	-124.08	-16.55
TLTRIB	6/6/12	-120.90	-16.60

Table 13 Dry Creek Experimental Watershed woody plant xylem water $\delta^2\text{H}$ and $\delta^{18}\text{O}$ values (‰). LG = Lower Gauge, TL = Treeline, BG = Bogus South. Plant individuals ending in a letter represent multiple samples from the same branch. A = base of branch, while letters following A in the alphabet were collected from closer to the leaf surface. σ = standard deviation. Standard deviations were included because spectral interference corrections (refer to Appendix C), which create larger uncertainties in isotope values, were often needed for plant xylem water samples. Locations are depicted in Figure 4. Plant sample coordinates are listed in Table 7.

Common Name	Plant Individual	Date Sampled	Mean $\delta^2\text{H}$	σ $\delta^2\text{H}$	Mean $\delta^{18}\text{O}$	σ $\delta^{18}\text{O}$
Chokecherry	BG-t5	06/06/12	-118.40	0.53	-16.58	0.18
Chokecherry	BG-t5	07/08/12	-125.80	1.02	-15.71	0.09
Chokecherry	BG-t5	09/04/12	-122.87	0.56	-16.26	0.09
Chokecherry	BG-t6	06/06/12	-122.19	2.41	-15.83	0.87
Chokecherry	BG-t6	07/08/12	-126.98	1.31	-16.32	0.58
Chokecherry	BG-t6	09/04/12	-125.52	0.14	-15.88	0.11
Chokecherry	BG-t7	06/06/12	-118.99	0.87	-17.32	0.10
Chokecherry	BG-t7	07/08/12	-122.44	0.77	-15.27	0.07
Chokecherry	BG-t7	09/04/12	-130.81	1.58	-17.61	0.21
Douglas-fir	BG-t2	11/29/11	-134.26	0.16	-17.00	0.04
Douglas-fir	BG-t2	06/06/12	-122.60	0.30	-15.28	0.05
Douglas-fir	BG-t2	07/08/12	-118.56	0.52	-15.60	0.08
Douglas-fir	BG-t2	09/04/12	-123.91	0.32	-16.71	0.05
Douglas-fir	BG-t4	11/29/11	-141.03	0.45	-19.34	0.12
Douglas-fir	BG-t4	06/06/12	-128.76	2.33	-15.83	0.13
Douglas-fir	BG-t4	07/08/12	-138.08	0.32	-18.77	0.58
Douglas-fir	BG-t4	09/04/12	-121.97	0.56	-16.26	0.10
Ponderosa pine	BG-t1	11/29/11	-138.29	0.37	-18.89	0.08
Ponderosa pine	BG-t1	06/06/12	-124.75	1.22	-16.03	0.59
Ponderosa pine	BG-t1	07/08/12	-128.62	0.80	-15.32	0.12
Ponderosa pine	BG-t1	09/04/12	-131.89	0.14	-14.93	0.09
Ponderosa pine	BG-t3	11/29/11	-140.18	0.37	-19.26	0.07
Ponderosa pine	BG-t3	06/06/12	-121.85	2.96	-15.02	0.65
Ponderosa pine	BG-t3	07/08/12	-123.90	0.19	-14.36	0.05
Ponderosa pine	BG-t3	09/04/12	-124.04	1.31	-16.55	0.20
Ponderosa pine	BG-t8	06/06/12	-120.56	0.55	-16.42	0.14
Ponderosa pine	BG-t8	07/08/12	-124.32	0.60	-13.98	0.08
Ponderosa pine	BG-t8	09/04/12	-126.21	0.45	-16.44	0.08
Chokecherry	LG-n-t2	04/08/12	-113.13	2.12	-12.40	0.29
Chokecherry	LG-n-t2	06/04/12	-125.30	0.56	-14.23	0.05
Chokecherry	LG-n-t2	09/13/12	-117.55	0.27	-11.82	0.05

Chokecherry	LG-n-t4	04/08/12	-89.00	0.17	-8.52	0.06
Chokecherry	LG-n-t4	06/04/12	-126.78	0.60	-16.12	0.04
Chokecherry	LG-n-t4	07/10/12	-127.73	0.53	-14.73	0.07
Chokecherry	LG-n-t4	09/13/12	-116.80	0.27	-11.88	0.11
Netleaf hackberry	LG-s-t6	07/19/11	-131.79	0.23	-15.50	0.08
Netleaf hackberry	LG-s-t6	04/08/12	-91.88	3.08	-5.15	0.98
Netleaf hackberry	LG-s-t6	06/04/12	-121.30	3.23	-14.08	0.31
Netleaf hackberry	LG-s-t6	07/10/12	-127.27	1.28	-14.15	0.11
Netleaf hackberry	LG-s-t6	09/13/12	-129.72	0.09	-14.29	0.33
Rabbitbrush	LG-n-s2	08/15/11	-132.48	0.31	-15.62	0.03
Rabbitbrush	LG-n-s2	04/08/12	-113.03	2.25	-12.66	0.60
Rabbitbrush	LG-n-s2	06/04/12	-120.08	0.46	-14.25	0.12
Rabbitbrush	LG-n-s2	09/13/12	-133.05	0.54	-14.76	0.15
Rabbitbrush	LG-n-s2a	07/10/12	-139.25	0.32	-16.62	0.16
Rabbitbrush	LG-n-s2b	07/10/12	-135.60	2.35	-15.07	0.10
Rabbitbrush	LG-n-s2c	07/10/12	-129.11	0.55	-14.35	0.18
Rabbitbrush	LG-n-s3	06/29/11	-127.71	0.30	-14.72	0.06
Rabbitbrush	LG-n-s3	08/15/11	-125.07	0.32	-15.33	0.05
Rabbitbrush	LG-n-s3	04/08/12	-98.47	0.09	-9.01	0.39
Rabbitbrush	LG-n-s3	06/04/12	-122.89	0.94	-14.73	0.66
Rabbitbrush	LG-n-s3	07/10/12	-126.70	0.73	-12.44	0.12
Rabbitbrush	LG-n-s3	09/13/12	-123.57	1.16	-14.17	0.82
Rabbitbrush	LG-s-s5	07/19/11	-130.53	0.44	-13.38	0.33
Rabbitbrush	LG-s-s5	04/08/12	-133.33	0.82	-15.25	0.11
Rabbitbrush	LG-s-s5	06/04/12	-127.95	0.83	-14.77	0.22
Rabbitbrush	LG-s-s5	07/10/12	-138.34	1.05	-15.67	0.26
Rabbitbrush	LG-s-s5	09/13/12	-137.91	0.91	-15.11	0.05
Sagebrush	LG-n-s1	08/15/11	-135.03	0.22	-14.84	0.01
Sagebrush	LG-n-s1	04/08/12	-123.17	1.19	-14.41	0.21
Sagebrush	LG-n-s1	06/04/12	-118.10	0.17	-13.51	0.16
Sagebrush	LG-n-s1	07/10/12	-140.15	2.19	-16.20	0.05
Sagebrush	LG-n-s1	09/13/12	-127.58	0.96	-12.73	0.13
Sagebrush	LG-n-s5	04/08/12	-118.28	2.20	-13.20	0.16
Sagebrush	LG-n-s5	06/04/12	-120.16	1.39	-14.05	0.14
Sagebrush	LG-n-s5	09/13/12	-131.47	2.20	-13.99	1.00
Sagebrush	LG-n-s5a	07/10/12	-137.99	0.52	-16.11	0.14
Sagebrush	LG-s-s1a	07/10/12	-131.23	0.52	-15.17	0.02
Sagebrush	LG-s-s1b	07/10/12	-126.27	NaN	-14.58	NaN
Sagebrush	LG-s-s1c	07/10/12	-125.26	1.09	-14.27	0.02
Sagebrush	LG-s-s2	07/19/11	-123.45	0.15	-12.88	0.04
Sagebrush	LG-s-s2	04/08/12	-134.07	1.03	-14.15	0.22
Sagebrush	LG-s-s2	06/04/12	-119.65	1.86	-13.79	0.26
Sagebrush	LG-s-s2	07/10/12	-127.46	0.18	-13.81	0.36

Sagebrush	LG-s-s2	09/13/12	-133.96	1.45	-14.26	0.06
Sagebrush	LG-s-s2b	03/23/12	-127.55	0.54	-15.32	0.15
Sagebrush	LG-s-s2c	03/23/12	-132.46	0.26	-16.35	0.10
Water birch	LG-n-t1	08/02/11	-132.02	0.03	-17.17	0.04
Water birch	LG-n-t1	04/08/12	-107.80	0.15	-9.09	0.04
Water birch	LG-n-t1	06/04/12	-123.12	1.44	-15.96	0.25
Water birch	LG-n-t1	07/10/12	-131.03	1.42	-16.16	0.08
Water birch	LG-n-t1	09/13/12	-124.74	0.59	-14.33	0.08
Water birch	LG-s-t1	04/08/12	-117.93	2.70	-14.11	0.60
Water birch	LG-s-t1	06/04/12	-128.07	0.66	-15.39	0.13
Water birch	LG-s-t1	09/13/12	-129.27	0.55	-15.56	0.28
Water birch	LG-s-t10	06/04/12	-121.44	1.34	-15.15	0.07
Water birch	LG-s-t1a	03/23/12	-120.60	0.62	-11.38	0.10
Water birch	LG-s-t3a	03/23/12	-120.42	0.88	-12.84	0.17
Yellow Willow	LG-s-t2	04/08/12	-108.37	0.87	-10.20	0.05
Yellow Willow	LG-s-t2	06/04/12	-135.58	1.25	-18.41	0.18
Yellow Willow	LG-s-t2	09/13/12	-125.59	0.67	-14.58	0.08
Yellow Willow	LG-s-t2a	07/10/12	-128.15	0.58	-15.52	0.08
Chokecherry	TL-t11	03/27/12	-113.52	1.74	-11.80	0.82
Chokecherry	TL-t11	05/17/12	-124.88	0.18	-15.85	0.29
Chokecherry	TL-t11	07/09/12	-131.57	1.50	-17.03	0.25
Chokecherry	TL-t11	09/07/12	-126.30	0.54	-16.76	0.12
Chokecherry	TL-t5	10/14/11	-129.81	0.84	-15.89	0.08
Chokecherry	TL-t5	03/27/12	-94.92	0.72	-10.70	0.12
Chokecherry	TL-t5	05/17/12	-126.66	0.64	-15.13	0.08
Chokecherry	TL-t5	07/09/12	-143.12	0.47	-17.70	0.08
Chokecherry	TL-t5	09/07/12	-133.94	0.21	-16.12	0.20
Chokecherry	TL-t7	10/14/11	-127.33	0.46	-14.25	0.11
Chokecherry	TL-t7	03/27/12	-89.83	0.31	-4.23	0.09
Chokecherry	TL-t7	05/17/12	-131.40	0.22	-16.58	0.13
Ponderosa pine	TL-t1	03/27/12	-132.04	0.48	-16.39	0.12
Ponderosa pine	TL-t1	05/17/12	-133.49	0.58	-14.71	0.16
Ponderosa pine	TL-t1	07/09/12	-123.75	1.83	-16.42	0.16
Ponderosa pine	TL-t1	09/07/12	-132.85	2.13	-15.84	0.26
Ponderosa pine	TL-t10	03/27/12	-133.88	0.19	-18.65	0.13
Ponderosa pine	TL-t10	05/17/12	-130.18	0.22	-17.41	0.06
Ponderosa pine	TL-t10	07/09/12	-125.62	1.38	-15.94	0.12
Ponderosa pine	TL-t10	09/07/12	-130.43	2.07	-16.43	0.20
Ponderosa pine	TL-t6	03/27/12	-135.54	1.07	-16.52	0.86
Ponderosa pine	TL-t6	05/17/12	-129.73	0.81	-14.38	0.17
Ponderosa pine	TL-t6	07/09/12	-134.47	0.60	-15.44	0.08
Ponderosa pine	TL-t6	09/07/12	-133.75	0.45	-15.75	0.10
Ponderosa pine	TL-t8	05/17/12	-123.23	0.35	-14.03	0.15

Ponderosa pine	TL-t8	07/09/12	-133.55	1.94	-16.95	0.14
Ponderosa pine	TL-t8	09/07/12	-134.36	0.62	-18.46	0.08
Ponderosa pine	TL-t9	03/27/12	-126.43	1.72	-16.05	0.86
Ponderosa pine	TL-t9	05/17/12	-122.96	1.02	-15.57	0.16
Ponderosa pine	TL-t9	07/09/12	-131.97	0.68	-17.07	0.19
Ponderosa pine	TL-t9	09/07/12	-130.42	2.81	-16.82	0.13
Sagebrush	TL-s1	03/27/12	-110.72	0.61	-11.05	0.38
Sagebrush	TL-s1	05/17/12	-119.70	2.75	-14.17	0.41
Sagebrush	TL-s1	09/07/12	-130.19	2.18	-13.72	0.01
Sagebrush	TL-s1a	03/23/12	-114.25	0.46	-11.06	0.23
Sagebrush	TL-s1b	03/23/12	-116.77	0.21	-12.89	0.11
Sagebrush	TL-s1c	03/23/12	-112.62	0.08	-11.59	0.04
Sagebrush	TL-s2	03/27/12	-100.32	0.46	-6.75	0.44
Sagebrush	TL-s2	05/17/12	-120.46	0.16	-13.71	0.27
Sagebrush	TL-s2	07/09/12	-131.68	0.12	-13.69	0.24
Sagebrush	TL-s2	09/07/12	-137.63	0.39	-16.09	0.09
Sagebrush	TL-s3	03/27/12	-117.55	0.49	-12.06	0.19
Sagebrush	TL-s3	05/17/12	-118.68	1.29	-13.04	0.70
Sagebrush	TL-s3	07/09/12	-125.73	0.18	-14.03	0.07
Sagebrush	TL-s3	09/07/12	-140.63	1.83	-16.00	0.78
Sagebrush	TL-s4	03/27/12	-114.39	0.49	-11.18	0.12
Sagebrush	TL-s4	05/17/12	-119.26	0.59	-13.53	0.07
Sagebrush	TL-s4	07/09/12	-128.80	0.19	-15.87	0.06
Sagebrush	TL-s4	09/07/12	-133.93	1.01	-14.11	0.75
Fire willow	TL-t4	10/14/11	-129.56	0.41	-15.90	0.09
Fire willow	TL-t4	03/27/12	-98.67	1.20	-8.60	0.76
Fire willow	TL-t4	05/17/12	-107.40	0.10	-8.58	0.19
Fire willow	TL-t4	07/09/12	-127.10	1.06	-14.30	0.10
Fire willow	TL-t4	09/07/12	-129.60	0.44	-16.36	0.05
Yellow willow	TL-t12	03/27/12	-107.02	1.54	-9.55	1.04
Yellow willow	TL-t12	05/17/12	-125.34	0.24	-16.79	0.06
Yellow Willow	TL-t2	03/27/12	-109.36	1.07	-10.72	0.99
Yellow Willow	TL-t2	05/17/12	-134.80	0.22	-15.95	0.09
Yellow Willow	TL-t2	07/09/12	-118.91	1.49	-14.47	0.10
Yellow Willow	TL-t2	09/07/12	-135.83	0.94	-15.97	0.33
Yellow Willow	TL-t3	05/17/12	-121.14	0.37	-15.55	0.11
Yellow Willow	TL-t3	07/09/12	-117.88	1.58	-13.13	0.06
Yellow Willow	TL-t3	09/07/12	-130.13	2.55	-16.33	0.16

Table 14a Stable Isotope Sourcing Using Sampling (SISUS) modeled median proportional source contributions to woody plant xylem water. Results represent the mean modeled proportional source contributions (% usage) of each potential water source. Bulk soil water isotope values were averaged at each sampled depth, at each field site, on each sampling date (e.g., 10 cm). The proportional source contributions are unbiased, and are derived from the differences between xylem water isotope values and source isotope values in dual-isotope ($\delta^2\text{H}$ and $\delta^{18}\text{O}$) plot space. For example, source water isotope values ($\delta^2\text{H}$ and $\delta^{18}\text{O}$) that plot near xylem water isotope values in dual-isotope space are likely to have a higher percent proportional contribution to the xylem water mixture. LG = Lower Gauge, TL = Treeline, BG = Bogus South. Locations are depicted in Figure 4. Plant sample coordinates are listed in Table 7.

Date Sampled	Species	Plant	10 cm	25 cm	45 cm	70 cm	100 cm	Ground water	Stream water
07/08/12	Chokecherry	bg-t5	0.10	NaN	0.13	0.54	0.13	0.04	0.04
09/04/12	Chokecherry	bg-t5	0.01	0.01	0.09	0.20	NaN	0.41	0.28
06/06/12	Chokecherry	bg-t6	0.31	0.05	0.37	0.11	0.07	0.03	0.02
07/08/12	Chokecherry	bg-t6	0.04	NaN	0.07	0.21	0.54	0.04	0.05
09/04/12	Chokecherry	bg-t6	0.02	0.07	0.41	0.35	NaN	0.07	0.07
07/08/12	Chokecherry	bg-t7	0.25	NaN	0.26	0.16	0.12	0.08	0.09
09/13/12	Chokecherry	lg-n-t2	0.39	0.16	0.05	0.06	NaN	0.16	0.15
07/10/12	Chokecherry	lg-n-t4	0.05	0.15	0.21	0.48	NaN	0.05	NaN
09/13/12	Chokecherry	lg-n-t4	0.40	0.11	0.04	0.05	NaN	0.40	NaN
07/09/12	Chokecherry	tl-t11	0.02	0.04	0.11	0.13	0.51	0.13	NaN
09/07/12	Chokecherry	tl-t11	0.00	0.00	0.01	0.01	0.18	0.79	NaN
09/07/12	Chokecherry	tl-t5	0.04	0.06	0.19	0.15	0.31	0.17	NaN
07/08/12	Douglas-fir	bg-t2	0.24	NaN	0.02	0.01	0.01	0.70	0.03
09/04/12	Douglas-fir	bg-t4	0.01	0.01	0.05	0.07	NaN	0.47	0.38
09/07/12	Fire willow	tl-t4	0.02	0.03	0.11	0.08	0.22	0.49	NaN
07/10/12	Netleaf hackberry	lg-s-t6	0.24	0.04	0.05	0.63	NaN	0.01	0.01

09/13/12	Netleaf hackberry	lg-s-t6	0.09	0.17	0.60	0.09	NaN	0.02	0.02
06/06/12	Ponderosa pine	bg-t1	0.05	0.01	0.74	0.14	0.02	0.01	0.01
09/04/12	Ponderosa pine	bg-t8	0.00	0.00	0.00	0.92	NaN	0.06	0.02
07/09/12	Ponderosa pine	tl-t1	0.02	0.04	0.06	0.07	0.09	0.69	NaN
09/07/12	Ponderosa pine	tl-t1	0.04	0.06	0.21	0.17	0.25	0.17	NaN
07/09/12	Ponderosa pine	tl-t10	0.08	0.11	0.12	0.12	0.14	0.36	NaN
09/07/12	Ponderosa pine	tl-t10	0.02	0.03	0.11	0.08	0.25	0.46	NaN
09/07/12	Ponderosa pine	tl-t6	0.05	0.07	0.23	0.19	0.27	0.09	NaN
07/09/12	Ponderosa pine	tl-t8	0.00	0.02	0.35	0.43	0.18	0.01	NaN
07/09/12	Ponderosa pine	tl-t9	0.02	0.04	0.11	0.13	0.54	0.11	NaN
09/07/12	Ponderosa pine	tl-t9	0.01	0.02	0.06	0.04	0.30	0.55	NaN
09/13/12	Rabbitbrush	lg-n-s3	0.09	0.10	0.18	0.24	NaN	0.38	NaN
07/10/12	Sagebrush	lg-s-s1	0.10	0.03	0.04	0.81	NaN	0.01	0.01
09/07/12	Sagebrush	tl-s1	0.34	0.04	0.07	0.10	0.39	0.01	NaN
07/09/12	Sagebrush	tl-s2	0.06	0.10	0.14	0.15	0.19	0.29	NaN
09/07/12	Sagebrush	tl-s2	0.15	0.03	0.06	0.09	0.62	0.01	NaN
07/09/12	Sagebrush	tl-s4	0.08	0.18	0.22	0.22	0.18	0.06	NaN
09/13/12	Water birch	lg-n-t1	0.09	0.11	0.24	0.25	NaN	0.16	0.14
09/13/12	Water birch	lg-s-t1	0.01	0.02	0.33	0.43	NaN	0.09	0.11
09/13/12	Yellow willow	lg-n-t2	0.07	0.09	0.26	0.28	NaN	0.15	0.14
07/10/12	Yellow willow	lg-s-t2	0.02	0.04	0.06	0.57	NaN	0.07	0.21
07/09/12	Yellow willow	tl-t2	0.26	0.08	0.06	0.06	0.07	0.42	NaN
09/07/12	Yellow willow	tl-t2	0.06	0.07	0.15	0.19	0.40	0.03	NaN
05/17/12	Yellow willow	tl-t3	0.38	0.09	0.14	0.10	0.08	0.05	0.07

07/09/12	Yellow willow	tl-t3	0.42	0.17	0.12	0.11	0.08	0.04	NaN
09/07/12	Yellow willow	tl-t3	0.02	0.03	0.12	0.09	0.23	0.45	NaN

Table 14b Stable Isotope Sourcing Using Sampling (SISUS) modeled minimum proportional source contributions to woody plant xylem water. Results represent the mean minimum proportional source contributions (% usage) of each potential water source. Bulk soil water isotope values were averaged at each sampled depth, at each field site, on each sampling date (e.g., 10 cm). The proportional source contributions are unbiased, and are derived from the differences between xylem water isotope values and source isotope values in dual-isotope ($\delta^2\text{H}$ and $\delta^{18}\text{O}$) plot space. For example, source water isotope values ($\delta^2\text{H}$ and $\delta^{18}\text{O}$) that plot near xylem water isotope values in dual-isotope space are likely to have a higher percent proportional contribution to the xylem water mixture. LG = Lower Gauge, TL = Treeline, BG = Bogus South. Locations are depicted in Figure 4. Plant sample coordinates are listed in Table 7.

Date Sampled	Species	Plant	10 cm	25 cm	45 cm	70 cm	100 cm	Ground water	Stream water
07/08/12	Chokecherry	bg-t5	0.00	NaN	0.00	0.28	0.00	0.00	0.00
09/04/12	Chokecherry	bg-t5	0.00	0.00	0.00	0.00	NaN	0.00	0.00
06/06/12	Chokecherry	bg-t6	0.14	0.00	0.00	0.00	0.00	0.00	0.00
07/08/12	Chokecherry	bg-t6	0.00	NaN	0.00	0.00	0.26	0.00	0.00
09/04/12	Chokecherry	bg-t6	0.00	0.00	0.00	0.00	NaN	0.00	0.00
07/08/12	Chokecherry	bg-t7	0.00	NaN	0.00	0.00	0.00	0.00	0.00
09/13/12	Chokecherry	lg-n-t2	0.08	0.00	0.00	0.00	NaN	0.00	0.00
07/10/12	Chokecherry	lg-n-t4	0.00	0.00	0.00	0.29	NaN	0.00	NaN
09/13/12	Chokecherry	lg-n-t4	0.19	0.00	0.00	0.00	NaN	0.36	NaN
07/09/12	Chokecherry	tl-t11	0.00	0.00	0.00	0.00	0.18	0.04	NaN
09/07/12	Chokecherry	tl-t11	0.00	0.00	0.00	0.00	0.15	0.78	NaN
09/07/12	Chokecherry	tl-t5	0.00	0.00	0.00	0.00	0.00	0.08	NaN
07/08/12	Douglas-fir	bg-t2	0.20	NaN	0.00	0.00	0.00	0.58	0.00
09/04/12	Douglas-fir	bg-t4	0.00	0.00	0.00	0.00	NaN	0.00	0.00
09/07/12	Fire willow	tl-t4	0.00	0.00	0.00	0.00	0.04	0.44	NaN
07/10/12	Netleaf hackberry	lg-s-t6	0.21	0.00	0.00	0.54	NaN	0.00	0.00

09/13/12	Netleaf hackberry	lg-s-t6	0.00	0.00	0.34	0.00	NaN	0.00	0.00
06/06/12	Ponderosa pine	bg-t1	0.00	0.00	0.34	0.07	0.00	0.00	0.00
09/04/12	Ponderosa pine	bg-t8	0.00	0.00	0.00	0.90	NaN	0.00	0.00
07/09/12	Ponderosa pine	tl-t1	0.00	0.00	0.00	0.00	0.00	0.63	NaN
09/07/12	Ponderosa pine	tl-t1	0.00	0.00	0.00	0.00	0.00	0.08	NaN
07/09/12	Ponderosa pine	tl-t10	0.00	0.00	0.00	0.00	0.00	0.23	NaN
09/07/12	Ponderosa pine	tl-t10	0.00	0.00	0.00	0.00	0.07	0.40	NaN
09/07/12	Ponderosa pine	tl-t6	0.00	0.00	0.00	0.00	0.00	0.00	NaN
07/09/12	Ponderosa pine	tl-t8	0.00	0.00	0.00	0.00	0.01	0.00	NaN
07/09/12	Ponderosa pine	tl-t9	0.00	0.00	0.00	0.00	0.21	0.01	NaN
09/07/12	Ponderosa pine	tl-t9	0.00	0.00	0.00	0.00	0.20	0.52	NaN
09/13/12	Rabbitbrush	lg-n-s3	0.00	0.00	0.00	0.00	NaN	0.29	NaN
07/10/12	Sagebrush	lg-s-s1	0.07	0.00	0.00	0.74	NaN	0.00	0.00
09/07/12	Sagebrush	tl-s1	0.30	0.00	0.00	0.00	0.22	0.00	NaN
07/09/12	Sagebrush	tl-s2	0.00	0.00	0.00	0.00	0.00	0.15	NaN
09/07/12	Sagebrush	tl-s2	0.11	0.00	0.00	0.00	0.46	0.00	NaN
07/09/12	Sagebrush	tl-s4	0.00	0.00	0.00	0.00	0.00	0.00	NaN
09/13/12	Water birch	lg-n-t1	0.00	0.00	0.00	0.00	NaN	0.00	0.00
09/13/12	Water birch	lg-s-t1	0.00	0.00	0.00	0.00	NaN	0.00	0.00
09/13/12	Yellow willow	lg-n-t2	0.00	0.00	0.00	0.00	NaN	0.00	0.00
07/10/12	Yellow willow	lg-s-t2	0.00	0.00	0.00	0.47	NaN	0.00	0.02
07/09/12	Yellow willow	tl-t2	0.14	0.00	0.00	0.00	0.00	0.34	NaN
09/07/12	Yellow willow	tl-t2	0.00	0.00	0.00	0.00	0.09	0.00	NaN
05/17/12	Yellow willow	tl-t3	0.11	0.00	0.00	0.00	0.00	0.00	0.00

07/09/12	Yellow willow	tl-t3	0.23	0.00	0.00	0.00	0.00	0.00	NaN
09/07/12	Yellow willow	tl-t3	0.00	0.00	0.00	0.00	0.03	0.39	NaN

Table 14c Stable Isotope Sourcing Using Sampling (SISUS) modeled maximum proportional source contributions to woody plant xylem water. Results represent the mean maximum proportional source contributions (% usage) of each potential water source. Bulk soil water isotope values were averaged at each sampled depth, at each field site, on each sampling date (e.g., 10 cm). The proportional source contributions are unbiased, and are derived from the differences between xylem water isotope values and source isotope values in dual-isotope ($\delta^2\text{H}$ and $\delta^{18}\text{O}$) plot space. For example, source water isotope values ($\delta^2\text{H}$ and $\delta^{18}\text{O}$) that plot near xylem water isotope values in dual-isotope space are likely to have a higher percent proportional contribution to the xylem water mixture. LG = Lower Gauge, TL = Treeline, BG = Bogus South. Locations are depicted in Figure 4. Plant sample coordinates are listed in Table 7.

Date Sampled	Species	Plant	10 cm	25 cm	45 cm	70 cm	100 cm	Ground water	Stream water
07/08/12	Chokecherry	bg-t5	0.28	NaN	0.45	0.74	0.44	0.16	0.17
09/04/12	Chokecherry	bg-t5	0.03	0.05	0.28	0.36	NaN	0.75	0.70
06/06/12	Chokecherry	bg-t6	0.57	0.26	0.60	0.35	0.41	0.16	0.14
07/08/12	Chokecherry	bg-t6	0.19	NaN	0.30	0.51	0.78	0.20	0.24
09/04/12	Chokecherry	bg-t6	0.08	0.17	0.79	0.87	NaN	0.26	0.24
07/08/12	Chokecherry	bg-t7	0.48	NaN	0.77	0.43	0.42	0.26	0.27
09/13/12	Chokecherry	lg-n-t2	0.53	0.56	0.18	0.23	NaN	0.40	0.35
07/10/12	Chokecherry	lg-n-t4	0.15	0.51	0.71	0.67	NaN	0.18	NaN
09/13/12	Chokecherry	lg-n-t4	0.49	0.37	0.12	0.16	NaN	0.44	NaN
07/09/12	Chokecherry	tl-t11	0.09	0.18	0.53	0.63	0.87	0.19	NaN
09/07/12	Chokecherry	tl-t11	0.01	0.02	0.07	0.05	0.19	0.79	NaN
09/07/12	Chokecherry	tl-t5	0.17	0.27	0.91	0.71	0.56	0.27	NaN
07/08/12	Douglas-fir	bg-t2	0.26	NaN	0.07	0.03	0.03	0.73	0.16
09/04/12	Douglas-fir	bg-t4	0.03	0.05	0.15	0.19	NaN	0.90	0.85
09/07/12	Fire willow	tl-t4	0.10	0.15	0.53	0.40	0.36	0.55	NaN
07/10/12	Netleaf hackberry	lg-s-t6	0.28	0.17	0.25	0.67	NaN	0.06	0.05

09/13/12	Netleaf hackberry	lg-s-t6	0.23	0.29	0.72	0.36	NaN	0.10	0.08
06/06/12	Ponderosa pine	bg-t1	0.27	0.09	0.88	0.38	0.14	0.06	0.05
09/04/12	Ponderosa pine	bg-t8	0.00	0.00	0.02	0.93	NaN	0.08	0.07
07/09/12	Ponderosa pine	tl-t1	0.07	0.14	0.27	0.28	0.31	0.71	NaN
09/07/12	Ponderosa pine	tl-t1	0.19	0.31	0.86	0.80	0.53	0.28	NaN
07/09/12	Ponderosa pine	tl-t10	0.18	0.37	0.53	0.53	0.59	0.42	NaN
09/07/12	Ponderosa pine	tl-t10	0.10	0.15	0.53	0.40	0.39	0.51	NaN
09/07/12	Ponderosa pine	tl-t6	0.21	0.34	0.93	0.89	0.57	0.22	NaN
07/09/12	Ponderosa pine	tl-t8	0.02	0.06	0.81	0.95	0.30	0.03	NaN
07/09/12	Ponderosa pine	tl-t9	0.09	0.18	0.53	0.62	0.90	0.17	NaN
09/07/12	Ponderosa pine	tl-t9	0.05	0.08	0.27	0.21	0.37	0.58	NaN
09/13/12	Rabbitbrush	lg-n-s3	0.19	0.23	0.40	0.52	NaN	0.45	NaN
07/10/12	Sagebrush	lg-s-s1	0.12	0.13	0.19	0.84	NaN	0.05	0.04
09/07/12	Sagebrush	tl-s1	0.42	0.17	0.33	0.47	0.52	0.07	NaN
07/09/12	Sagebrush	tl-s2	0.16	0.34	0.61	0.62	0.69	0.35	NaN
09/07/12	Sagebrush	tl-s2	0.22	0.16	0.30	0.43	0.73	0.06	NaN
07/09/12	Sagebrush	tl-s4	0.16	0.51	0.80	0.81	0.55	0.13	NaN
09/13/12	Water birch	lg-n-t1	0.20	0.25	0.48	0.61	NaN	0.41	0.36
09/13/12	Water birch	lg-s-t1	0.04	0.05	0.68	0.86	NaN	0.33	0.30
09/13/12	Yellow willow	lg-n-t2	0.17	0.21	0.52	0.66	NaN	0.40	0.35
07/10/12	Yellow willow	lg-s-t2	0.08	0.21	0.28	0.64	NaN	0.34	0.30
07/09/12	Yellow willow	tl-t2	0.32	0.38	0.30	0.30	0.33	0.48	NaN
09/07/12	Yellow willow	tl-t2	0.21	0.34	0.68	0.87	0.66	0.14	NaN
05/17/12	Yellow willow	tl-t3	0.63	0.32	0.83	0.49	0.40	0.23	0.33

07/09/12	Yellow willow	tl-t3	0.48	0.64	0.50	0.51	0.32	0.13	NaN
09/07/12	Yellow willow	tl-t3	0.11	0.17	0.58	0.44	0.38	0.51	NaN

APPENDIX B

Figures

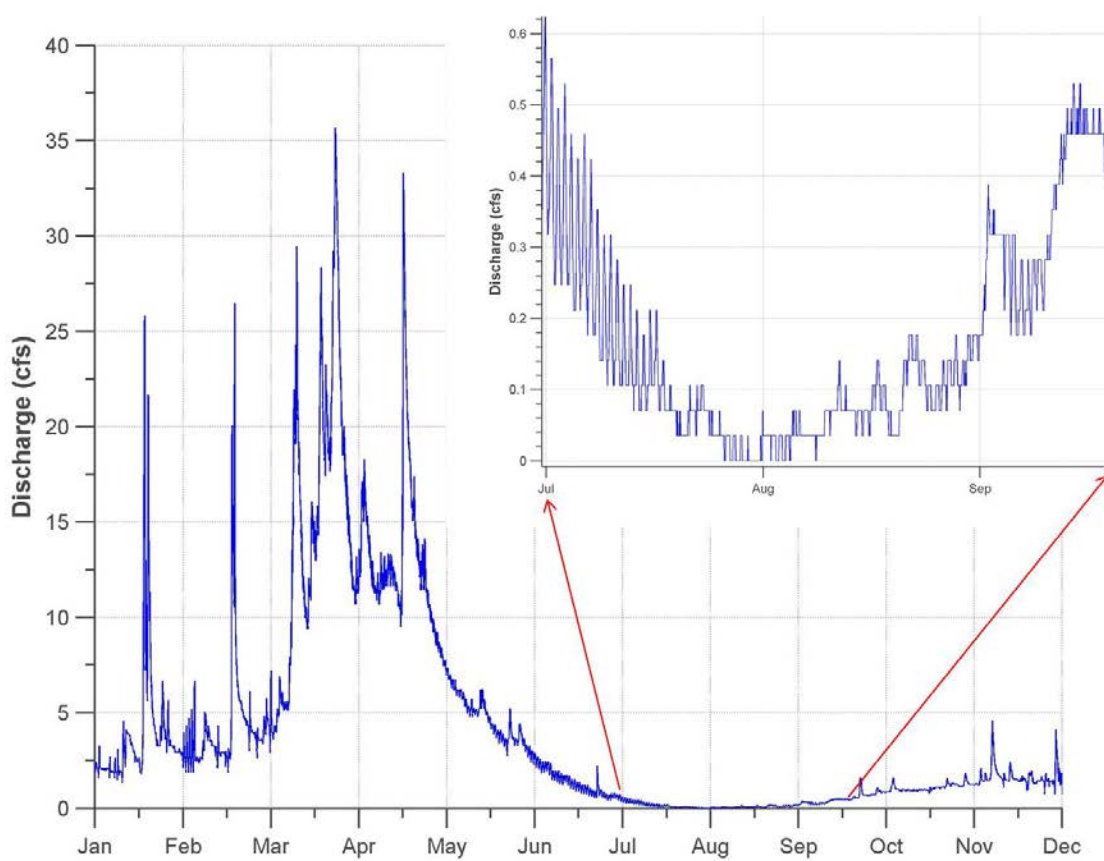


Figure 1. Dry Creek Hydrograph (Lower Gauge, 2012). Lower Gauge monitors discharge of Dry Creek at the outlet of Dry Creek Experimental Watershed. The gauge location is depicted in Figure 4.

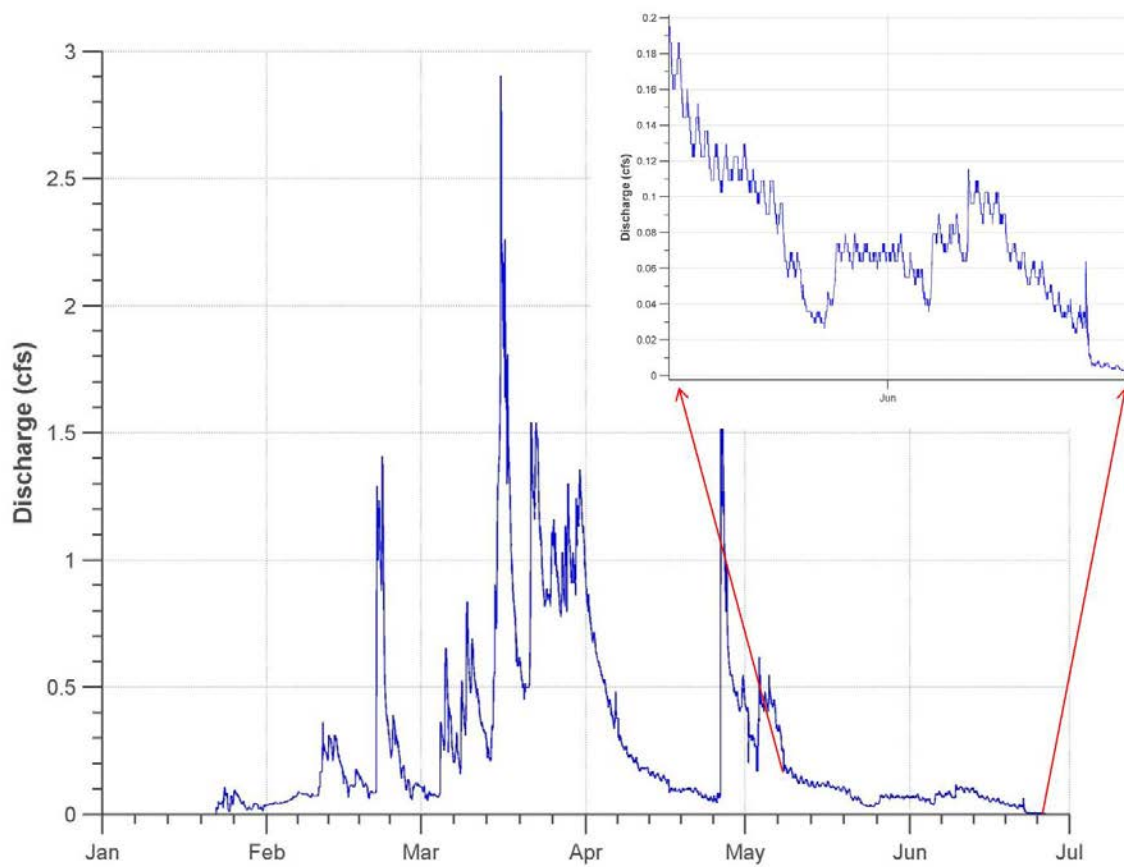


Figure 2. Treeline Stream Hydrograph (2012). Discharge only plots until late June because Treeline stream ceased to flow at this time. The gauge location is depicted in Figure 4.

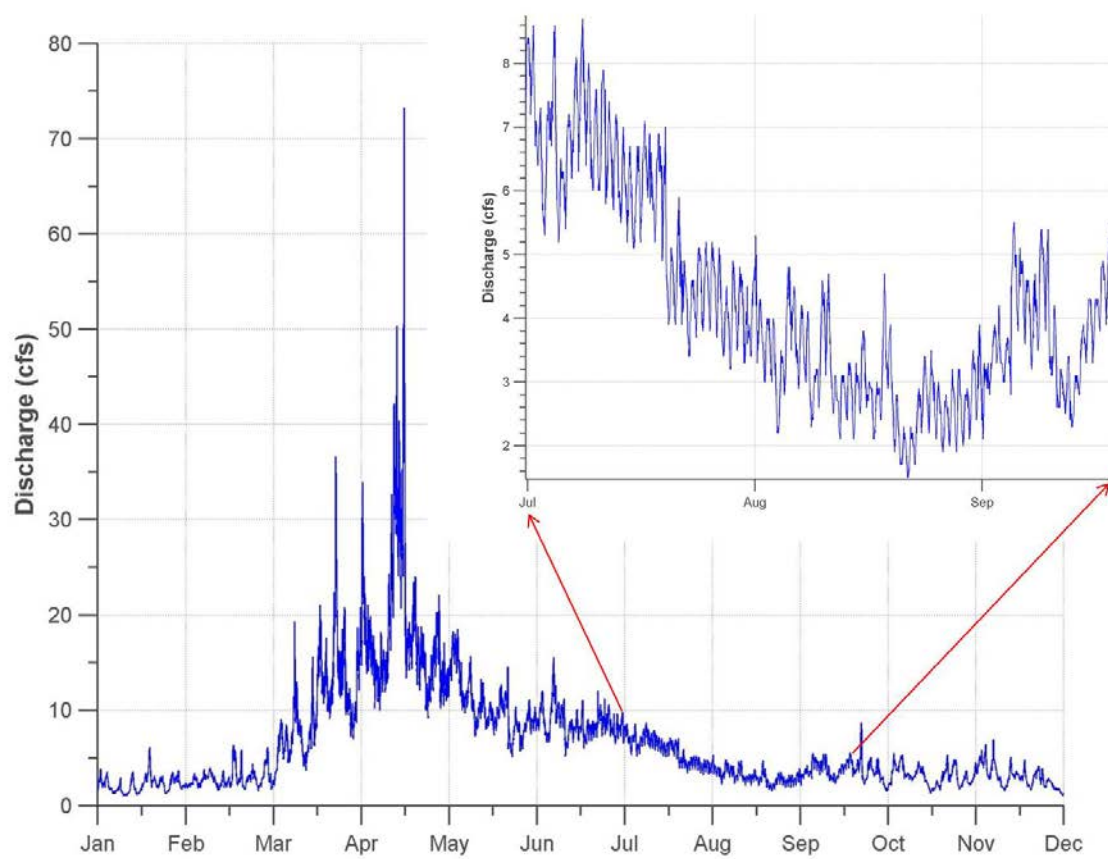


Figure 3. Dry Creek Hydrograph (Bogus South, 2012). Bogus South monitors discharge near the headwaters of Dry Creek. The gauge location is depicted in Figure 4.

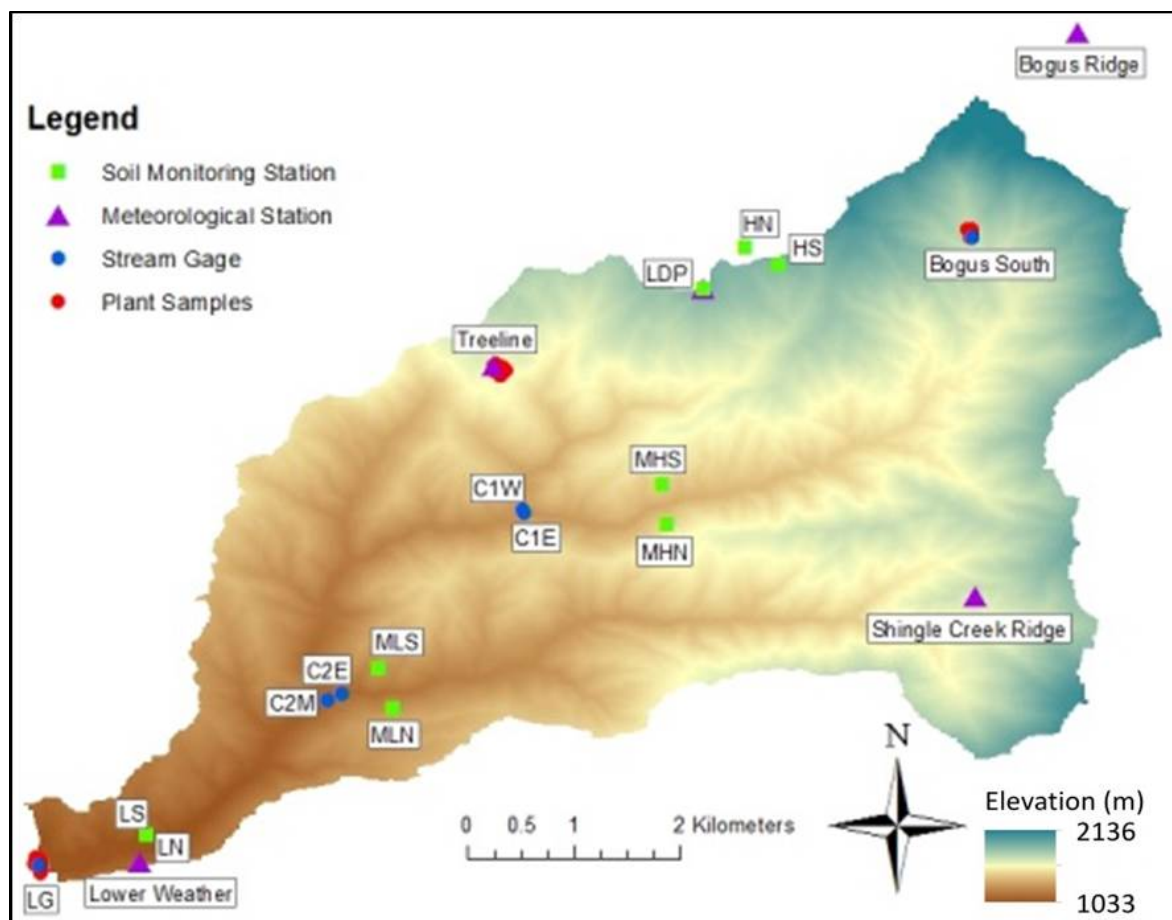


Figure 4. Dry Creek Experimental Watershed Topographic Map, including sampling sites, elevation, weather stations, stream gauges, and soil moisture monitoring stations. Refer to CHAPTER THREE: STUDY AREA or <http://earth.boisestate.edu/drycreek/> for site descriptions.

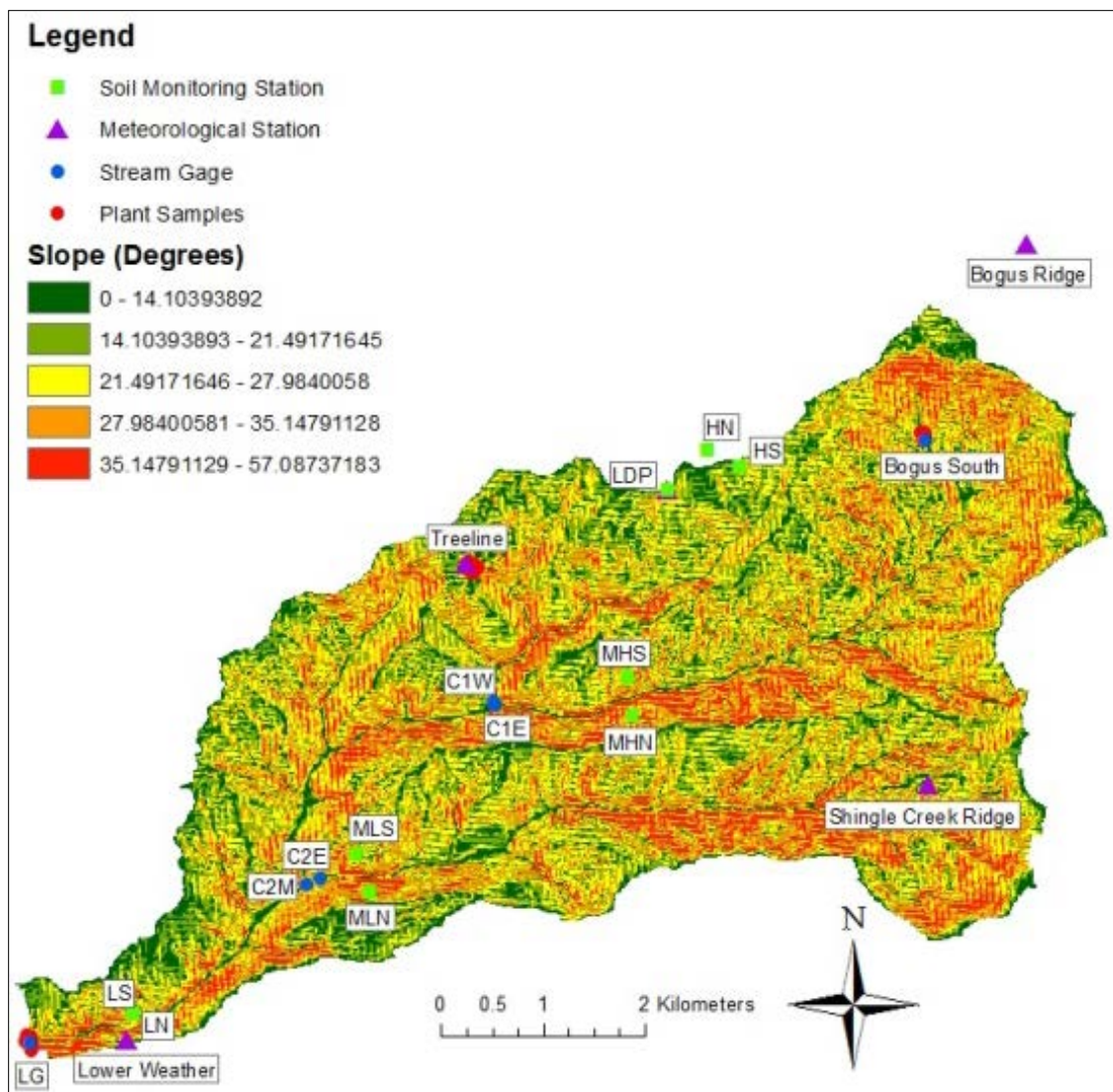


Figure 5. Dry Creek Experimental Watershed Slope Distribution, including sampling sites, elevation, weather stations, stream gauges, and soil moisture monitoring stations. Refer to **CHAPTER THREE: STUDY AREA** or <http://earth.boisestate.edu/drycreek/> for site descriptions.

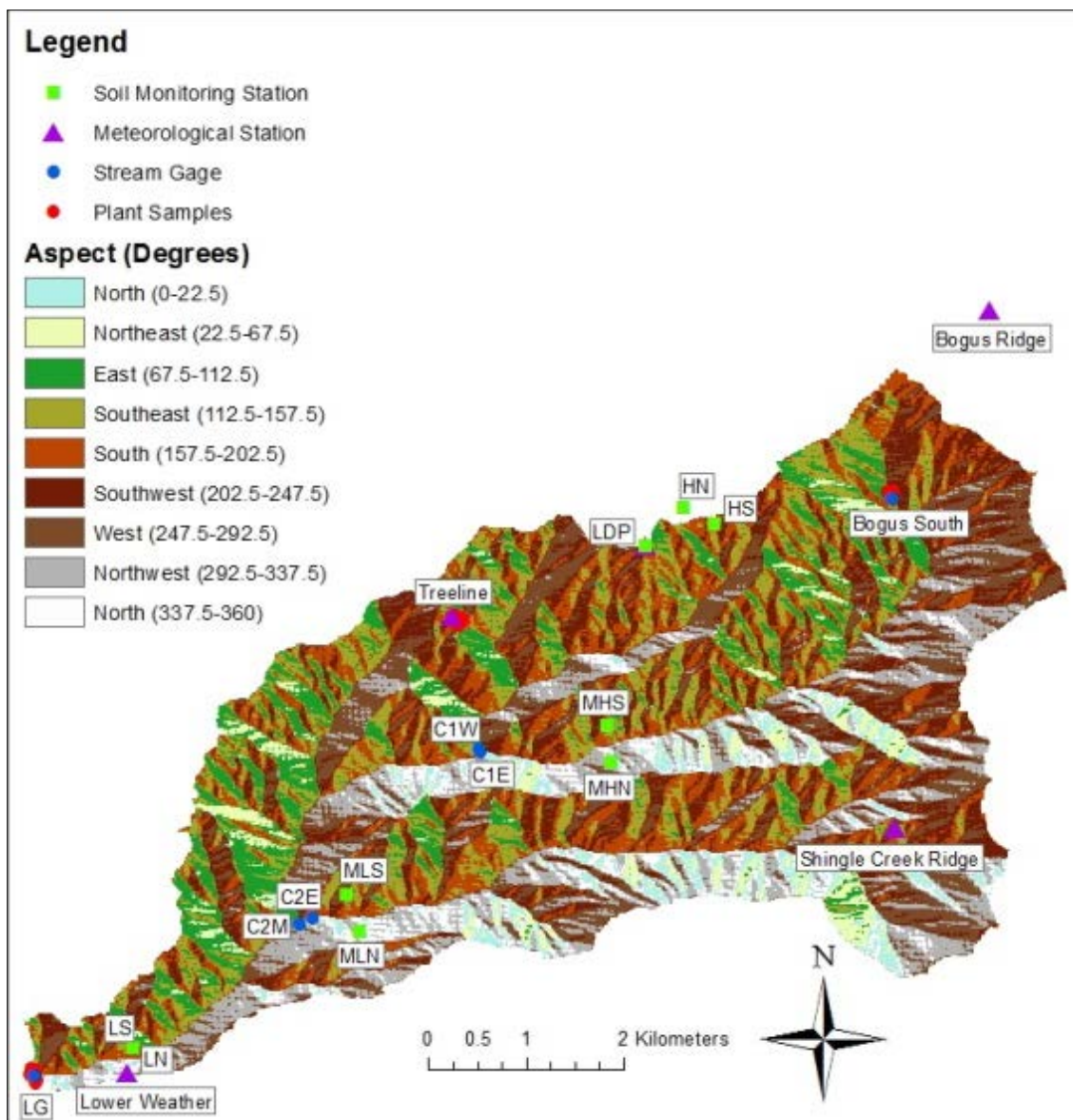


Figure 6. Dry Creek Experimental Watershed Aspect Distribution, including sampling sites, elevation, weather stations, stream gauges, and soil moisture monitoring stations. Refer to CHAPTER THREE: STUDY AREA or <http://earth.boisestate.edu/drycreek/> for site descriptions.

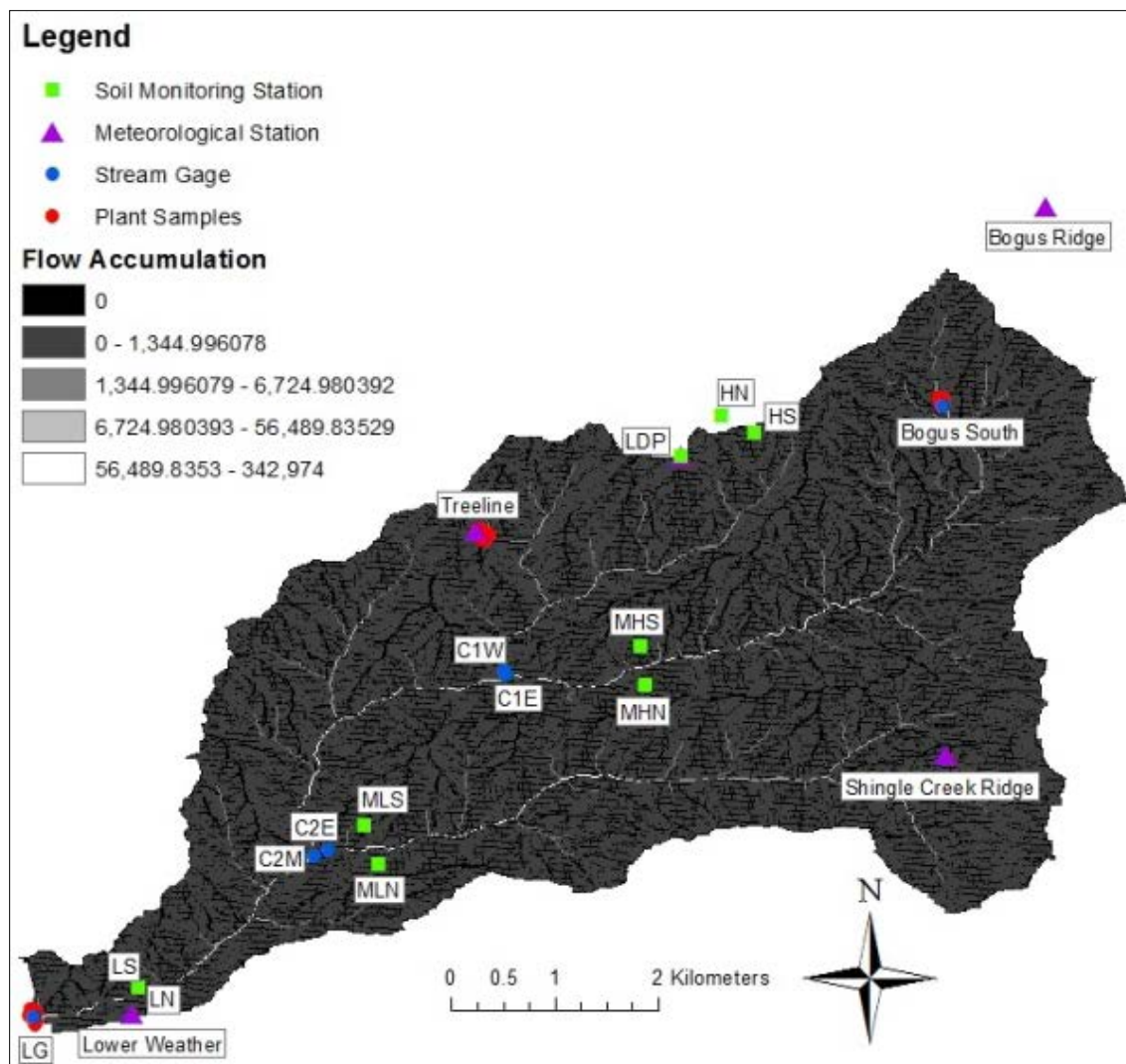


Figure 7. Dry Creek Experimental Watershed flow accumulation, including sampling sites, elevation, weather stations, stream gauges, and soil moisture monitoring stations. Refer to **CHAPTER THREE: STUDY AREA** or <http://earth.boisestate.edu/drycreek/> for site descriptions.

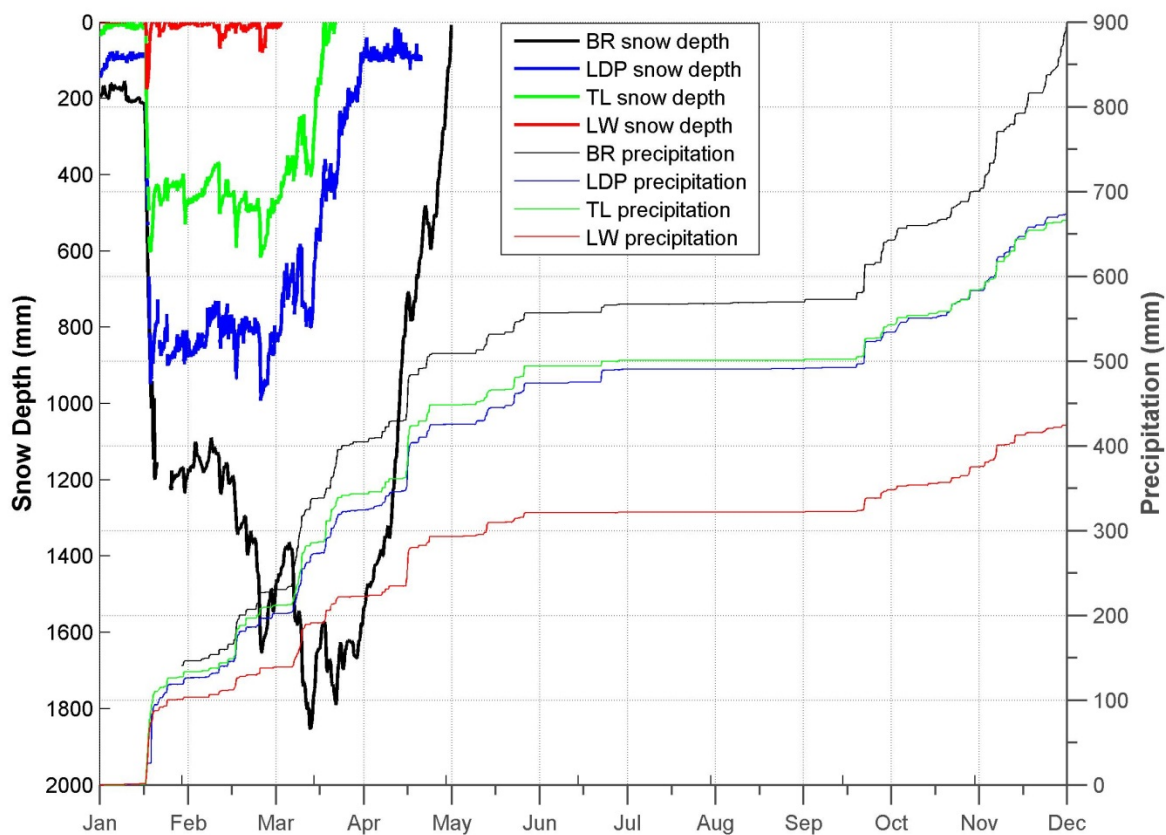


Figure 8. Dry Creek Experimental Watershed spatiotemporal variation of precipitation and snow depth (2012). BR = Bogus Ridge, LDP = Lower Deer Point, TL = Treeline, LW = Lower Weather. Elevations: BR = 2114 m, LDP = 1850 m, TL = 1610 m, LW = 1151 m. Locations are depicted in Figure 4.

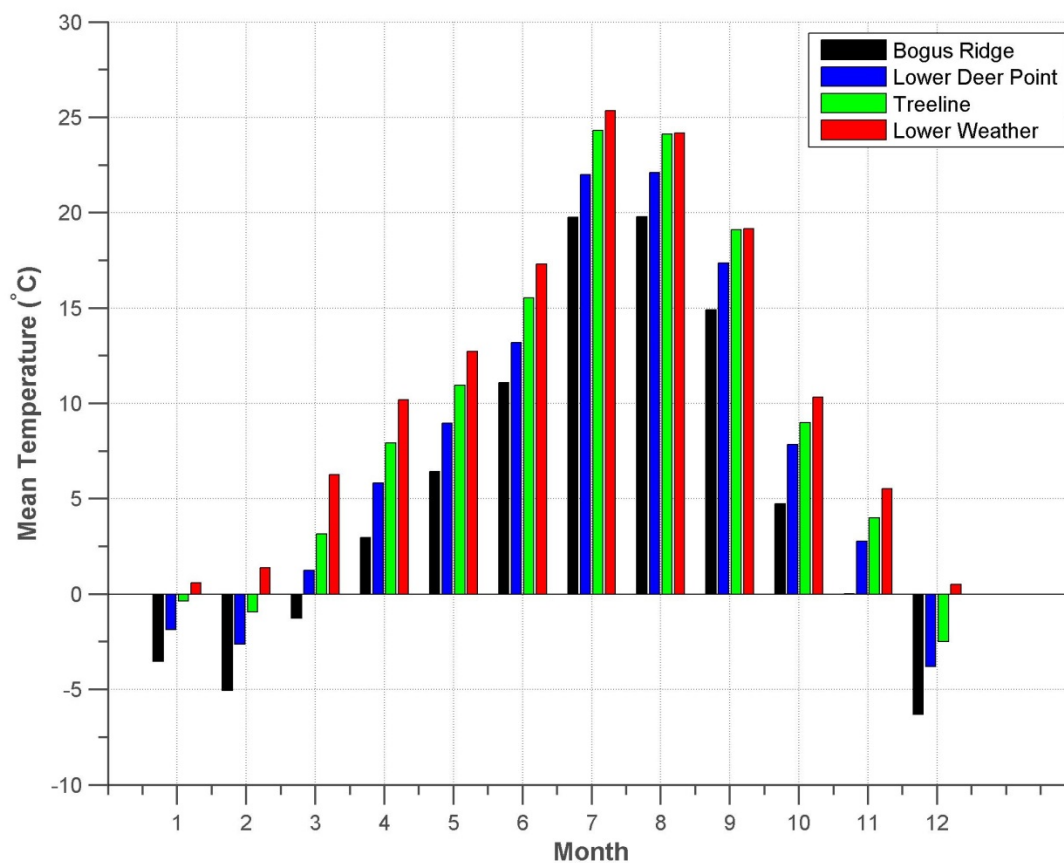


Figure 9. Dry Creek Experimental Watershed spatiotemporal variation of temperature (2012). BR = Bogus Ridge, LDP = Lower Deer Point, TL = Treeline, LW = Lower Weather. Elevations: BR = 2114 m, LDP = 1850 m, TL = 1610 m, LW = 1151 m. Locations are depicted in Figure 4.

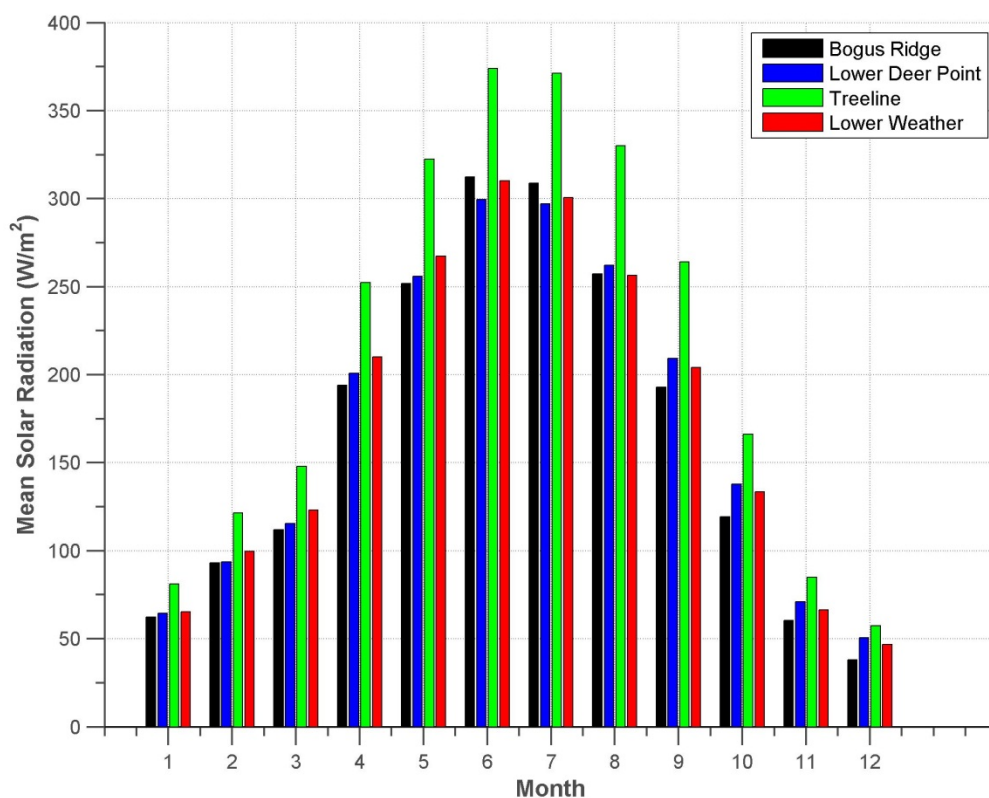


Figure 10. Dry Creek Experimental Watershed spatiotemporal variation of solar radiation (2012). BR = Bogus Ridge, LDP = Lower Deer Point, TL = Treeline, LW = Lower Weather. Elevations: BR = 2114 m, LDP = 1850 m, TL = 1610 m, LW = 1151 m. Locations are depicted in Figure 4.

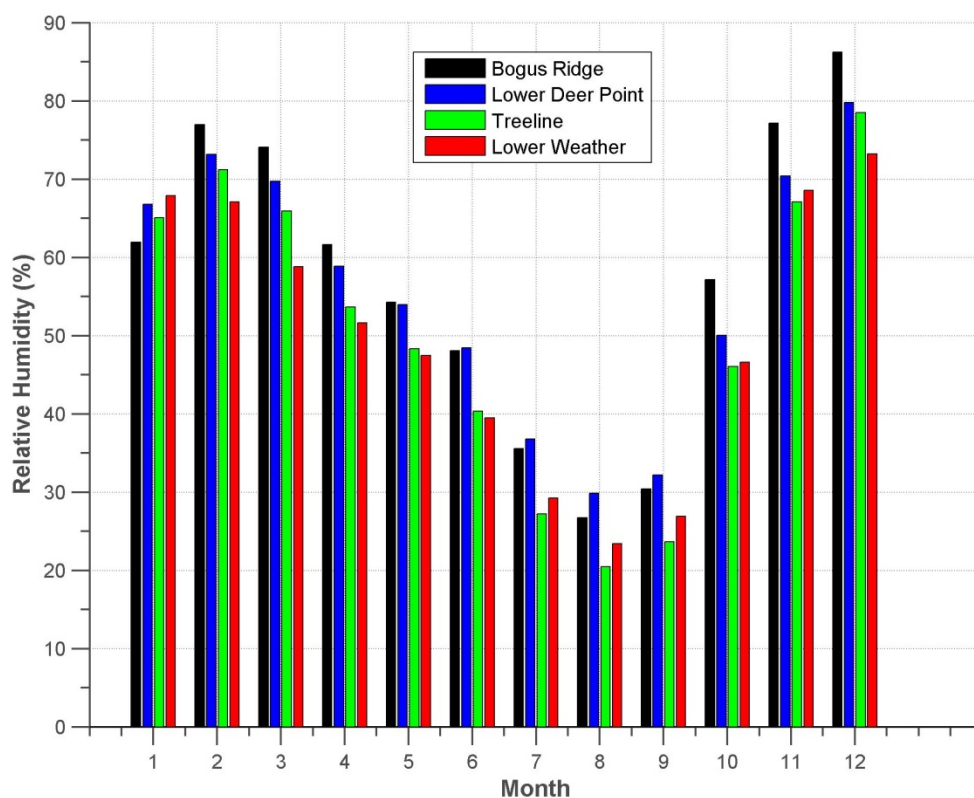


Figure 11. Dry Creek Experimental Watershed spatiotemporal variation of relative humidity (2012). BR = Bogus Ridge, LDP = Lower Deer Point, TL = Treeline, LW = Lower Weather. Elevations: BR = 2114 m, LDP = 1850 m, TL = 1610 m, LW = 1151 m.

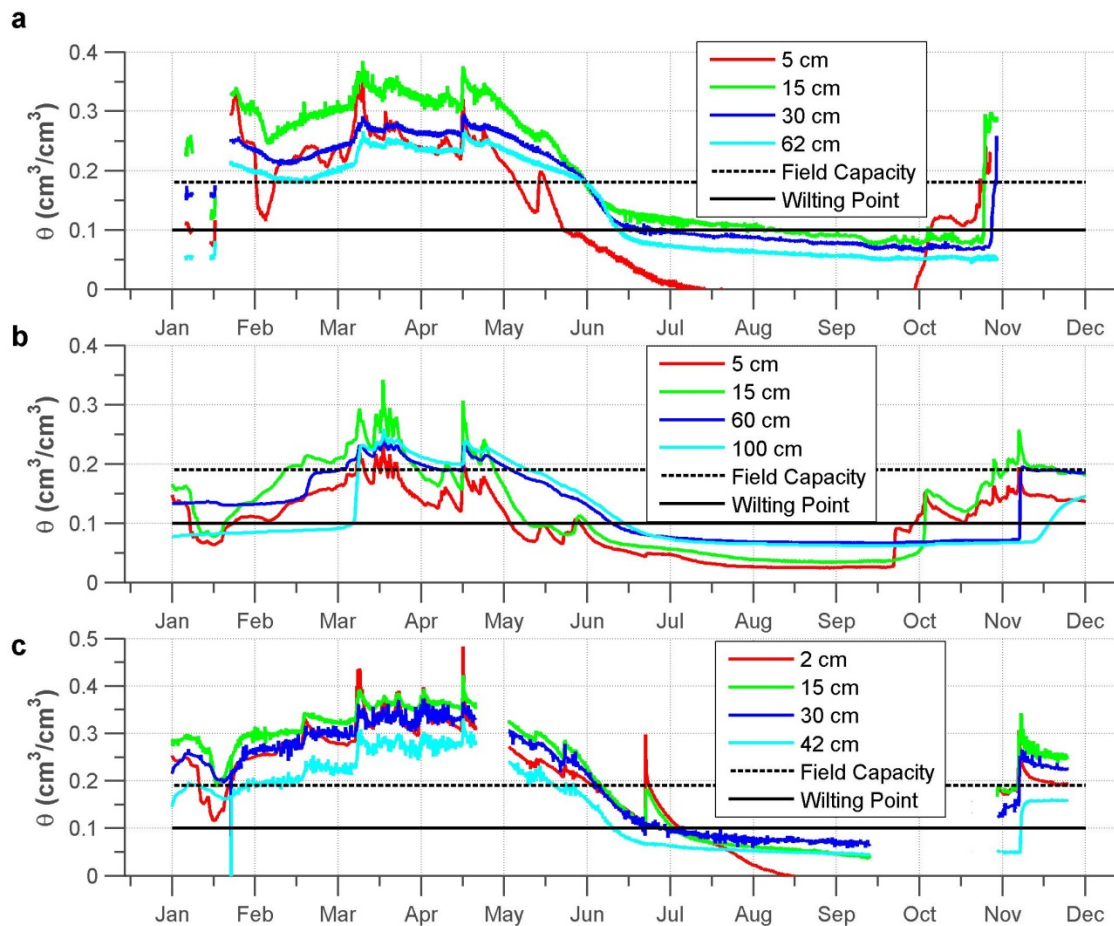


Figure 12. Dry Creek Experimental Watershed spatiotemporal variation in volumetric soil moisture content (2012). Field capacity and wilting point estimates from Smith (2010). HN is used as a proxy for BG soil moisture, field capacity and wilting point. MHN is used as a proxy for TL field capacity and wilting point. (a) LN, (b) Treeline, (c) HN. LN is used as a proxy for Lower Gauge soils and HN is used as a proxy for Bogus Gauge soils, though it is expected that BG soils generally contain more moisture than HN soils. Locations are depicted in Figure 4.

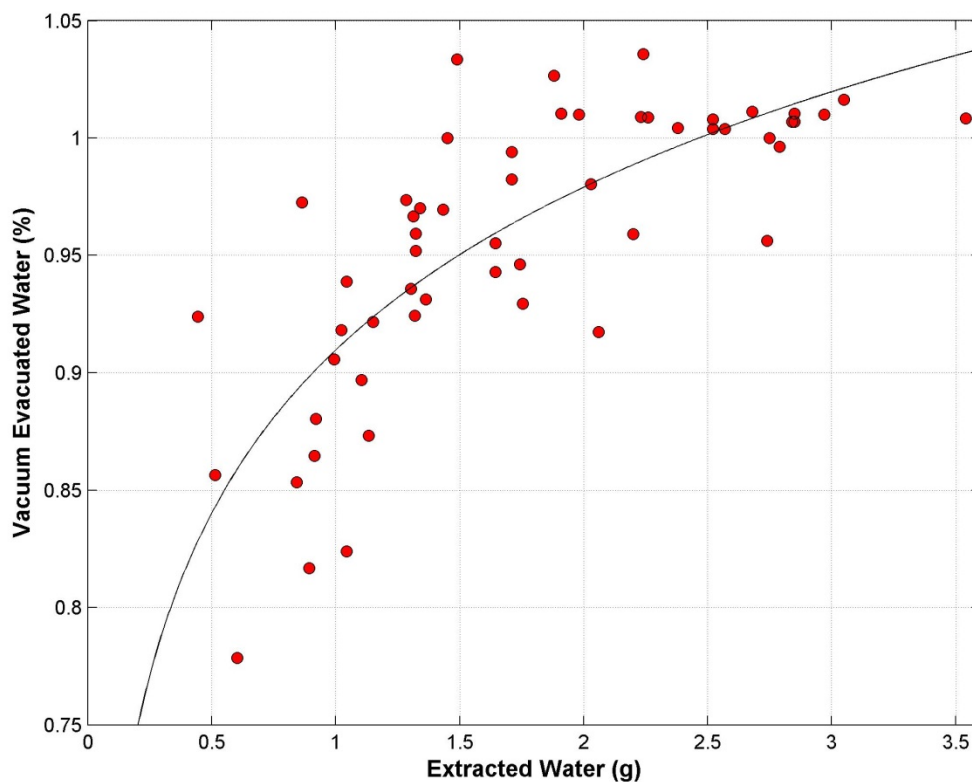


Figure 13. Total soil extracted water (grams) is plotted against vacuum evacuated soil water (%). Total extracted water is the sum of vacuum evacuated water and oven extracted water. Water was vacuum extracted from soils using cryogenic vacuum distillation (West et al., 2006 method) for 40 minutes. Remaining water was extracted via evaporation by placing samples in an oven at 100 °C for 24 hours. The percent vacuum evacuated water is calculated by vacuum evacuated water (g) / vacuum evacuated water (g) + 24 hour oven evaporated water (g).

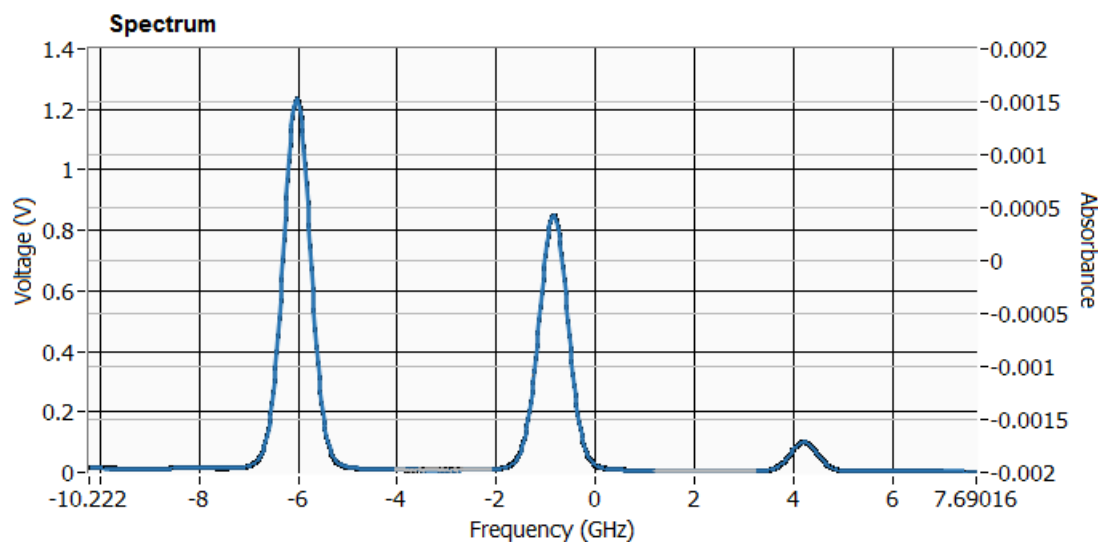


Figure 14. Example water sample spectral absorption behavior (LGR LWIA run, 02-26-2012). The Los Gatos Research Liquid Water Isotope Analyzer uses the spectral absorbance features of water isotopologues as a proxy to calculate the concentrations of hydrogen and oxygen isotopes in each water sample.

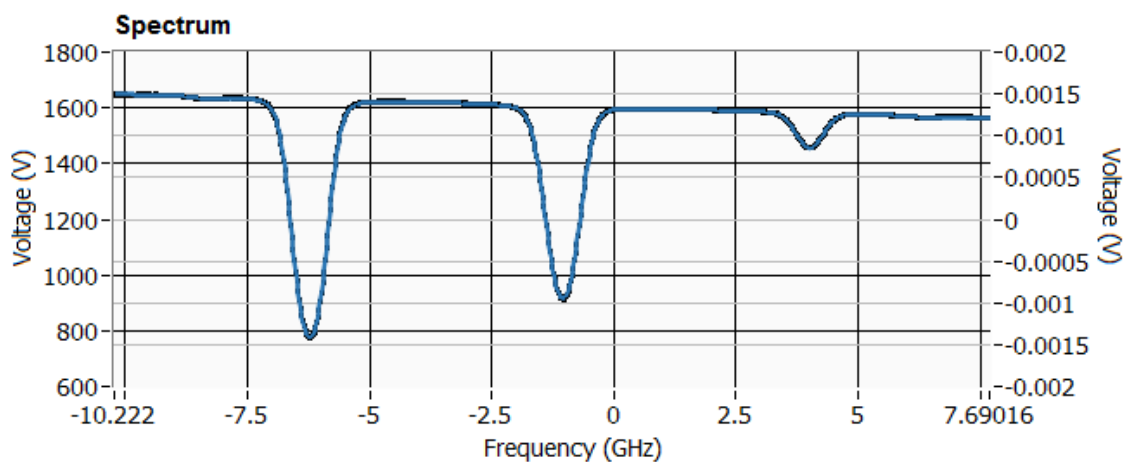


Figure 15. Example water sample spectral transmission behavior (LGR-LWIA run, 02-26-2012). The Los Gatos Research Liquid Water Isotope Analyzer uses the spectral absorbance features of water isotopologues as a proxy to calculate the concentrations of hydrogen and oxygen isotopes in each water sample. The Los Gatos Research Liquid Water Isotope Analyzer uses the spectral absorbance features of water isotopologues as a proxy to calculate the concentrations of hydrogen and oxygen isotopes in each water sample.

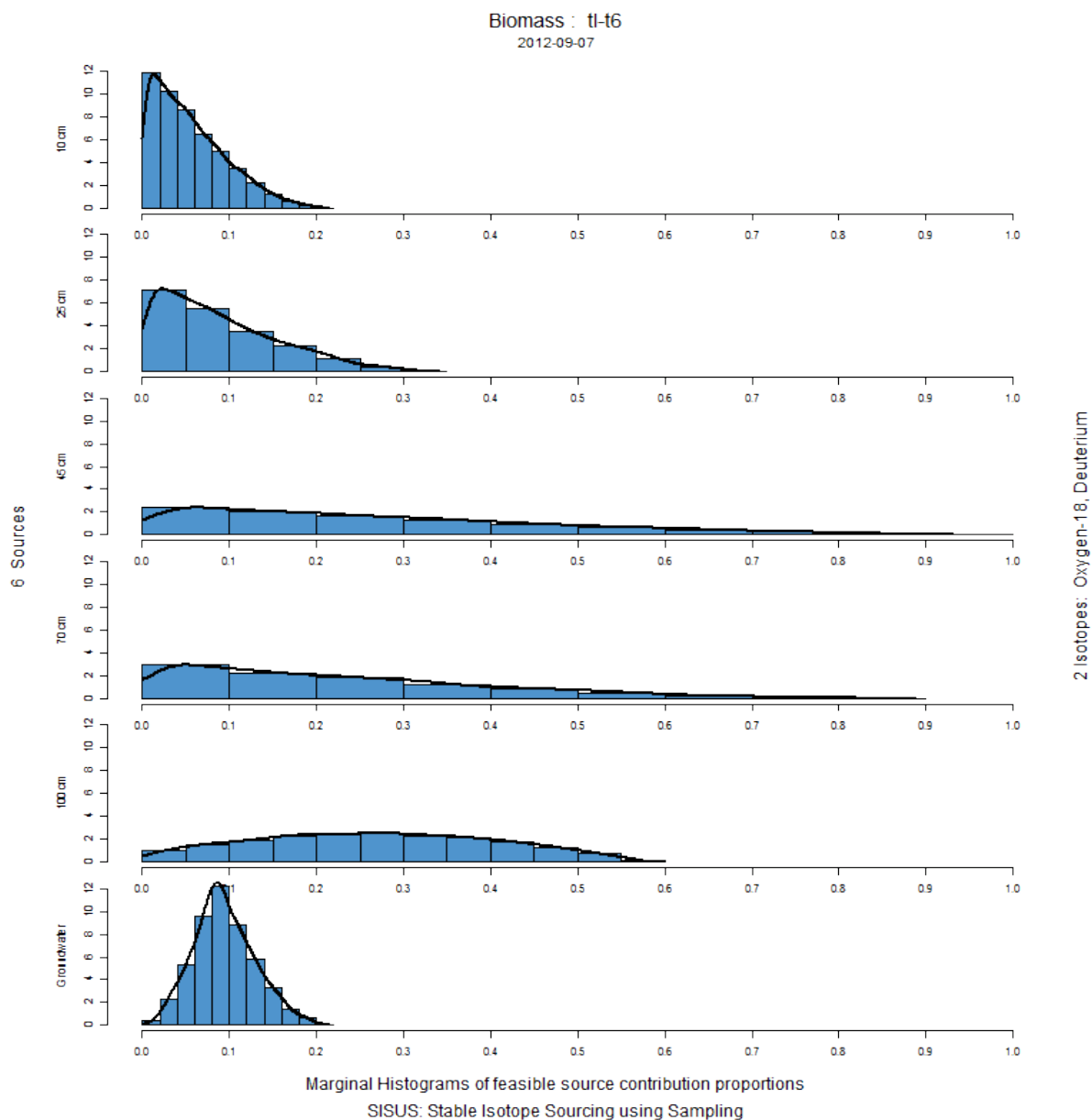


Figure 16. SISUS Modeling Output Example: Feasible water source contributions to the plant xylem water mixture. This model uses the Markov Chain Monte Carlo method to calculate unbiased proportional contribution estimates of each source (e.g., groundwater) to the mixture (woody plant xylem water). The x-axis labels percentage usage of each potential water source, while the y-axis labels the water source.

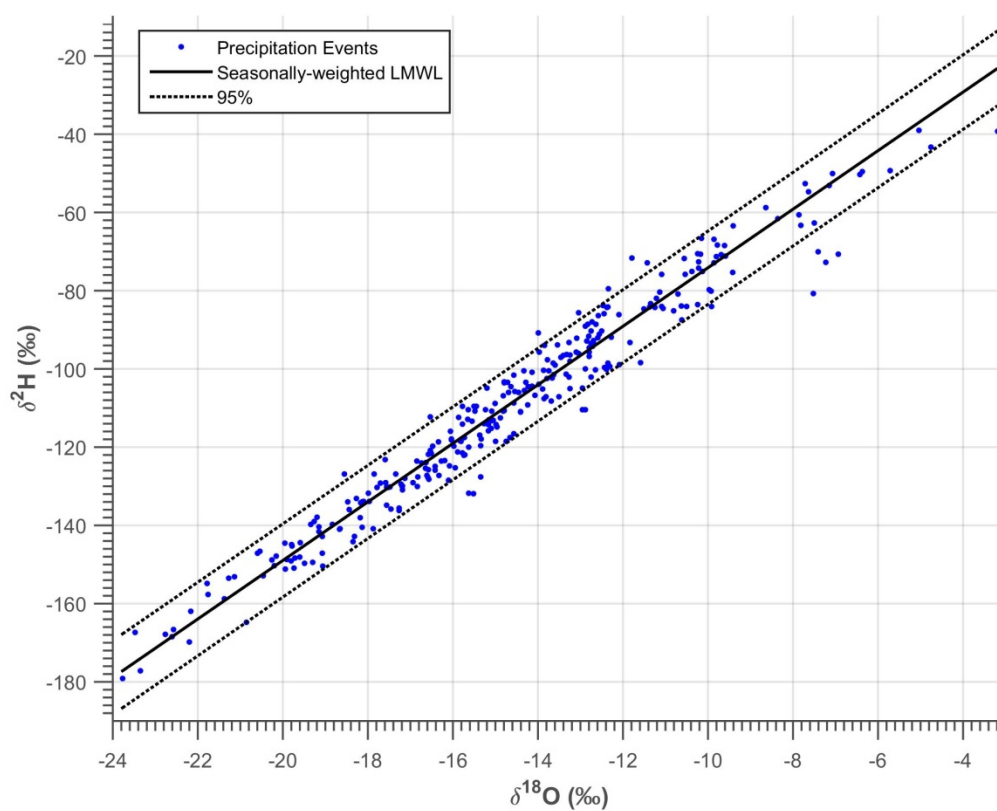


Figure 17. Dry Creek Experimental Watershed Seasonally-Weighted LMWL. Precipitation data collected at Lower Weather, Treeline and Lower Deer Point field sites from 2009 to 2012. Refer to Tappa (2013) for data collection and weighting-method information. Locations are depicted in Figure 4.

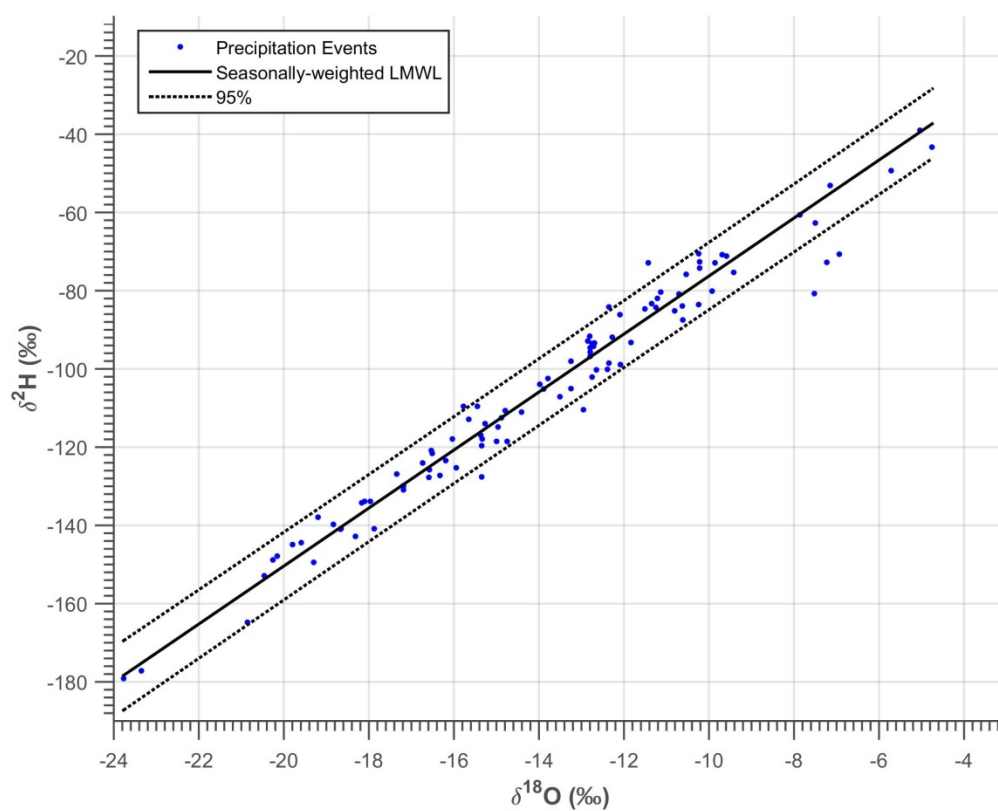


Figure 18. Lower Gauge Field Site Seasonally-Weighted LMWL. Precipitation data collected at Lower Weather from 2009 to 2012. Refer to Tappa (2013) for data collection and weighting-method information. This location is depicted in Figure 4.

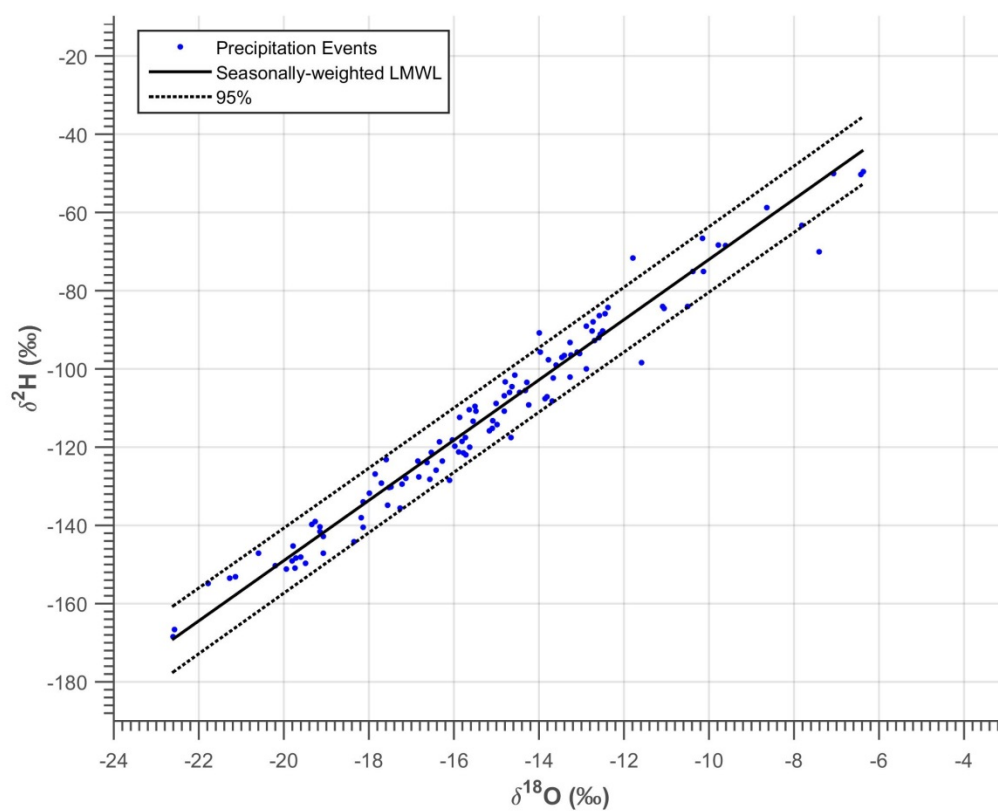


Figure 19. Treeline Field Site Seasonally-Weighted LMWL. Precipitation data collected at Treeline from 2009 to 2012. Refer to Tappa (2013) for data collection and weighting-method information. This location is depicted in Figure 4.

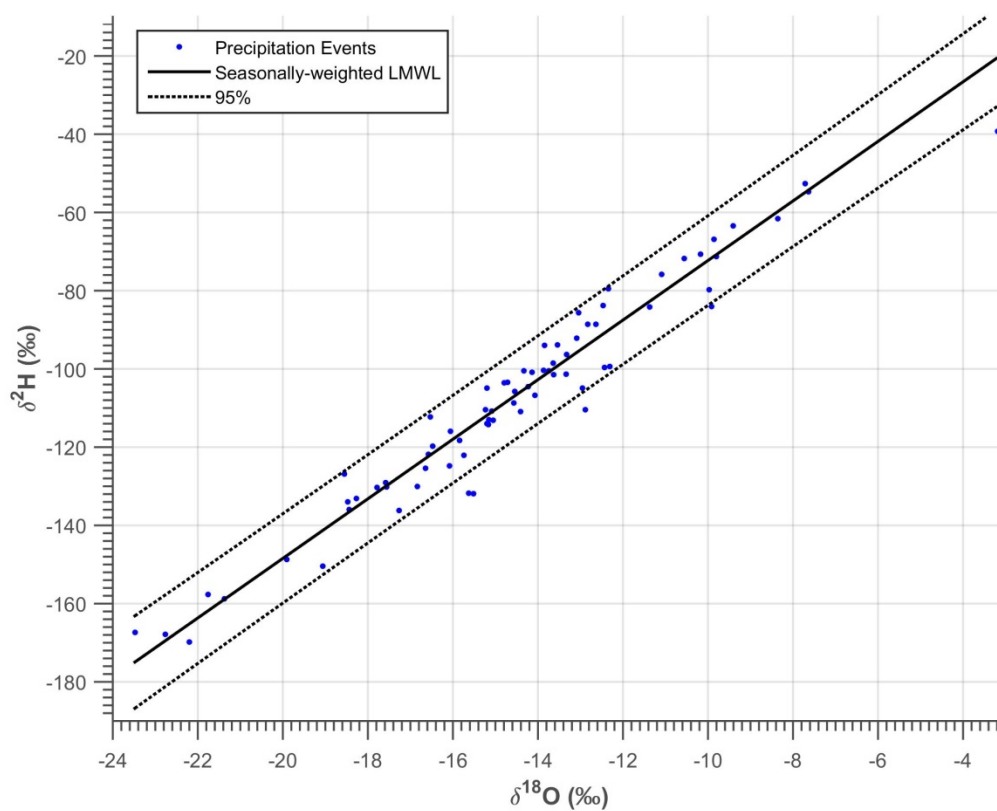


Figure 20. Lower Deer Point Field Site Seasonally-Weighted LMWL. Precipitation data collected at Lower Deer Point 2009 to 2012. Refer to Tappa (2013) for data collection and weighting-method information. This LMWL was used as a proxy for a LMWL at Bogus South. This location is depicted in Figure 4.

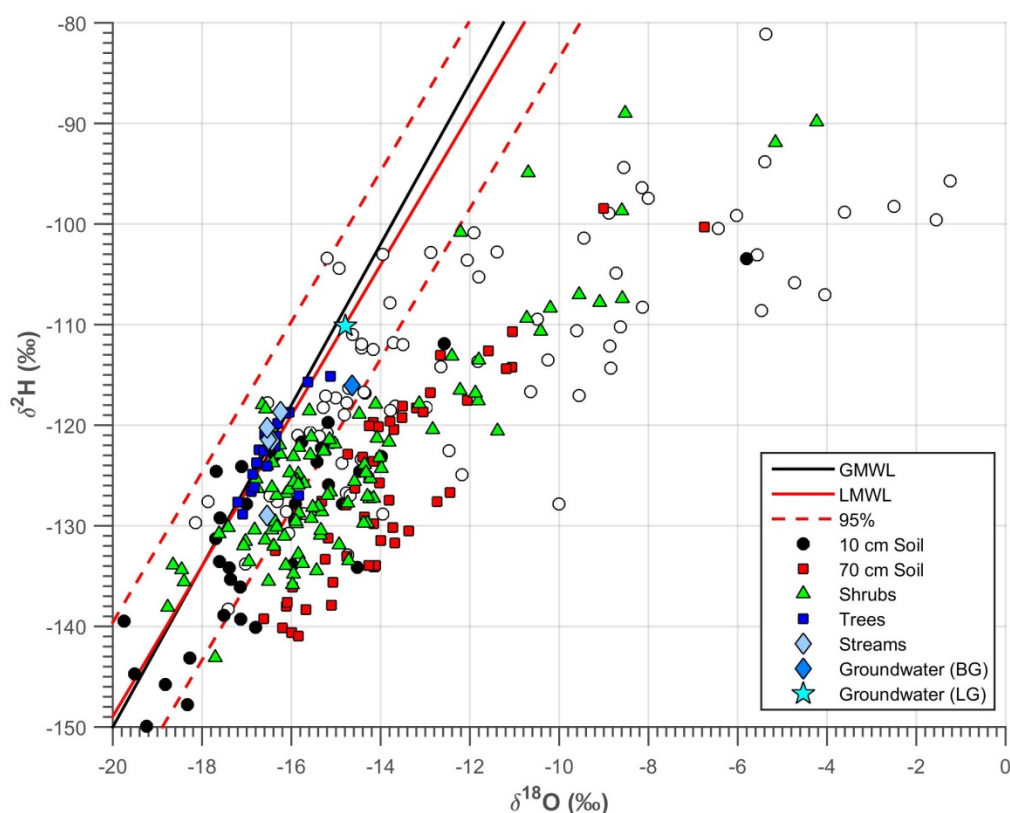


Figure 21. Dry Creek Experimental Watershed $\delta^2\text{H}$ and $\delta^{18}\text{O}$ isotope values (2012). Plotted values include water removed from trees, shrubs, streams, groundwater, and bulk soil water collected from 10 cm and 70 cm depths. Plant and soil samples collected from 03/27/2012 to 09/13/2012 are shown, while steamwater and groundwater samples were collected from 11/27/2011 to 10/9/2012. The Global Meteoric Water Line (Equation 4) and Dry Creek Experimental Watershed Seasonally-Weighted Local Meteoric Water Line (Equation 6) provide reference points for evaporative isotopic fractionation. The LMWL was derived from precipitation collected at Lower Gauge, Treeline and Lower Deer Point from 2009 to 2012 (see Tappa, 2013 for data and LMWL weighting method). Locations are depicted in Figure 4.

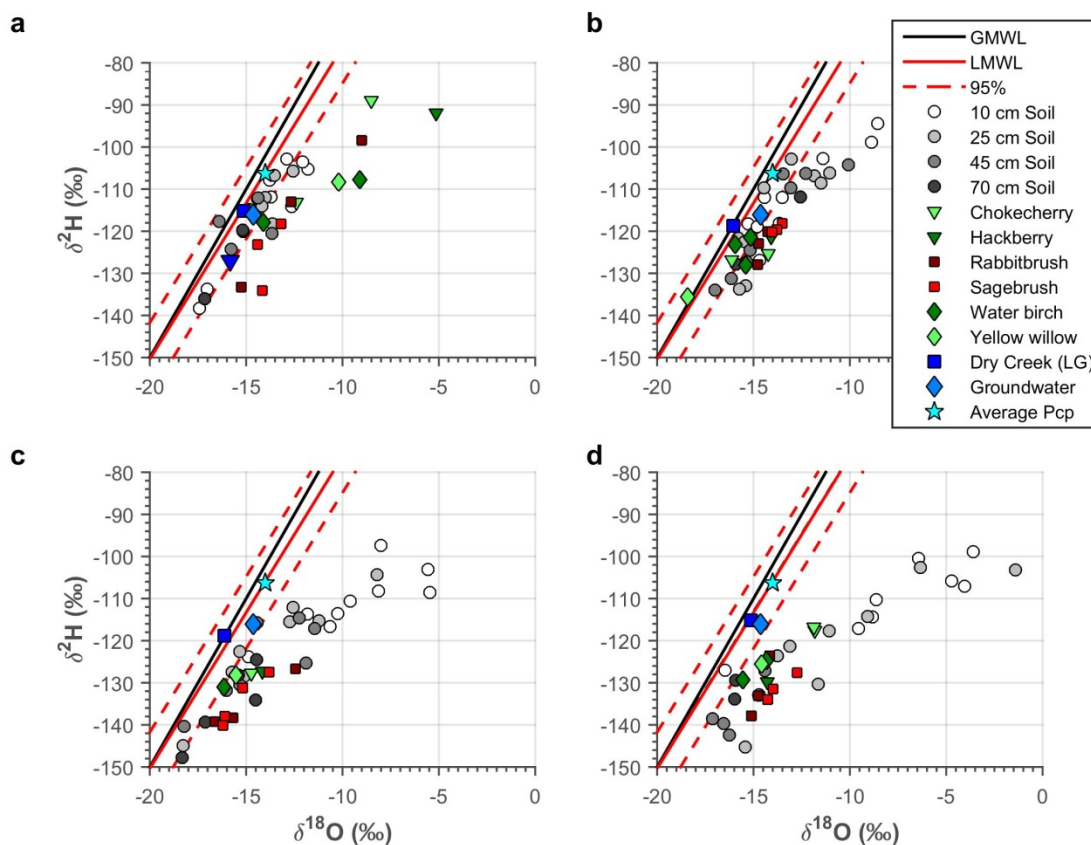


Figure 22. Lower Gauge (location depicted in Figure 4) $\delta^2\text{H}$ and $\delta^{18}\text{O}$ isotope values (2012). Samples shown include trees, shrubs, streams, groundwater, and soil water at 10 cm, 25 cm, 45 cm and 70 cm depths. Woody plants sampled from the Lower Gauge field site include Chokecherry, Hackberry, Rabbitbrush, Sagebrush, Water birch and Yellow willow. Groundwater was sampled on 03-23-2012 from a residential well near Lower Gauge (Table 8). Streamwater was sampled during each field site visit. The Global Meteoric Water Line (Equation 4) and Seasonally-Weighted Local Meteoric Water Line (Equation 7) from precipitation collected at Lower Gauge from 2009 to 2012 provide reference points for evaporative isotopic fractionation (see Tappa, 2013 for data and LMWL weighting method). (a) 04-08-2012, (b) 06-04-2012, (c) 07-10-2012, (d) 09-13-2012

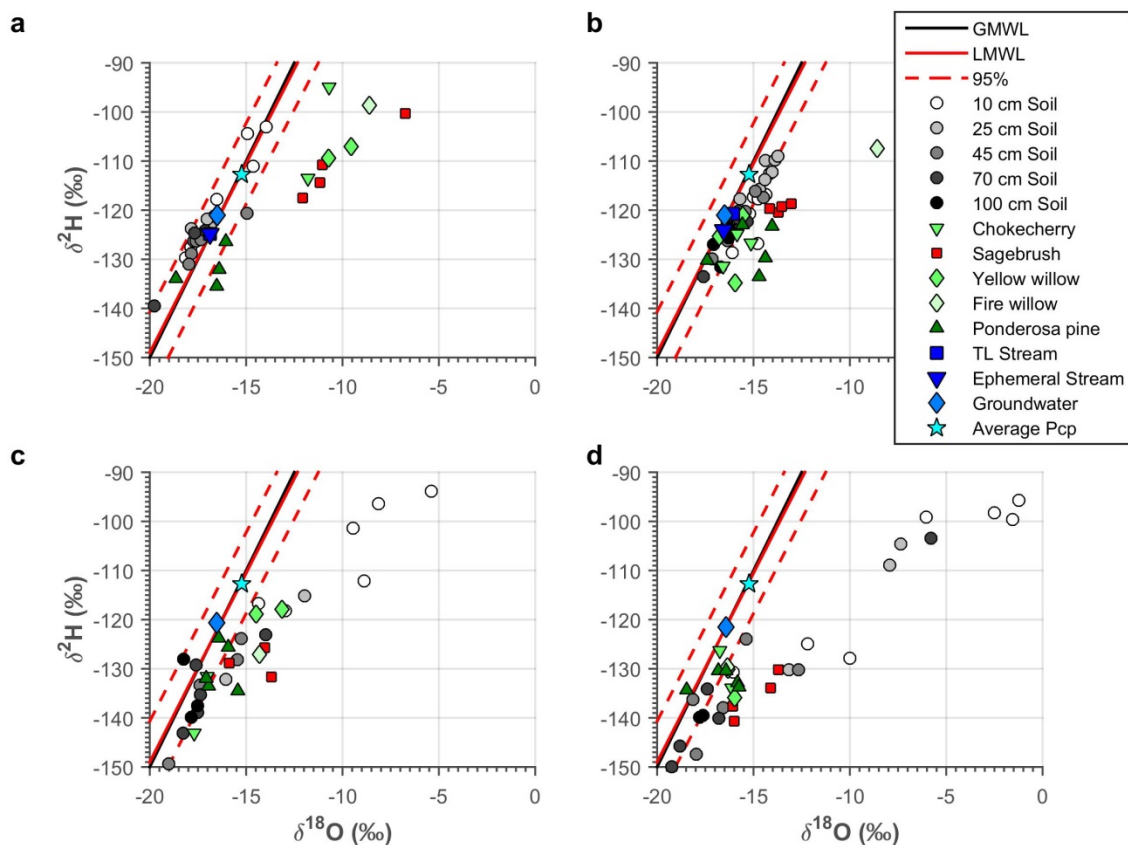


Figure 23. Treeline (location depicted in Figure 4) $\delta^2\text{H}$ and $\delta^{18}\text{O}$ isotope values (2012). Samples shown include trees, shrubs, streams, groundwater, and soil water at 10 cm, 25 cm, 45 cm, 70 cm and 100 cm depths. Woody plants sampled from Treeline field site include Chokecherry, Sagebrush, Yellow willow, Fire willow and Ponderosa pine. Groundwater was sampled during each field site visit from a freshwater spring between Lower Deer Point and Bogus Gauge (Table 8). The Global Meteoric Water Line (Equation 4) and Seasonally-Weighted Local Meteoric Water Line (Equation 8) from precipitation collected at Treeline from 2009 to 2012 provide reference points for evaporative isotopic fractionation. (a) 03-27-2012, (b) 05-17-2012, (c) 07-09-2012, (d) 09-07-2012.

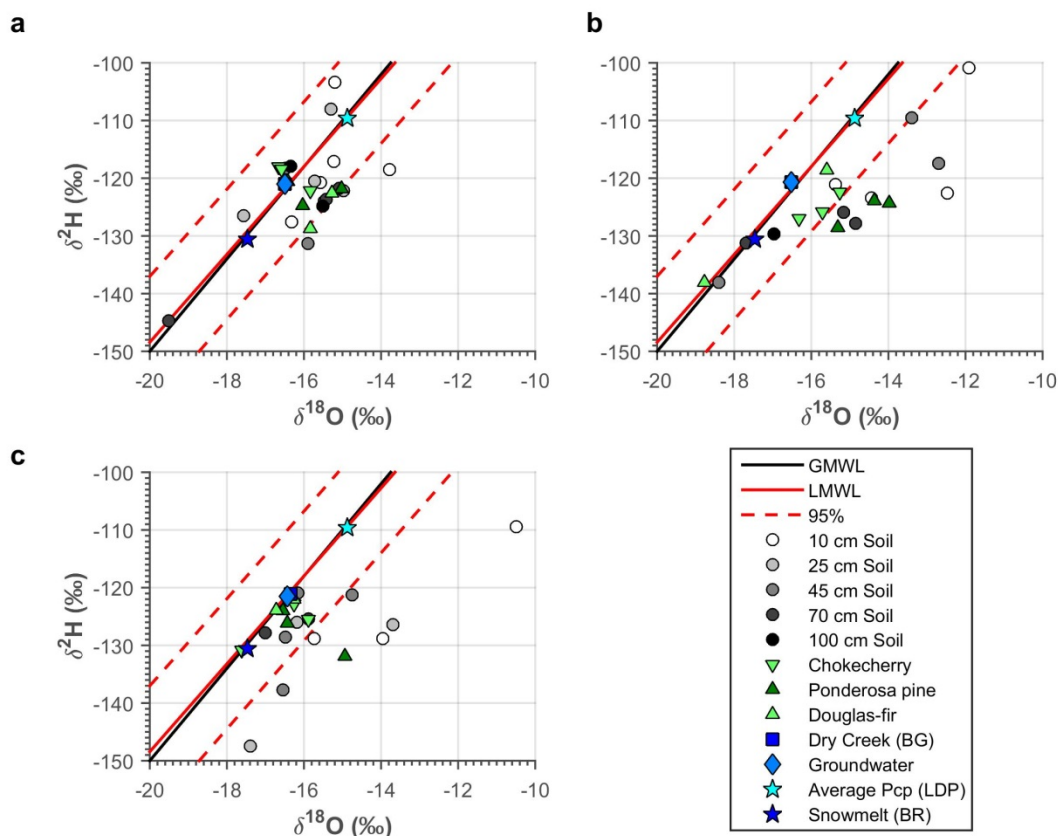


Figure 24. Bogus South (location depicted in Figure 4) $\delta^2\text{H}$ and $\delta^{18}\text{O}$ isotope values (2012). Samples shown include trees, shrubs, streams, groundwater, and soil water at 10 cm, 25 cm, 45 cm, 70 cm and 100 cm depths. Woody plants sampled from Treeline field site include Chokecherry, Sagebrush, Yellow willow, Fire willow and Ponderosa pine. Groundwater was sampled during each field site visit from a freshwater spring between Lower Deer Point and Bogus Gauge (Table 8). The Global Meteoric Water Line (Equation 4) and Seasonally-Weighted Local Meteoric Water Line (Equation 7) from precipitation collected at Bogus South from 2009 to 2012 provide reference points for evaporative isotopic fractionation. Note that the axes were shrunk and some evaporatively-enriched soil water isotope values plotted outside of the axis limits. This was done in an effort to zoom in on the plants because Bogus South plants and bulk soil water lie closer to streamwater and groundwater values than other field sites. (a) 06-06-2012, (b) 07-08-2012, (c) 09-04-2012.

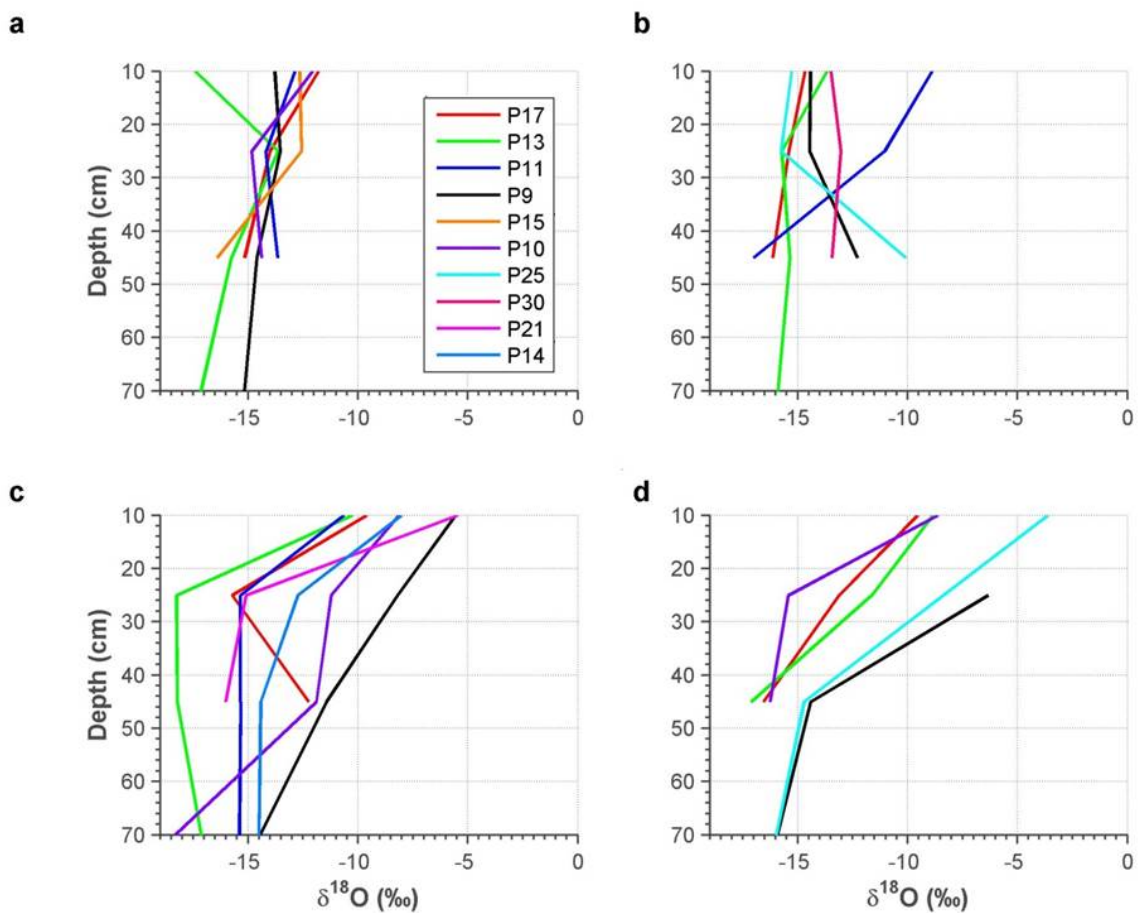


Figure 25. Lower Gauge soil pit $\delta^{18}\text{O}$ values. Each line represents a linear interpolation between $\delta^{18}\text{O}$ value data points from bulk soil water collected at 10 cm, 25 cm, 45 cm and 70 cm depths. Note that the legend denotes soil pits dug on each sampling date, within 5 meters of a specific plant individual (Table 7). This location is depicted in Figure 4. (a) 04-08-2012, (b) 06-04-2012, (c) 07-10-2012, (d) 09-13-2012

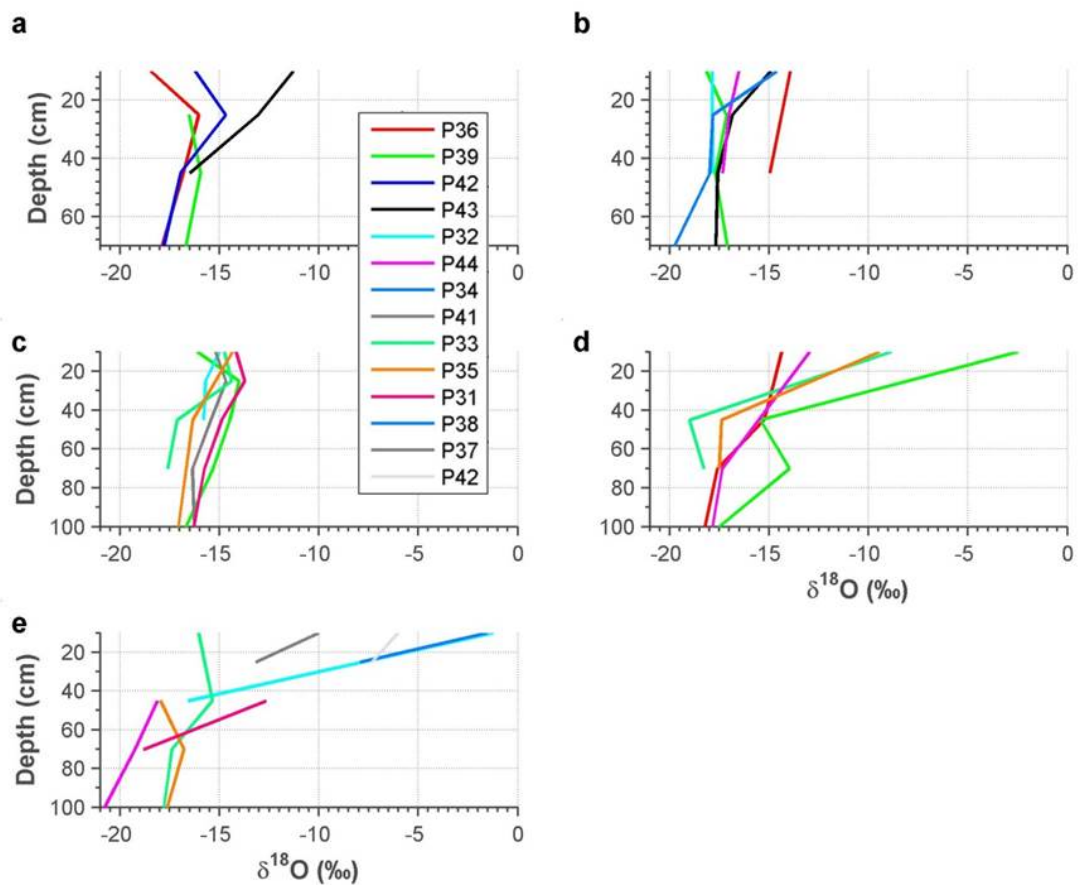


Figure 26. Treeline soil pit $\delta^{18}\text{O}$ values. Each line represents a linear interpolation between $\delta^{18}\text{O}$ value data points from bulk soil water collected at 10 cm, 25 cm, 45 cm and 70 cm depths. Note that the legend denotes soil pits dug on each sampling date, within 5 meters of a specific plant individual (Table 7). This location is depicted in Figure 4. (a) 10-14-2011, (b) 03-27-2012, (c) 05-17-2012, (d) 07-09-2012, (e) 09-07-2012

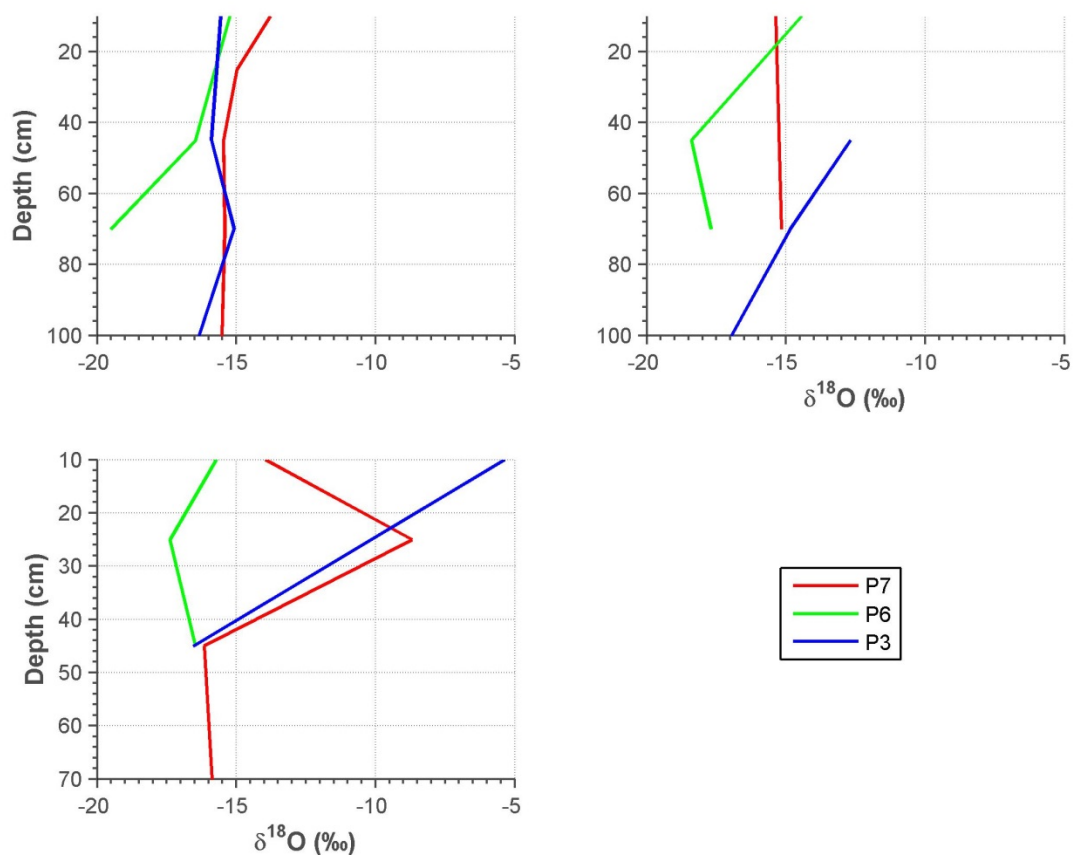


Figure 27. HN (a field site proxy for Bogus South) soil pit $\delta^{18}\text{O}$ values. Each line represents a linear interpolation between $\delta^{18}\text{O}$ value data points from bulk soil water collected at 10 cm, 25 cm, 45 cm and 70 cm depths. Note that the legend denotes soil pits dug on each sampling date, within 5 meters of a specific plant individual (Table 7). This location is depicted in Figure 4. (a) 06-06-2012, (b) 07-08-2012, (c) 09-04-2012

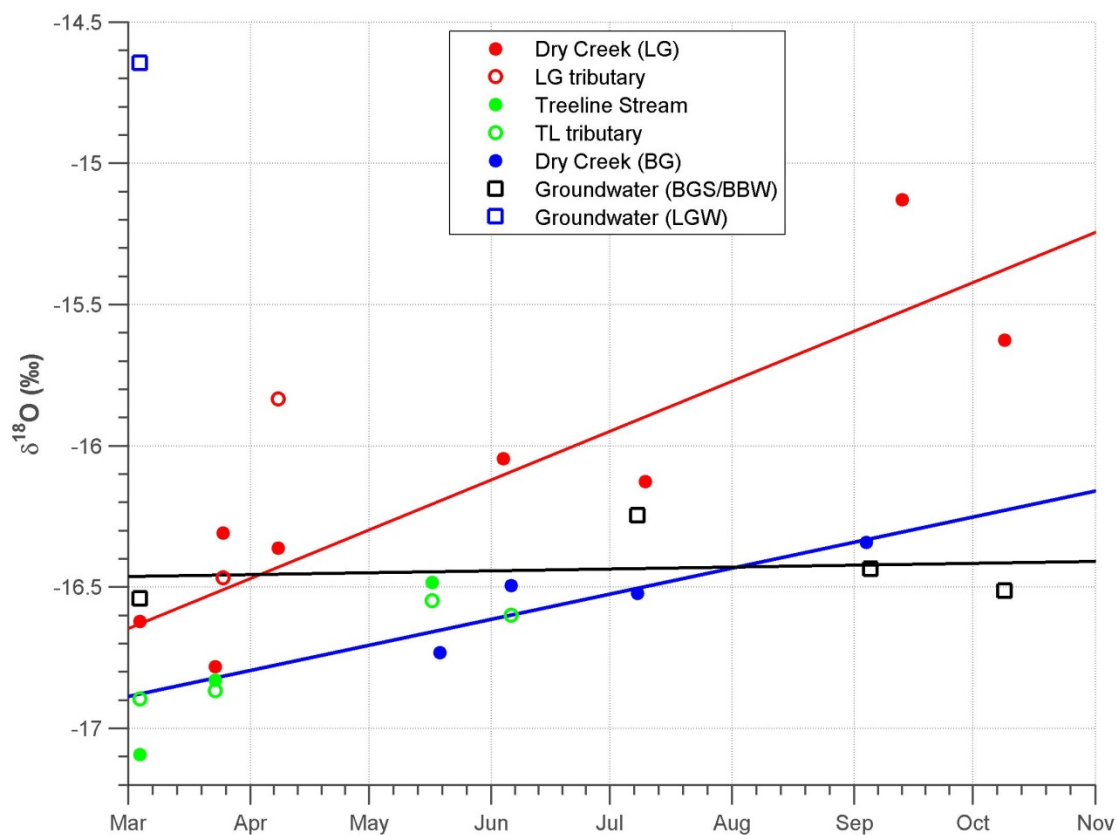


Figure 28. Temporal variability of Dry Creek Experimental Watershed groundwater and stream water $\delta^{18}\text{O}$ values (2012). High elevation groundwater was acquired from a freshwater spring between Lower Deer Point and Bogus South (BGS) and a well near Bogus Basin (BBW), while low elevation groundwater (LGW) was acquired from a residential well near Lower Gauge. Note that groundwater from LGW was only collected once. LG = Lower Gauge. TL = Treeline. BG = Bogus South. Locations are depicted in Figure 4.

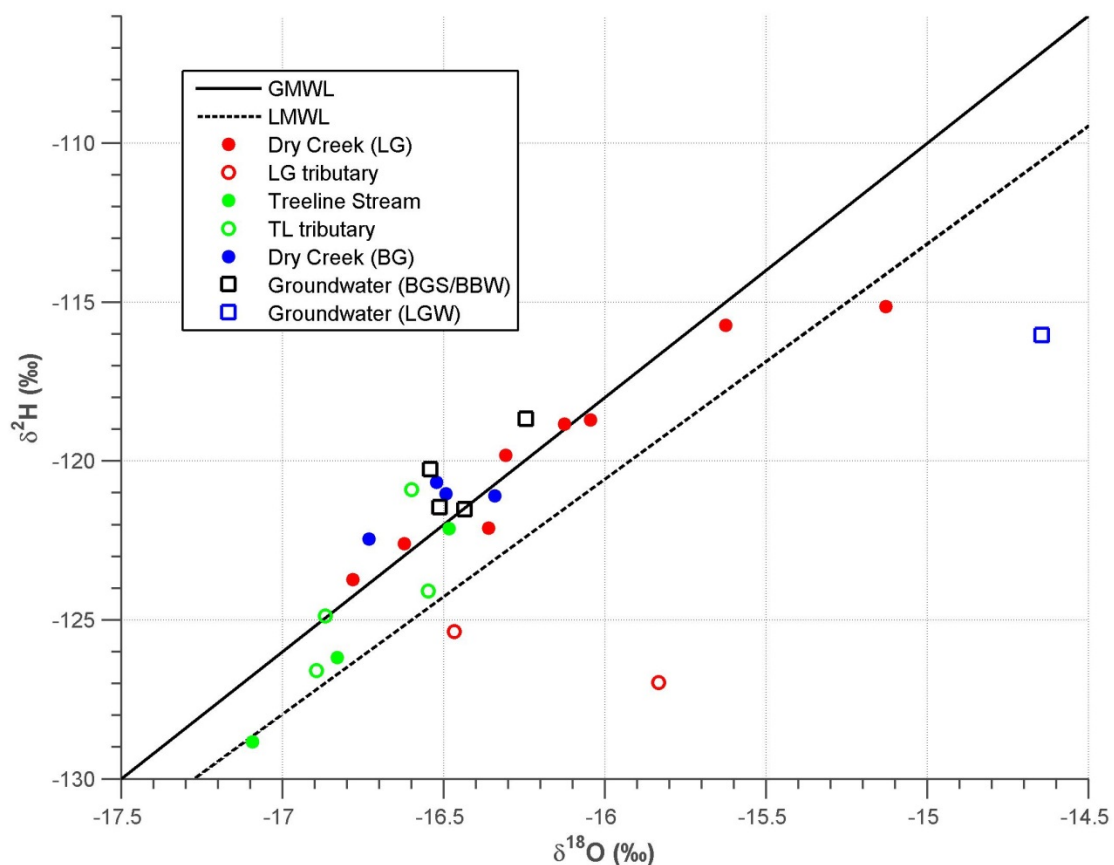


Figure 29. Temporal variability of Dry Creek Experimental Watershed streamwater and groundwater (outliers removed) along the LMWL (2012). Groundwater (BGS/BBW) was acquired from a freshwater spring between BG and a well near Bogus Basin, while Groundwater (LGW) was acquired from a residential well near LG. Locations are depicted in Figure 4.

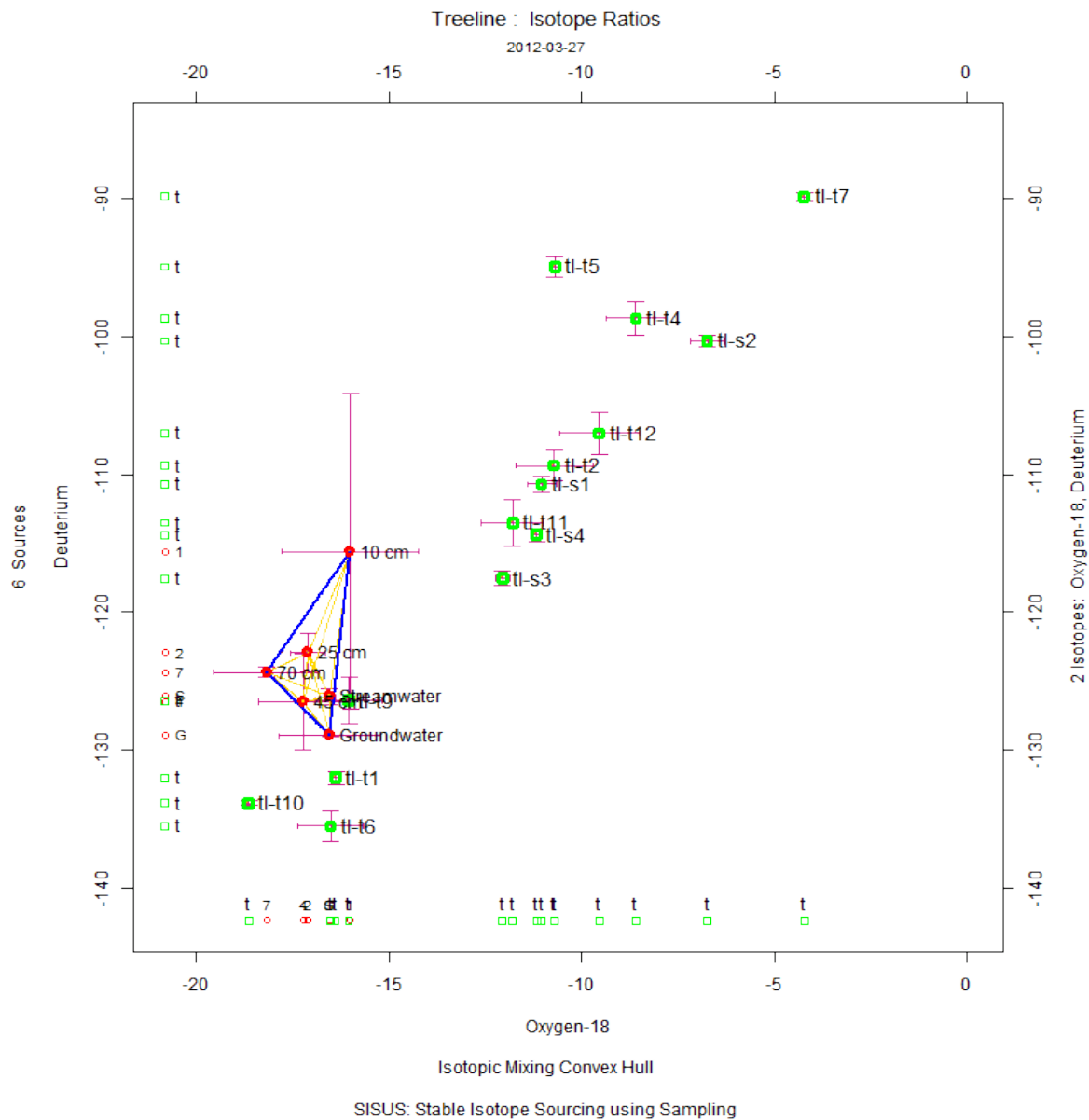


Figure 30. SISUS modeled Isotopic Mixing Convex Hull output for Treeline samples collected on 03-27-2012. This location is depicted in Figure 4.

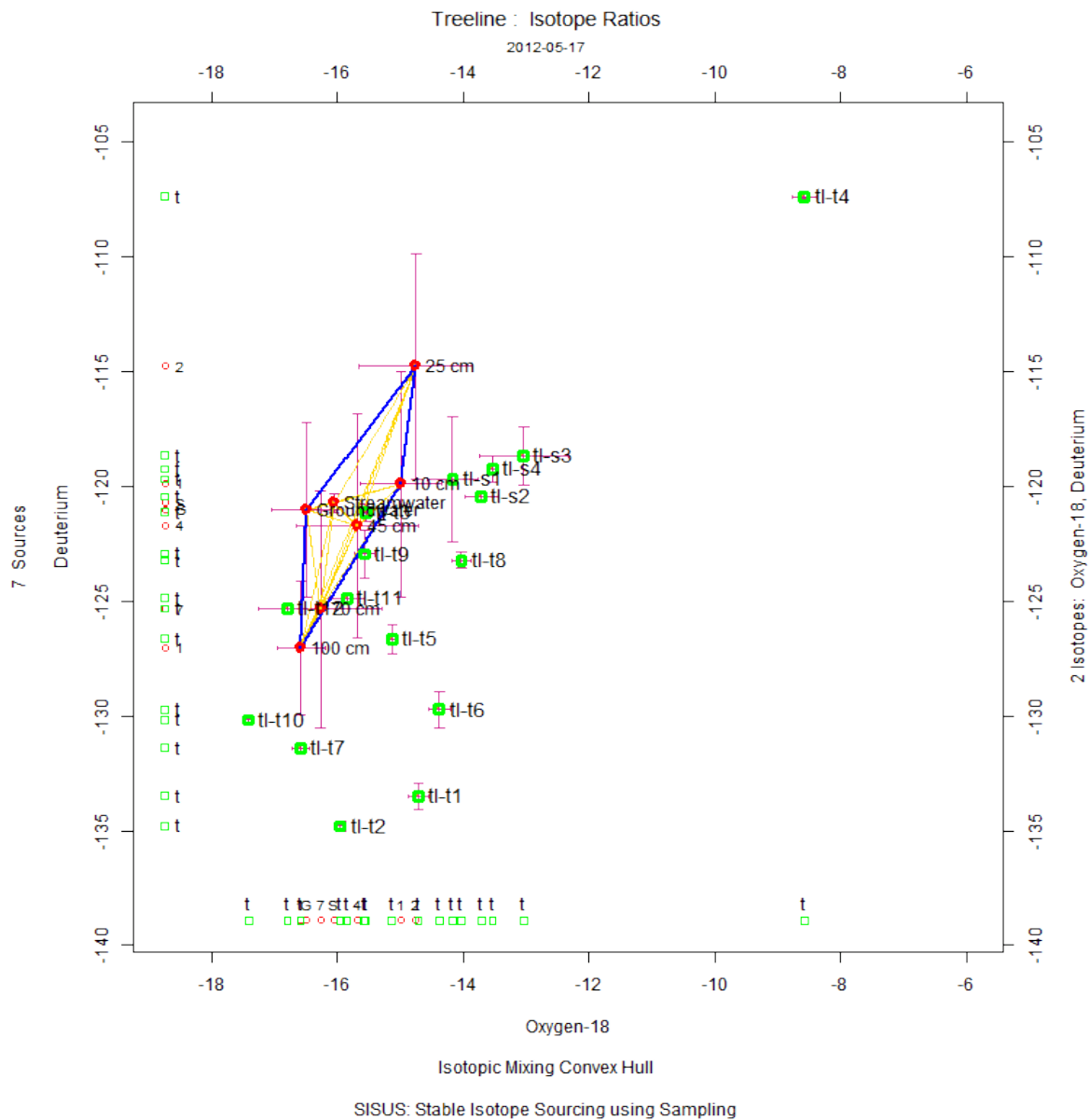


Figure 31. SISUS modeled Isotopic Mixing Convex Hull output for Treeline samples collected on 05-17-2012. This location is depicted in Figure 4.

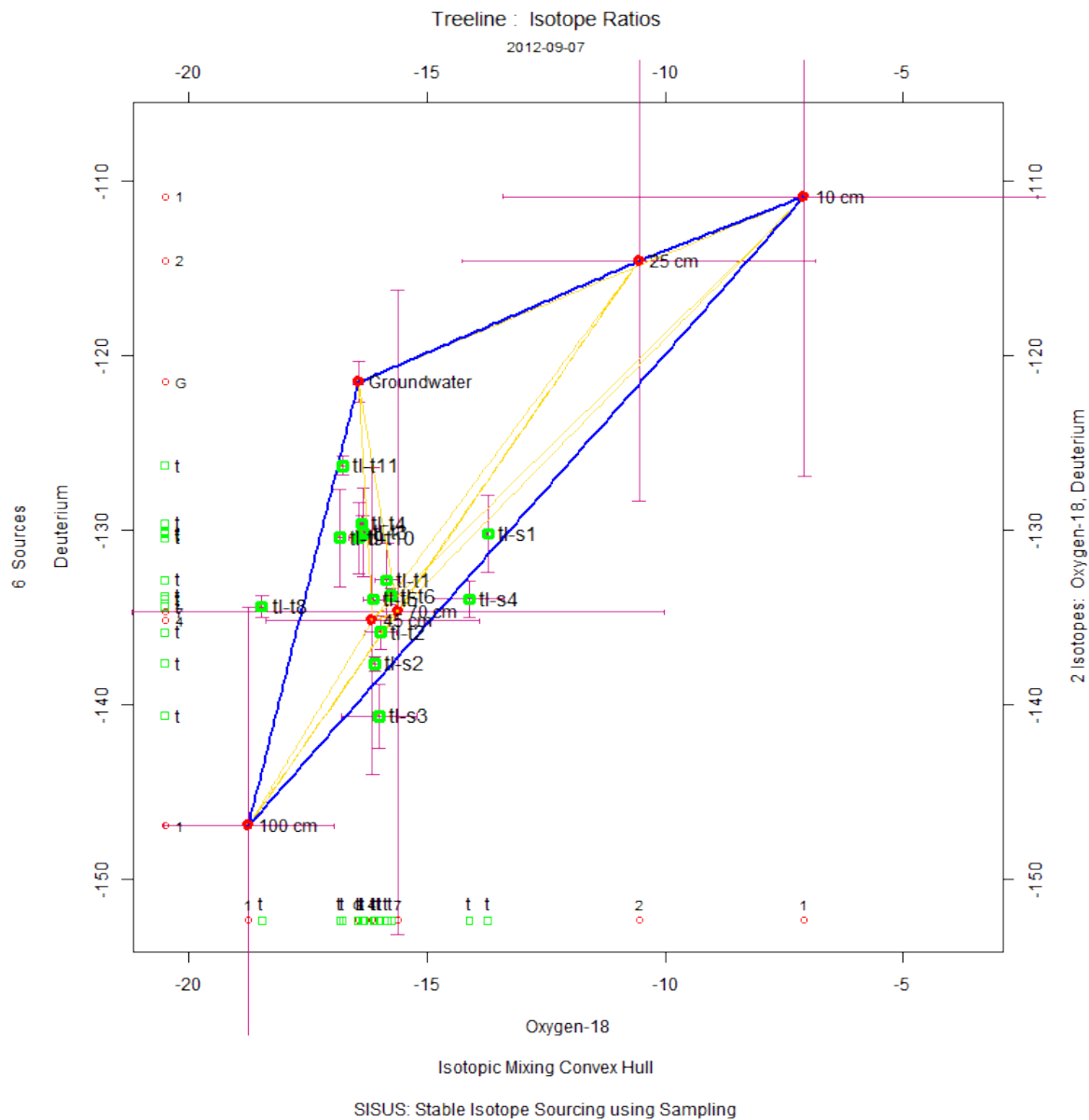


Figure 32. SISUS modeled Isotopic Mixing Convex Hull output for Treeline samples collected on 09-07-2012. This location is depicted in Figure 4.

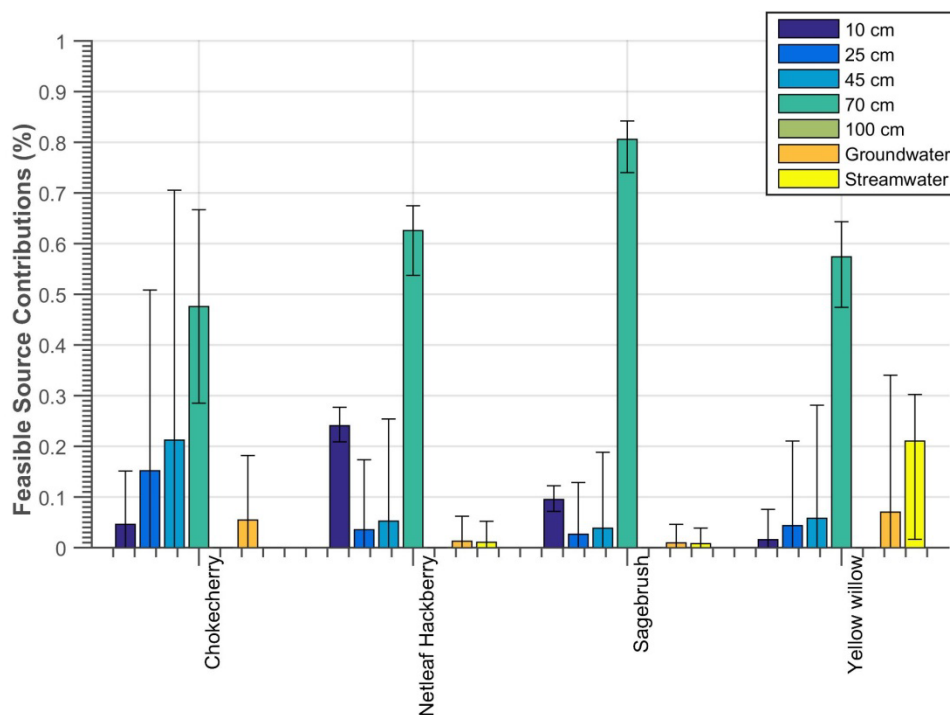


Figure 33. Lower Gauge (07-10-2012) SISUS modeled woody plant individual mean feasible contributions (y-axis) of water sources (x-axis) for each successfully modeled woody plant (Table 14). The bar represents the median, while the errorbars represent the minimum and maximum modeled source contributions to the plant individual. This location is depicted in Figure 4.

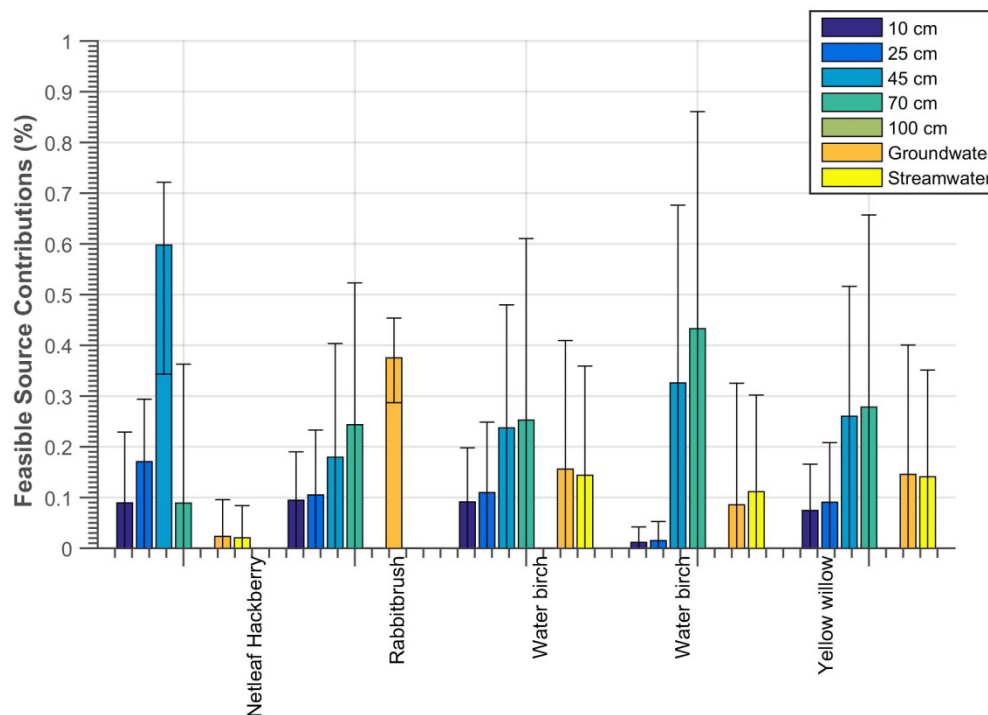


Figure 34. Lower Gauge (09-13-2012) SISUS modeled woody plant individual mean feasible contributions (y-axis) of water sources (x-axis) for each successfully modeled woody plant (Table 14). The bar represents the median, while the errorbars represent the minimum and maximum modeled source contributions to the plant individual. This location is depicted in Figure 4.

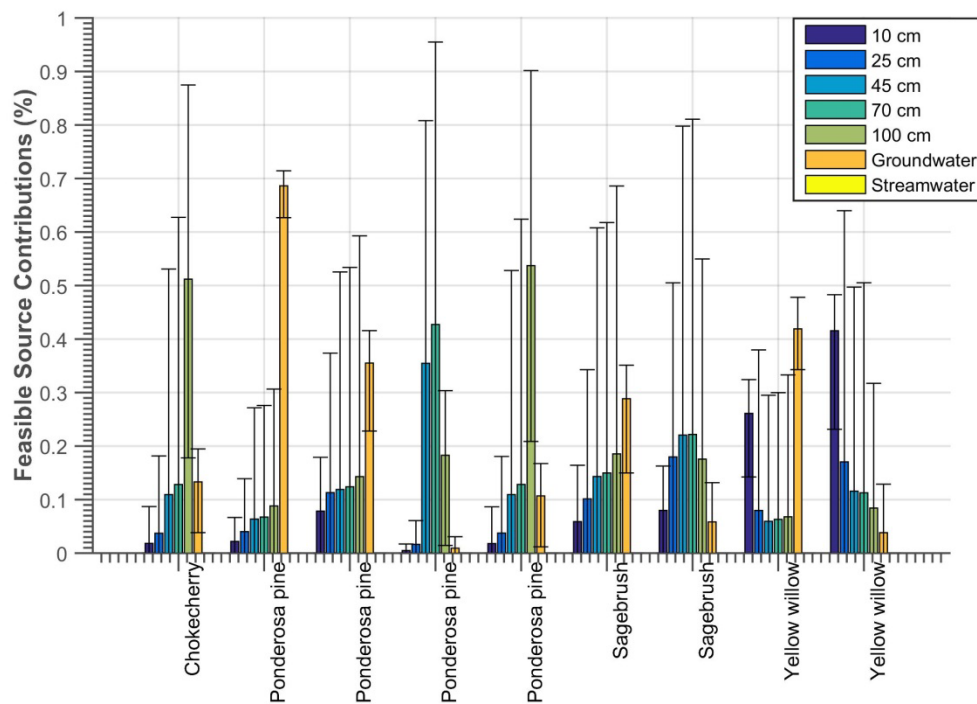


Figure 35. Treeline (07-09-2012) SISUS modeled woody plant individual mean feasible contributions (y-axis) of water sources (x-axis) for each successfully modeled woody plant (Table 14). The bar represents the median, while the errorbars represent the minimum and maximum modeled source contributions to the plant individual. This location is depicted in Figure 4.

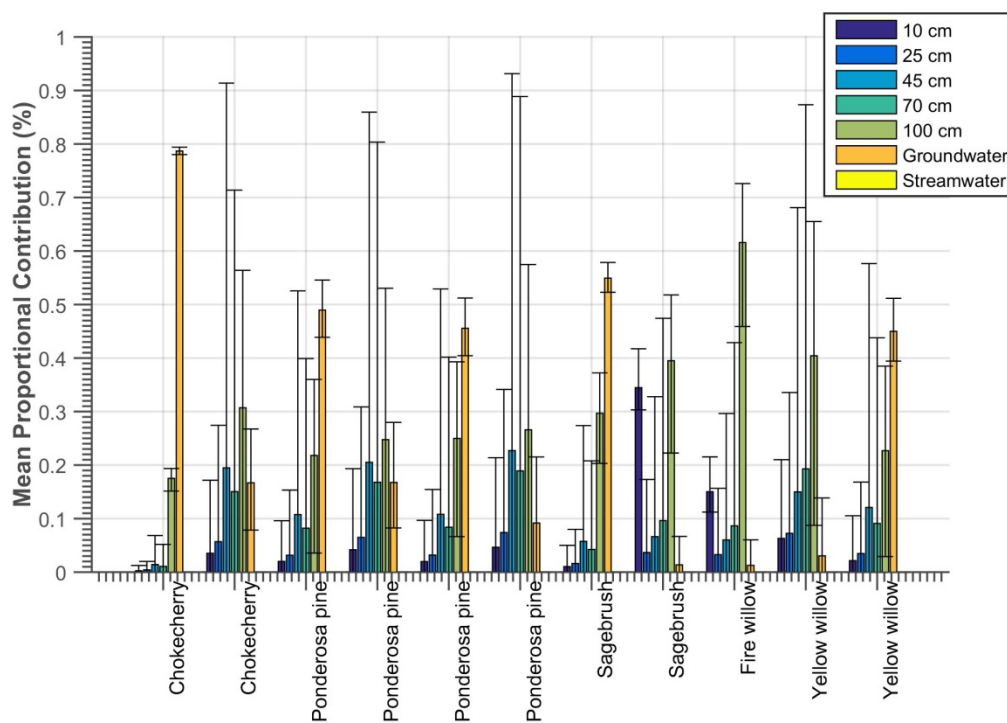


Figure 36. Treeline (09-07-2012) SISUS modeled woody plant individual mean feasible contributions (y-axis) of water sources (x-axis) for each successfully modeled woody plant (Table 14). The bar represents the median, while the errorbars represent the minimum and maximum modeled source contributions to the plant individual. This location is depicted in Figure 4.

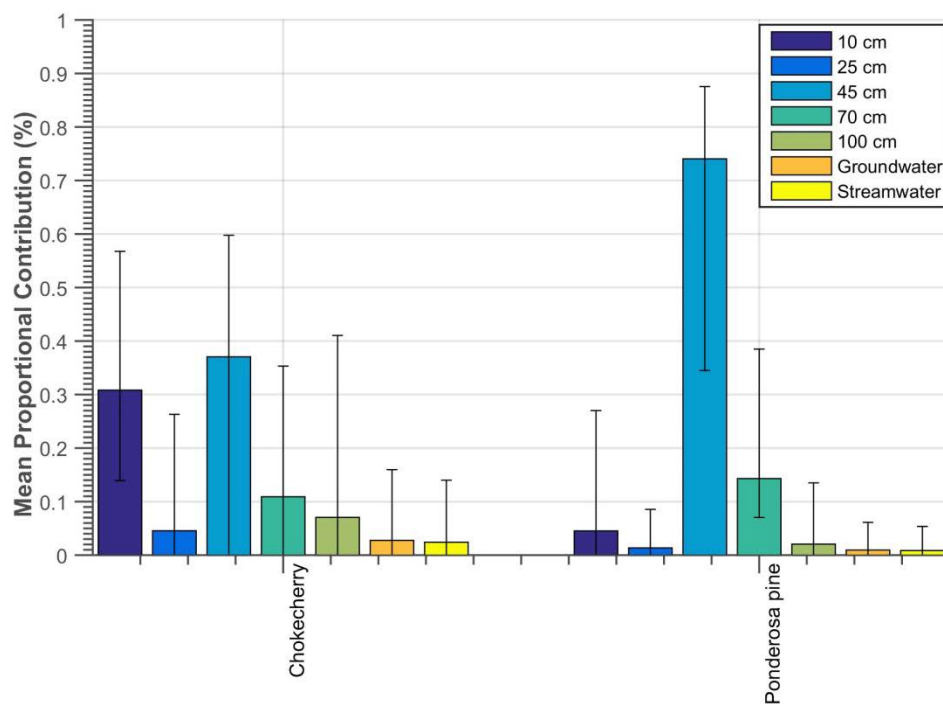


Figure 37. Bogus South (06-06-2012) SISUS modeled woody plant individual mean feasible contributions (y-axis) of water sources (x-axis) for each successfully modeled woody plant (Table 14). The bar represents the median, while the errorbars represent the minimum and maximum modeled source contributions to the plant individual. This location is depicted in Figure 4.

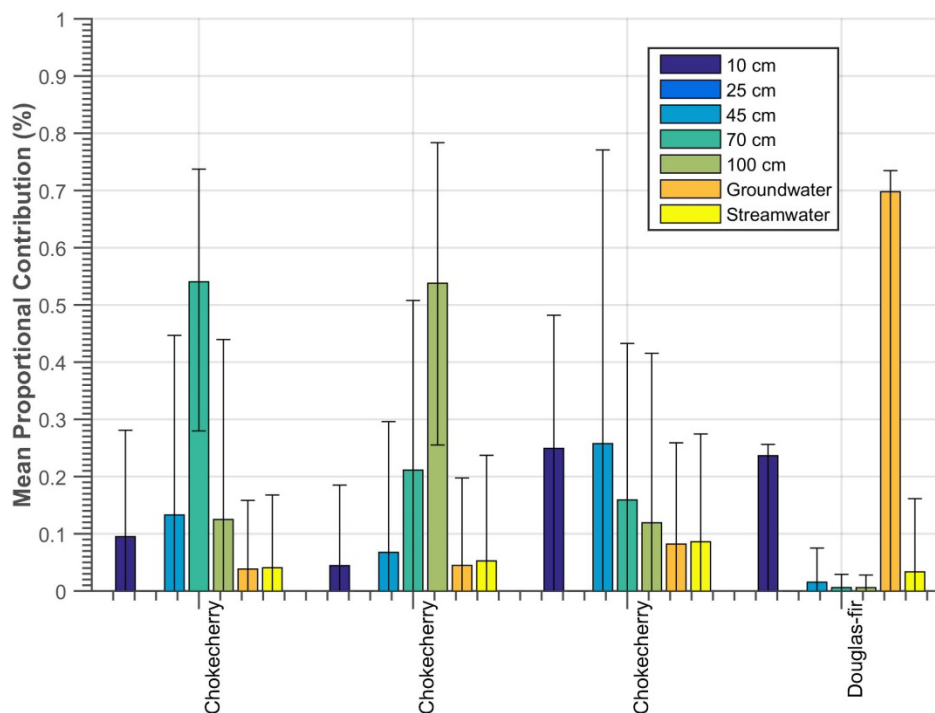


Figure 38. Bogus South (07-08-2012) SISUS modeled woody plant individual mean feasible contributions (y-axis) of water sources (x-axis) for each successfully modeled woody plant (Table 14). The bar represents the median, while the errorbars represent the minimum and maximum modeled source contributions to the plant individual. This location is depicted in Figure 4.

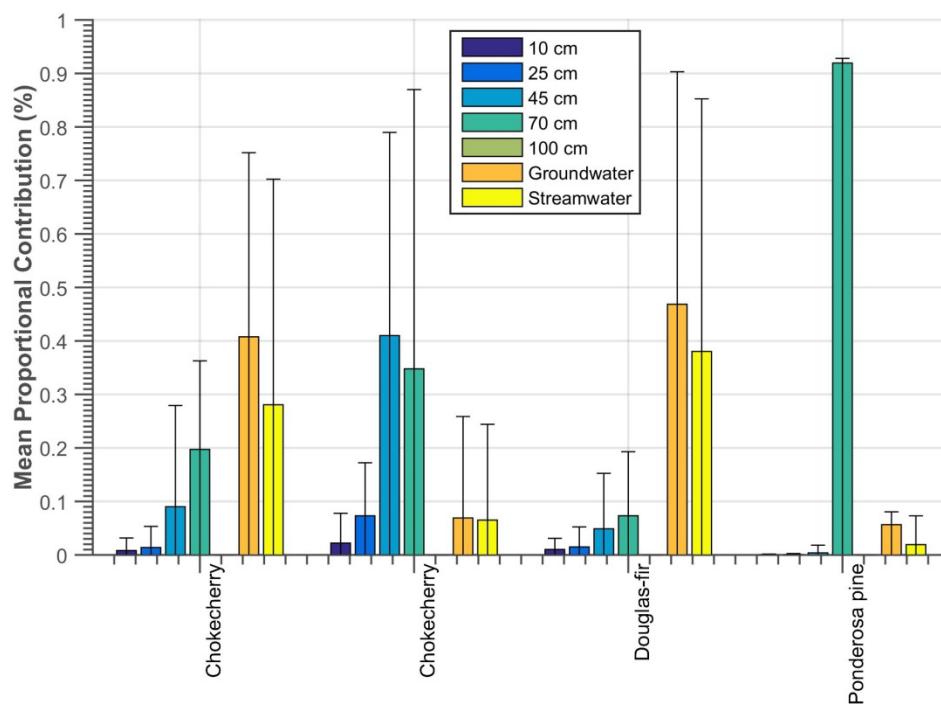


Figure 39. Bogus South (09-04-2012) SISUS modeled woody plant individual mean feasible contributions (y-axis) of water sources (x-axis) for each successfully modeled woody plant (Table 14). The bar represents the median, while the errorbars represent the minimum and maximum modeled source contributions to the plant individual. This location is depicted in Figure 4.

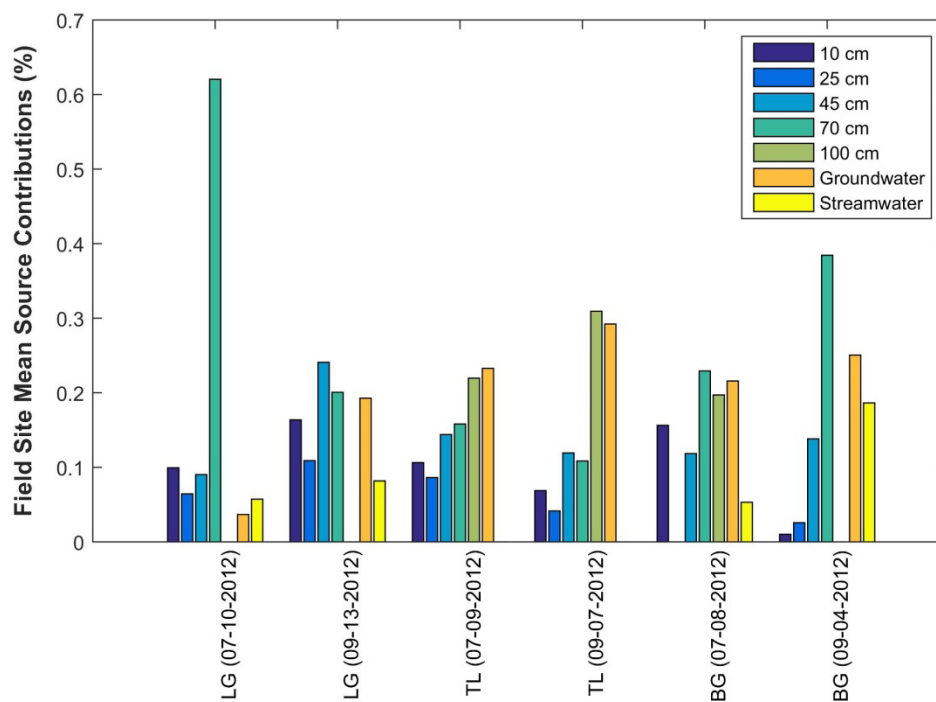


Figure 40. SISUS modeled mean field site scale proportional contributions of source water to woody plant xylem water. The bars of the graph represent the average of the median feasible source contributions for each plant individual modeled at each field site, collected on each sampling date. Locations are depicted in Figure 4.

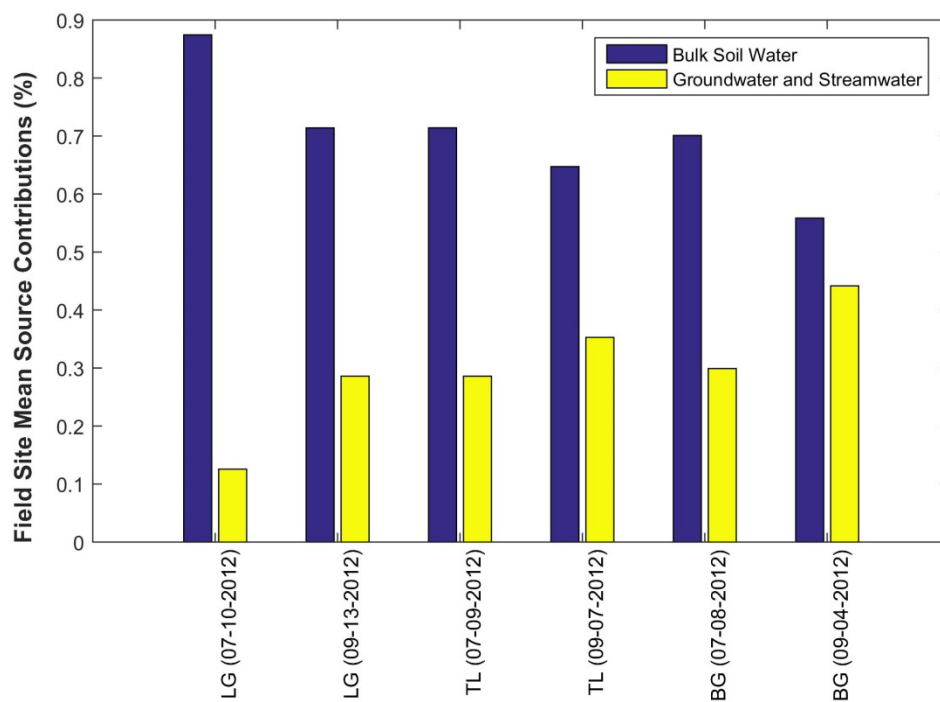


Figure 41. SISUS modeled mean field site scale proportional contributions of source water to woody plant xylem water. The bars of the graph represent the average of the median feasible source contributions for each plant individual modeled at each field site, collected on each sampling date. Locations are depicted in Figure 4.

APPENDIX C**Los Gatos Liquid Water Isotope Analyzer – Correcting for Spectral Interference****Caused by Organic Contaminants**

LOS GATOS LIQUID WATER ISOTOPE ANALYZER – CORRECTING FOR SPECTRAL INTERFERENCE CAUSED BY ORGANIC CONTAMINANTS

Post Analysis Software

The LWIA-PAS was used upon completion of each LWIA run (see Materials and Methods). A full review of the LWIA-recorded data that this software can analyze is available online via the LWIA Post Analysis Software User's Guide. The LWIA collects six injections from each sample, yielding six $\delta^2\text{H}$ and $\delta^{18}\text{O}$ values from which sample averages can be calculated. However, standard data processing methods ignore the first two injections in an effort to mitigate memory effects. Therefore, each sample mean stable isotope value is the average of four injections (assuming that no injections were filtered by the LWIA instrument or LWIA-PAS). Flags and filters related to injection volume, temperature variations, etc. were set up according to standard LWIA-PAS specifications. Refer to the LWIA Post-Analysis User's Guide Version 2.1 for information about conditions that exclude single injection isotope values from sample mean calculations.

After the LWIA measured raw $\delta^2\text{H}$ and $\delta^{18}\text{O}$ values, the LWIA-PAS was used to correct all raw isotope ratio data to match fluctuations in raw isotope ratios reported for standards of known isotope values. Sample isotope ratios are corrected to these standards of known isotope value to prevent machine error. Figure 44 shows temporal variability of the standards for a normal LWIA run. Five LGR standards ($\delta^2\text{H} = -154.10$ to -9.80 , $\delta^{18}\text{O} = -19.57$ to -2.96) were used. These standards were chosen because their range of stable isotope values encompasses the stable isotope values of the vast majority of our plant, soil, stream, and groundwater samples. A standard was run after every six samples, and

one of each standard comprises a standard group (Figure 45). Every sample belongs to a standard group, to which its isotope value is corrected. Following isotope value correction to the standards, LGR-LWIA data was loaded into the Spectral Contaminant Identifier software (LWIA-SCI) for further processing.

Spectral Contaminant Identification Software

The Spectral Contaminant Identification Version 1.0.0 (LWIA-SCI) was created by LGR in 2010. Its original purpose was to flag water samples that contain contaminants with spectral absorption properties similar to water isotopologues so that those samples could be omitted from analysis. These contaminants cause errors in LWIA $\delta^2\text{H}$ and $\delta^{18}\text{O}$ values because they influence the spectral transmission fitting routine (Equation 5), as it is not trained to recognize them. The LWIA-SCI characterizes contaminants as either broadband absorbers or narrowband absorbers, measured by the broadband metric and narrowband metric respectively (LWIA-SCI manual). Fortunately for IRIS users, several recent studies have suggested that clear relationships between these metrics and errors in LWIA $\delta^2\text{H}$ and $\delta^{18}\text{O}$ values can be characterized (West & Goldsmith, 2010; West et al., 2011; Zhao et al., 2011; Brand, 2010; Brand, 2009). Using these relationships, the LWIA-SCI software may be used to correct LWIA isotope data for such interference (Brian Leen et al., 2012; Schultz et al., 2011; West et al., 2011).

Contaminants flagged by the LWIA-SCI broadband and narrowband metrics are commonly organic, and are therefore commonly found in plant water and soil water of high organic carbon concentration. These contaminants can interfere with the LWIA's calculation of isotope ratios if they are volatile enough to enter the absorbance cavity and they absorb light within the range of wavelengths used to identify isotopologues of water

(West & Goldsmith, 2010). Organic contaminants from plant and soil water often fit these criteria because some of them are quite volatile and their atomic structures feature an O-H bond similar to water isotopologues, giving them similar spectral absorption properties.

Broadband absorbers are defined as contaminants that absorb light across the entire spectrum within which water isotopomers absorb, resulting in a decrease in light transmission at all wavelengths (LWIA-SCI Manual). The broadband metric (mBB) is calculated as the difference between the baseline absorption of the sample and the mean baseline absorption of the standards (Equation 10) (Brian Leen et al., 2012).

Contaminants found to co-distill with plant and soil water and exhibit broadband absorption include ethanol (CH₃CH₂OH) and larger organics containing –OH functional groups (Brian Leen et al., 2012). Broadband absorbers can change the baseline absorbance, which can in turn cause LWIA stable isotope measurement errors (refer to Equation 10). The relationship between LWIA δ²H error and mBB (x=LWIA error, y = mBB) can sometimes be described by 3rd order polynomials but is usually relatively unclear (Brian Leen et al., 2012). The relationship between LWIA δ¹⁸O error and mBB has been shown to be linear, where raw LWIA isotope values are overly depleted (Schultz et al., 2011; Brian Leen et al., 2012). Of the broadband absorbers, ethanol causes the largest LWIA isotope value errors, and has been shown to cause changes in δ²H as large as ± 3 ‰ and δ¹⁸O as high as -3 ‰ (Schultz et al., 2011).

EQUATION 10

$$mBB = \frac{\bar{b}_0^s}{b_0^m}$$

where \bar{b}_0^s is the average baseline offset coefficient of the standards and b_0^m is the baseline offset coefficient for the measured spectrum of the current injection (Brian Leen et al., 2012).

Narrowband absorbers are contaminants that absorb light at discrete wavelength bands within the light spectrum that water isotopomers absorb (LWIA-SCI Manual). The narrowband metric is calculated as the spectrum fit difference in two spectral regions of interest (gray shaded area of $I(\nu)$ fit in Figure 14). The regions of interest are in wavelength bands where water isotopomers lack strong absorbers (Equation 11) (LWIA-SCI Manual; Brian Leen et al., 2012). Narrowband absorbers include methanol (CH_3OH), H_2O_2 , and CH_4 (Brian Leen et al., 2012). The relationship between LWIA isotope value errors and the narrowband metric (mNB) is exponential in nature. Raw LWIA output $\delta^2\text{H}$ and $\delta^{18}\text{O}$ values are enriched relative to their true values. Methanol is the dominant narrowband absorber found in plant and soil water, and has been shown to cause changes in $\delta^2\text{H}$ as high as +29 ‰ and $\delta^{18}\text{O}$ as high as +19 ‰ (Schultz et al., 2011). The presence of methanol, therefore, creates larger LWIA isotope value errors per unit concentration than the presence of ethanol.

EQUATION 11

$$mNB = \frac{1}{N^2} \left(\sum_{\nu \in R_1} (r(\nu) - \bar{r}_1)^2 \right) \left(\sum_{\nu \in R_2} (r(\nu) - \bar{r}_2)^2 \right)$$

where $N = (\text{molecules}/\text{cm}^3) * (1 * 10^{-22})$, ν = laser frequency (GHz), R_n is the n-th region of interest, and $r(\nu)$ is the fit residual at frequency ν (the difference between the measured and fit laser transmission curve at ν , and \bar{r}_n is the average residual in the n-th region of interest (Brian Leen et al., 2012).

Correcting LWIA Isotope Values for Spectral Interference

Once data from the LWIA-PAS and LWIA-SCI had been thoroughly gleaned for errors, we developed a time-efficient and cost-effective method for correcting plant and soil water $\delta^2\text{H}$ and $\delta^{18}\text{O}$ values for spectral interference caused by broadband and narrowband absorbers. The method used was similar to the methods employed by Schultz et al. (2011) and Brian Leen et al. (2012). However, slight modifications were made to the suggested methods in an effort to cater to the strengths and weaknesses of our particular LGR LWIA machine, minimize the length of each LGR LWIA run, and reduce the total cost of stable isotope analysis. The correction process used was as follows:

1. Assess the temporal variability of $m\text{BB}_{\text{standard}}$ and $m\text{NB}_{\text{standard}}$ on your LGR LWIA machine. Determine an appropriate method to define the baseline narrowband and broadband metrics for each LGR LWIA run. Note that LWIA-SCI software default is to average the metrics of the standards for the LGR LWIA run. However, if intra-run temporal variability of either of these metrics is significant, a more temporally-dependent baseline value must be established.
2. Subtract the user-defined baseline metric_{standards} from metric_{samples}, and use the differences to evaluate the need for narrowband absorber or broadband absorber correction functions.
3. Include methanol (increases narrowband metric) or ethanol (increased broadband metric) solutions in LGR LWIA runs. Use regression analyses to create isotope value correction equations that describe the relationships between the applicable metric(s) and LWIA raw isotope value errors.
4. Use correction functions to adjust LWIA isotope values ($\delta^2\text{H}$ and $\delta^{18}\text{O}$) of every sample injection when ($m\text{NB}_{\text{sample}} > m\text{NB}_{\text{standard}} + 2\sigma$).
5. Compare LGR LWIA isotope values to IRMS to validate correction methods.
6. Average the corrected injections to report spectral-interference corrected sample mean $\delta^2\text{H}$ and $\delta^{18}\text{O}$ and standard deviations for each water sample.

Table 15 shows temporal variability of $m\text{NB}_{\text{standard}}$ on Boise State's LGR LWIA machine. Broadband metrics of standards had little temporal variance, and rarely deviated more than 0.012 from the expected 1.00. In contrast, $m\text{NB}_{\text{standard}}$ had very high temporal

variance. According to Manish Gupta (written communication, 2013), our standards had unusually high narrowband metrics (much larger than 0.1-0.2). The unusually high narrowband metrics and significant intra-run temporal variability of our standards demonstrated a need for further spectral-interference analysis.

Figure 44 shows an example of intra-run variability of mNB_{standard} on 09-25-2012. This level of variability was relatively common for Boise State's machine (Table 16). There are two possibilities for how mNB_{standard} could be this much higher than normal and exhibit this level of variability. The first possibility is that a narrowband absorber was transferred from one vial to another (Brian Leen, written communication, 2013). The second possibility is that the standards were contaminated via LWIA memory effects (Brian Leen, personal communication, 2013). The first possibility is particularly unfortunate because it suggests that water is being mixed between sample vials, eliminating the validity of the LGR-LWIA output isotope values (Brian Leen, personal communication, 2013). If the second possibility occurs, an accurate data set can be salvaged if the isotope values of the standards are unchanged despite the unusually high narrowband metrics.

Fortunately, our standards appear to have been contaminated via a memory affect rather than transfer of contaminated water from one vial to another. Evidence for this stems from the fact that the standards showed elevated narrowband metrics during isolated parts of the analysis following LWIA injections into samples containing narrowband contaminants (Figure 44). In addition, measured isotope values of standards with elevated narrowband metrics did not differ significantly from standards with small narrowband metrics (Table 16). If the standards had been contaminated with narrowband

absorbers, the measured isotope values would be expected to change accordingly, as the fitting routine (Equation 5) does not account for the presence of narrowband absorbers.

After assessing the temporal variability of mBB_{standard} and mNB_{standard} , we determined that the LWIA-SCI software baseline mBB_{standard} at $mBB + 3\sigma$ is suitable for our applications. However, memory effects may have caused mNB_{standard} to be too variable to use the standard LWIA-PAS $\text{average}(mNB_{\text{standard}}) + 3\sigma$ as a benchmark for contaminated sample identification. Instead, we used Matlab's Piecewise Cubic Hermite Interpolating Polynomial (PCHIP) function to connect mNB_{standard} values (Figure 44) and model how the baseline mNB_{standard} may change between the standards (e.g., the 6 samples between standards). We used the PCHIP interpolation modeled $mNB_{\text{standard}} + 2\sigma$ line as a baseline, above which, samples were considered to be contaminated. Note that this line connects LGR LWIA measured $mNB_{\text{standard}} + 2\sigma$, where the standard deviation is derived from the four injections averaged to arrive at a sample mean.

Now that we have established a baseline above which samples are considered contaminated by narrowband absorbers, we must evaluate the need for narrowband absorber correction functions. Table 17 below evaluates narrowband contamination in our plant and soil water samples. Table 17 shows that plant stem water samples were contaminated 72.7% of the time, while soil water samples were only contaminated 10.5% of the time. These results are similar to Schultz et al. (2011) because plant stem water is usually found to be contaminated. However, unlike Schultz et al. (2011), we did find some of our soil water samples to be contaminated. These soil samples may contain root fragments or high levels of organic carbon, which could be dissolved into methanol in soil water. We believe that this method identifies the vast majority of contaminated

samples, while excluding samples that may simply be exhibiting organic contaminant memory effects, similar to the standards.

Now that we have identified contaminated water samples, we must correct the isotope values of each contaminated sample accordingly. Broadband interference correction curves were excluded from our spectral interference correction process for a number of reasons. First, broadband contamination creates lesser changes in LWIA isotope values than narrowband contamination (Schultz et al., 2011; Brian Leen et al., 2012). For example, Schultz et al. (2011) and Brian Leen et al. (2012) had previously determined that broadband metrics similar to those witnessed in our analyses yielded LWIA $\delta^2\text{H}$ and $\delta^{18}\text{O}$ value errors ranging from negligible to 1‰ and negligible to 0.2‰, respectively. Also, high levels of broadband contamination were not commonly observed in our water samples, as only 118 of 4444 injections were flagged for high concentrations of broadband absorbers ($\text{mBB} = \text{mBB}_{\text{standard}} + 3\sigma$). When injections were flagged for broadband contamination, they were commonly a statistical anomaly amongst the four injections into the sample vial. Given this information, we determined that the creation of correction curves for broadband absorbers was unnecessary for our applications. The inclusion of ethanol solutions in each LWIA run increases the time and expense of stable isotope analysis, and was not seen to be worthwhile given its lack of applicability to $\delta^2\text{H}$ corrections, and lesser effect on LWIA $\delta^{18}\text{O}$ values.

Narrowband interference correction curves were necessary given our applications (Table 17). To correct LWIA isotope values for narrowband spectral interference, one must establish the relationship between the narrowband metric and errors in LWIA stable isotope value output. This requires mixing methanol (the most common narrowband

absorber in plant and soil water) into solution with water of known $\delta^2\text{H}$ and $\delta^{18}\text{O}$ values. Once mixed, these solutions must be included in the LWIA run list. Following a LWIA run, $(\text{mNB}_{\text{solution}} - \text{mNB}_{\text{standard}})$ vs. $(\delta_{\text{solution}} - \delta_{\text{standard}})$ data can be plotted, and a regression analysis may yield a narrowband spectral interference correction equation.

In total, we created nine correction curves between 09-05-2012 and 02-26-2013. Each LGR LWIA run during this time contained seven or more methanol and DI water solutions containing from 20 ppmv to 500 ppmv methanol. The results of Schultz et al. (2011) showed promising LGR LWIA stable isotope value precision over a two-week period (Brian Leen et al., 2012). However, we ran methanol samples on Boise State's LGR LWIA machine periodically over a 6 month period in an attempt to investigate the long-term temporal variability of these relationships. Understanding temporal variability in LWIA sensitivity to narrowband absorbers is important because it informs LWIA users of how often methanol solutions must be included in LWIA runs to produce accurate stable isotope values.

Tables 17 and 18 describe intra-run variability in LGR LWIA sensitivity to narrowband absorbers. The tables list the ability of best fit equations of the form $-\ln(x/a + 1)/b$ to predict changes in isotope values based on changes in the narrowband metric over 5 discrete time windows during a LGR LWIA run on 09-19-2012. For example, correction curve A was generated from data at the beginning of the LWIA run, while correction curve E was generated from data at the end of the run. The RMSE values of the regression analyses demonstrate that full LWIA run correction curves predict isotope errors nearly as well as discrete time window intra-run correction curves. The results of our inter-run variability tests are in tables 19 and 20, and visualized in figures 43 and 44.

Figures 43 and 44 suggest that Boise State's LWIA stable isotope measurement errors ($\delta^2\text{H}$ and $\delta^{18}\text{O}$) correlate negatively with $\text{mNB} - \text{mNB}_{\text{standard}}$. This trend is similar to the results of Schultz et al. (2011) and Brian Leen et al. (2012). Additionally, the RMSE values in tables 19 and 20 suggest that inter-run temporal variability in the LGR LWIA response to narrowband absorbers is great enough to warrant the use of individual narrowband absorber correction equations for each LGR LWIA run. However, unfortunately, this study did not include methanol solutions in our early LGR LWIA isotope analyses. Therefore, we were forced to make due with narrowband absorber correction equations generated using all of our data. Fortunately, however, we were able to create piecewise-functions to improve the RMSE of our narrowband absorber correction equations.

It follows logic that one function for both $\delta^2\text{H}$ and $\delta^{18}\text{O}$ could be used to describe the LGR LWIA sensitivity to narrowband absorbers because the LWIA transmission fitting routine (Equation 5) is the same regardless of the reported narrowband metric. However, this logic does not transfer to the results of these tests. Schultz et al. (2011) used piecewise functions to describe these relationships for narrowband metrics ranging from 0 to 100,000. Despite the smaller narrowband metric values present in our tests, piecewise functions were appropriate for describing our data set as well. Piecewise functions were used because residuals plots indicated that modeled $\delta^2\text{H}$ and $\delta^{18}\text{O}$ corrections were generally under predicted when $\text{mNB} < 10$ (Figure 47; Figure 48).

Table 22 and figures 49 and 50 contain the piecewise correction functions fitted for $\delta^2\text{H}$ and $\delta^{18}\text{O}$ raw isotope value errors, respectively. Note that the coefficient of determination was not listed for the correction functions at $\text{mNB} < 10$, as variability is

too great at this resolution to predict accurate isotope value errors. Nonetheless, we believe that this piecewise function approach is more effective, because it reduces the residuals at $mNB < 10$, while the larger fit equations are good predictors of isotope value error, and yield relatively low root mean squared errors.

Spectral Interference Correction Method Validation

Now that we have finalized our narrowband interference correction equations, we must test the accuracy of our correction method. We tested our spectral interference correction method by running 16 stem samples and 9 de-ionized water samples on both the LGR LWIA and the Finnigan TC/EA IRMS. First, we compared the LWIA isotope values ($\delta^2\text{H}$ and $\delta^{18}\text{O}$) of uncontaminated de-ionized water samples to the IRMS (Table 23). Mean IRMS isotope values were $\delta^2\text{H} = -127.34 \text{‰}$ ($\sigma = 2.86$) and $\delta^{18}\text{O} = -16.98 \text{‰}$ ($\sigma = 0.44$). Mean IRIS values were $\delta^2\text{H} = -129.16 \text{‰}$ ($\sigma = 0.84$) and $\delta^{18}\text{O} = -16.93 \text{‰}$ ($\sigma = 0.07$). According to a two-tailed paired t-test, neither difference is statistically significant, as $\delta^2\text{H } t_{\text{calc}} = 1.81$ and $\delta^{18}\text{O } t_{\text{calc}} = 0.33$, whereas $t_{\text{critical}} (p=0.05) = 2.3$.

Now that we've established that isotopes of clean water are quite comparable ($\delta^2\text{H}$ differences $< 5\text{‰}$ and $\delta^{18}\text{O}$ differences $< 1\text{‰}$) on the Finnigan TC/EA IRMS and Los Gatos Research Liquid Water Isotope Analyzer, we can compare isotope values of samples contaminated with narrowband absorbers. We selected plant stem water samples that contained enough water to run simultaneous LGR LWIA and Finnigan TC/EA IRMS analyses. Tables 24 and 25 compare IRMS, LWIA raw, and LWIA corrected isotope values. Figures 51 and 52 show Finnigan TC/EA IRMS isotope values plotted on the x-axis and LGR LWIA IRIS isotope values plotted on the y-axis. If the IRMS values are viewed as the true values, then a one to one ratio indicates that the LWIA isotope values

are accurate $\delta^2\text{H}$ and $\delta^{18}\text{O}$ values. For both figures, the black line is a 1 to 1 ratio, while the black dotted lines indicate the IRMS σ (n=9). Error bars represent $\delta^2\text{H}$ and $\delta^{18}\text{O}$ value standard deviations.

Unfortunately, many of the water samples had narrowband metrics (mNB) that were nearly equal to the narrowband metrics of the standards, so spectral interference corrections were generally minor in magnitude. It is important to note that due to the logarithmic nature of the mNB vs. LWIA isotope value error relationship, as well as the larger relative uncertainty of small narrowband metric values, correcting samples where $\text{mNB} < 10$ presents the most difficult challenge. We would expect the accuracy of our corrections to increase with increased narrowband metric values. Regardless of the increased uncertainty associated with correcting these samples, our results were encouraging. The accuracy of the LWIA $\delta^2\text{H}$ and $\delta^{18}\text{O}$ values ($\text{IRMS} - \text{IRIS}_{\text{raw}}$) were 0.56 ‰ and -0.82 ‰, respectively. The standard deviations of the raw isotope value differences were 2.73 ‰ and 0.55 ‰. The accuracy of the corrected LWIA $\delta^2\text{H}$ and $\delta^{18}\text{O}$ values ($\text{IRMS} - \text{IRIS}_{\text{corrected}}$) were 0.96 ‰ and -0.55 ‰. The standard deviations of the corrected isotope value differences were 2.64 ‰ and 0.48 ‰, respectively.

Correction for narrowband spectral interference slightly improved the accuracy of our LWIA $\delta^{18}\text{O}$ values. However, this method increased the average difference between our LWIA and IRMS $\delta^2\text{H}$ values. This seems discouraging and counterintuitive until one considers that our clean DI water analysis showed an $\text{IRMS} - \text{LWIA}$ difference of about 1.82‰. If this offset is accurate for our LWIA, then the corrected $\delta^2\text{H}$ values ($\text{IRMS} - \text{IRIS}_{\text{corrected}} = 0.96$ ‰) are closer to the clean water LWIA $\delta^2\text{H}$ values than the uncorrected values ($\text{IRMS} - \text{IRIS}_{\text{raw}} = 0.56$ ‰).

Schultz et al. (2011) conducted a similar LWIA spectral interference correction study where they corrected 78 leaf water samples. The accuracy of their LWIA isotope values were $\delta^2\text{H} = -3.45\text{‰}$ and $\delta^{18}\text{O} = 0.19\text{‰}$, while the standard deviations of the corrected isotope value differences were 1.98‰ and 0.58‰. The directions of our IRMS-IRIS_{corrected} offsets differ for both $\delta^2\text{H}$ and $\delta^{18}\text{O}$; however the magnitude of our offsets is similar. The standard deviations of the differences between our IRMS and IRIS_{corrected} values were slightly greater for $\delta^2\text{H}$ and slightly less for $\delta^{18}\text{O}$.

Differences in our $\delta^2\text{H}$ offsets may result from the fact that we analyzed stem water rather than leaf water. Water distilled from leaves commonly contains more organic material than water from stems (Zhao et al., 2011). Therefore it is likely that leaf water contains more large alcohols, glycols, acids, and organics that don't contain O-H functional groups. Such contaminants affect IRMS machines but not the LGR LWIA, as their absorptive properties are not similar to water isotopologues (Brian Leen et al., 2012). These contaminants are commonly extremely depleted compared to plant water (Sessions, 2006) and cause IRMS machines to produce depleted $\delta^2\text{H}$ values. The minor differences in our $\delta^{18}\text{O}$ values may be caused by the increased difficulty of correcting samples where $m\text{NB} \approx m\text{NB}_{\text{standard}}$ with natural logarithm equation forms. Despite these differences, our results suggest that the Boise State Stable Isotopes Laboratory LWIA yields stem water $\delta^2\text{H}$ and $\delta^{18}\text{O}$ values to within 2.64 ‰ and 0.48 ‰ of our Finnigan High Temperature Conversion Elemental Analyzer IRMS. These standard deviations include measurement noise in both instruments.

Tables

Table 15 LWIA Inter-run temporal variability of mBB_{standard} and mNB_{standard} output from the Los Gatos Research Liquid Water Isotope Analyzer, Spectral Contaminant Identifier Software. mBB = broadband metric. mNB = narrowband metric. n = number of samples in analysis.

LGR Standards	mBB mean	mBB σ	mNB mean	mNB σ	n
All LWIA runs	1.00	0.00815	1.88	3.32	221
11-11-2011	1.00	0.00240	0.27	0.21	10
12-02-2011	1.00	0.00247	0.14	0.07	10
02-17-2012	1.00	0.00326	0.21	0.09	10
04-26-2012	1.00	0.00974	1.39	1.67	35
08-02-2012	1.00	0.00681	0.82	0.65	25
09-25-2012	1.00	0.01196	0.94	1.19	25
10-15-2012	1.00	0.01159	0.61	0.63	25
11-21-2012	1.00	0.01048	6.05	6.39	21
02-12-2013	1.00	0.00562	1.52	0.65	28
02-20-2013	1.00	0.00394	3.41	2.31	20
02-26-2013	1.00	0.00241	5.24	7.42	12

Table 16 One-tailed Wilcoxon rank sum test for LWIA measured $\delta^2\text{H}$ and $\delta^{18}\text{O}$ values. Measured isotope values were compared between standards where $mNB < 1$ and $mNB \geq 1$. The null hypothesis stated that these populations have the same isotope values ($h=0$). The alternate hypothesis stated that standards where $mNB > 1$ are more enriched than standards where $mNB < 1$ ($h=1$). n = number of samples in analysis.

LGR Standard	$\delta^2\text{H}$ p-value	$\delta^{18}\text{O}$ p-value	h ($\delta^2\text{H}$)	h ($\delta^{18}\text{O}$)	n ($mNB < 1$)	n ($mNB > 1$)
LGR1	0.2947	0.2063	0	0	31	19
LGR2	0.0700	0.9685	0	0	28	22
LGR3	0.2021	0.1748	0	0	22	28
LGR4	0.2415	0.7825	0	0	25	18
LGR5	0.6640	0.4765	0	0	17	3

Table 17 Plant xylem water and bulk soil water sample LWIA narrowband interference. n = number of samples analyzed. In total, 73.3 % of xylem water samples and 10.5% were found to contain narrowband absorber concentrations sufficient to significantly alter raw isotope value output.

Date	Contaminated Plants	n Plants	Contaminated Soils	n Soils
All samples	173	236	38	361
11-11-2011	6	8	0	0
12-02-2011	26	33	0	2
02-17-2012	20	26	2	9
04-26-2012	3	5	5	52
08-02-2012	20	25	0	19
09-25-2012	29	35	10	42
10-15-2012	15	17	5	46
11-21-2012	16	28	2	33
02-12-2013	21	26	10	61
02-20-2013	15	31	2	67
02-26-2013	2	2	2	30

Table 18 Intra-run LWIA $\delta^2\text{H}$ value sensitivity to narrowband absorbers. All trendlines are of the form $f(x) = -\ln(\frac{x}{a} + 1)/b$.

Samples	a	b	SSE	r^2	Adj r^2	RMSE	n
9-19-12 all	9.042	0.4066	104.4	0.902	0.9	1.475	50
9-19-12 (A)	5.725	0.4643	28.83	0.8353	0.8147	1.898	10
9-19-12 (B)	24.47	0.3456	13.97	0.9274	0.9184	1.322	10
9-19-12 (C)	12.97	0.357	10.91	0.9633	0.9587	1.168	10
9-19-12 (D)	1.627	0.5661	10.9	0.9373	0.9295	1.167	10
9-19-12 (E)	9.934	0.3777	16.96	0.922	0.9122	1.456	10

Table 19 Intra-run LWIA $\delta^{18}\text{O}$ value sensitivity to narrowband absorbers. All trendlines are of the form $f(x) = -\ln(\frac{x}{a} + 1)/b$.

Samples	a	b	SSE	r^2	Adj r^2	RMSE	n
9-19-12 all	7.865	0.6039	20.65	0.9583	0.9575	0.6559	50
9-19-12 (A)	8.709	0.598	0.8071	0.9914	0.9904	0.3176	10
9-19-12 (B)	9.906	0.564	4.429	0.9563	0.9508	0.7441	10
9-19-12 (C)	9.575	0.6089	5.396	0.9488	0.9424	0.8213	10
9-19-12 (D)	2.318	0.7585	4.447	0.948	0.9415	0.7456	10
9-19-12 (E)	11.35	0.5339	1.581	0.9855	0.9837	0.4446	10

Table 20 Inter-run LWIA $\delta^2\text{H}$ value sensitivity to narrowband absorbers. All trendlines are of the form $f(x) = -\ln(\frac{x}{a} + 1)/b$.

Date	a	b	r^2	SSE	Adj r^2	RMSE	n
All	7.473	0.428	0.9209	227.9	0.9204	1.276	142
All < 200	2.147	0.6724	0.7101	132.2	0.7072	1.167	99
9/5/2012	14.59	0.3779	0.979	21.54	0.9782	0.8771	30
9/19/2012	9.041	0.4066	0.902	104.4	0.9	1.475	50
9/25/2012	8.749	0.4388	0.8983	7.956	0.8813	1.152	7
10/15/2012	0.586	0.8183	0.9353	2.454	0.9224	0.7005	8
11/21/2012	1.296	0.6039	0.8889	7.399	0.8889	1.216	7
11/29/2012	1.236	0.5646	0.9796	2.072	0.9755	0.6438	7
2/12/2013	27.63	0.1972	0.8679	14.12	0.849	1.42	10
2/20/2013	1.621	0.6362	0.8365	11.49	0.8161	1.198	11
2/26/2013	1.44	0.6139	0.8655	8.922	0.8487	1.056	11

Table 21 Intra-run LWIA $\delta^{18}\text{O}$ value sensitivity to narrowband absorbers. All trendlines are of the form $f(x) = -\ln(\frac{x}{a} + 1)/b$. n = number of samples analyzed.

Date	a	b	r^2	SSE	Adj r^2	RMSE	n
All	9.893	0.5931	0.9531	61.91	0.9528	0.665	142
All < 200	2.26	1.014	0.7957	35.6	0.7936	0.6059	99
9/5/2012	17.51	0.5213	0.9812	9.15	0.9805	0.5717	30
9/19/2012	7.865	0.6039	0.9583	20.65	0.9575	0.6559	50
9/25/2012	4.652	0.8242	0.9832	0.5938	0.9804	0.3146	7
10/15/2012	14.84	0.5587	0.9822	0.5587	0.9786	0.3343	8
11/21/2012	8.531	0.7539	0.9853	0.4101	0.9824	0.2864	7
11/29/2012	0.7336	1.05	0.9697	0.902	0.9636	0.4247	7
2/12/2013	1.441	1.18	0.9809	0.2423	0.9782	0.186	10
2/20/2013	6.375	0.7914	0.9703	0.8262	0.9665	0.3214	11
2/26/2013	0.4932	1.223	0.9507	1.109	0.9446	0.3723	11

Table 22 LWIA isotope data piecewise narrowband spectral interference correction equations. All trendlines are of the form $f(x) = -\ln(\frac{x}{a} + 1)/b$. mNB = narrowband metric. n = number of samples analyzed.

Stable Isotope	mNB Range	a	B	r^2	SSE	Adj r^2	RMSE	n
$\delta^2\text{H}$	< 10	0.2595	1.549	N/A	41.47	N/A	1.006	43
$\delta^2\text{H}$	10 - 5000	8.786	0.4149	0.9218	130.8	0.9209	1.18	99
$\delta^{18}\text{O}$	<10	0.3572	2.005	N/A	12.83	N/A	0.5594	43
$\delta^{18}\text{O}$	10 -5000	11.98	0.563	0.9616	31.84	0.9612	0.582	99

Table 23 Clean water LWIA (IRIS) vs. Finnigan High Temperature Conversion Elemental Analyzer (IRMS) performance.

Sample	IRMS $\delta^2\text{H}$ (‰)	IRIS $\delta^2\text{H}$ (‰)	IRMS $\delta^{18}\text{O}$ (‰)	IRIS $\delta^{18}\text{O}$ (‰)	$\delta^2\text{H}_{\text{IRMS}} - \delta^2\text{H}_{\text{IRIS}}$ (‰)	$\delta^{18}\text{O}_{\text{IRMS}} - \delta^{18}\text{O}_{\text{IRIS}}$ (‰)
DI-1	-133.80	-128.80	-17.04	-16.86	-4.99	-0.18
DI-2	-128.04	-128.83	-18.00	-17.01	0.79	-0.99
DI-3	-127.12	-128.43	-16.85	-16.82	1.31	-0.03
DI-4	-124.17	-128.49	-17.04	-16.96	4.32	-0.07
DI-5	-125.49	-130.25	-16.78	-16.98	4.76	0.20
DI-6	-126.28	-130.85	-16.82	-16.91	4.57	0.09
DI-7	-129.38	-129.31	-17.14	-16.88	-0.07	-0.25
DI-8	-126.29	-128.87	-16.76	-17.01	2.58	0.26
DI-9	-125.48	-128.63	-16.38	-16.92	3.15	0.54

Table 24 LWIA (IRIS) vs. Finnigan High Temperature Conversion Elemental Analyzer (IRMS) plant xylem water $\delta^2\text{H}$ values (11-29-2012).

Plant Stem	IRMS $\delta^2\text{H}$ (‰)	IRIS raw $\delta^2\text{H}$ (‰)	σ	IRIS corrected $\delta^2\text{H}$ (‰)	σ	IRMS – IRIS raw	IRMS - IRIS corrected
Douglas-fir	-140.36	-144.45	0.82	-144.45	0.82	4.09	4.09
Bitter cherry	-124.33	-124.72	0.67	-125.23	0.43	0.39	0.90
Pacific willow	-133.49	-131.11	0.68	-131.11	0.68	-2.38	-2.38
Bitter cherry	-131.14	-129.27	0.86	-129.27	0.86	-1.87	-1.87
Sagebrush	-132.37	-134.22	0.45	-135.76	0.43	1.85	3.39
Pacific willow	-119.63	-119.90	0.18	-120.55	0.39	0.27	0.91
Pacific willow	-128.56	-127.66	0.29	-127.76	0.20	-0.90	-0.80
Ponderosa pine	-126.33	-129.60	0.72	-129.60	0.72	3.27	3.27
Sagebrush	-131.35	-129.88	1.17	-131.00	0.98	-1.47	-0.35
Ponderosa pine	-132.47	-129.87	0.44	-130.57	0.27	-2.61	-1.90
Ponderosa pine	-130.97	-134.38	0.54	-134.67	0.36	3.41	3.70
Ponderosa pine	-128.34	-126.60	0.51	-127.33	0.52	-1.74	-1.01
Ponderosa pine	-128.73	-127.15	0.53	-127.15	0.53	-1.58	-1.58
Ponderosa pine	-132.75	-138.10	0.42	-138.10	0.42	5.35	5.35
Ponderosa pine	-135.85	-140.19	0.62	-140.19	0.62	4.34	4.34
Rabbitbrush	-140.75	-139.27	0.40	-140.09	0.76	-1.48	-0.66

Table 25 LWIA (IRIS) vs. Finnigan High Temperature Conversion Elemental Analyzer (IRMS) plant xylem water $\delta^{18}\text{O}$ values (11-29-2012)

Plant Stem	IRMS $\delta^{18}\text{O}$ (‰)	IRIS raw $\delta^{18}\text{O}$ (‰)	σ	IRIS corrected $\delta^{18}\text{O}$ (‰)	σ	IRMS -IRIS raw	IRMS -IRIS corrected
Douglas-fir	-18.46	-18.35	0.06	-18.35	0.06	-0.10	-0.10
Bitter cherry	-16.41	-15.70	0.05	-16.02	0.21	-0.71	-0.39
Pacific willow	-16.07	-15.67	0.09	-15.67	0.09	-0.41	-0.41
Bitter cherry	-15.70	-15.17	0.04	-15.17	0.04	-0.53	-0.53
Sagebrush	-14.17	-13.38	0.08	-14.43	0.06	-0.79	0.26
Pacific willow	-14.14	-13.25	0.07	-13.68	0.43	-0.89	-0.47
Pacific willow	-15.96	-14.60	0.10	-14.66	0.22	-1.35	-1.29
Ponderosa pine	-14.73	-15.01	0.07	-15.01	0.07	0.29	0.29
Sagebrush	-15.28	-13.75	0.13	-14.49	0.17	-1.53	-0.79
Ponderosa pine	-16.35	-15.17	0.06	-15.62	0.18	-1.18	-0.73
Ponderosa pine	-16.87	-16.26	0.03	-16.45	0.38	-0.61	-0.42
Ponderosa pine	-15.98	-14.98	0.13	-15.46	0.42	-1.00	-0.53
Ponderosa pine	-16.33	-15.15	0.04	-15.15	0.04	-1.18	-1.18
Ponderosa pine	-18.05	-17.01	0.22	-17.01	0.22	-1.04	-1.04
Ponderosa pine	-18.02	-17.80	0.04	-17.80	0.04	-0.22	-0.22
Rabbitbrush	-16.45	-14.66	0.10	-15.19	0.35	-1.80	-1.26

Figures

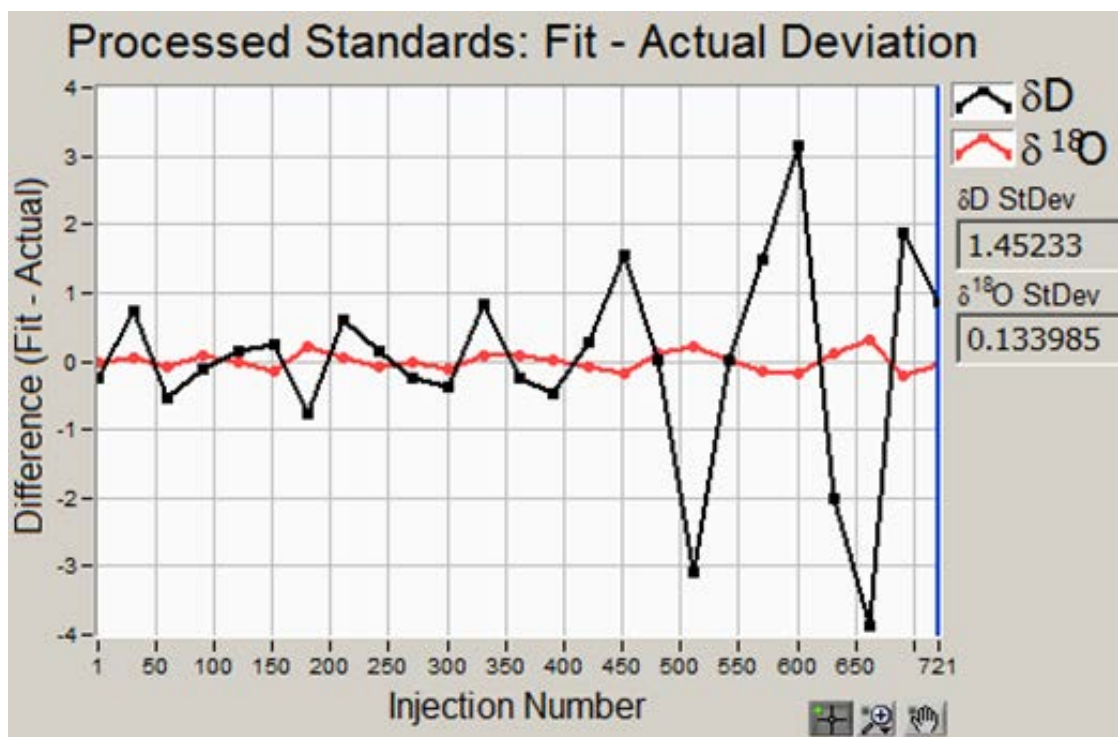


Figure 42. LWIA measured standards values vs. actual known isotope values (09-25-2012)

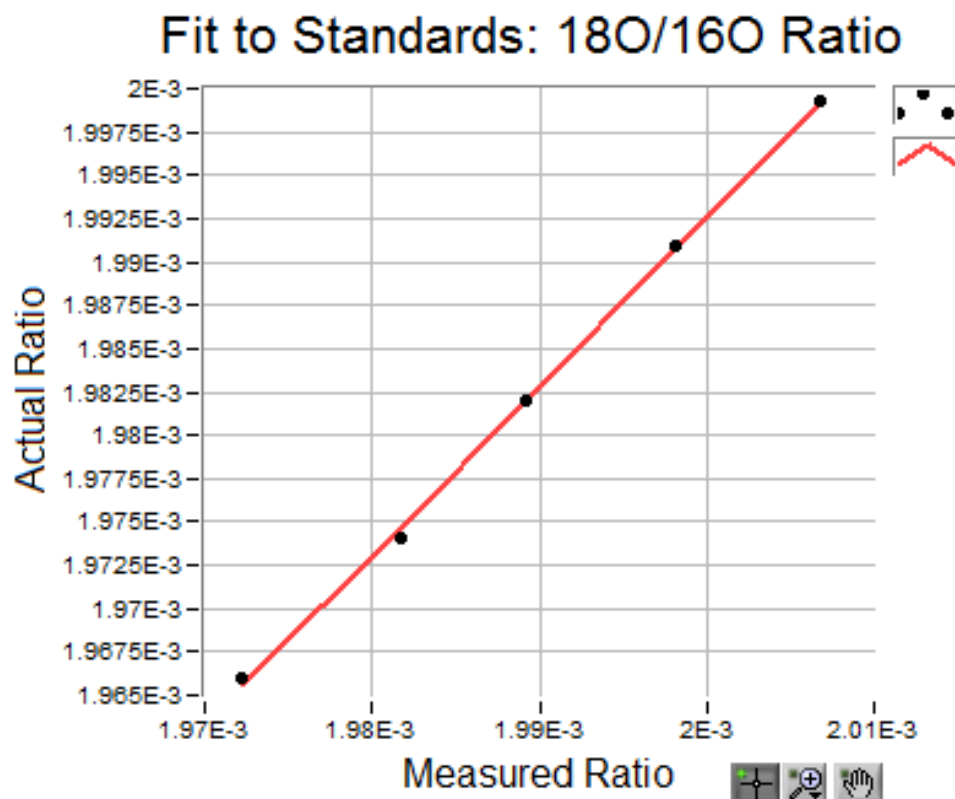


Figure 43. LWIA Isotopic Analysis Standard Group Example (08-02-2012)

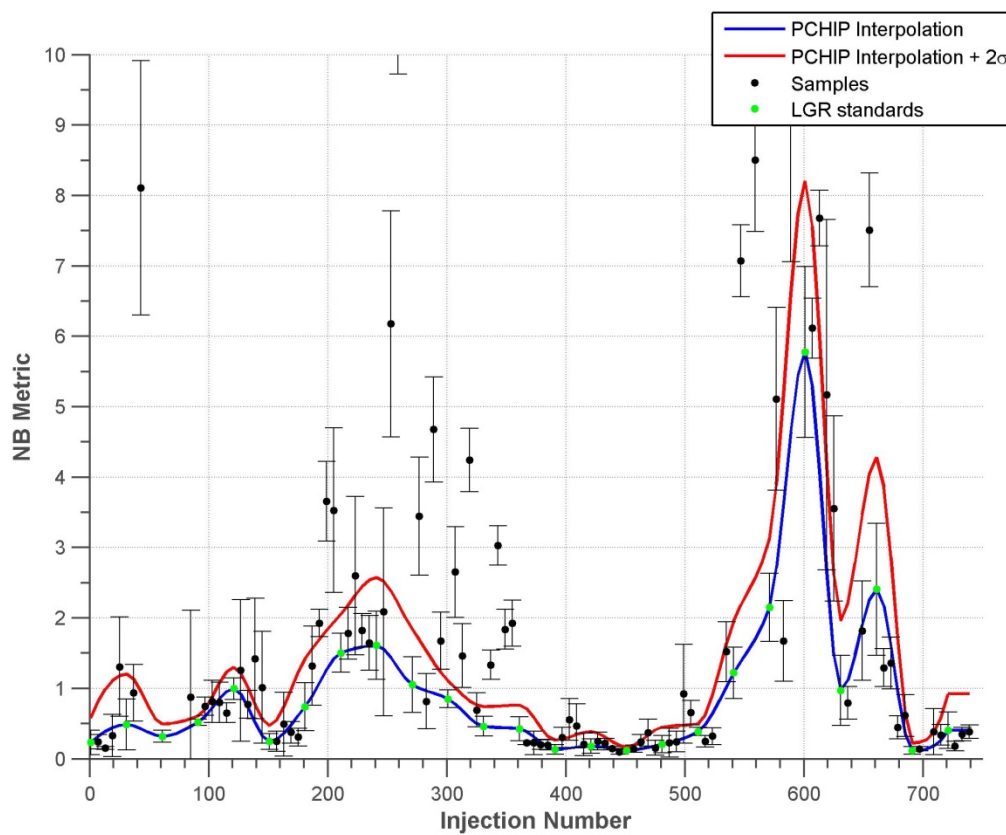


Figure 44. LWIA intra-run mNB_{standard} temporal variability (run on 09-25-2012)

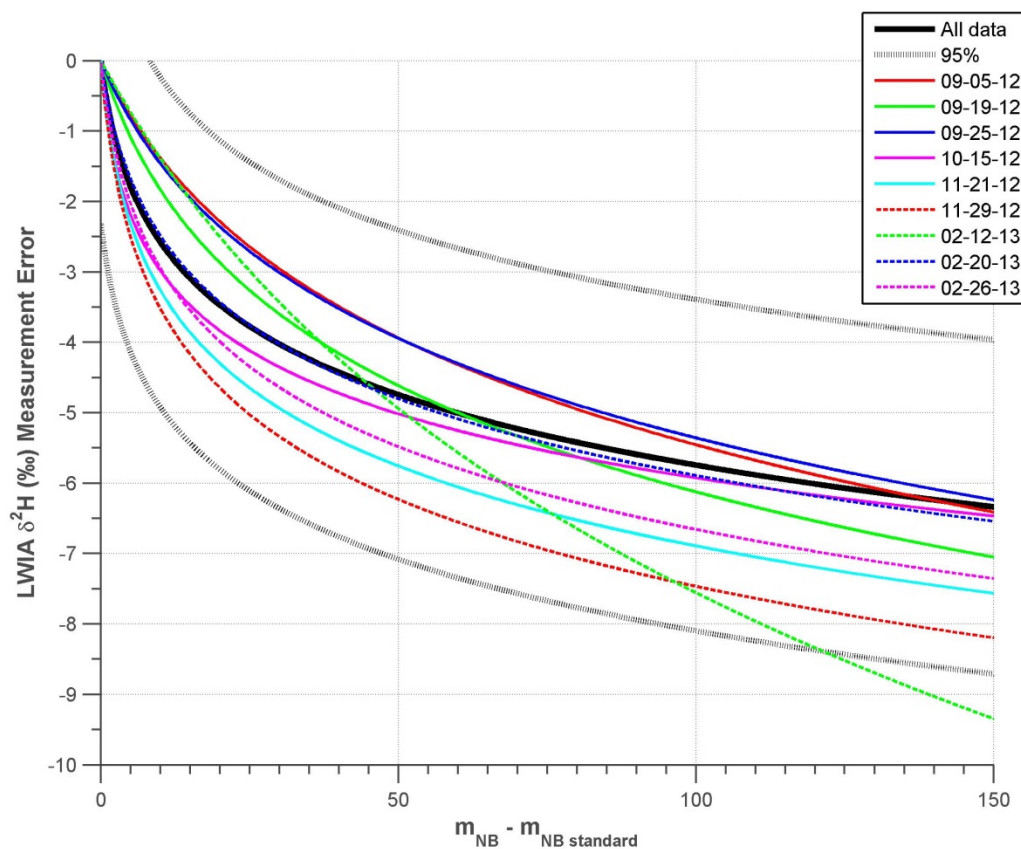


Figure 45. LWIA inter-run $\delta^2\text{H}$ sensitivity to narrowband absorbers. All trendlines are of the form $f(x) = -\ln\left(\frac{x}{a} + 1\right)/b$. Note that 95% represents confidence bounds on the All data fit.

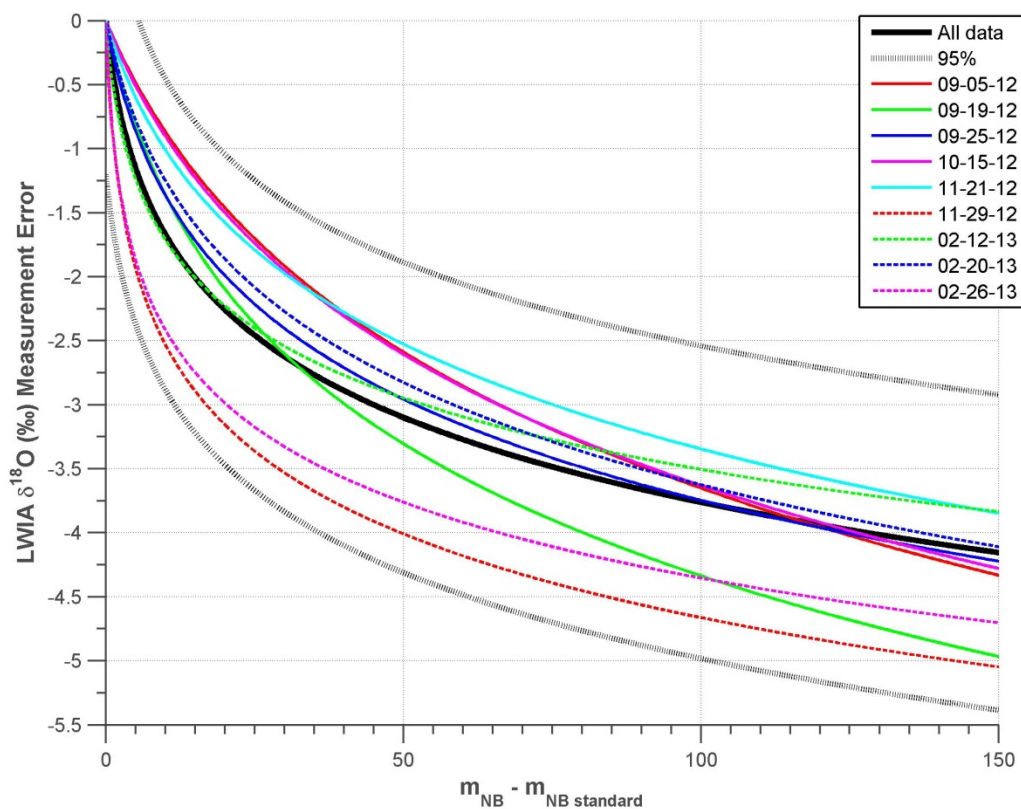


Figure 46. LWIA $\delta^{18}\text{O}$ sensitivity to narrowband absorbers. All trendlines are of the form $f(x) = -\ln\left(\frac{x}{a} + 1\right)/b$. Note that 95% represents confidence bounds on the All data fit.

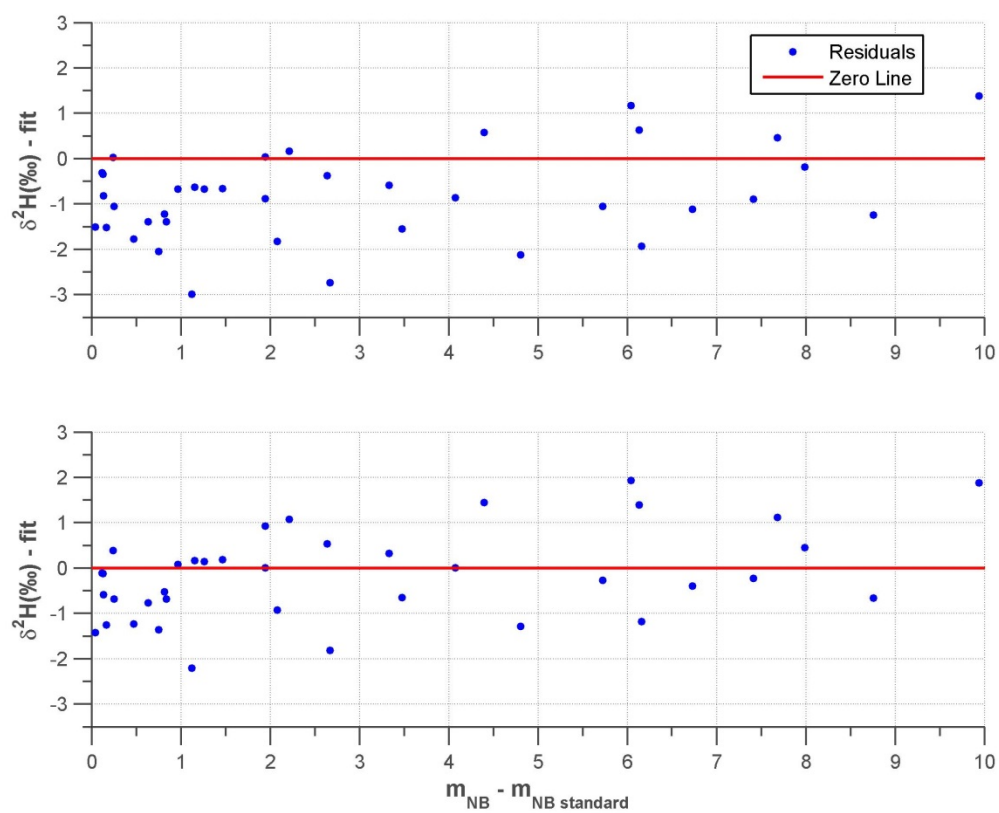


Figure 47. LWIA $\delta^2\text{H}$ residuals plots for the all data function (top) and the function generated using on $m_{\text{NB}} < 10$ (bottom).

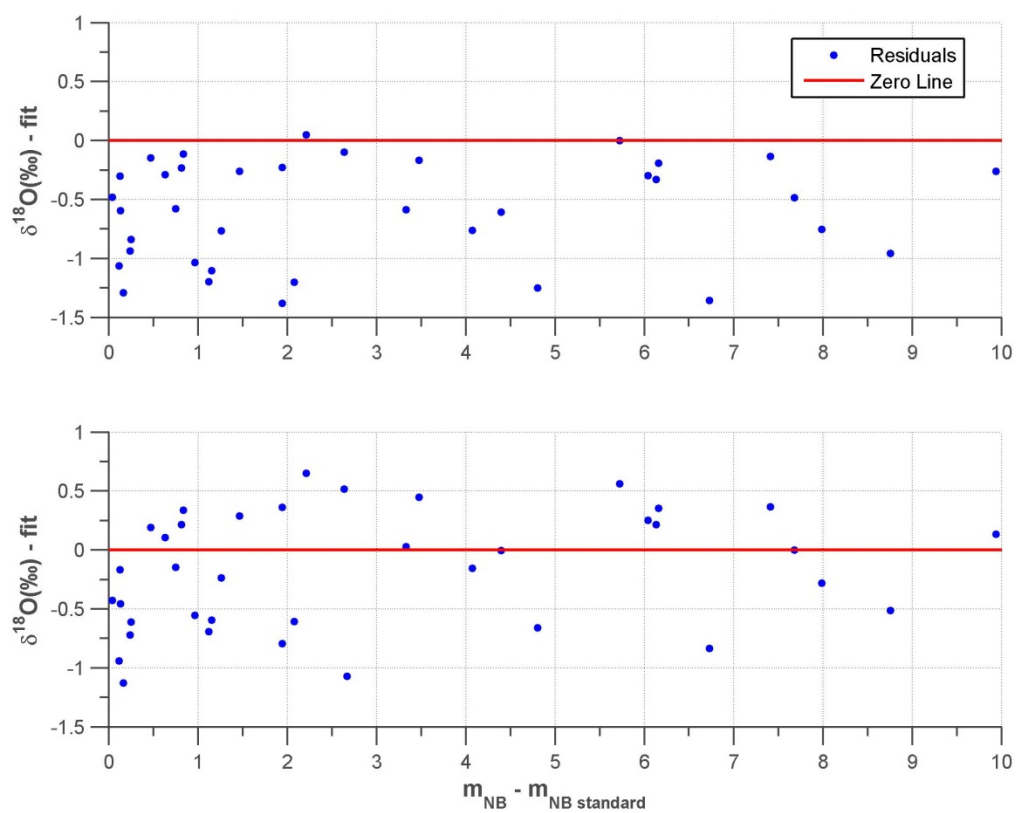


Figure 48. LWIA $\delta^{18}\text{O}$ residuals plots for the all data function (top) and the function generated using only $m_{\text{NB}} < 10$ data (bottom).

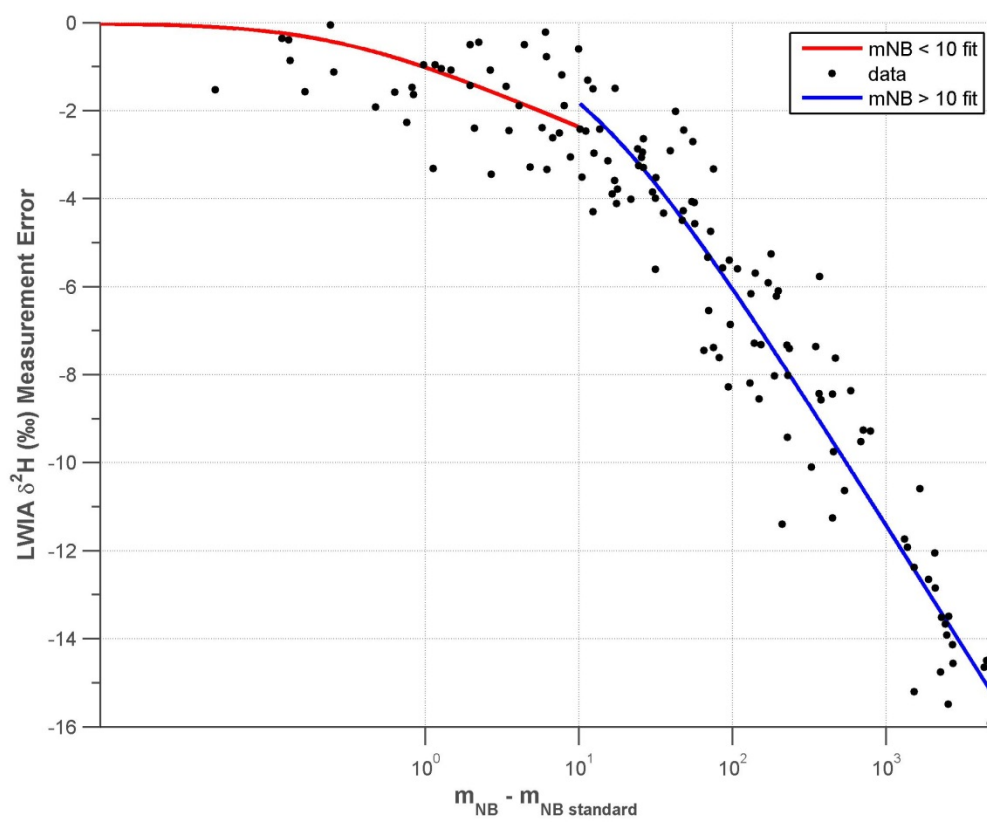


Figure 49. LWIA fitted $\delta^2\text{H}$ isotope value correction functions. All trendlines are of the form $f(x) = -\ln\left(\frac{x}{a} + 1\right)/b$.

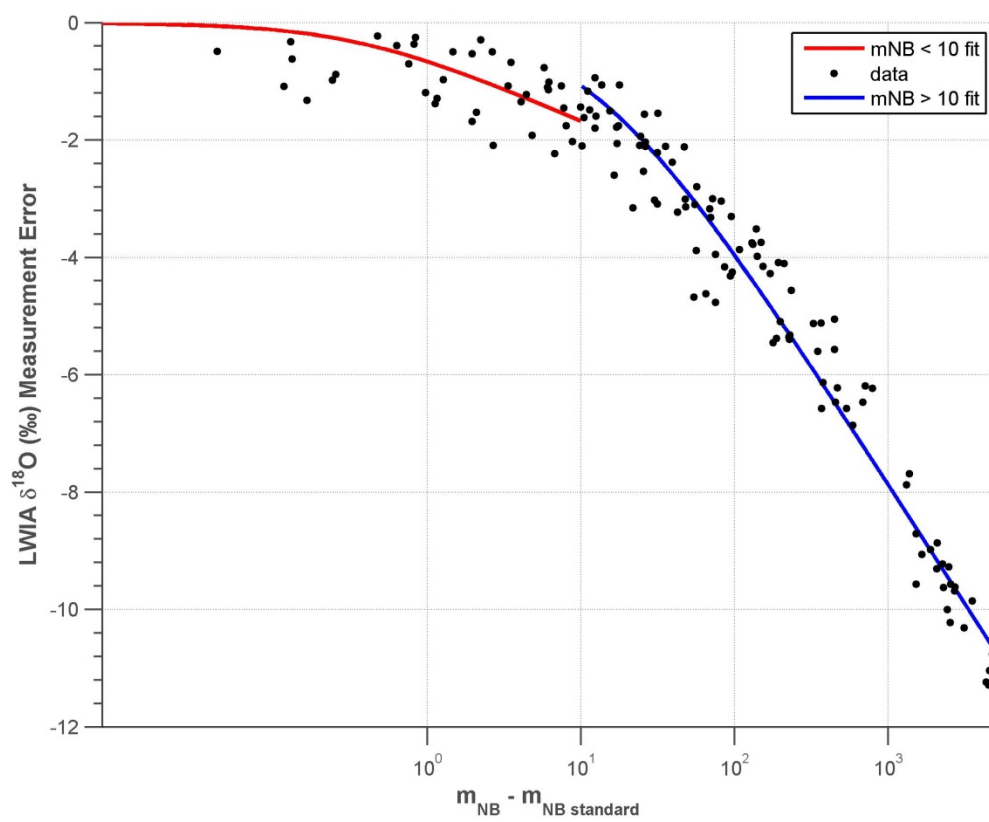


Figure 50. Fitted $\delta^{18}\text{O}$ isotope value correction function. All trendlines are of the form $f(x) = -\ln\left(\frac{x}{a} + 1\right)/b$.

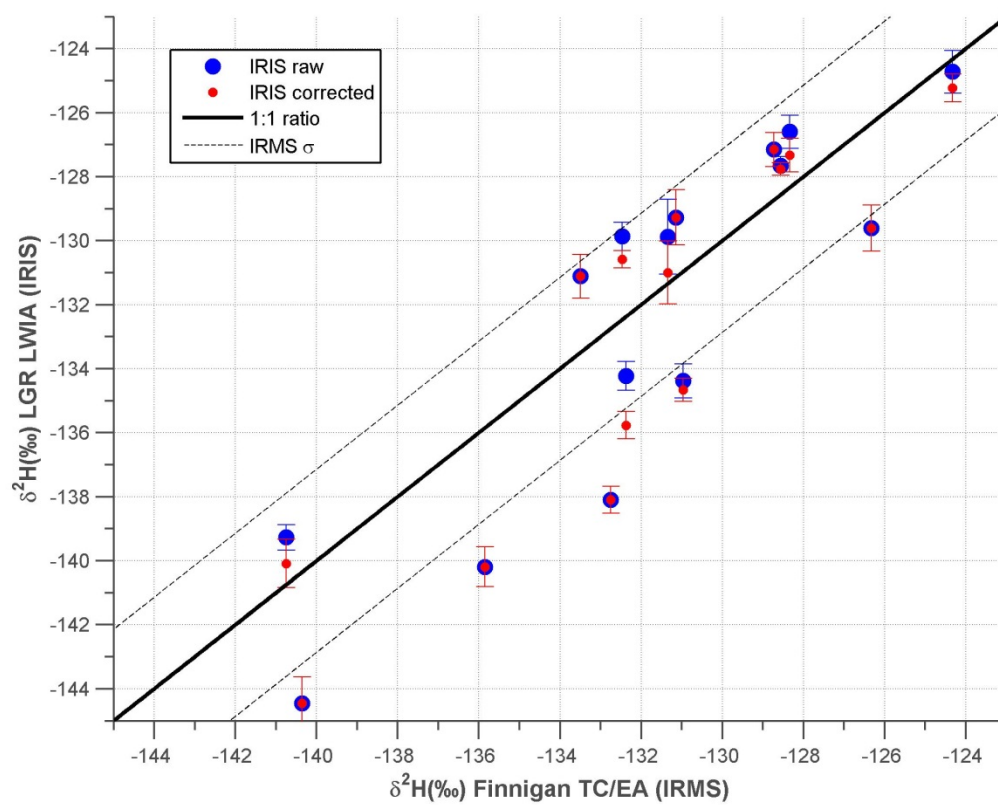


Figure 51. LWIA vs. FINNIGAN TC/EA IRMS $\delta^2\text{H}$ values.

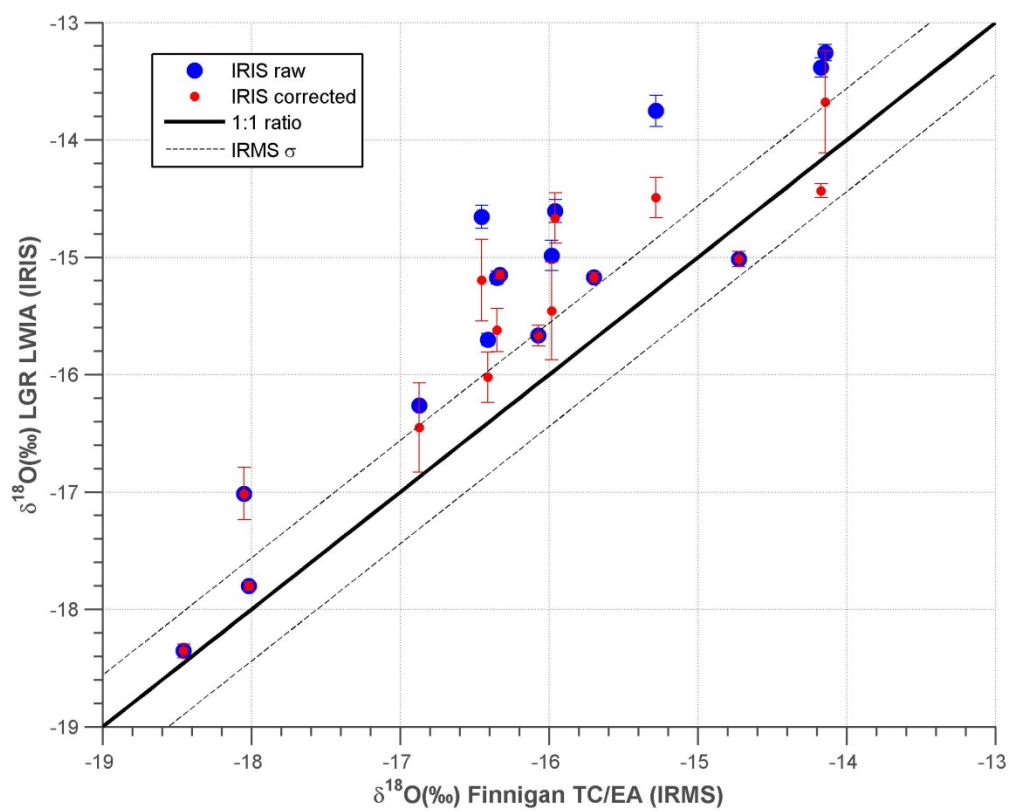


Figure 52. LGR LWIA vs. FINNIGAN TC/EA IRMS $\delta^{18}\text{O}$ values